Development of perylene and silicon rhodamine imaging reagents for fluorescence guided surgery

Gutachter:
1. Prof. Dr. Peneva, Gutachterin, Institut für Organische Chemie und Makromolekulare Chemie (IOMC)
2. Prof. Dr. Arndt, Gutachter, Institut für Organische Chemie und Makromolekulare Chemie (IOMC)

Tag der Verteidigung: 25.10.2022

"Prendete la vita con leggerezza. Che leggerezza non è superficialità, ma planare sulle cose dall'alto, non avere macigni sul cuore. […] La leggerezza per me si associa con la precisione e la determinazione, non con la vaghezza e l'abbandono al caso"

Italo Calvino

LIST of most used abbreviations:

$CHCl_3$ Chloroform

CT Computerized tomography

DCM Dichloromethane

DIPEA Diisopropylethylamine

DMABN 4-N,N-Dimethylamino benzonitrile

DMF Dimethylformamide

DPAP 2,2-dimethoxy-2-phenyl-acetophenone

DPAP 2,2-dimethoxy-2-phenyl-acetophenone

FDA Food and drug administration

FGS Fluorescence guided surgery

GPMI Guanidine peri-fused perylene monoimide

HRMS High Resolution Mass Spectrometry

ICG Indocyanine green

MB Methylene Blue

MRI Magnetic resonance imaging

NBS N-bromo succinimide

NIR Near infrared

PA Photoacustic

PET Positron emission tomography

PET Positron emission tomography

PMI Perylene monoimide

PY Pyronine

RP HPLC MS Reverse Phase High Performance Liquid Chromatography

SN_2 Second order nucleophilic substitution reaction

TEA Triethylamine

TEC Thiol-ene coupling

TFA Trifluoroacetic acid

CONTENTS

Chapter 1-Introduction

1.1 Fluorescence guided surgery

The death associated to cancer are increasing every year and according to the National Cancer Institute, in 2017, 1,7 million people have died because of cancer related diseases[1], in 2020 the number of affected patients reached 1,8 million and the limited access to hospitals during COVID-19 pandemic hampered the time needed for diagnosis and cancer treatment[2]. Surgery remains one of the most useful and rapid methodology to fight cancer together with adjuvant therapies such as chemo and immunotherapies[3]. Early-stage cancer resection is the first approach to treat non hematogenous localized cancer and the detection and visualization of all malignant lesions remains a consistent challenge in the hand of the surgeon. To date, the first operation needed to detect the tumour mass relies on visual localization, palpation, and frozen section pathologic analysis[4]. The difficulty to detect tumour margins often leads to incomplete removal of the tumour. While modern imaging technologies based on computerized tomography (CT) and magnetic resonance imaging (MRI) are effective in detecting abnormalities on the anatomical level, only techniques based on the use of targeted exogenous molecular contrast agents can shed light on the residual positive margins at the cellular level[5]. Among them, fluorescence guided surgery (FGS) is becoming a popular methodology of choice in the operating rooms[1, 3]. As an alternative to radionuclide imaging, the use of low energy near infrared (NIR) photons transparent to tissues together with compact optical imaging systems, reduces the space demanding equipment of nuclear medicine allowing surgeons to improve in real time, the quality of surgical resections without causing any damage to normal structures such as nerves, blood vessels ureters and bile ducts[1]. To date, the use of fluorescent contrast agents has been documented in several medical applications ranging from sentinel lymph node mapping to laparoscopic and robot assisted surgeries. Between them, vascular fluorescence angiography in reconstructive surgery, liver function assessment are the most common techniques[6]. A fluorescent contrast can be a small molecule synthetic organic chromophore or a macromolecular entity (molecular weight >1000 Da). It should possess high extinction coefficients and high quantum yield in water, large Stokes shift (> 80 nm)[7], biocompatibility and low toxicity. In 1959 Food and Drug Administration (FDA) approved Indocyanine Green (ICG) as contrast in fluorescence guided surgery[8]. ICG represents the first fluorophore to be used in the clinics. It belongs to the family of cyanine dyes and gave substantial results in surgery to measure cardiac output, to study the anatomy of retinal vessels and to assess the

liver functional reserve before hepatic resection in cirrhotic livers[9]. Under excitation light at 750-800 nm, ICG emits around 820 nm, exhibits low toxicity, binds to plasma proteins with a short half-life in bloodstream (3-5 min). It is quickly eliminated by the liver and concentrated unchanged into the bile[10].However, ICG suffers from several drawbacks such as poor water solubility, small Stokes shift and low quantum yield in water ranging from 1 to 10 %. This makes the fluorescent signal from ICG difficult to detect, while it necessitates higher doses and multiple intravenous injections of contrasts in the same operation setup[11]. The dye photostability is also an important parameter, ICG undergoes degradation after short irradiation time with visible light (20 min)[12]. For these reasons, the synthesis of novel NIR agents that can replace the use of ICG green in the clinic represents nowadays an important challenge. Companies make use nowadays of NIR imaging agents based on chemically improved version of cyanine dye scaffolds. In particular, LiCOR® biotechnology have experience in advancing research with IRDye® probes in phase I and phase II clinical trials[3]. NIR agents are useful to study drug delivery systems, targeted therapeutics, surgical contrast agents and monitoring the molecular basis of disease. Nevertheless, research is moving to different class of dyes to overcome the limitations of cyanine dyes. Push-pull perylene dyes represent a novel class of NIR absorbing chromophores with excellent photostability and water solubility. They are derived from perylene monoimides following the installation of electron donating groups, like primary aryl amines or water-soluble groups like guanidine functions, on the peri positions. Push-pull Perylene dyes are known in the literature as material resistant to photobleaching and suitable to long term irradiation condition during live cell imaging[13, 14], Peneva and co-workers achieved for the first-time the synthesis of a push-pull perylene dye with emission in the NIR up to 720 nm using a guanidine function as donor group on the peri position[15]. Push-pull perylene dyes and most of cyanine dyes can be classified as "always ON probes". According to the definition of Chen et al[16], the emission signal of always ON probes remain constant upon irradiation at the excitation wavelength used in the experimental setup. As a result of this property, the excess of signal coming from unbound always ON probes on the diseased tissue *in vivo* may result in a low target to background ratio on the diseased tissue of interest[17, 18]. To overcome these disadvantages, activatable dyes has been developed, these fluorophores can be designed to swich their fluorescence from a dark OFF state to an ON fluorescent state to sense specific pathological conditions associated with diseased tissues, for example the change of pH in tumour acidosis[19]. Between activatable dyes used nowadays *in vivo*, silicon rhodamines are also versatile tools to arm antibodies and small peptides and their versatile synthesis can be performed to allow the functionalization of primary thiols in cysteine residues in

macromolecular entities chosen ad vector molecules. In the following chapters, the potential use of push-pull perylene dyes and activatable silicon rhodamine dyes is provided followed by an extensive description of the state of the art of the substances already in use in FGS. Subsequently, the description of IRDye® probes advancing in phase I and II clinical trials and the modern strategies that make use of activatable dyes is provided. For this purpose, the strategies used to achieve the signal confinement on the region of interest are explained in the context of FGS.

1.2 NIR light, tissue penetration and the biological window

A fluorescent substance used as contrast in FGS should emit photons which wavelength lies inside the near infrared (NIR) range (650-900 nm) that are poorly absorbed by blood chromophores such as haemoglobin, myoglobin, lipids and water typically found in the blood or the so called biological window[20] (Figure 1). In this range, optical effects affecting photon propagation can be described as a result of both scattering events[21].
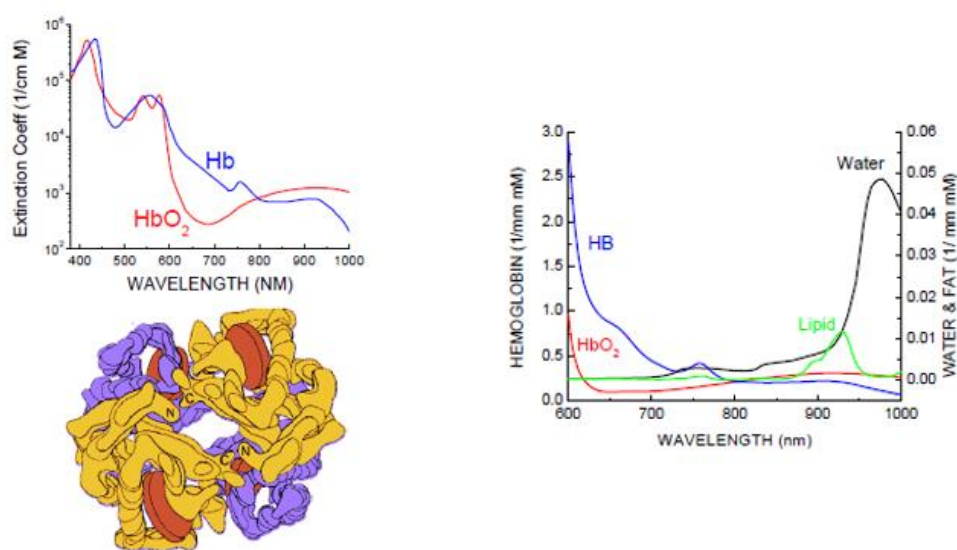
Figure 1 Imaging in the NIR window and hemoglobin absorption[20]

NIR light does not interact with common biological small molecules like NAD(P)H, flavins, vitamin A, porphyrins, lipofuscins and proteins[21] and it is commonly used in FGS. In a fluorescence image guided operational setup, photons interacting with particles that are smaller than their wavelength are scattered in all the directions in respect to the incident light (Rayleigh scattering), instead, when the particle has a size comparable or higher than the incident light wavelength, scattering occurs mostly in forward direction (Mie scattering)[22]. Photon propagation in tissues, depends on the extent of forward scattering[20]. Gradients of refractive

index are also commonly present and are associated with the density of subcellular organelles in tissues such as mitochondria nuclei, lysosomes, striations in collagen fibers and macromolecular aggregates. Those particles and organelles have a diameter that range from 0,1 μm to 1 μm and scatters NIR light forward being responsible for the high penetration depth in biological tissues[23, 24].To image deeper in tissues, detection of NIR photons have been achieved up to few millimeters thanks to the use of optical systems with large aperture lenses for high photon collection efficiency[24]. Detection of low energy photons are based on charge coupled device cameras (CCD) with appropriate band pass filter for NIR light, between them, intensified charge coupled devices and electron multiplying charge coupled devices (EMCCD) are the most commonly used in FGS[25]. Imaging on large animal living systems is based on planar imaging techniques that can be divided in two sub-categories: reflectance and transillumination imaging, the former having the source of the detector in the same side of the tissue, the latter between the source and the detector[26] (Figure 2).
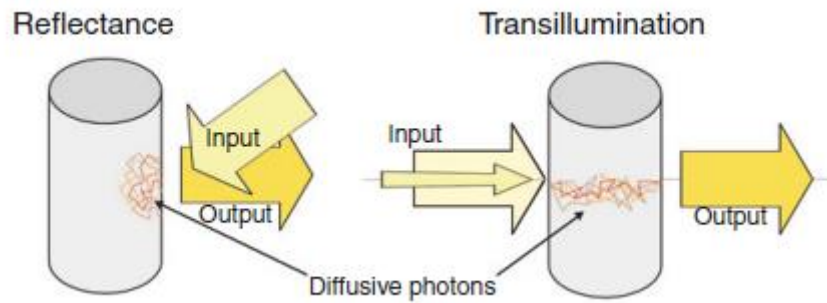
Figure 2 Reflectance and transillumination imaging taken from the work of Weissleder and coworkers[26]

Signal intensity relates linearly to the concentration of the fluorophore in the desired tissue but nonlinearly with its size and accumulation depth[27]. The quality of the signal is further attenuated by the high scattering nature of the media depending on the tissue. Brain, muscle and breast have the lowest reduced scattering coefficient while lungs scatters NIR light more[28]. Therefore, it is important to select the appropriate excitation wavelength and use high sensitivity CCD cameras to have the maximum image signal to background ratio (SBR). Optical imaging systems for FGS are assembled following the scheme depicted in Figure 3.
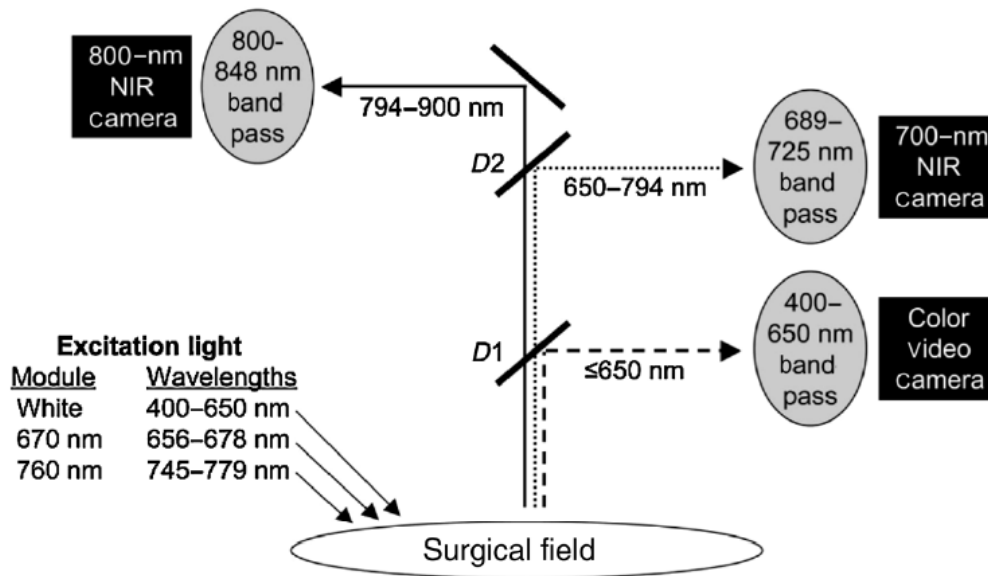
Figure 3 Schematic image of a NIR fluorescence imaging setup on the surgical field taken from the work of Pogue and coworkers[6]

The surgical field is irradiated with white light containing all the excitation wavelengths in the visible range and the reflected light is deviated by dichroic mirrors achieving band pass filters before reaching the CCD camera. Sensors are installed to impose images with white light and NIR light. Up to three channels have been installed depending on the imager used[6]. The most common commercially available imager systems are Perkin Elmer Solaris® Novadaq SPY-Elite® Quest Spectrum® CuradelTesVet LAB-flare® VisionSense Iridium® SurgVision prototype®. Between them, Novadaq, SPY ® and Fluoroptics Fluorobeam 800® operates in single channel modality, however, imagers that contains more than one channel and the ability to overlay the NIR image on the white light illuminated red, blue, green (RGB) image, can provide more accurate detection of fluorophore concentration in tissues[6]. Nevertheless, the most important factor determining the quality of the image and therefore of the instrument, is the ability to differentiate fluorescence light (>650 nm) from visible light (<650 nm) therefore, not only band pass filters and dichroic mirrors have a unique role in the system design but also the fluorophore itself, with its optical properties like high extinction coefficient, photostability, large Stokes shift and quantum yield. Since the excitation light coming from the fluorescence imager is emitted mostly by light-emitting diodes (LED) that have a large spectral bandwidth in the visible range[6] (Figure 4), it results difficult to filter all the excitation light close to the emission of the fluorophore. Because of these limitations, the image can have a low signal to background ratio (SBR).
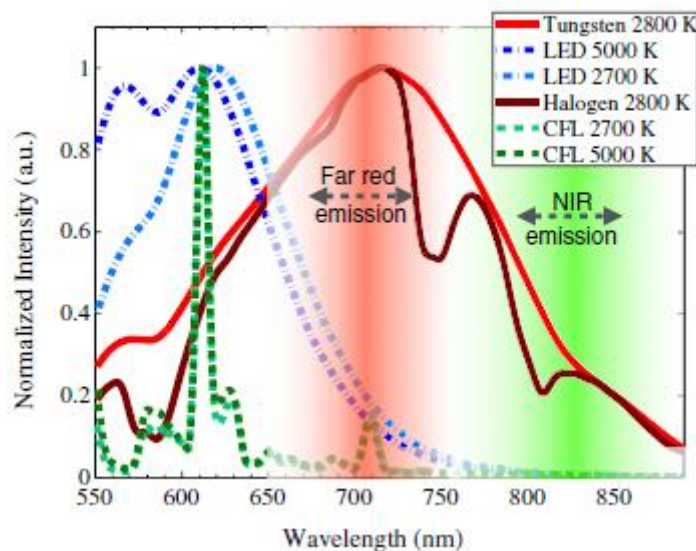
Figure 4 Common LED excitation sources used in FGS taken from the work of Pogue and coworkers[6]

The choice of the fluorophore is therefore crucial in every FGS setting and should be calibrated according to the excitation source used and the NIR imager channel. Probes should be tailored with a specific emission maximum centered at 700 nm or 800 nm. Most of the systems are manufactured with the 800 nm channel only, but imaging systems like Quest® and Fluorobeam® can image nowadays also with the 700 nm channel. Multichannel imagers expand the applicability of fluorophores which emission wavelengths lies outside the conventional ICG emission and open new challenges in the design of fluorophores to be used in conjunction with vector molecules like antibodies or small peptides[29]. Most of the surgical operations setups needs nowadays two targets to be detected simultaneously to highlight malignant cells and different tumor types but also to define the position of nerves and to avoid damages to normal structures like the ureters and blood vessels. Accidental nerve transection is associated with chronic pain, paralysis and it is responsible for example for the preservation of the urinary continence and erectile disfunction after prostatectomies[30]. The research on new fluorophores therefore, is expanding to different class of NIR emitting dyes to be used at the same time. Between them, special interest has been paid to always ON probes for the visualization of vessel anatomy bile ducts and nerves while activatable dyes have been proposed to reduce the nonspecific background fluorescence signal. Nevertheless, research is also focusing on the improvement of the specific binding, uptake and retention of the probe in the region of interest by studying the net charge distribution on the fluorophore structure[31]. Gibbs and coworkers highlight in a graph the probes that have been used in the clinics in the visible and in the two NIR channels[29] (Figure 5).
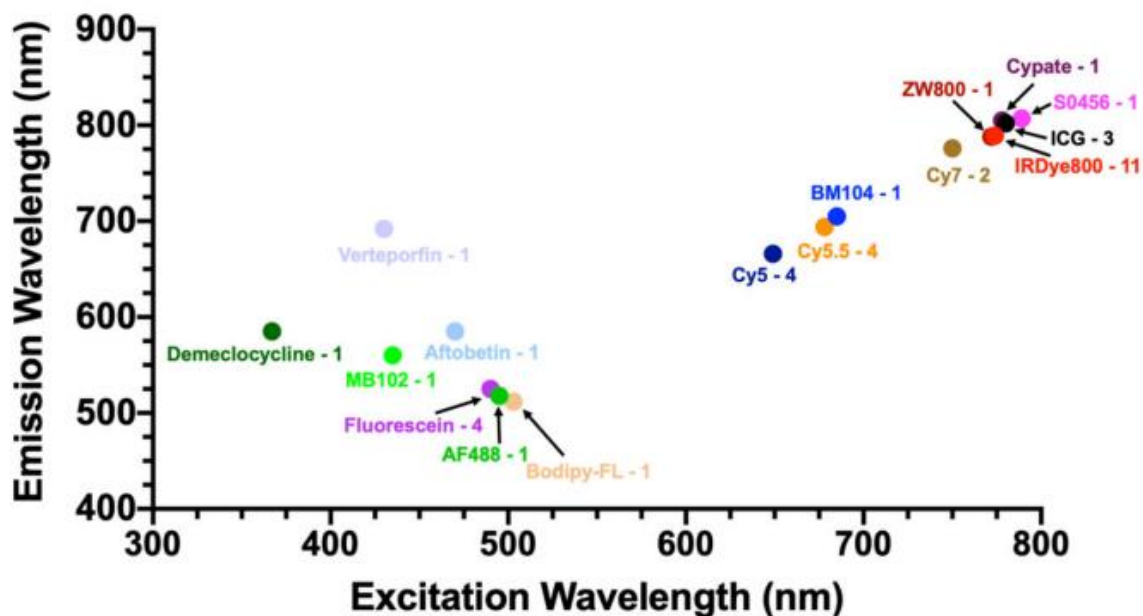
Figure 5 Most used fluorophores in FGS and their emission wavelength matching the conventional visible NIR channels in commercially available imaging devices. Taken from the work of Gibbs and coworkers[29]

Between the commercially available fluorophores only few that does not belong to the cyanine dyes family cover the range of the dual channel imagers. The aim of this thesis is to provide more accessible class of dyes that can improve the signal to background ratio in biological systems and image quality on the main NIR imager channels. We focused on NIR absorbing Perylene APMI dyes emitting up to 780 nm and silicon rhodamine dyes emitting in the 675 nm range. The two class of dyes offers several advantages including improved water solubility large Stokes shift (APMI dyes) and activatability in the physiological range (pH responsive silicon rhodamines).

1.3 FDA approved fluorescent based contrast agents

It is the aim of this section is to describe the FDA approved substances nowadays in clinical use as NIR contrasts. In particular, a detailed description of their chemical structure and photophysical properties will be provided and the applications that these contrasts find in surgery, their associated drawbacks and the limits that they represent in the clinic will be discussed. Fluorescent substances used in the clinics does not have a change in their emission wavelength under physiological condition and are defined as "Always ON" non-targeted probes[3] as they do not target any specific antigen associated to cancer cells, for this reason, they are still limited to applications that does not require a specific accumulation of the probe on the desired tissue. Always ON probes are useful in solid organ transplantation where

vascular reconstruction should be intraoperatively monitored. An always ON probe, is useful to confirm the position and physical state of the reconstructed vessels and, for example, to identify specific blockages. Teraoka et al. confirmed the success of vascular reconstruction in kidneys and liver transplantations using ICG[32]. Intraoperative use of ICG was also reported in colorectal cancer surgeries to evaluate the blood flow at the marginal artery in rectosigmoid junctions[33] and in the evaluation of coronary artery bypass grafts[34].

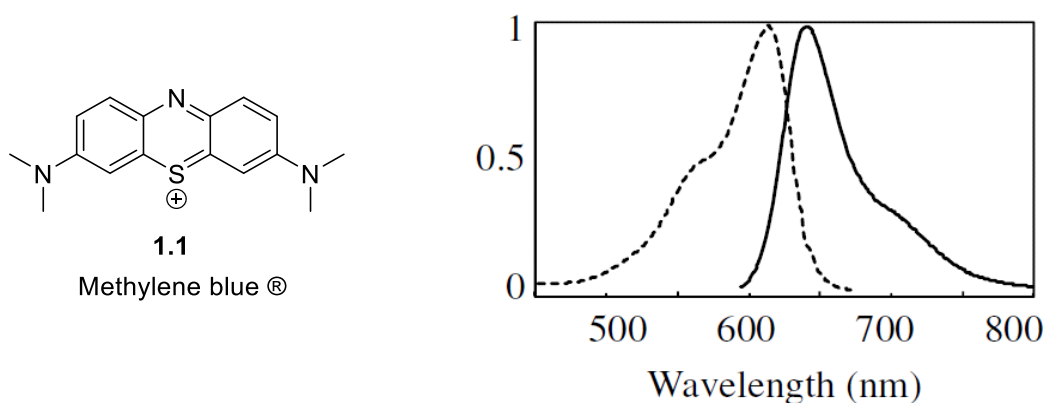### 1.3.1 Methylene Blue (1891)

1.1
Methylene blue ®

Figure 6 Chemical structure of methylene blue® and its absorption emission spectra in water[6]

Methylene blue® (MB) (Compound **1.2**) is the first synthetic dye used for medical applications, it was first discovered by Paul Gottmann and Paul Ehrlich as antimalarial agents in 1891[35] (Figure 6). MB is a heterocyclic aromatic compound with a small molecular weight (320 g/mol). It absorbs and emit light in water at 670 nm and 690 nm respectively and it is excreted through the kidneys upon intravenous injection. It can be used for breast cancer as well as neuroendocrine and urologic tumors imaging[3, 36]. Methylene blue cannot be used in higher concentration rather than 20×10^{-6} M because of loss of fluorescence in plasma and urine[36]. This phenomena, can be explained by the formation of the leuco methylene blue form under reducing conditions in plasma[37]. Methylene blue is also known to cause elevation of methemoglobin levels in blood, therefore, to limit the risk of toxicity, it should be applied in lower dosage (0,1 mg/kg)[36]. It is also important to exclude patients with known glucose-6-phosphate dehydrogenase deficiency due to the risk of severe hemolysis[38, 39]. Important side effects associated with the use of methylene blue in humans have been reported in clinical settings, among them, there is a potential risk of cardiac arrhythmias, coronary vasoconstriction and a decrease of renal blood flow[3, 35].

1.3.2 Fluorescein sodium (1947)
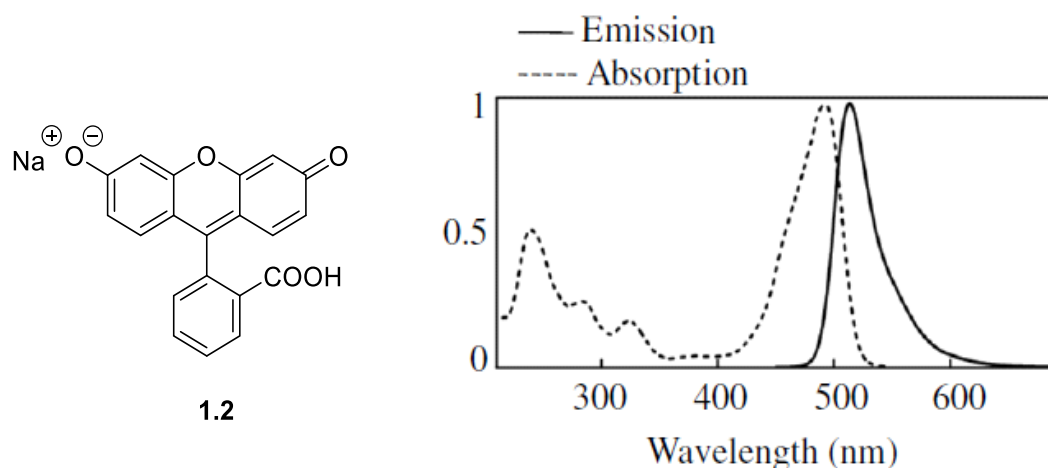
Figure 7 Chemical structure of Fluorescein sodium and its absorption and emission spectra in water[6]

Fluorescein sodium (Compound **1.4**) (Figure 7) is an anionic dye that absorbs and emits in the visible range with an excitation peak at 494 nm and an emission at 512 nm. It can be administered intravenously from aqueous sterile solution and finds the main application in ophthalmology for retinal angiography nevertheless, the historical use of fluorescein sodium belongs to intracranial tumors surgery (1947)[3]. Being a small molecule (332 g/mol), it is mainly found in plasma in the unbound state from serum proteins in blood upon intravenous injection. The dye can cross the Blood Brain Barrier (BBB) and help the identification of metastatic brain tumors upon nonvascular leakage[3, 40].

1.3.3 ICG green (1955)
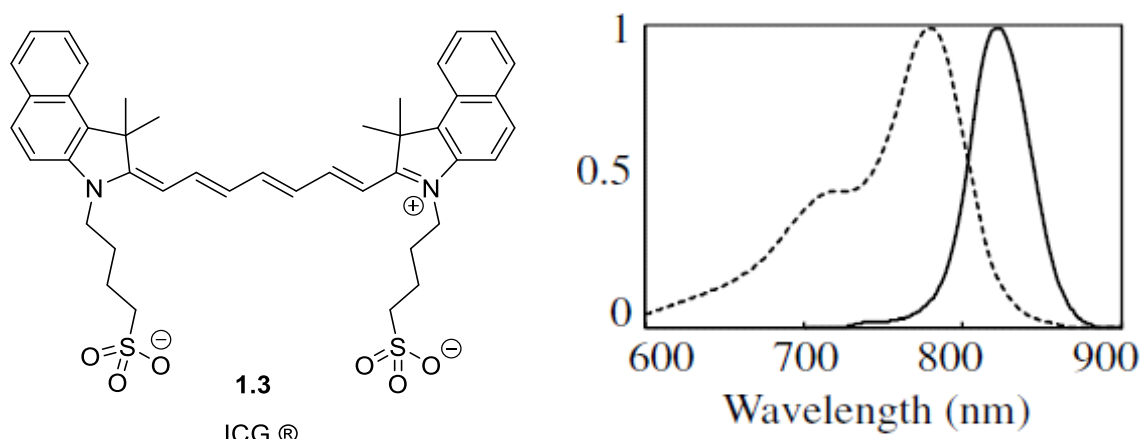
ICG green ® (Compound **1.1**) (Figure 8) was developed by Kodak laboratories in 1955 and FDA approved for clinical use in 1959. It is a water souluble anionic amphiphilic tricarbocyanine dye with relatively small molecular weight (776 g/mol) it belongs to the cyanine family and it is characterized by two heterocyclic units connected by a polimethyne bridge of seven carbon atoms. The absorption at 780 nm and emission at 820 nm makes it suitable for *in vivo* imaging. The molar extinction coeffcient in water is exceptionally high and reaches 200.000 $M^{-1}cm^{-1}$.The quantum yields are poor, about 10 % in water and they represents one of the main limitation togheter with the limited photostability[41]. It has been shown that ICG green undergoes rapid photobleaching after 20 min irradiation[12] and the degradation products have been extensively studied in the literature[42, 43]. Upon intravenous injection, ICG binds to plasma proteins like albumin, it has a relatively short half life (3-5 min), it is rapidly excreted by the liver and accumulated unchanged into the bile[10]. The most common applications of ICG green in surgery are related to hepatic function assetement, cardiac output measure and retinal angiorapy but they can be extended to sentinel lymph node (SLN) mapping, lymphography and tumor imaging[3].

1.3.4 Protoporphyrin IX (2017)

1.4
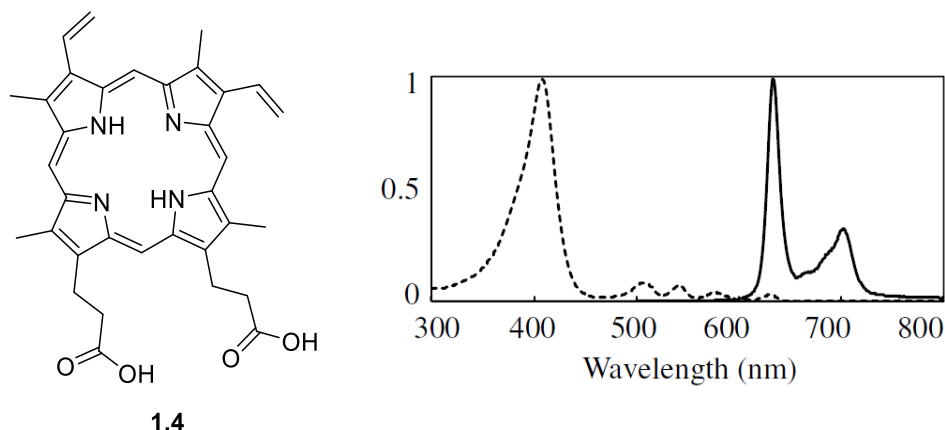
Figure 9 Chemical structure of Protoporphyrin IX and its absorption and emission spectra in water[6]

5-Aminolevulinic acid (5-ALA) (Compound **1.3**) (Figure 9) was approved by the FDA in 2017 for the surgery of gliomas[44]. 5-ALA is used as a substrate for the synthesis of protoporphyrin IX (PpIX) (Figure 9) *in vivo*, it can be administered topically or orally some hours before the surgical operation of glioma[44]. 5-ALA induces the synthesis of the fluorophore PpIX directly in epithelia and neoplastic tissues. Upon irradiation with blue light (380-440 nm) the emission peak can be detected with an exceptionally large Stokes shift at 620 nm or 634 nm depending on the pH of the tumor microenvironment (Figure 9). The major drawback associated with the use of 5-ALA is represented by the use of the blue light as excitation source around 400 nm as it can excite endogenous chromophores causing tissue autofluorescence. Patients can also be exposed to the risk of skin sensitization and they should be protected by sunlight days before the administration[3].

1.4 Targeted NIR imaging agents advancing in clinical trails

NIR dyes can be designed to achieve specificity on the target diseased tissue of interest. Many of the new NIR probes advancing in clinical trials possess bioconjugation linkers to covalently label vector molecules like antibodies, aptamers and small peptides targeting specific antigens overexpressed in cancer cells[45]. Macromolecular probes of this type, concentrates the signal in the region of interest while unbound probe rapidly clears with the bloodstream[45]. NIR dyes such as IRDye800CW® and ICG green have been recently used to study antibody pharmacokinetics and plasma clearance[46]. According to the analysis of Gibbs and coworkers most of the NIR agents nowadays advancing in clinical research are covalently linked to macromolecular entities to achieve tumor target specificity[29] (Figure 10).
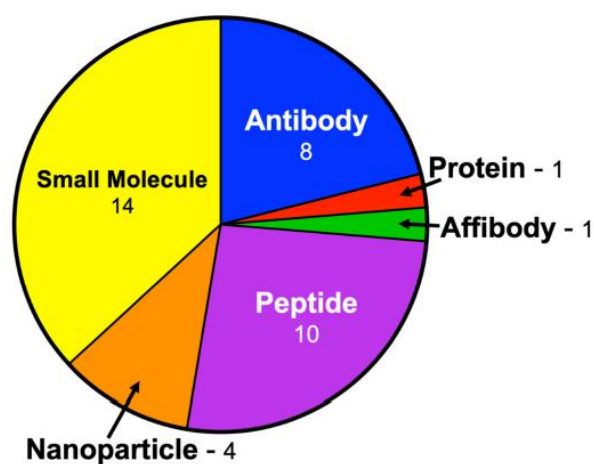

Figure 10 Pie chart of novel optical agents for FGS for clinical use[29]

In this section, NIR dyes possessing bioconjugation linkers to label vector molecules will be described, in particular, I will focus on the photophysical properties and applications of IRDye800CW® and IRDye700DX® advancing nowadays in clinical trials.

1.4.2 IRDye 800CW
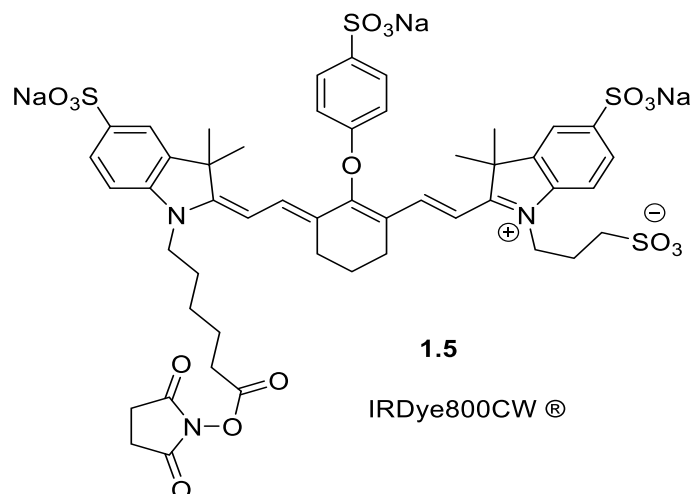
Figure 11 Chemical structure of IRDye800CW®

IRDye 800CW® (Compound **1.5**) is a commercially available cyanine dye patented by Li-Cor® (Figure 11). It absorbs and emits in 680 nm and 800 nm respectively, it possesses high water solubility, salt tolerance and low non-specific binding. It is manly used in conjugation with antibodies and manufactured as NHS ester or bearing maleimide linkers. It has been used in several phase I and phase II clinical trials and cited in clinical research worldwide[3]. In 2007 showed to be non toxic in animal studies and the complete report have been concluded and published in 2010 on record with U.S and European regulatory authorities. Nevertheless, FDA approval is still under current process and revision. The major drawbacks of IRDye800CW® are associated with the instability of the ether bond in the central carbon atom of the polymethine unit. It has been shown that the replacement of this function with a carbon carbon bond, improve the photostability of the chromophore, nevertheless, a consistent H-dimer formation in aqueous solutions have been observed. These phenomena limit the use if IRDye 800CW® for in vivo applications[47].

1.4.3 IRDye 700DX

1.6
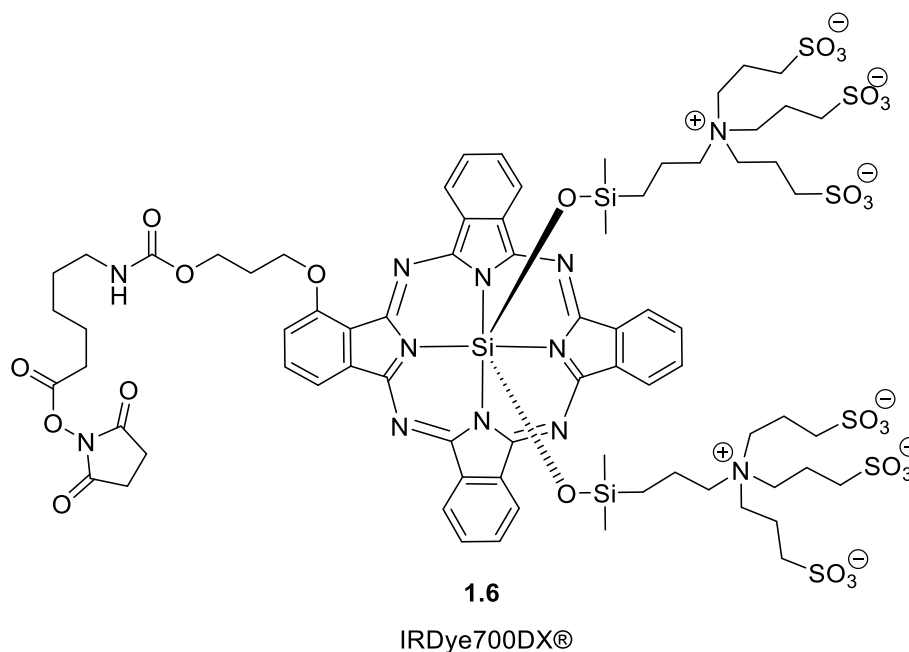
IRDye700DX®

Figure 12 Chemical structure of IRDye700DX®

IRDye 700DX® (Compound **1.6**) (Figure 12) is a near infrared phthalocyanine dye that absorbs and emits at 689 nm and 700 nm, possess a unique combination of properties like water solubility, lack of aggregation phenomena, photochemical stability, and high extinction coefficients up to 165000 $M^{-1}cm^{-1}$. It has been manufactured as NHS ester and advanced in phase II and phase I clinical trials by Li-Cor®. The main applications of IRDye700DX ® are associated with modern photo immunotherapies[48].

1.5 Activatable dyes in fluorescence guided surgery:

1.5.1 H-dimers formation and photoinduced electron transfer (PeT)

Fluorescent probes can be made more specific in conjugation with vector macromolecules targeting specific regions of diseased tissues, nevertheless, unspecific signal from unbound probes may persist limiting the spatial and temporal resolution[49,31]. To achieve signal confinement and improve the target to background ratio on the target region of diseased tissue, activatable probes have been designed[50]. Their mechanism of action consists on fluorescence activation upon specific cellular event or enzymatic cleavage of a functional group. The probe is remains non fluorescent outside the region of interest and become emissive only upon internalization in cancer cells (Figure 13). Activatable probes, help the surgeon to detect solid tumors and their boundaries in high resolution, limiting incomplete removal during dissection, avoiding metastatic lesions, tumor recurrence and the need of reoperation in patients[4].
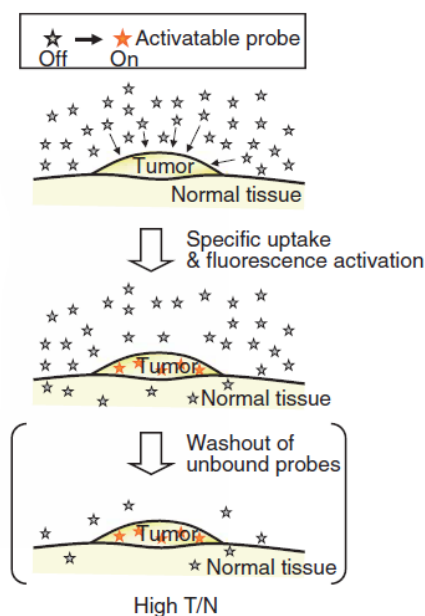
Figure 13 Image showing the mechanism of action of an activatable probe. The macromolecule once internalized in the cancer cell, gives the fluorescence signal thus improving the target to background ratio showing the difference in contrast between the healthy and the diseased the tissue[49].

Efficient quenching of a NIR active fluorophore can be achieved by the formation of H-dimers upon conjugation with a macromolecule targeting the receptor of interest. Ogawa et al. showed that commercially available dyes like TAMRA® forms homodimer pairs upon conjugation with Avidin tetramer and monoclonal antibody Trastuzumab ®. When the probe is internalized in cancer cells, the signal is restored thus improving the signal to background ratio[51]. Lacivita

et al. interpreted the mechanism of fluorescence activation with the action of protease enzymes in endosomes and lysosomes that disrupt the lysine backbone of the protein conjugate allowing the fluorophores to separate from each other thus restoring their fluorescence[52](Figure 14)
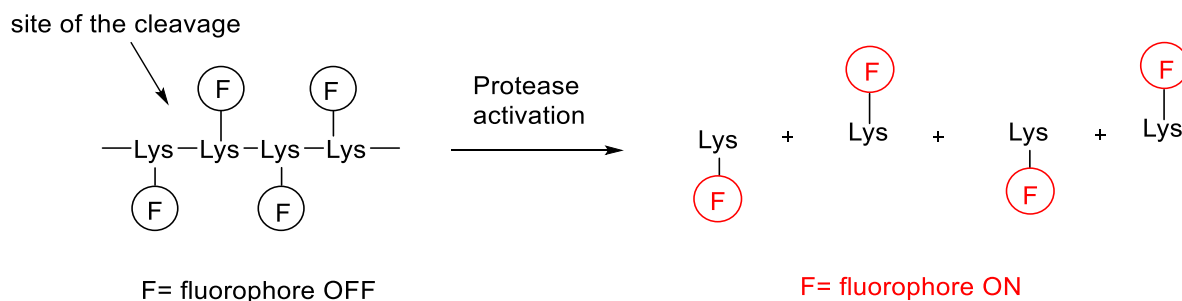
Figure 14 Fluorescence activation of bioconjugates by the action of proteases[52]

When a probe undergoes an intramolecular photophysical process to quench its fluorescence, it can be used to sense the environmental change in biological media such pH and the dielectric constant[53]. Photo induced electron transfer, for example[54], is an intrinsic mechanism of fluorescence activation that can be used to detect the pH change in the physiological range. pH activation through PeT, has been first described on a series of boron dipyrromethene (BODIPY) dyes[49]. The installation of N,N dialkyl aniline groups on the fluorophore scaffold, (Compound **1.7**) (Figure 15), resulted in a different fluorescent activation response in respect to the environmental pH. In basic pH, the fluorophore absorbs a photon achieving an excited electronic state. Subsequently, the transfer of an electron from the lone pair of the aniline nitrogen, provides a faster deactivation pathway thus preventing fluorescence to occur. In acidic pH, protonation of the nitrogen atom occurs, therefore, lone pair electrons are not anymore involved in electron transfer processes. In this state, the fluorescence of the probe is restored[19] (Figure 15). Other examples that use this mechanism to sense acidification pathways are under current investigation.
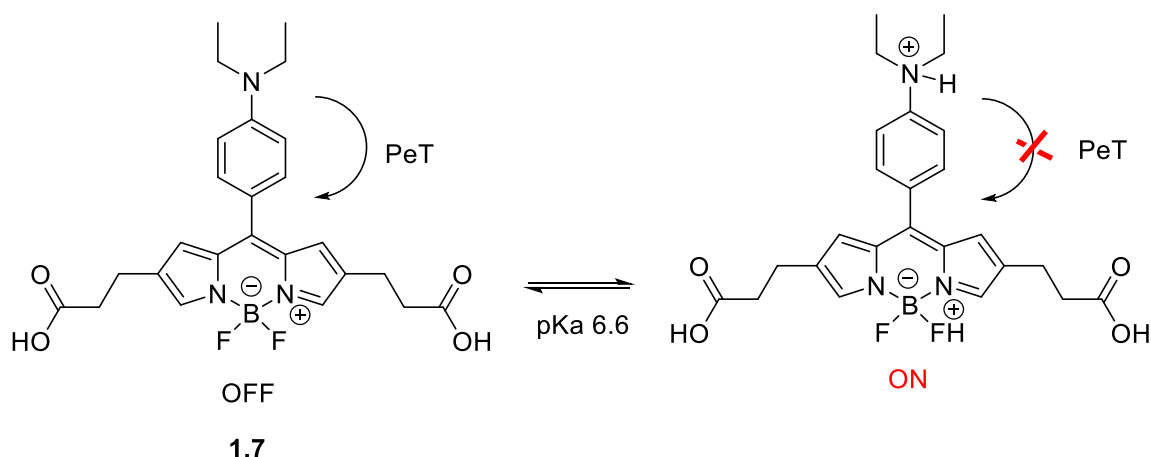
Figure 15 Chemical structure of pH responsive BODIPY dye and mechanism of action by photoinduced electron transfer based on protonation deprotonation equilibria in water[49].

NIR absorbing tetraryl azadipirromethene derivatives developed by O'Shea and coworkers possess emission in the NIR, they show typical absorption at 688 nm and emission up to 716 nm. Due to their intrinsic high hydrophobicity, they have been prepared with terminal alkynes and further functionalized through azide-alkyne click chemistry with sugars like 1-azido-1-deoxy-β-D-galactopyranoside. Compound **1.8** was prepared following this strategy[55]. The resulting dye is highly water soluble and presents a linker to a galactose mioety (Figure 16). Compound **1.8** (Figure 16) give a pH response to environmental conditions controlled by intramolecular charge transfer (ICT) through deprotonation of the free phenol moiety. In particular, a phenolate anion is formed at pH 6.9 that quench the fluorescence in the desired physiological range. (Figure 16)[55, 56].

Figure 16 pH responsive water-soluble tetraaryl aza dipyrromethene dye and equilibria based on phenol/phenolate anion equilibria showing the pKa value in water.

Combining both mechanism of intrinsic PeT fluorescence quenching, and intermolecular H-dimer formation, Kobayashi and coworkers proposed the use of pHrodo® (Compound **1.9**) (Figure 17) a commercially available chromophore patented by Invitrogen®. Once co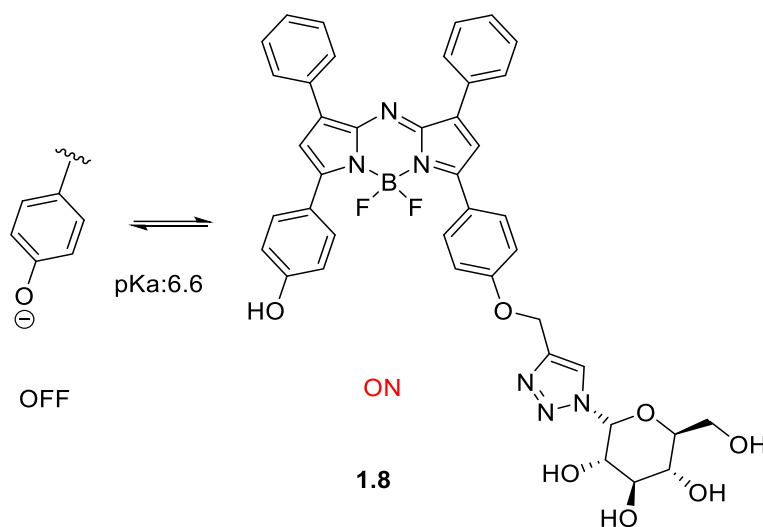njugated to biological macromolecules like antibody Trastuzumab ® and Avidin tetramer, pHrodo® forms H-dimer pairs and, at the same time, improves the fluorescence quenching process through a pH responsive PeT process. This is the first synthetic fluorophore combining two fluorescence quenching mechanism, H-dimer and photo induced electron transfer, that have been tested in fluorescence guided surgery[57] (Figure 17).

1.9
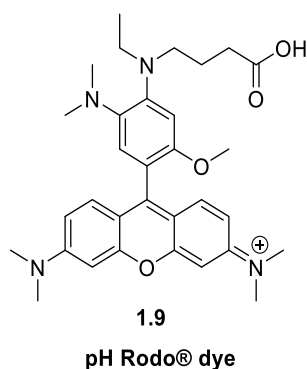
pH Rodo® dye

Figure 17 Chemical structure of pHrodo® dye provided by Invitrogen®

1.5.2 Enzyme activatable fluorescent probes

NIR emitting probes have also been employed to image superficial tumors expressing high levels of metalloproteinases[58]. Gamma glutamyl transferases (GGT) and aminopeptidase N are common examples of overexpressed proteases by cancer cells, they are mostly extracellular membrane anchoring enzymes and their activity is associated with angiogenesis, cancer cell migration and metastasis[59]. Kobayashi and coworkers developed the first series of rhodamine probes based on intramolecular spiro cyclization mechanism of fluorescence activation upon enzymatic cleavage (Figure 18)[60]. Probe **1.10** can be applied topically in the region of interest and was able to image the enzymatic activity with a penetration depth of a fraction of millimeter[60] (Figure 18).

Figure 18 Chemical structure of Rhodamine gamma glutamyl transferase targeting probe based on spiro cyclization mechanism of fluorescence activation upon enzymatic cleavage[60].

Based on the same synthetic approach, NIR absorbing silicon rhodamine dyes targeting gamma aminotransferases have been developed (Compound **1.11**) [61] (Figure 19).

Figure 19 Chemical structure of silicon rhodamine gamma glutamyl transferase targeting probe based on spiro cyclization mechanism of fluorescence activation upon enzymatic cleavage[61].

Another important achievement in the development of synthetic enzyme activatable probes have been proposed by Peng and coworkers[62] that prepared dicyanoisophorone dyes with large Stokes shift (205 nm) targeting aminopeptidase N in one step enzymatic reaction. The probe **1.12** was able to give fast activation response upon topical administration and image metastatic lesion large less than 1 mm in mice[4] (Figure 20)[62].

Figure 20 Dicyanoisophorone enzyme activatable dye and its mechanism of action based of enzymatic cleavage by aminopeptidase N[4]

1.6 Push-pull NIR absorbing perylene dyes

Push-pull dyes have attracted considerable attention because of their broad applicability in organic electronics in particular, photovoltaics, OLED, field effect transistors and dye sensitized solar cells[63]. A push-pull dye can be described as a molecule bearing electron donor (D) and electron acceptor (A) groups at the two terminal carbon atoms of a polyene system or an aromatic compound bearing D/A substituents para to each other (Figure 21)[64]. Typical electron donors (D) are hydroxy (-OH) amino ($-NH_2$) methoxy (-OMe) and dimethylamino ($-NMe_2$) groups, while common electron acceptors are nitro ($-NO_2$) cyano (-CN) and aldehyde (-CHO) groups[63] (Figure 21).
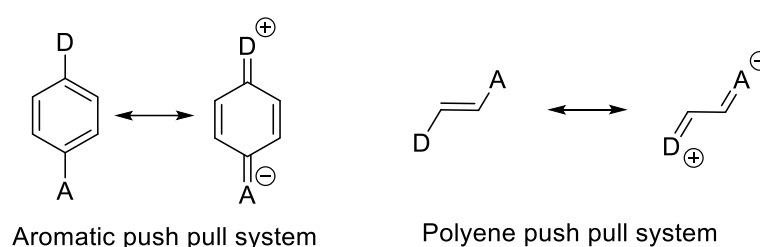

Figure 21 Aromatic and polyene push-pull systems and their resonance form leading to dipolar species

Upon photoexcitation, the transfer of an electron from the donor group (D) through the acceptor group (A) occurs giving rise to dipolar species with two separate charges at the end of the conjugated system (Figure 21). This process has been called intramolecular charge transfer (ICT)[65] and have been extensively studied especially to enhance the Stokes and the bathochromic shift in the absorption and emission of dyes with an extended conjugated system. The entity of the red shift depends on the type and position of the donor-acceptor (D/A) substituents as well as on the extent of the conjugation of the chromophore[65]. Bures Philip et al. reported 4-nitroaniline, Compound **3.0** (Figure 22). This aromatic compound, shows a red shifted absorption profile at 370 nm in comparison with bulk chemicals like nitrobenzene, 4-nitroaniline and 3-nitrobenzene[63] which absorption lies mainly in the UV range (250-260 nm) (Figure 22). This phenomenon has been explained by the formation of a dipolar species upon photoexcitation due to the para position of the donor and acceptor groups in the phenyl ring (Figure 22).

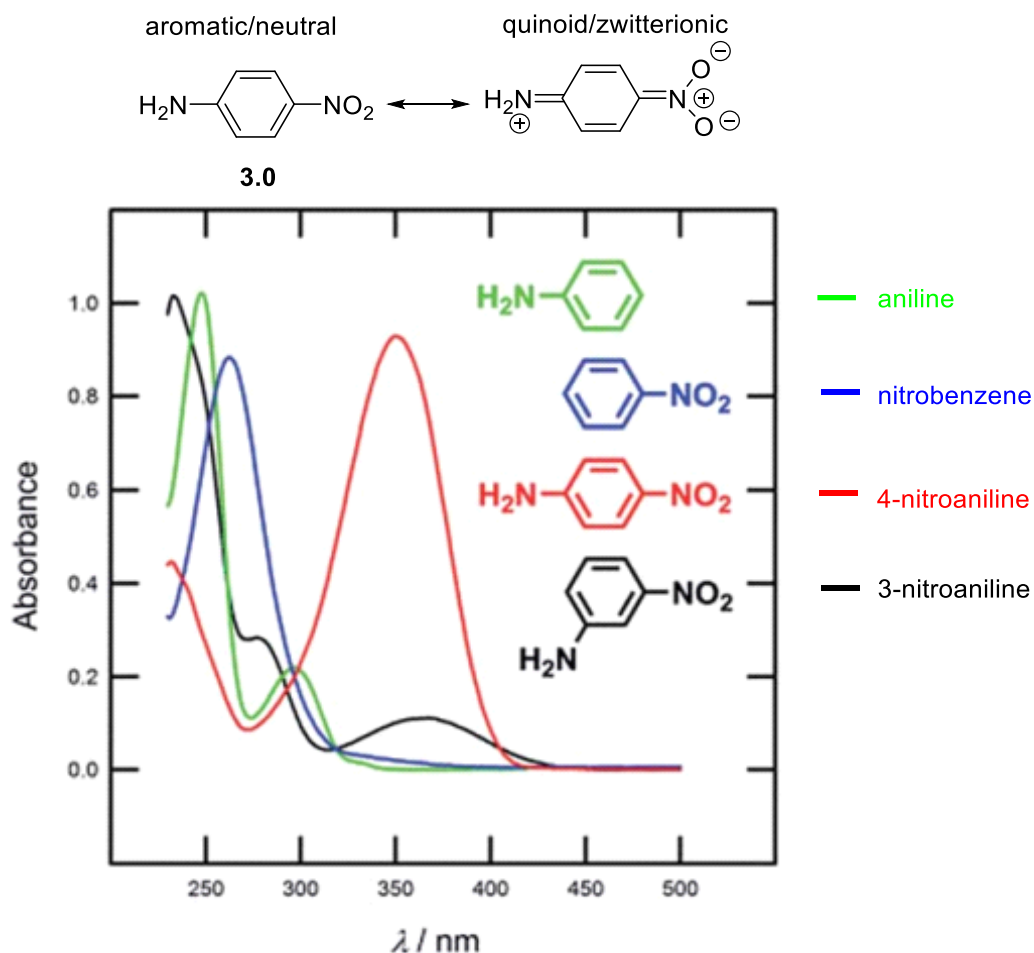aromatic/neutral   quinoid/zwitterionic

3.0

Figure 22 Example of a push-pull dye, 4-nitroaniline, Compound **3.0** showing its absorption at 360 nm in DCM. Bulk chemicals like aniline, nitro benzene and 3-nitroaniline absorbs mainly in the UV range (Bures, 2014)[63].

One of the most studied push-pull dye is 4-N,N-dimethylamino benzonitrile (DMABN) Compound **3.1** (Figure 23) reported for the first time by Lippert and coworkers in 1962[66]. DMABN is a push-pull dye that exhibits two emission peaks depending on the solvent used, the red shifted one was assigned as the emission arising from an ICT state[66] (Figure 23). Solvents with a low dielectric constant like hexane, dibuthylether, diethyl ether favor the emission at 28.000 cm^{-1} (357 nm) (Figure 23). When polar solvents are used like buthylchloride and acetonitrile, the emission shifts to lower frequencies (20.000 cm^{-1}) (500 nm). These observations indicate that polar solvents stabilize the formation of the dipolar species of DMABN and stabilize the low energy emission[66-68] (Figure 23).
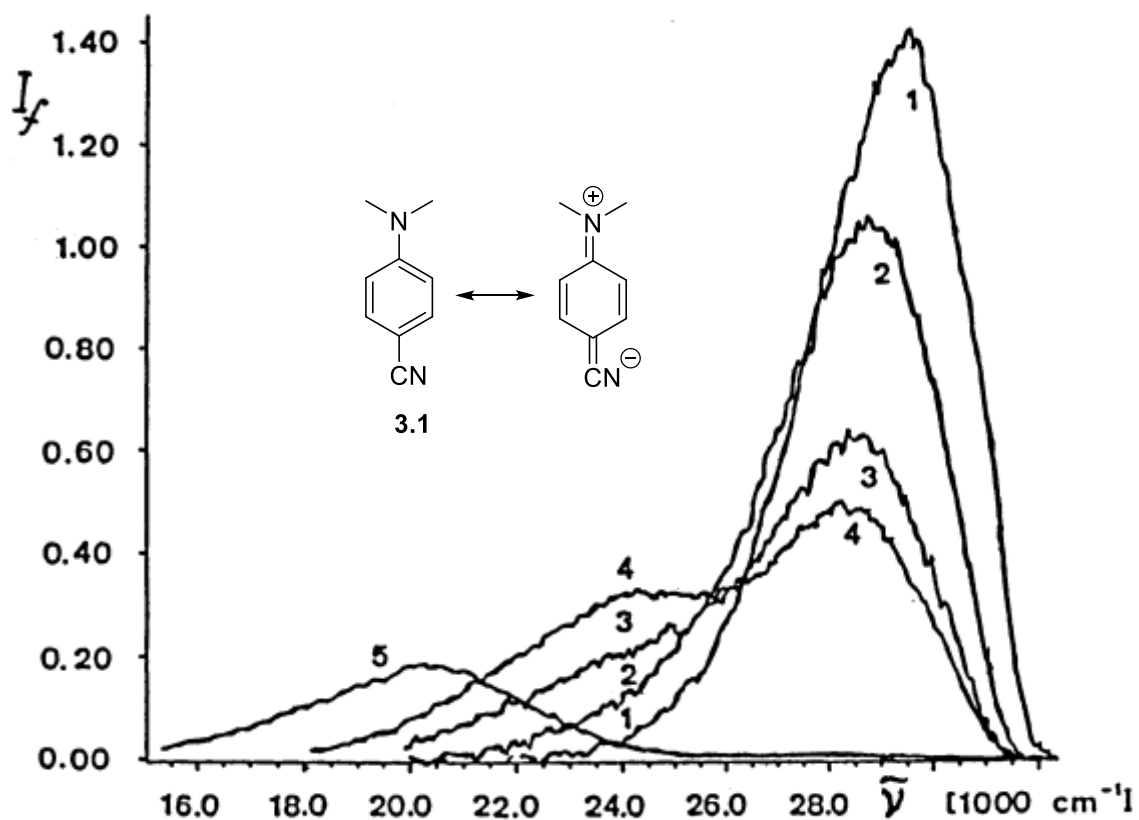
Figure 23 4-N,N-dimethylamino benzonitrile (DMABN) fluorescence spectra in hexane (1) dibuthylether (2) diethyleteher (3) buthylchloride (4) acetonitrile (5) (Grabowsky et al. 2003)[66].

Donor and acceptor groups can be installed also on rylene derivatives leading to large bathochromic shift in the absorbance and emission in the NIR region. The rylene dyes are based on poly(peri-naphthalene) units covalently fused in the peri positions **3.2** (Figure 24). A dye belonging to rylene family is perylene 3,4,9,10-tetracarboxy dianhydride (Compound **3.3**)[69] (Figure 24). This perylene dianhydride, is well-known in the literature for its photostability as a pigment and vat dye[69]. It is commonly used as a starting material in the synthesis of perylene 3,4-dicarboximides.
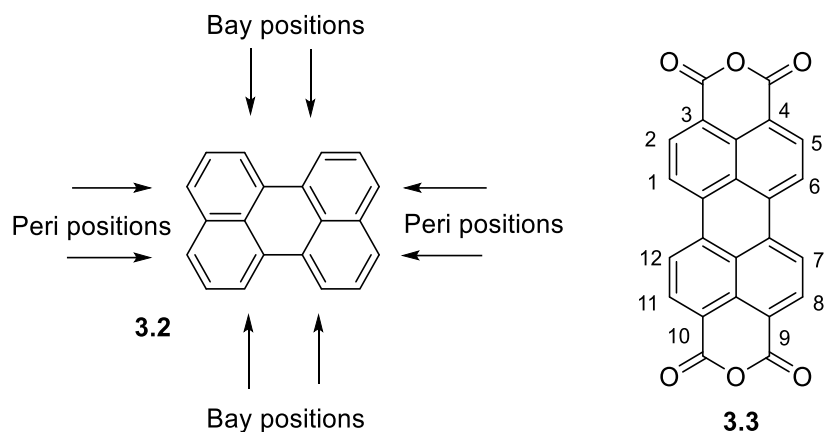
Figure 24 Chemical structure of rylene derivatives and numbering system of perylene (left). Perylene-3,4,9,10-tetracarboxylic dianhydride is shown (right).

Perylene 3,4,9,10-tetracarboxylic dianhydride, Compound **3.3** (Scheme 1), can be obtained from naphthalene dicarboximide **3.5** (Scheme 1) through oxidative dimerization with alkali (potassium hydroxide of sodium hydroxide) and via saponification with sulfuric acid (Scheme 1)
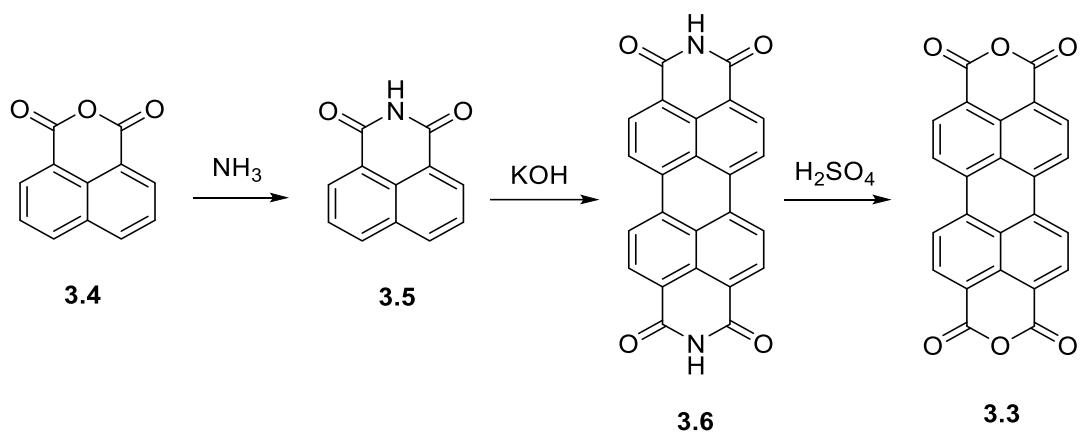
Scheme 1 Synthesis of perylene-3,4,9,10-tetracarboxylic dianhydride Compound **3.3**.

In addition, perylene 3,4,10-tetracarboxydianhydride **3.3** (Scheme 2) undergoes decarboxylation reaction using 2,5-di-tert-buthylaniline in water in presence of zinc acetate at 190°C for 24 hours gi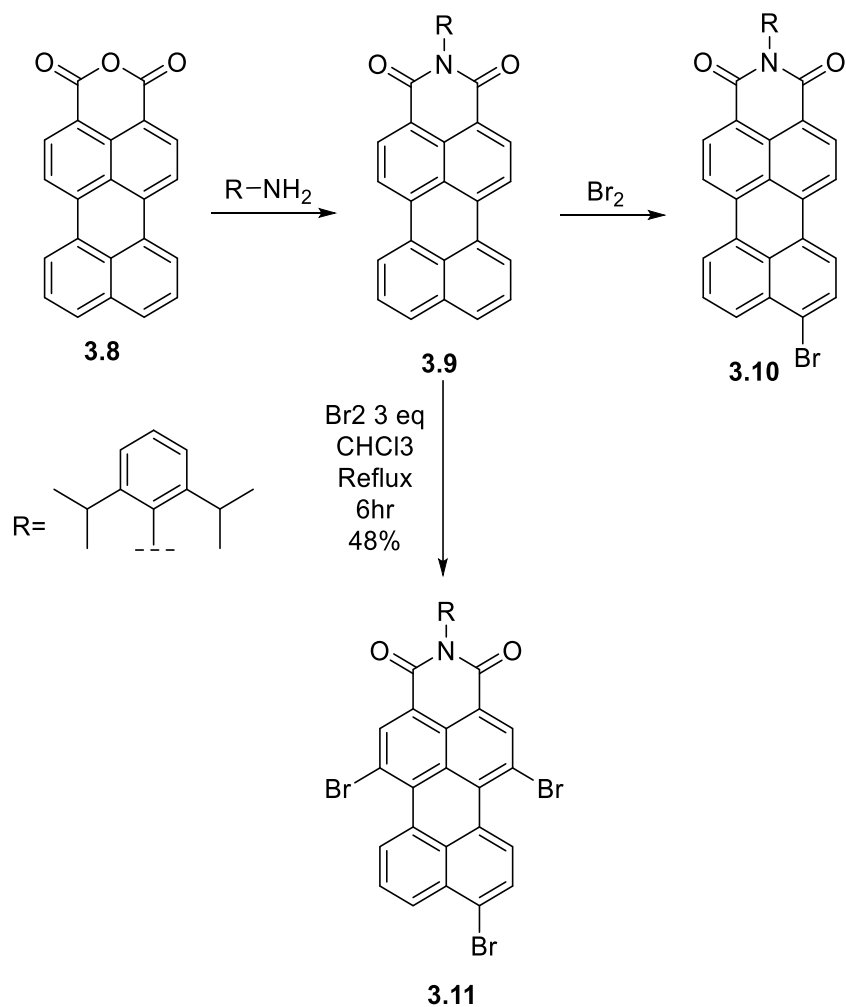ving perylene monoimide Compound **3.7** (Scheme 2). Moreover, Compound **3.7**, treated in acetic acid under reflux, gives perylene 3,4-monoanhydride, Compound **3.8**[69] (Scheme 2).
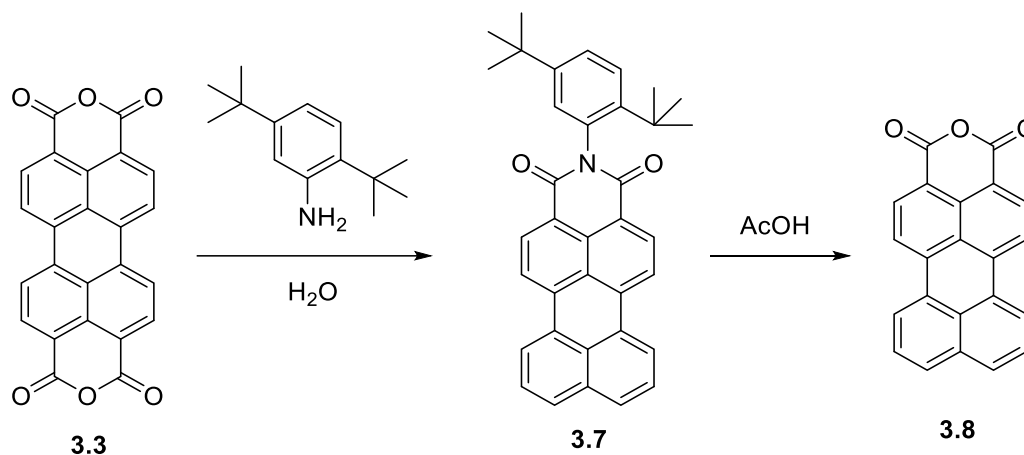

Scheme 2 Decarboxylation and imidization of perylene 3,4,0,10-tetracarboxydianhydride in water and zinc acetate in presence of 2,5-di-tert-buthylaniline[69].

Perylene monoimides (PMI) like Compound **3.7** (Scheme 2), are useful starting materials for the preparation of NIR emitting dyes and have found extensive applications in organic electronic devices due to their exceptional photostability[70, 71]. This class of chemical compounds are obtained through imidization of the anhydride function of Compound **3.8** (Scheme 2) in presence of aromatic and aliphatic amines. Perylene monoimides can be further modified with bromine and nitrating agents (Scheme 3). In particular, it is possible to perform selective monobromination in position 9 or tribromination in position 1,6,9 giving Compound **3.10** and Compound **3.11** (Scheme 3). Brominated PMI are used as starting materials for the preparation of push-pull rylene derivatives with NIR emission[72].

Scheme 3 Preparation of brominated perylene monoimides

Brominated perylene monoimide Compound **3.11** (Scheme 3) undergoes nucleophilic aromatic substitution reactions with aromatic thiols on position 1,6[72] . This transformation affords compounds **3.12** and **3.13** (Scheme 4) as main products.
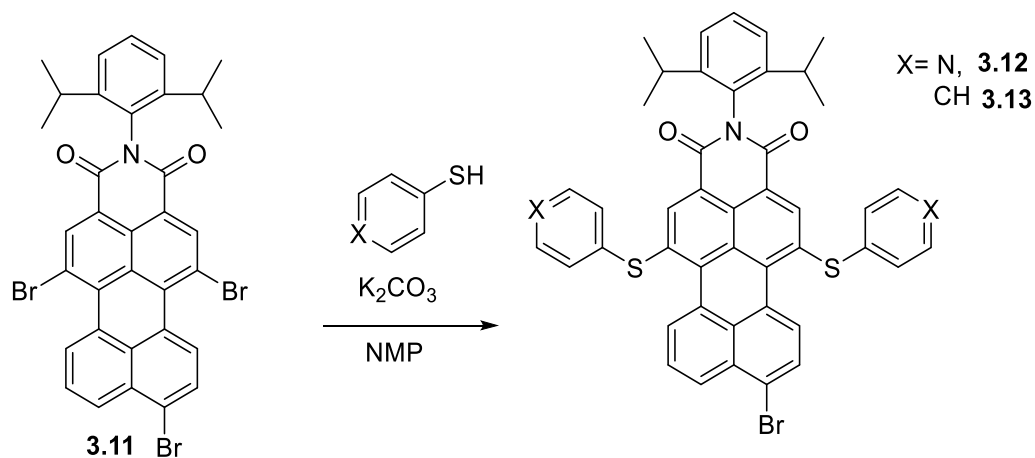

Scheme 4 Nucleophilic aromatic substitution on perylene monoimide scaffolds with aromatic thiols

Furthermore, compound **3.12** and **3.13** can undergo substitution on position 9 with secondary aromatic amines as donor groups affording push-pull perylene Compound **3.14** (Scheme 5) and Compound **3.15** (Scheme 5)[72]. The installation of a nitrogen atom on position 9, is responsible for the ICT absorption band in the NIR in DCM at 736 nm (Compound **3.14**) and at 681 nm (Compound **3.15**) [72] respectively (Scheme 5).
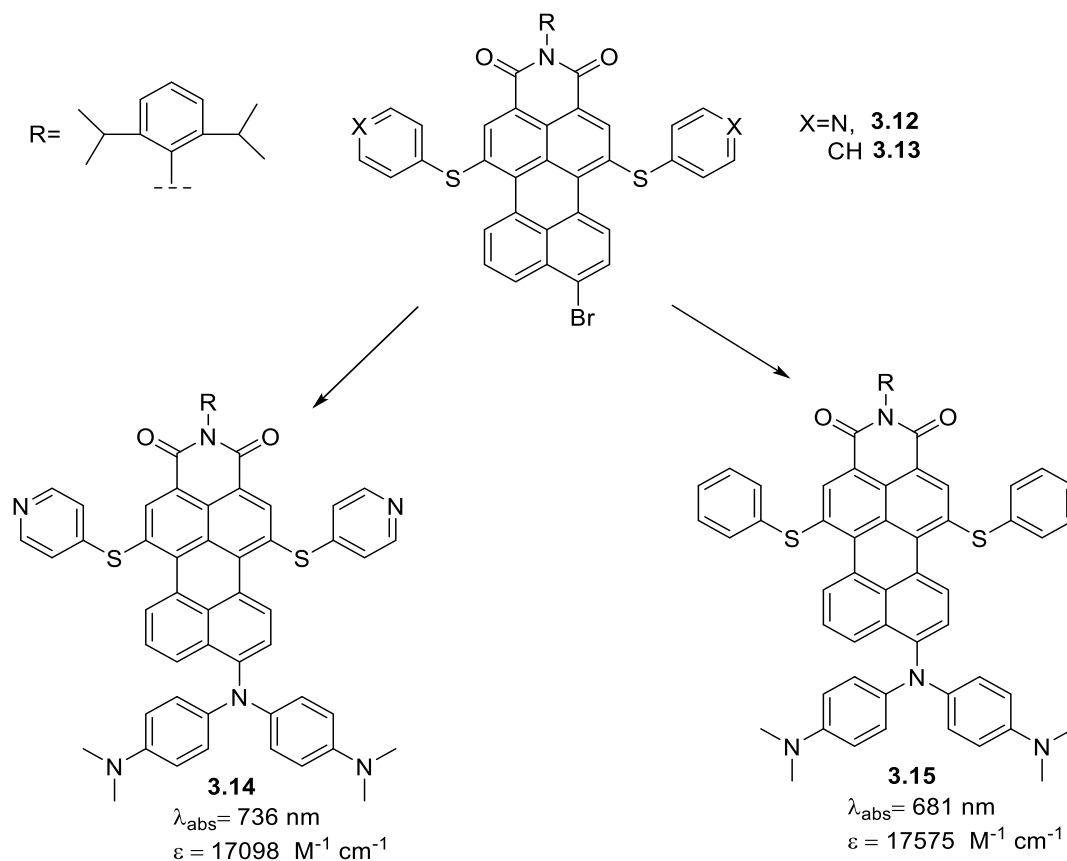
Scheme 5 Substitution with donor substituents at the *peri* position with aromatic diamines give NIR push-pull absorbing perylene chromophores in DCM.

To enhance the push-pull character of perylene monoimides, Zagranyarski et al. performed, for the first time, a double donor substitution on position 9, 10 starting from perylene tetracarboxy dianhydride Compound **3.16** (Scheme 6). Compound **3.16** reacts with elemental bromine in water/acetic acid mixtures to give perylene monoimide Compound **3.17** with two bromine atoms installed on 9,10 position[73] (Scheme 6).
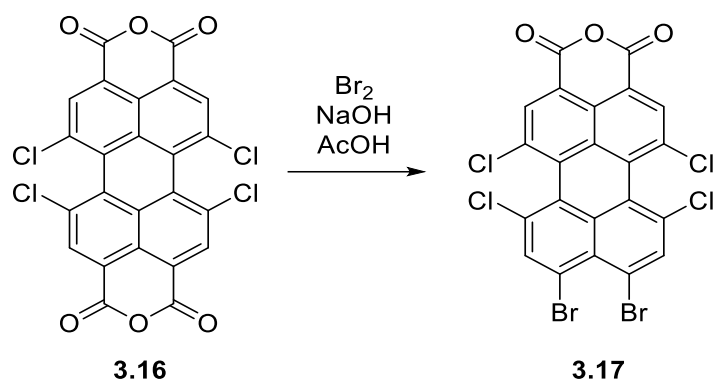
Scheme 6 Hunsdiecker reaction on perylene-3,4,9,10-tetracarboxylic dianhydride giving selective substitution of the 9, 10 position with bromine atoms [73].

Subsequently, the installation of donor groups on position 9,10 was achieved by Suspension of **3.17** (Scheme 7) in aniline at 180° for 5 hours giving one-pot imidization on the anhydride function and substitution on position 9,10. This reaction, affords Compound **3.18** (Scheme 7) as main product. Compound **3.18** is a push-pull dye presenting aromatic primary amines as donor groups (Scheme 7). Further bridging of the donor nitrogen atoms on position 9, 10 with a methylene bridge with paraformaldehyde gives Compound **3.19** (Scheme 7). This modification on the *peri*-fused nitrogen atoms rises the value of the molar absorptivity and slightly shift the absorbance to longer wavelength[73] (Scheme 7).
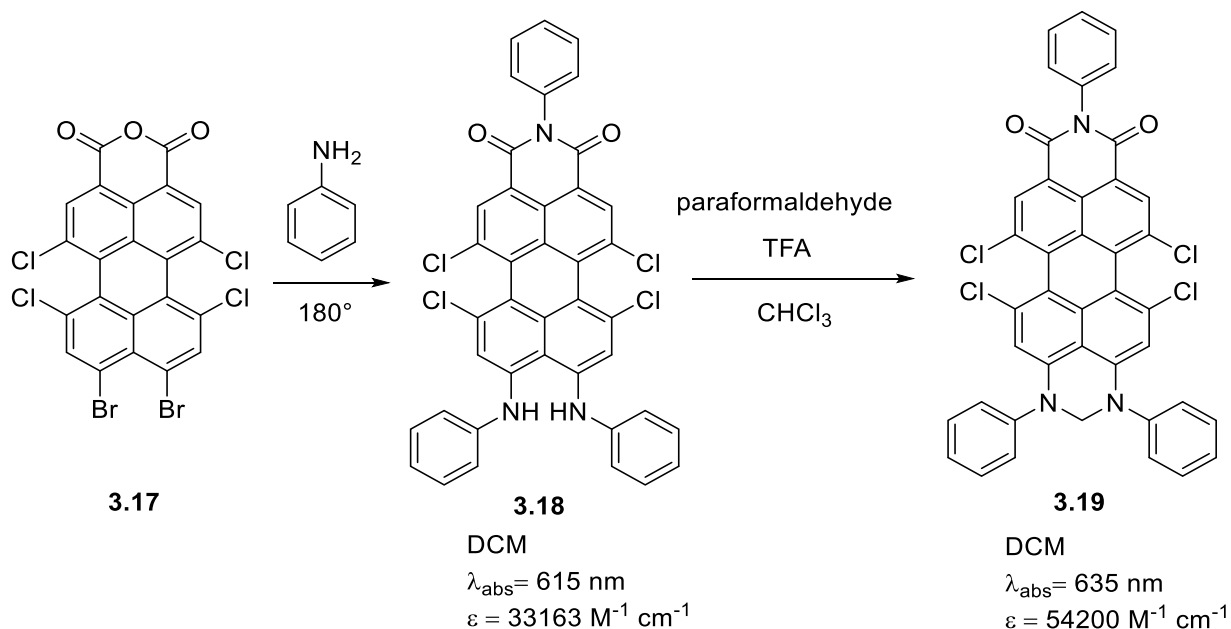
Scheme 7 Preparation of push-pull perylene dyes refluxing perylene monoanhydride **3.17** in aniline (right) and modification of the *peri*-fused nitrogen atoms with paraformaldehyde (left).

1.7 NIR absorbing push-pull water soluble rylene chromophores.

Perylene monoimides are useful starting materials for the preparation of push-pull dyes with absorption and emission in the NIR. They can be prepared through the installation of nitrogen atoms as donor groups on the peri position (position 9,10) (Scheme 7) Nevertheless, when donor substituents from bulky aromatic amines are used, the dye hydrophobicity considerably increases. To overcome this limitation, Kaloyanova et al. proposed the installation of a guanidine function on Compound **3.21**[15] (Scheme 8) to give a water-soluble push-pull dye **3.21** (Scheme 8). Compound **3.21** (Scheme 8) can be modified on the hydroxy group with phosphorus tribromide to give Compound **3.22** bearing a primary bromide function. In the last step, the primary bromide is substituted by triphenyl phosphine to give compound **3.23**. This dye is active in the NIR with emission up to 710 nm and possess two positive charges on its chemical structure, for this reason, it is used as cellular stain for the visualization of internal membranes of mitochondria in super resolution microscopy[15].
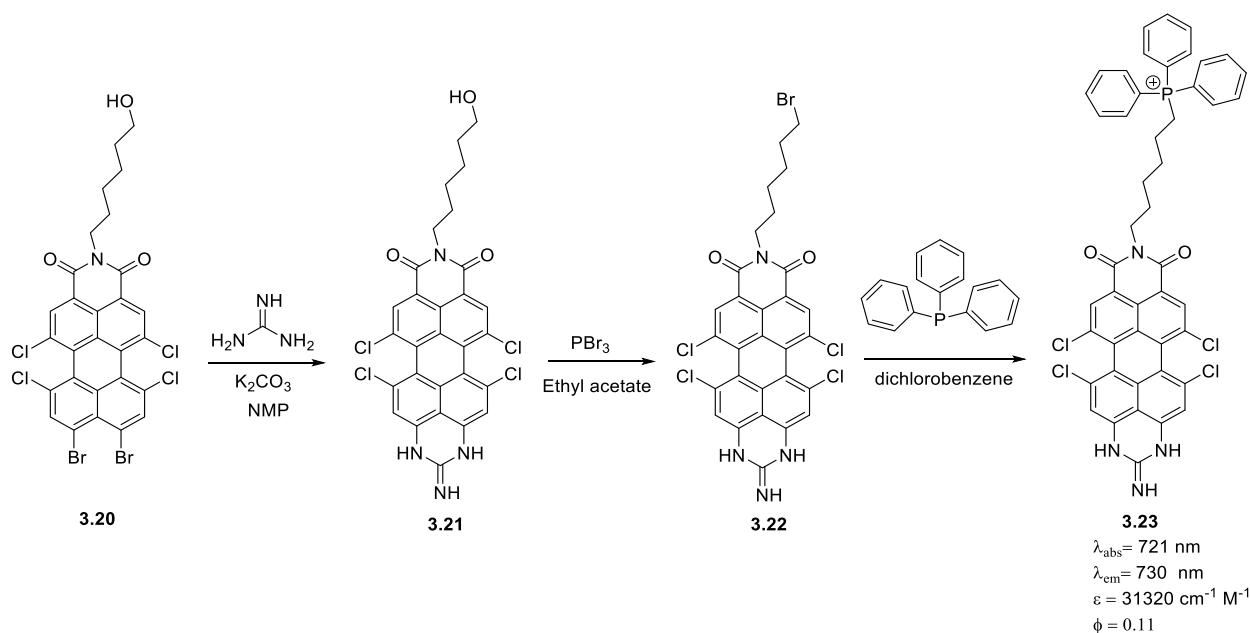
Scheme 8 Synthesis of water-soluble push-pull NIR absorbing perylene chromophores.

The synthesis of new water-soluble perylene push-pull dyes offers a unique way to achieve NIR emission bringing together the characteristics of photostability and water solubility of the rylene family in a single structure.

1.8 Other strategies to achieve NIR emission in rylene derivatives.

NIR emission in perylene dyes can also be achieved by extension of the rylene core to form higher-rylene derivatives such as quarterrylene teracarboxy diimide or through the anhydride function leading to perylene bisarylamidines[74].

1.8.1 Perylenebisamidine derivatives

The synthesis of perylenebisamidine dyes is considered the first attempt to enlarge the conjugated system of the chromophore. The condensation of perylene-3,4,9,10-tetracarboxylic dianhydride with ortho-diamino arenes produced bisamidine derivatives as a mixture of syn and anti-isomers **3.24** achieving absorption maxima in the range of 629-659 nm.[74, 75] (Scheme 9).

3.3

anti **3.24** sin
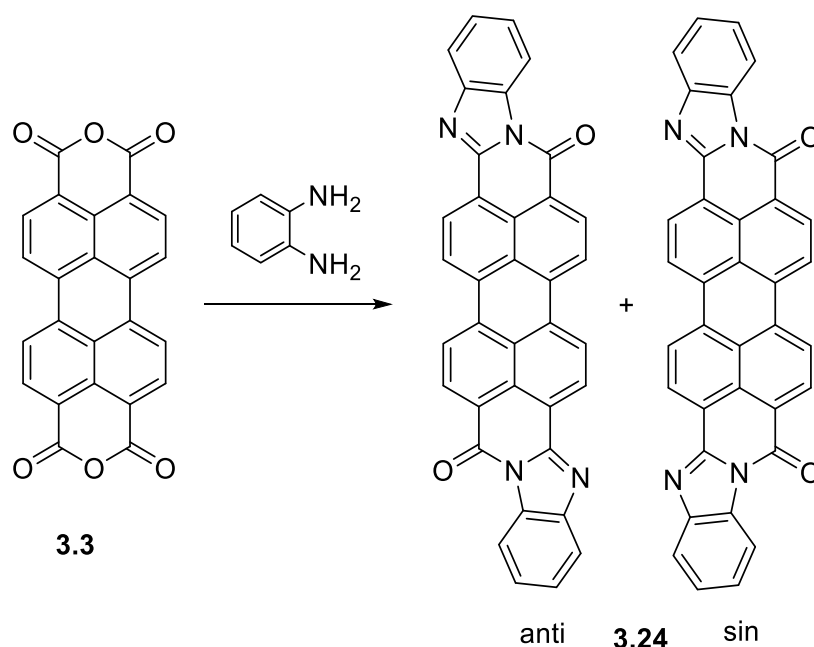
Scheme 9 Imidization of perylene-3,4,9,10-tetracarboxylic dianhydride with ortho diaminoarenes to produce a mixture of isomers sin, anti absorbing in the range of 629-659 derivatives.

Perylenebisamidines like Compound **3.24** (Scheme 9) are poorly soluble in organic solvents. To overcome this limitation, aryloxy and alkyloxy derivatives were installed on the bay position of perylene 3,4,9,10 tetracarboxydianhydride prior to imidization with ortho diamino arenes leading to NIR emissive materials highly soluble in organic solvents. Compound **3.25** for example, was obtained as a mixture of sin, anti-isomers with emission up to 768 nm[74] (Scheme 9).

3.25
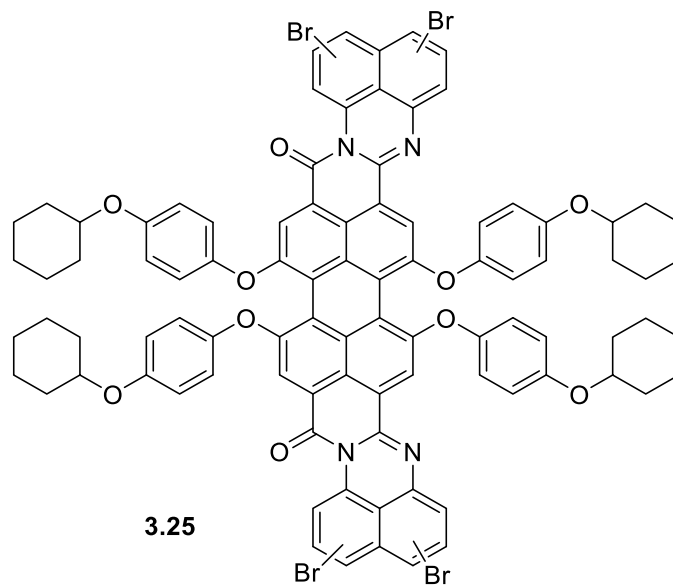
sin/anti

Methylene Chloride

λ_{abs}= 712 nm

λ_{em}= 768 nm

$\varepsilon = 59000$ cm^{-1} M^{-1}

Figure 25 Chemical structure of a NIR absorbing 1,6,7,12-tetrakis((hexyloxy)-phenoxy)-3,4,9,10-perylenetetracarboxdiimide dye with high solubility in organic solvents[74]

1.8.2 Core enlarged perylene dyes

Terrylene dyes contains three *peri* naphthalene units covalently fused to each other, they can be prepared by Suzuki coupling between 4-bromo naphthalene monoimide Compound **3.27** (Scheme 10) with perylene monoimide **3.26** (Scheme 10) and final dehydrogenation and coupling to form the extended rylene core **3.29**[76] (Scheme 10).
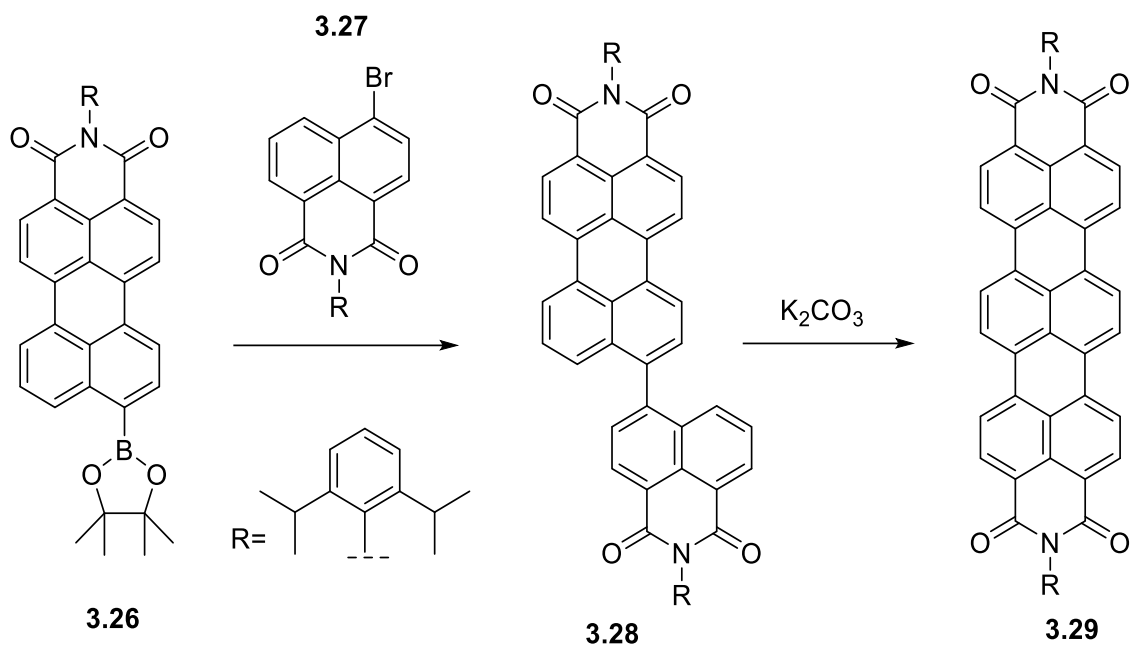
Scheme 10 Synthesis of terrylene bisimde dyes

Quaterrylene diimide dyes can be prepared by two coupling 9-bromo perylene monoimide **3.10** and further cyclodehydrogenation to give **3.31**[76] (Scheme 11).
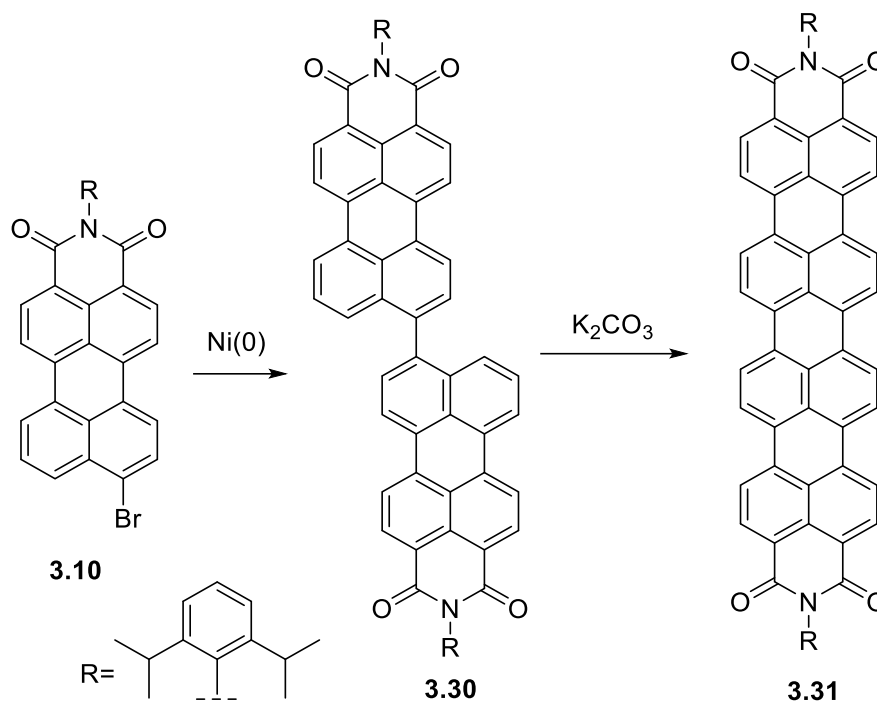
Scheme 11 Synthesis of quaterrylene diimide dyes

It has been found that by extending the rylene core by condensation of naphthalene units, it is possible to obtain bathochromic shifts to the NIR and very high extinction coefficients up to $300000 \text{ M}^{-1}\text{cm}^{-1}$(Figure 26)[76].
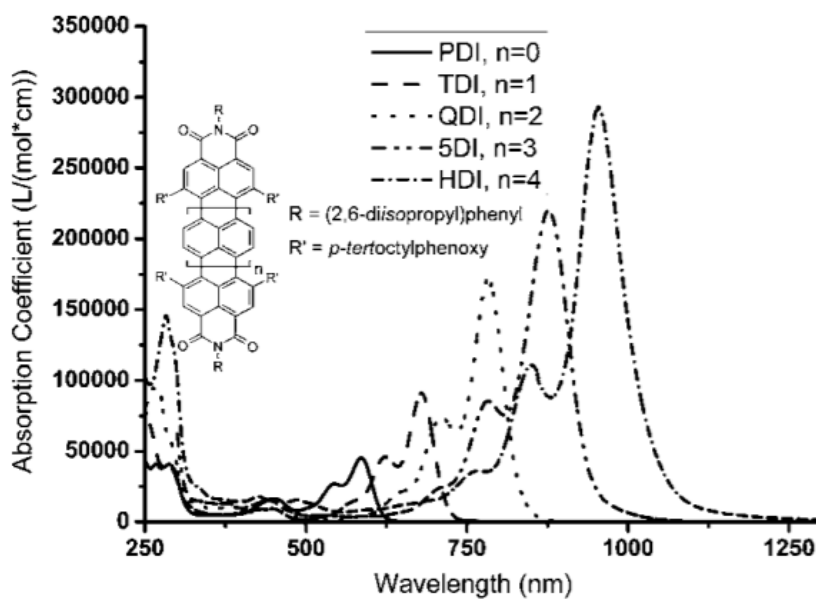
Figure 26 Extinction coefficients of core enlarged rylene dyes and bathochromic shift to the NIR[76]

1.9 Silicon rhodamine dyes as NIR active imaging reagents for *in vivo* applications

Silicon Rhodamines emerged as new NIR absorbing class of dyes after the discovery that the substitution of the oxygen atom with a silicon atom in the pyronine scaffold gave a bathochromic shift in the absorption and emission about 90 nm (Figure 27)[77]. This effect has been expanded to rhodamine derivatives giving a new series of chromophores active in the NIR (655 nm) with high extinction coefficients (64191 $M^{-1}cm^{-1}$) and quantum yield (31%) in water[77, 78] (Figure 28).
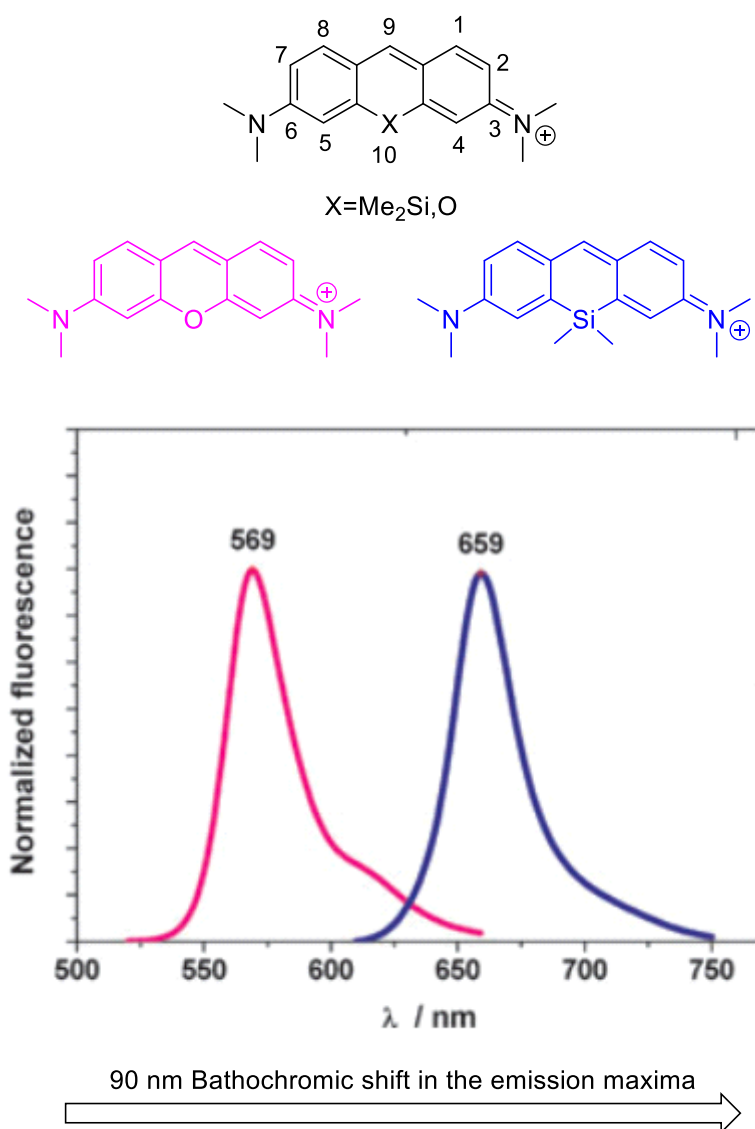
Figure 27 Numbering system of a pyronine scaffold (top) and effect of the substitution of the oxygen atom with the silicon atom in position 10th with relative bathochromic shift of 90 nm (bottom)[77].

To expand the applicability of silicon rhodamines, Koide et al. developed the first series of pH activatable silicon rhodamines with an intrinsic mechanism of fluorescence activation based on photo induced electron transfer[79]. As an example, Compound **4.22** is shown in Figure 28[79] its fluorescence activation threshold was tuned by a protonation-deprotonation equilibria on the aniline nitrogen installed on the phenyl ring (Figure 28) and was used to sense the acidity in mitochondria of Hela cells showing co staining with mito tracker green FM®[78].
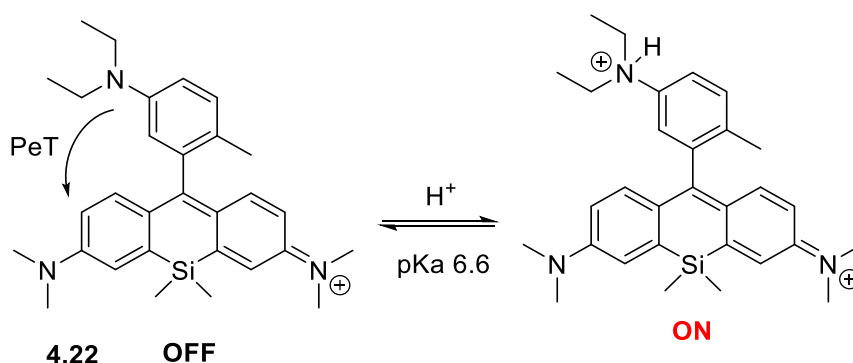

Figure 28 pH responsive silicon rhodamine dye based on photo induced electron transfer developed by Koide et al.[79]

A modified structural version SiR700 was proposed by Koide at al. SiR700 achieving an emission maximum at 700 nm (Compound **4.34**) (Figure 29)[80]. The installation of a succinimidyl ester on the phenyl ring in position 4' of **4.34** (Figure 29), was used to prepare a fluorescent conjugate with anti-tenascin-C-antibody to image extracellular matrix glycoprotein tenascin-C expressed in malignant gliomas. This work is the first example of use of silicon rhodamines *in vivo* for the imaging of solid tumours[81]. Nevertheless, to date, an activatable version of a silicon rhodamine dye has never been used for the preparation of macromolecular injectable conjugates for diagnostic purposes. The application and properties of activatable silicon rhodamine dyes will be further explained in chapter 4.

4.34
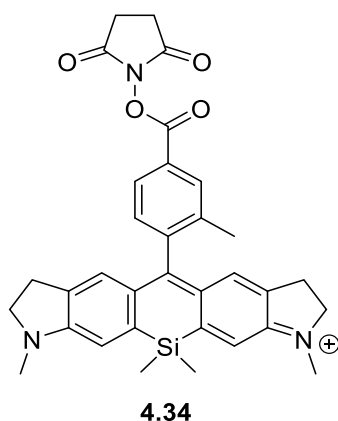
Figure 29 Chemical structure of SiR700 dye

1.10 From siloles and silyl antracenes to silicon rhodamine dyes

Siloles are chemical analogs of cyclopentadiene arising from the substitution of the tetrahedral carbon with a dimethyl silyl function. They are known in the literature for their high electron accepting properties due to their low lying LUMO level[82]. Comparison with cyclopentadiene electronic orbitals with *ab initio* calculations, show small difference of 0,4 eV in the HOMO energy and markedly higher difference for the LUMO levels for siloles reaching 1,3 eV. These phenomena are ascribed to the unique conjugation between the σ*-π* orbitals of the Si-C bond with the butadiene moiety respectively[82]. (Figure 30[83])
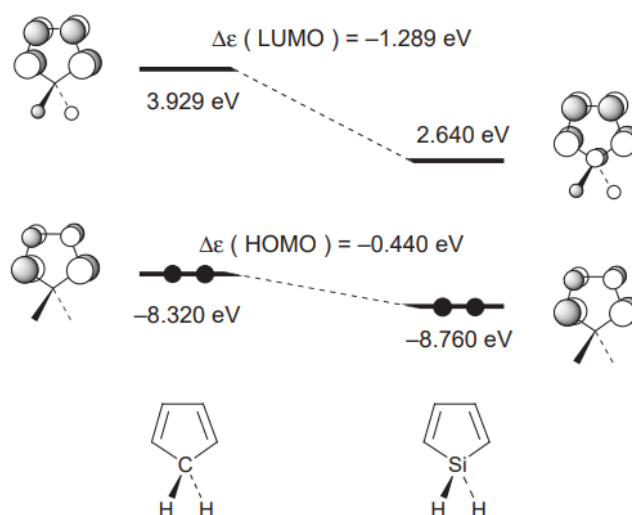
Figure 30 Comparison between the molecular orbitals (MO) of cyclopentadiene and siloles showing 1,2 eV difference in energy in the LUMO levels. Picture from the work of Yamaguchi et al.[83].

To study the effect of the silicon atom on anthracene-like systems, biphenyl methane compound **4.1** have been used in lithium halogen exchange reactions to install silicon functions with bulky substituents like 2,4,6-tris[bis(trimethylsilyl)methyl]phenyl (Tbt) (Scheme 12). Silyl anthracene **4.5** (Scheme 12) have absorption and emissions maxima at 270 nm and 550

nm respectively and is considered the first stable compound of this class of fluorophore at room temperature[84] (Scheme 12).
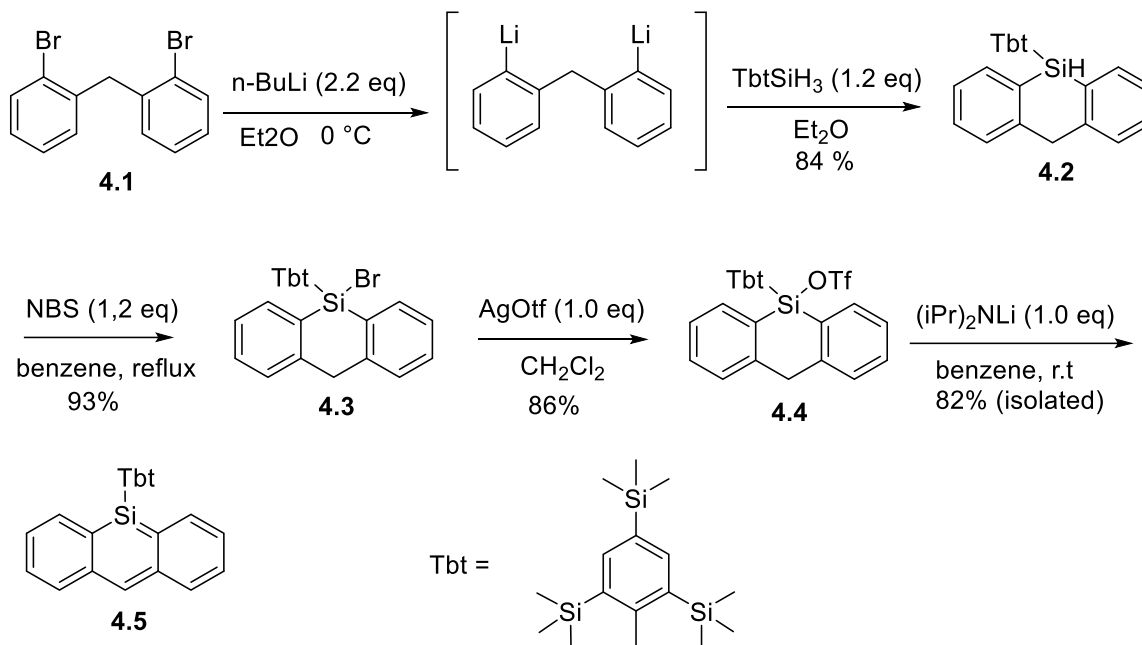
Scheme 12 Synthesis of silyl anthracene compound **4.5** with bulky substituents (Tbt) to improve the photostability of the fluorophore.

To exploit the potential of silyl anthracene compounds and expands the functional modifications on this scaffold, in 2009, Fu et al[77]. proposed the use of biphenylmethane **4.8** obtained from 3-bromo-N,N-dimethylaniline **4.7** in lithium halogen exchange conditions giving silicon pyronine **4.9** after dichloro dicyano quinone (DDQ) oxidation in methanol[77] (Scheme 13).
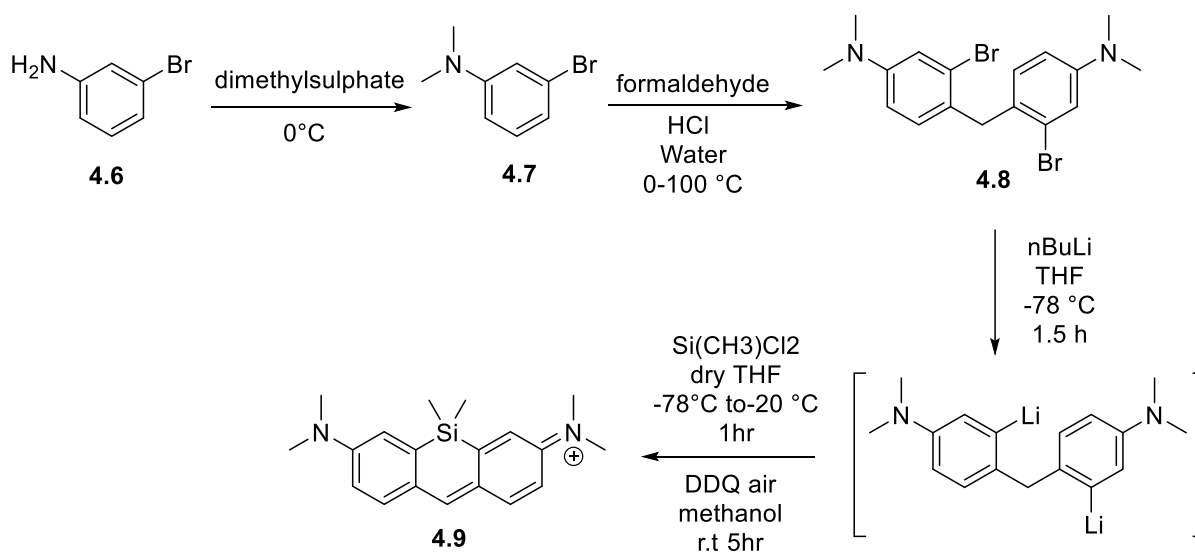
Scheme 13 Synthesis of Silicon pyronine **4.9** from a biphenyl methane compound **4.8**

Compound **4.9** (Scheme 13) exhibits a large bathochromic shift in the emission maxima of 90 nm in respect to the commercially available pyronine (PY), it is stable at room temperature and soluble in water with emission in the NIR (653 nm) in high quantum yield 18% (QY). These findings indicate that the silicon atom substitution dramatically improves the optical properties of the fluorophore not only in terms of red shifted absorption but also in terms of extinction coefficients, quantum yield and solubility in both organic solvents and water[77] (Figure 27). The discovery leads the foundations for the development of novel water-soluble fluorophores active in the NIR for biological imaging applications. In 2011, the group of Tetsuo Nagano proposed the first series of Silicon rhodamine compounds through the installation of a phenyl ring on position 9 of pyronine scaffold **4.9**[85]. A series of 12 water soluble silicon rhodamines were obtained with fluorescence emission in the NIR (660 nm) in high QY (31% in water). The proposed synthesis shows, as a key step, the oxidation of **4.9** (Scheme 14) with potassium cyanide in water in presence of ferric chloride giving silicon xanthone compound **4.10** in low yield (35%) (Scheme 14). Other oxidation process of the same scaffold can be performed by the method of Pastierik et al.[86] with $KMnO_4$ in acetone in comparable reaction yields (30%)[87].

$X=Me_2Si,O$

i) KCN/H2O reflux
ii) $FeCl_3$ 2N HCl aq.
iii) $NaHCO_3/H_2O$ reflux

35%

4.9

4.10
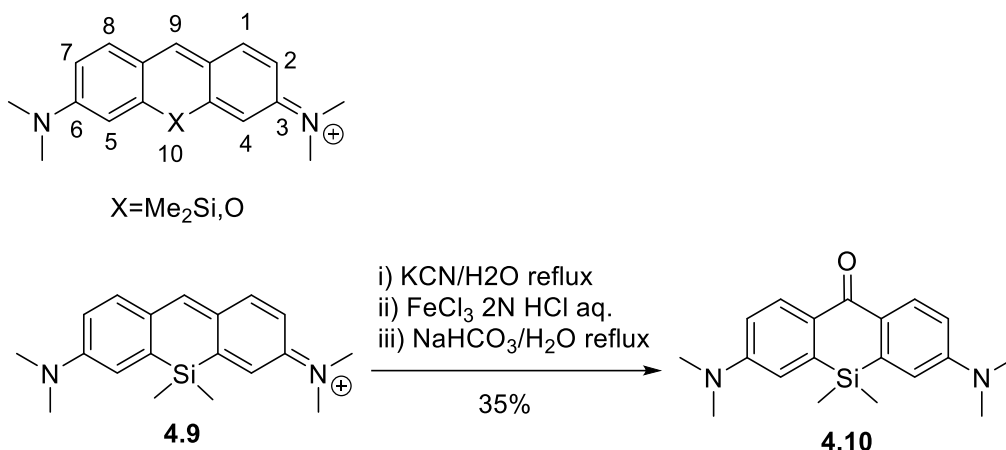
Scheme 14 Oxidation of Silicon Pyronine **4.9** on position 9

4.10 represents an important building block for the synthesis of silicon rhodamine scaffolds[85] Its synthesis represents anyway a strong limiting factor due to low reaction yield and to the use of toxic oxidizing reagents (Scheme 14). To overcome these disadvantages, the use biphenyl silanes **4.13** were first proposed by Lavis et al. for the synthesis of carboxy silicon rhodamines[88] and further expanded by Hell group for the synthesis of silicon xanthones. In the work of Butkevich et al., for example, Compound **4.13** was treated with NBS (2 equivalents) in acetonitrile to give selective bromination para to the N,N dimethyl amino functions giving

4.14[89] (Scheme 15). Further lithium halogen exchange with tert-Butyl lithium in dry THF and quenching with dimethyl carbamyl chloride gave **4.10** in high yield (83%)[90] (Scheme 15).
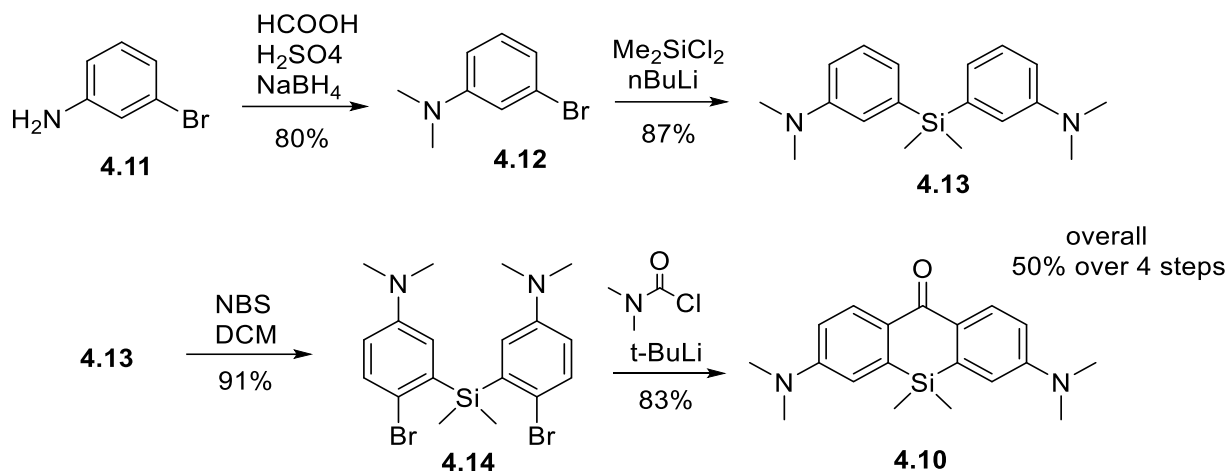
Scheme 15 Alternative route for the synthesis of silicon xanthones from biphenyl silane Compound **4.13**

The addition of phenyl lithium compounds to the carbon-oxygen double bond of **4.10**, can be performed starting from the *in situ* generation of aryl lithium nucleophiles from N,N-dialkyl-bromoanilines bearing substituents in position 1, 4 (Scheme 16). Between them, lithium-halogen exchange on Compounds **4.15** and **4.16** (Scheme 16) is taken an example from the work of Koide et al[79]. When a N,N-dialkyl-bromoaniline is treated with a lithium reagent like n-BuLi sec-BuLi or tert-BuLi, a phenyl lithiun nucleophile is formed *in situ*. Further addition on silicon xanthone Compound **4.10**, give silicon rhodamines **4.17** and **4.18** (Scheme 16). These compounds present a lack of fluorescence emission in basic media. This effect, was ascribed to the low value of the oxidation potential due to the presence of an electron rich aniline system (0.65-0.66 eV)[79] and to the high reduction potential (-0.62 eV). The two parameters taken together with the small separation in the zero-zero transition to the lowest excited singlet state $\Delta E_{0\text{-}0}$ (1.90 eV), gave a favorable value for the photo induced electron transfer to occur spontaneously in basic media[79]. The Rehm-Weller equation $\Delta G_{PeT} = E(D^+/D)$-$E(A/A^-)$-$\Delta E_{0\text{-}0}$-C. $E(D^+/D)$ (Scheme 16) describes the energetics of PeT processes. $E(A/A^-)$ represents the one electron reduction potential of the silicon rhodamine scaffold (Scheme 16) $E(D^+/D)$, the oxidation potential of the phenyl ring installed on position 9 that act as a quencher and the C term is the work term needed for the charge separation[79](Scheme 16). For silicon rhodamine compounds bearing N,N dialky amino substituents on the phenyl ring, ΔG_{PeT} gives a negative value thus allowing PeT process to occur[85] (Scheme 16).
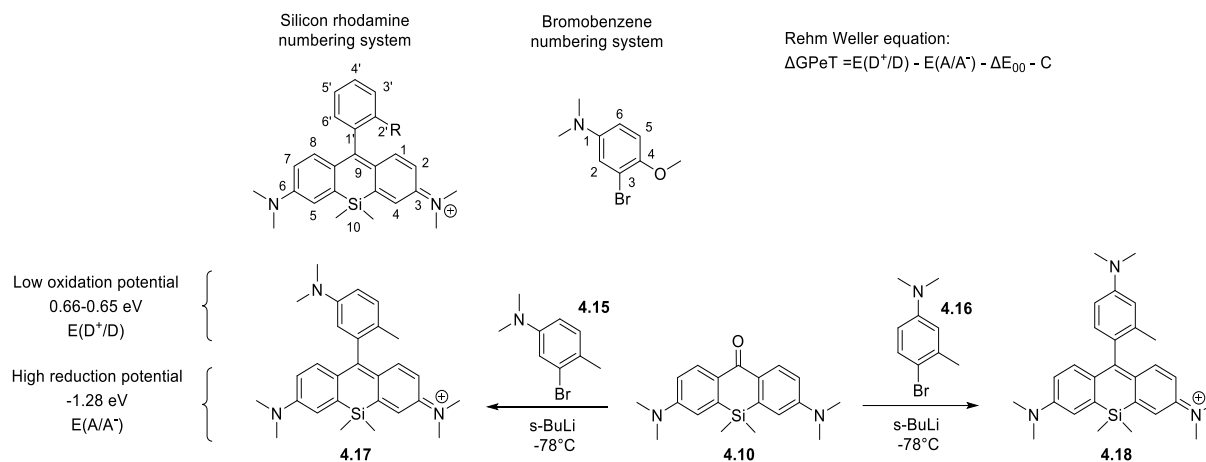
Scheme 16 Silicon rhodamine and bromobenzene numbering systems and Rehm Weller equation describing the energetics of photo induced electron transfer processes (Top). Phenyl lithium addition on silicon xanthone compound **4.10** giving pH responsive silicon rhodamines **4.17** and **4.18** (bottom). Values of oxidation potential and reduction potential are reproduced from the work of Koide et al.[79] (bottom left).

Silicon rhodamines **4.17** and **4.18** restore their fluorescence emission under aqueous acidic conditions. Their pKa can be efficiently modulated varying the length of the alkyl chain on the aniline nitrogen on position 5'(Scheme 16). This strategy has been used to fine tune the fluorescence activation threshold of Compound **4.17**[85] (Scheme 17). The use of N,N diethyl amino function, for example, greatly enhance the pKa of the fluorophore **4.22** reaching the value of 6.6 (Scheme 17).
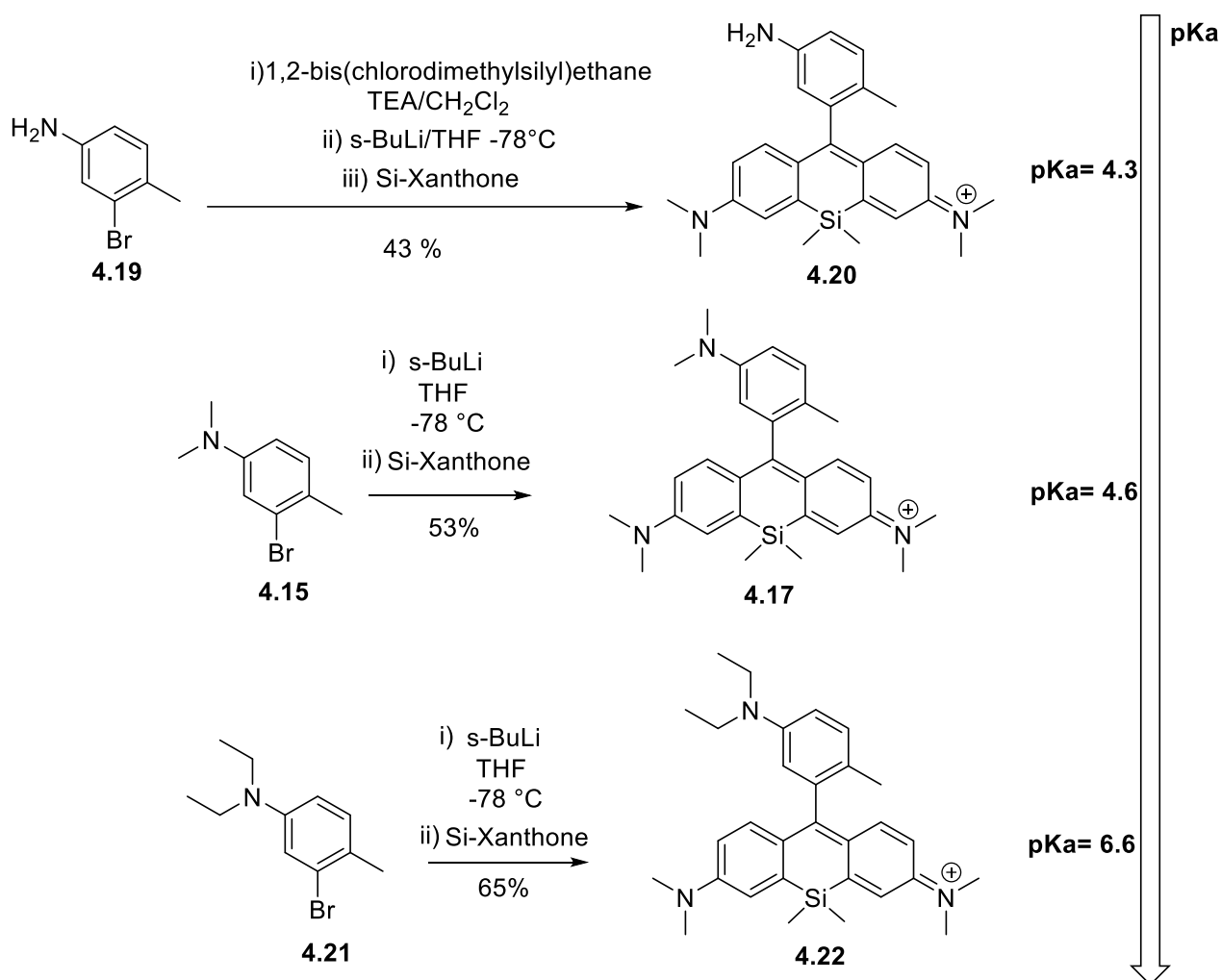
Scheme 17 Effect of the alkyl chain length installed as N,N dialkyl aniline substituents on the pKa of silicon rhodamine scaffolds Compound **4.20**, **4.17** and **4.22**[79].

Probes with a pKa value close to physiological range, have a unique advantage as they present an activation threshold suitable for cellular internalization imaging studies. pH activatable probes can also be used in conjugation with vector molecules like antibodies and short peptide sequences to target overexpressed receptors in cancer cells[49]. The time required for the fluorescent activation, is strictly dependent on the stage of probe internalization (Figure 31). In early endosome, the pH value is close to 6.9 following maturation and fusion with lysosomes where pH, reaches the value of 4[91, 92] (Figure 31).When the pKa value of the probe is not sufficiently high, the fluorescent spot require more time to appear (4 hours) in respect to probes with a value suitable to sense the early endosomal environment[49]. FGS, requires activatable probes that can give a fluorescence signal rapidly after few hours upon intravenous injection[3, 49].It is therefore highly desirable to design PeT quenchers based on the silicon rhodamine scaffolds with a pKa range close to the physiological range giving a suitable fluorescence response in early endosomes (Figure 31).
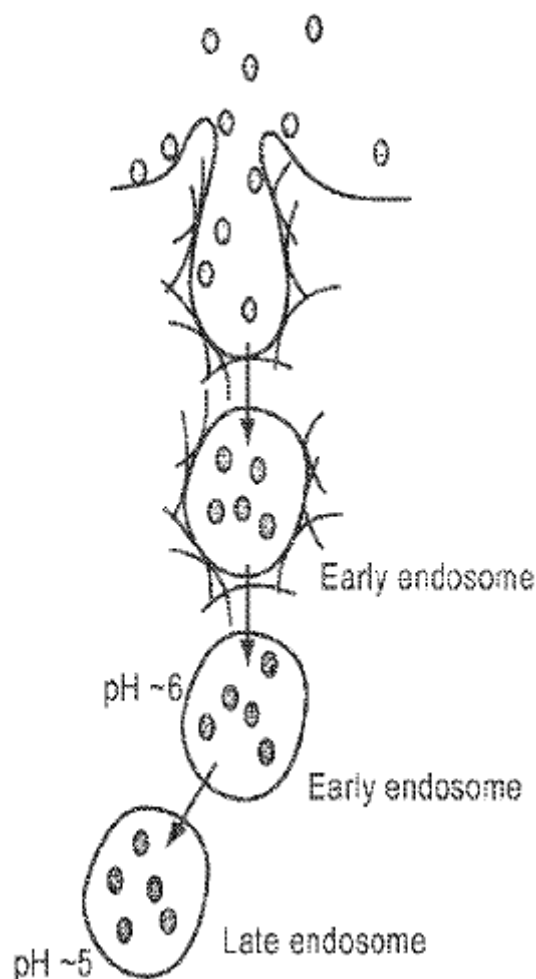
Figure 31 Internalization process of macromolecules in eukaryotic cells showing the process of endosome maturation with the associated pH value.

The fluorescence activation response and sensing properties of a rhodamine dye are associated with its pKa value. A pKa value is related to chemical structural effects due to the specific spatial arrangements of substituents installed on the aniline function on the phenyl ring (Figure 32; Figure 33). When the phenyl ring installed on position 9 of the rhodamine scaffold present two N,N dialkyl aniline functions ortho to each other, the pKa value achieve a value close to 7.0-7.4 due to the unique strain restricted arrangement of N,N dialkyl substituents (Figure 32; Figure 33). It is well known that ortho substituents installed on N,N dialkyl anilines, twist the non-bonding electrons out of the conjugation thus increasing their basicity, this effect is known under the name of "secondary steric effect"[93-95]. When the ortho substituent is another N,N dialkyl amino substituent, additional stabilization due to hydrogen bonding on the strain restricted monoprotonation site, enhance the basicity of the compound. Depending on the entity of the secondary steric effect, pKa value can be close to the physiological range (7.0-7.4) (Figure 32). Aromatic systems like **4.24** (Figure 32) are known as "proton sponges"[96]. The

pKa values of aniline proton sponges have been measured in water: ethanol (20%) mixtures. Compound **4.23** (Figure 32) for example, bears alkyl substituents on the ortho position twisting the N,N diethyl aniline function achieving a value close to 5.15, while **4.24** reaches the highest value of 6.19 due to additional stabilization by hydrogen bond formation[96] (Figure 32).
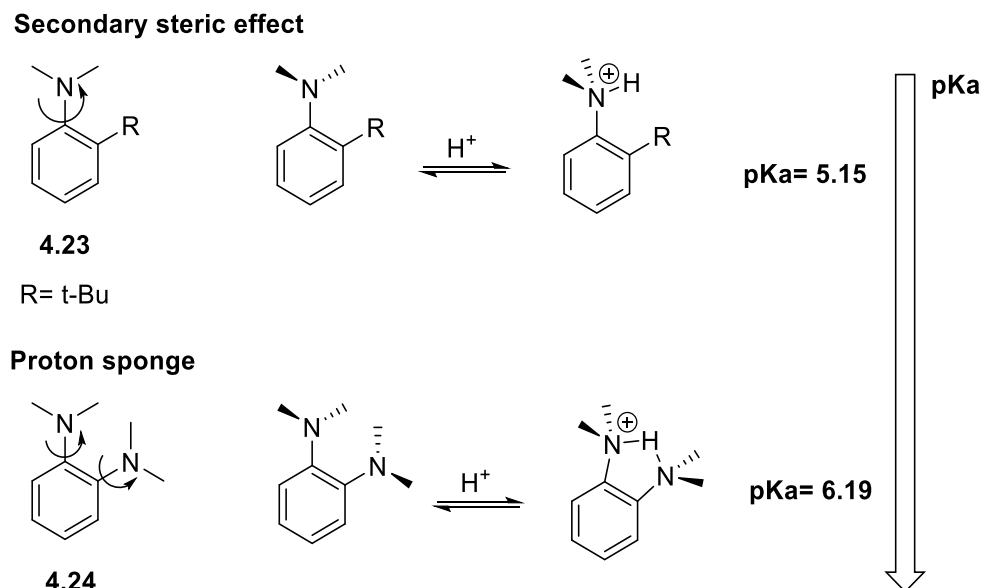
Figure 32 Secondary steric effect on simple aniline systems giving high pKa value in water: ethanol (20%) media (top). An example of proton sponge system installed on a benzene unit Compound **4.24** achieving pKa value 6.19 close to the physiological range.

The use of proton sponges as fluorescence quencher moieties installed on a rhodamine scaffold lies at the basis of the pH rodo® series patented by Invitrogen Corp.® (Figure 33).
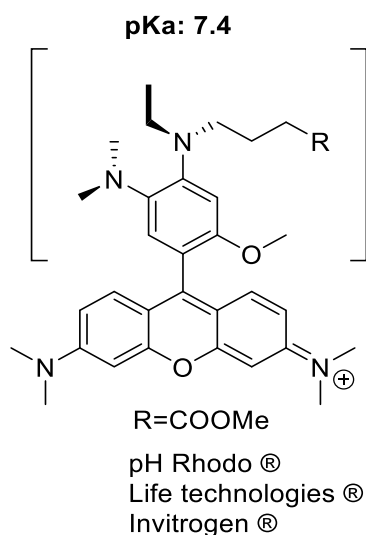
Figure 33 Chemical structure of pHrodo® fluorophore and spatial arrangement of substituents on the aniline nitrogen giving the proton sponge system responsible for the fluorophore pKa 7.0-7.4 value in the physiological range.

The unique arrangement of the substituents on the phenyl ring of pHrodo®, not only allow the fluorophore to have a fluorescence threshold in the range of 7.0-7.4 but also a linker to label tumor targeting vector macromolecules. This approach will be applied on silicon rhodamine systems and further expanded in Chapter 4.

Chapter 2-Motivation and objectives

Water soluble NIR absorbing agents are powerful tools in the hand of the surgeon to image physiological mechanisms and to shed light on anatomical structures otherwise difficult to discern by visual palpation like nerves, bile ducts and ureters. Commercially available devices that detect NIR light from exogenous contrasts have been developed by companies like Frangioni Laboratory® Fluoptics® and Quest Medical Imaging® [29]. The need to image more than one chemical probe simultaneously in the same operational setup lies at the basis of the so called dual-channel imaging systems[97]. Complementary fluorescent readouts in the same operational setting are routinely used as multi wavelength fluorescence guidance technologies for precision surgery to improve tissue specific resections[97]. For example, dual channel imagers are widely used in reconstructive surgery to assess anastomosis quality and to detect perioperative graft occlusions. This imaging technique is useful in coronary artery bypass grafting (CABG) surgery[98]. Tanaka et al., for example, described a clinically relevant study on coronary arteriography and myocardial perfusions demonstrating that NIR light can be used intraoperatively in real time improving graft patency assessment thus reducing the risk of early graft failure in patients[98]. On the other hand, Wada et al., used a dual channel NIR imager to expand the use of cyanine and phenothiazine dyes in gastrointestinal surgeries of patients with an high risk of pancreatic injuries. These includes colectomy splenectomy and urologic surgeries like nephrectomy and adrenalectomy[99]. Multi wavelength fluorescence imaging is also applied in ophthalmology for the study and diagnosis of retinal and choroidal disorders. In this specific case ICG green and fluorescein sodium are used as contrasts[100]. One of the most important criteria in the choice of a contrast agent is the emission wavelength that should be close to 700 nm or 800 nm where most of the commercially available devices are designed to collect NIR photons. NIR light is then processed through photon collecting devices called NIR channels[99] (Figure 34). It is important to note that most of the dyes like FDA approved ICG green and Methylene Blue (MB) used in clinical settings are designed to have an emission as close as possible to this photon energy value. As it is summarized in the work of Van et al.[97], an imager can collect photons from different class of dyes thus enhancing the versatility of the technique and expanding the synthetic challenges for the preparation of novel water soluble biocompatible NIR active contrasts.
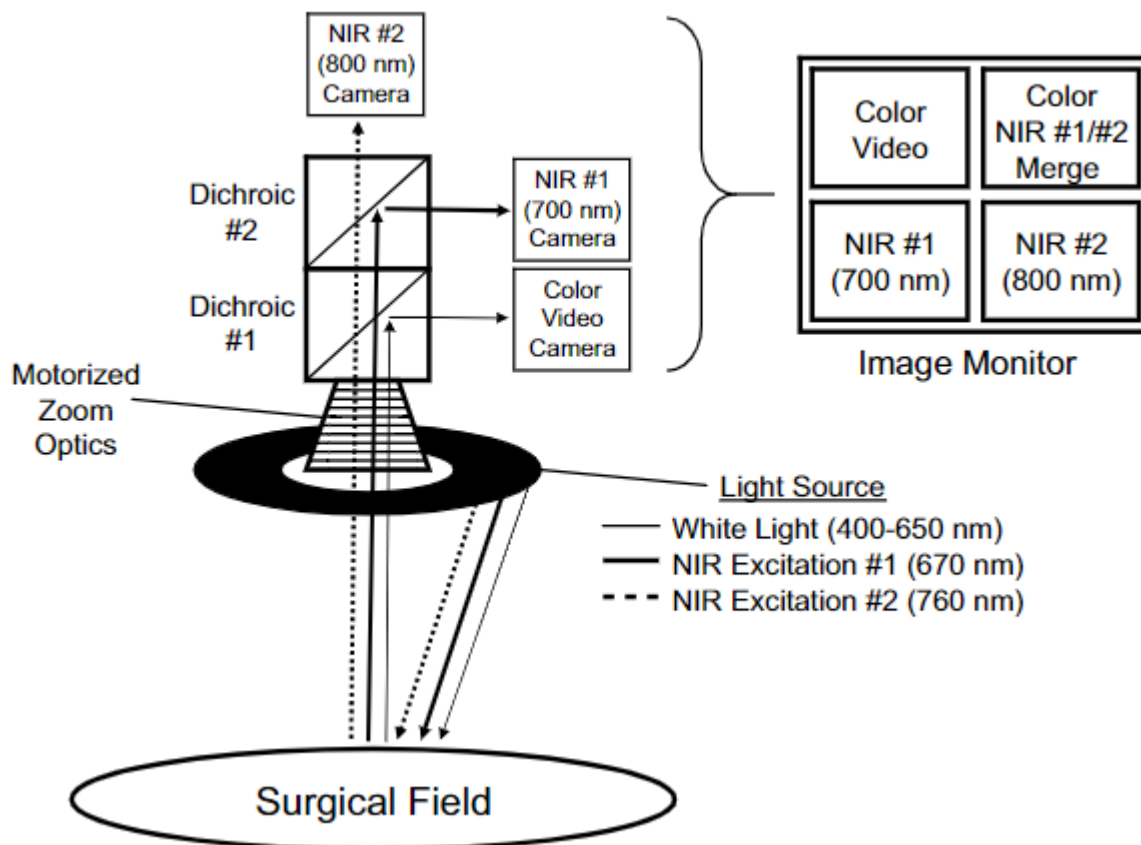
Figure 34 Dual channel imager schematic of the imaging system showing the light pathways of the excitation light source and the detection of the emitted light from commercially available fluorophores like methylene blue and ICG green. Taken from the work of Tanaka et al.

Between the contrast used in the clinics, ICG green is the most used and FDA approved with an emission maximum at 820 nm, nevertheless, ICG presents several drawbacks like aggregation phenomena in water, and poor photostability that limit its applications in clinical settings. The development of new cyanine dyes like IRDye800CW® from LiCOR®, also present limitations associated with poor photostability due to the central ether bond that is responsible for the rapid degradation of the fluorophore under prolonged irradiation conditions[47, 99] (section 1.4.1). On the other hand, the only one FDA approved contrast used in the clinics active on the 700 nm channel, is methylene blue (MB) (Chapter 1.3). MB emits at 680-690 nm in water is a cationic dye and its use is associated with the formation of toxic leucomethylene blue form especially with patients with known glucose-6-phosphate dehydrogenase (G6PD) deficiency[101]. Its photophysical properties are summarized by Sikka et al.[101] and Tanaka et al.[98] (Figure 35).

Figure 35 Absorption and emission profile of methylene blue MB in water from the work of Tanaka et al.

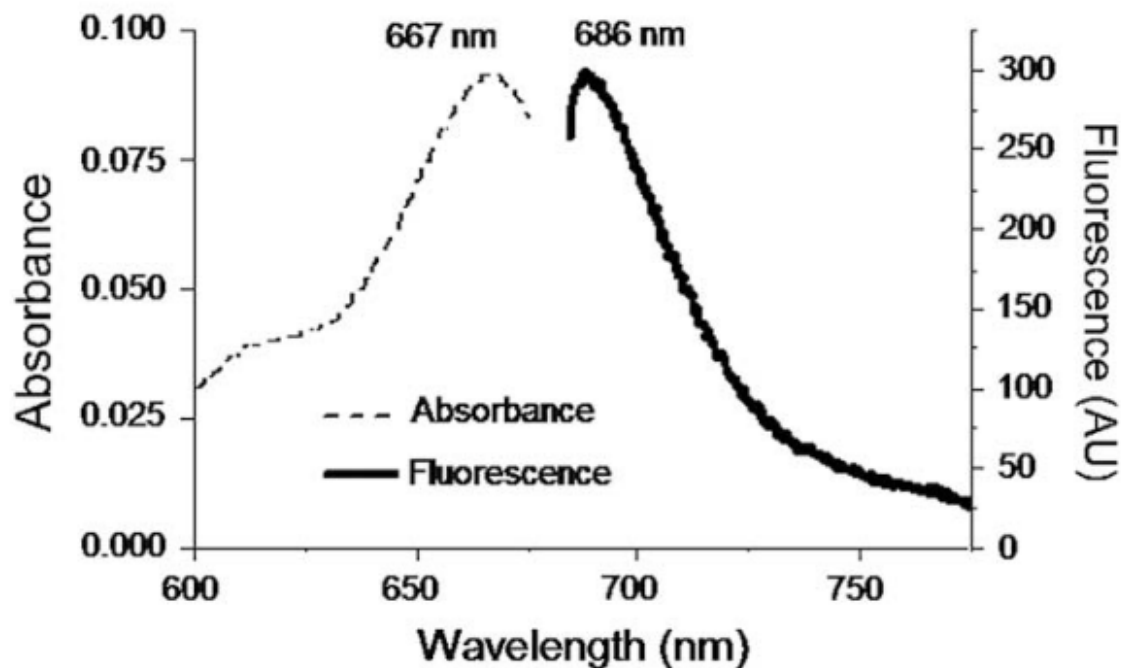To overcome the limitation of FDA approved contrasts used in operational rooms, I worked on NIR absorbing fluorophores belonging to two different class of dyes, perylene and silicon rhodamines, active on the commonly used NIR channels of commercially available devices (Figure 34). Push-pull Perylene dyes, are designed to be compatible with Quest medical imaging® imager and may find possible implications as valid alternatives of FDA approved indocyanine green. The chromophore possess improved photostability, large Stokes shift (130 nm) and emission maxima in the NIR up to 770 nm. On the other hand, the Silicon rhodamine probe I developed, is designed to be active in a shorter wavelength range (Figure 36). The proposed chemical structure is a modified version of the commercially available pHrodo® (Figure 17) described in section 1.10. The substitution of the oxygen atom with a dimethyl silyl function gave a substantial bathochromic shift of 90 nm in the emission maxima reaching the value of 675 nm exceptionally close to the emission wavelength of Methylene Blue (MB) in water[98](Figure 35). The emission close to the far red represents a valuable improvement in respect to the commercially available analog pHrodo® to image in higher penetration depth in tissues while, keeping the same advantages of being an activatable probe. Probe activatability is mediated by the pH of the media and it occurs through photoinduced electron transfer mediated by protonation deprotonation equilibria of proton sponge moieties installed on the phenyl ring on position 9 of the rhodamine scaffold. In particular, the specific spatial arrangements of the substitutents gave a significant shift in the pKa value reaching the

physiological range (7.4). In addition, the fluorophore showed the ability to form H-dimers in concentrated aqueous solutions. This property may be used to enhance the quenching ability of dye pairs in concentrated aqueous solution and, as future perspective, for the preparation of macromolecular probes with dual quenching modality like those described in the work of Ogawa et al.[57] To continue the studies on pH responsive silicon rhodamine dyes I also installed an allyl functional group for UV mediated click thiol-ene coupling toward site-specific labelling of cysteine containing peptides and antibodies (Figure 36) this function will be considered in future perspectives described in chapter 5.
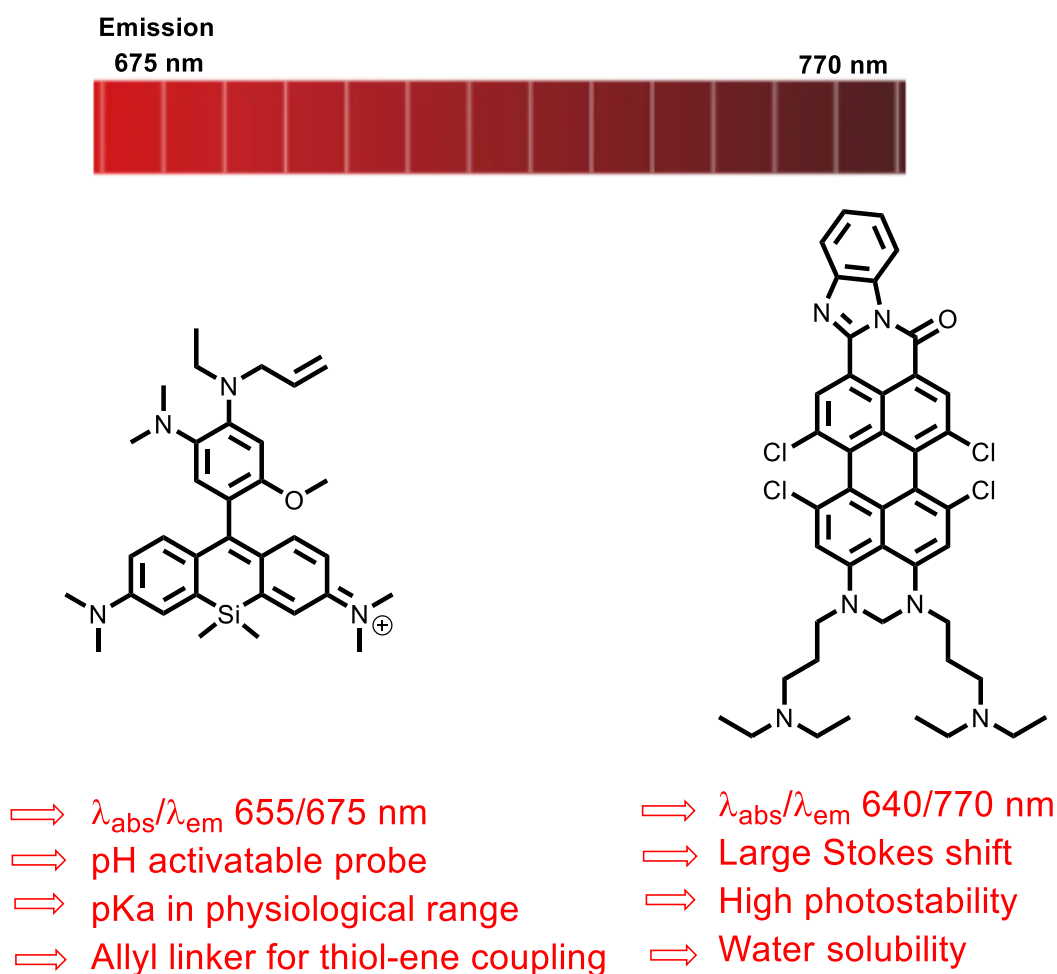
Figure 36 Two class of dyes, perylene (left) and silicon rhodamines (right) matching the two imaging emission maxima detectable by the common NIR imaging devices.

In the context of my dissertation, the research on perylene monoimides is provided giving insight on the preparation of NIR absorbing dyes as optical contrast agents for applications in fluorescence guide surgery[73] (Chapter 3). In Chapter 4 I will focus on pH responsive silicon rhodamine dye analog of the commercially available pHrodo®. It will follow the optical characterization of the dye showing the determination of the pKa value in physiological range

(7.4) and the study on the formation of H-dimers in concentrated aqueous solutions. Chapter 5 and 6 will describe the summary and the experimental part of my work respectively, including materials and methods.

Chapter 3-Preparation of alkylamine perylene monoimide dyes

Perylene monoimides are important building blocks for the preparation of water soluble NIR absorbing fluorophores. To achieve NIR emission, primary alkylamines as donor substituents and a benzimidazole function as an acceptor group has been installed on the *peri* positions of the perylene core (Figure **37**). This modification gave access to a new series of fluorophores with emission in the NIR up to 770 nm. To improve the photophysical properties of the fluorophore, the nitrogen atoms on the peri position were modified in form of chemical bridge. In particular, aminal and urea functions has been selected as chemical protective group (Figure 37). The chemical bridge between the *peri* nitrogen improved the fluorophore Stokes shift (130 nm), quantum yield and photostability upon prolonged irradiation conditions in water. The resulting chromophores are also highly soluble in water.
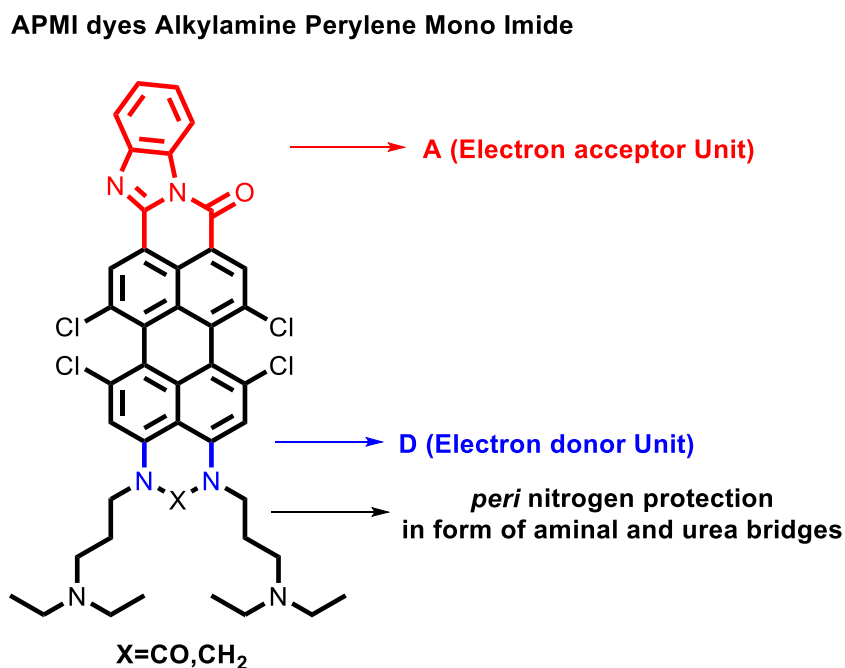
Figure 37 Schematic picture showing the chemical structure of APMI dyes Alkylamine Perylene Mono Imides. The benzimidazole acceptor group is shown in red; the donor groups are shown in blue.

The chromophores have been named alkylamine perylene monoimide (APMI) dyes, for simplicity, and their staining properties have been investigated in live cell imaging setups. The dyes resulted nontoxic, cell permeable and showed the ability to concentrate in intracellular compartments like cell nucleus, endoplasmic reticulum, and cell membrane. This property was

exploited to label therapeutic CD+ macrophages to be used in longitudinal imaging studies in mice. At the same time, I continued to explore the applicability of APMI dyes *in vivo* by direct infusion in rats. In particular, an ultrabright angiography of the mesenteric vessels followed by hepatic excretion of the chromophore through the bile has been observed. To conclude the studies on APMI dyes, their potential role as novel contrast agents in photoacoustic imaging have also been evaluated. For this purpose, I demonstrated that the chromophores absorb pulse NIR light and release a photoacoustic signal making them useful candidates to be used in commercially available devices like LAZR-X® Vevo Visualsonics from Fujifilm®. The data provided in the next paragraphs aim to present APMI dyes as good candidates for *in vivo* applications in FGS especially those that make use of NIR imaging technologies to track post transferred therapeutic immune cells for cancer immunotherapies or to improve fluorescence image assisted surgeries.

3.3.1 Synthesis of perylene 9,10-dibromo perylene amidine compounds

Compound **3.17** (Scheme **18**) was obtained according to the procedures described by Zagranyarski et al. (Scheme **6**) and was used as starting material for further imidization with ortho diamino arenes to perform the installation of a benzimidazole subunit as electron acceptor unit. (Scheme 18).
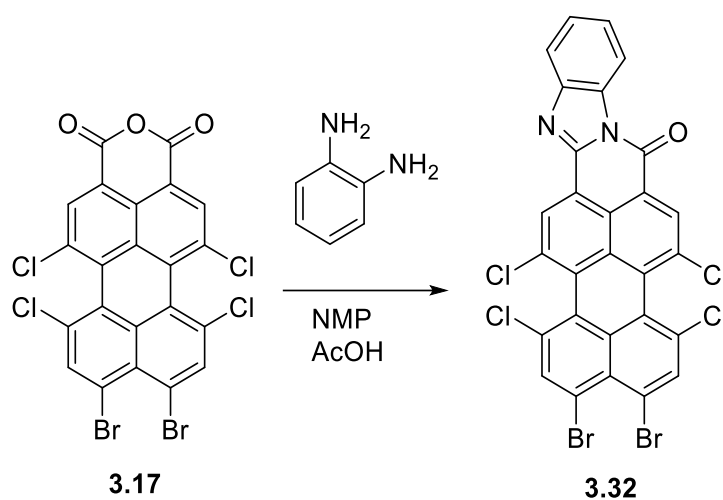
Scheme 18 Synthesis of perylene monoimide compound **3.32** from perylene monoanhydride **3.17** in presence of ortho diamino benzene in NMP and acetic acid.

The imidization reaction was carried out in presence of ortho diaminobenzene in NMP/AcOH (1:1) stirred and heated at 140 °C for 24 h affording the desired product **3.32** in 80% yield. The material was obtained as a precipitate solid and characterized by high resolution mass spectrometry (HRMS) (Figure 38).
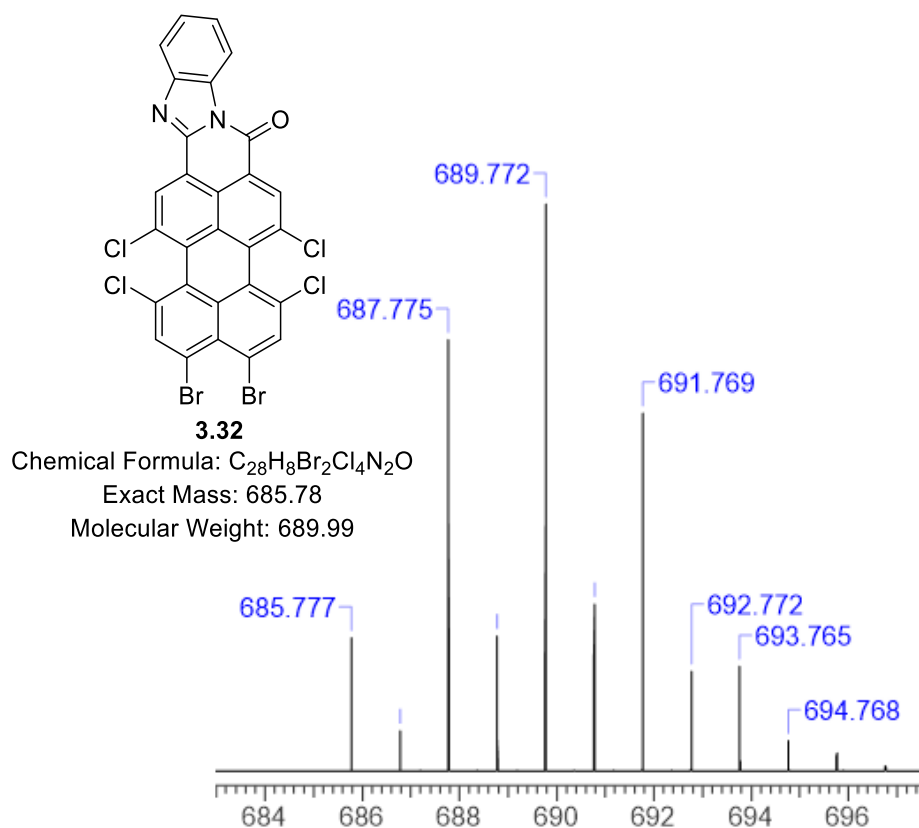
Figure 38 ESI-HRMS mass spectrum of **3.32** 689.772 [M+]

Further characterization of **3.32** by NMR spectroscopy was not possible due to poor solubility in organic solvents. **3.32**, was used without purification in the next step (Scheme 19), dissolved in NMP treated with TEA and 3-(N,N-diethylamino) propylamine at 110 °C for 1,5 hours giving **3.33** in 32 % yield. The material was obtained as a dark blue powder (Scheme 19).
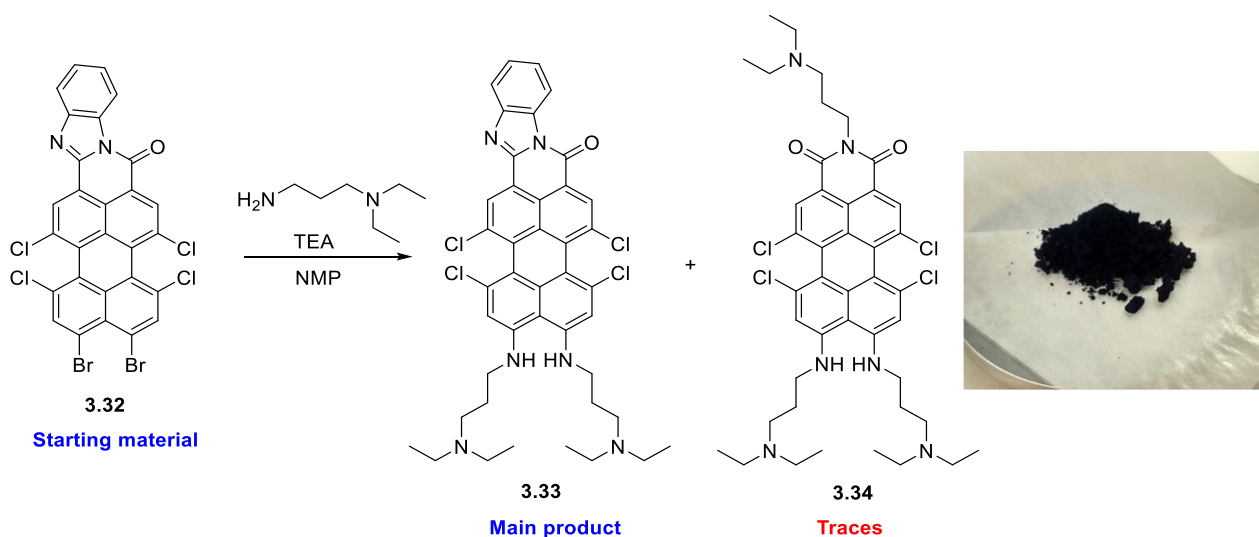
Scheme 19 Installation of donor groups (primary alkyl amines) in the peri positions of the perylene monoimide **3.32** giving **3.33** (main product) and **3.34** (side product)

Analysis of the raw material from the reaction mixture was performed by reverse phase ultra-high-performance liquid chromatography coupled with high resolution mass spectrometry (RP-HPLC-MS) showing the presence of two peaks with different retention time belonging to **3.33** (5.4 minutes) (Figure 39) and **3.34** (3.8 minutes) (Figure 41). Compound **3.33** has been characterized by NMR spectroscopy (Figure 40). Compound **3.34** was investigated with RP-HPLC-MS (Figure 41) and by ^{1}H NMR spectroscopy (Figure 42). In particular, ^{1}H peaks at 8.01 and 6.79 ppm were visible and were assigned to the protons installed on the ortho position of the perylene core (Signal g, f in Figure 42). On the other and, also the signal from the methylene (CH_2) in alpha position from the imide nitrogen was found at 4.12 ppm (Figure 42).

Figure 39 RP-HPLC chromathogram showing retention time of **3.33** at 5.4 minutes (top), the absorbption profile (bottom left) and ESI-HRMS spectrum of **3.33 (**789.219 [M⁺]) (bottom right)
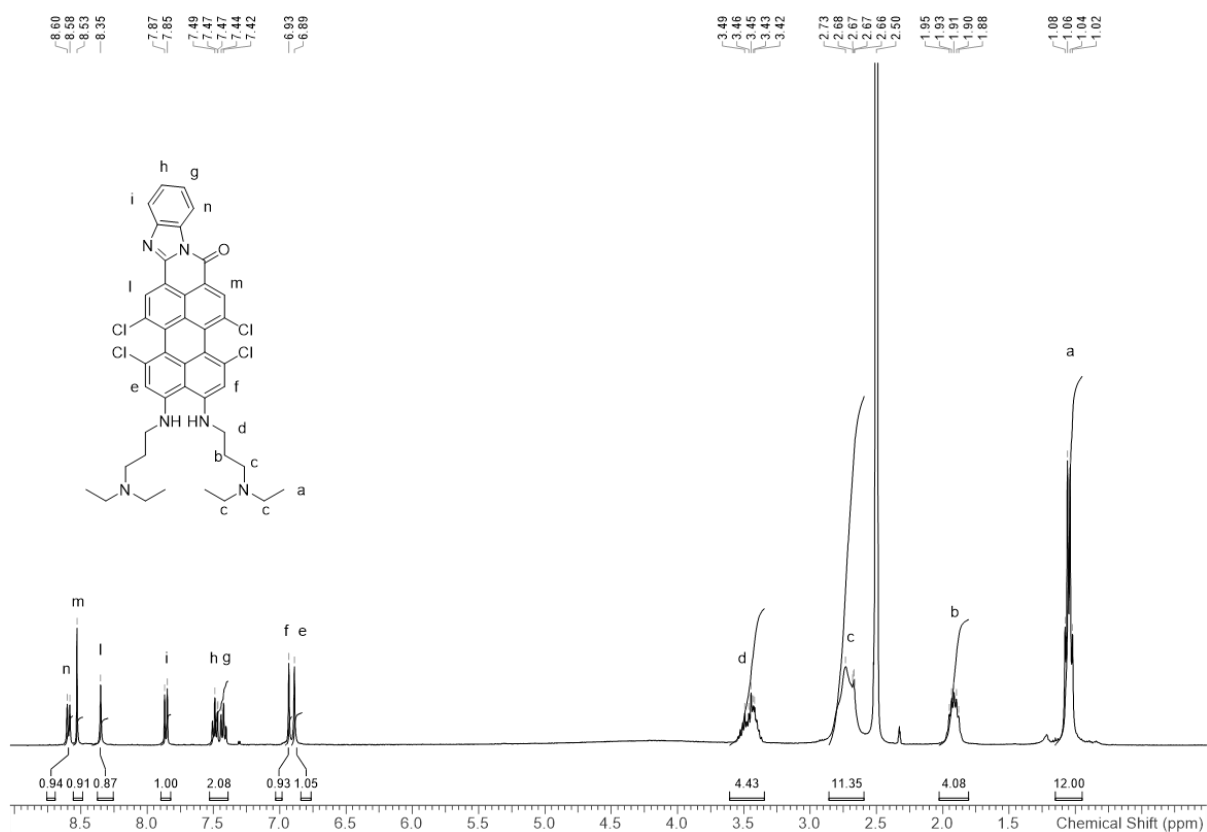
Figure 40 ¹H-NMR spectrum of **3.33** in DMSO-d6 at room temperature (300 MHz)
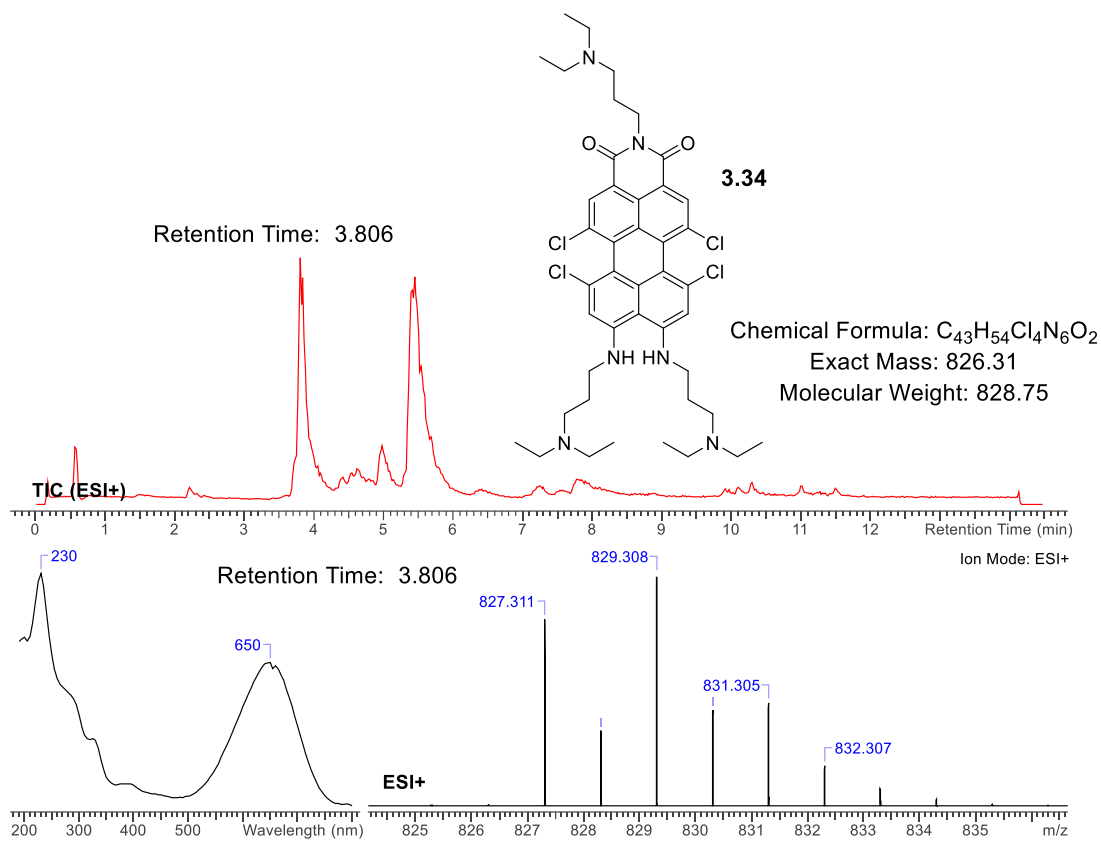
Figure 41 RP-HPLC-MS chromatogram showing retention time of **3.34** at 3.8 minutes (Top) the absorption profile (Bottom left) and high resolution mass isotopic pattern (Bottom right).
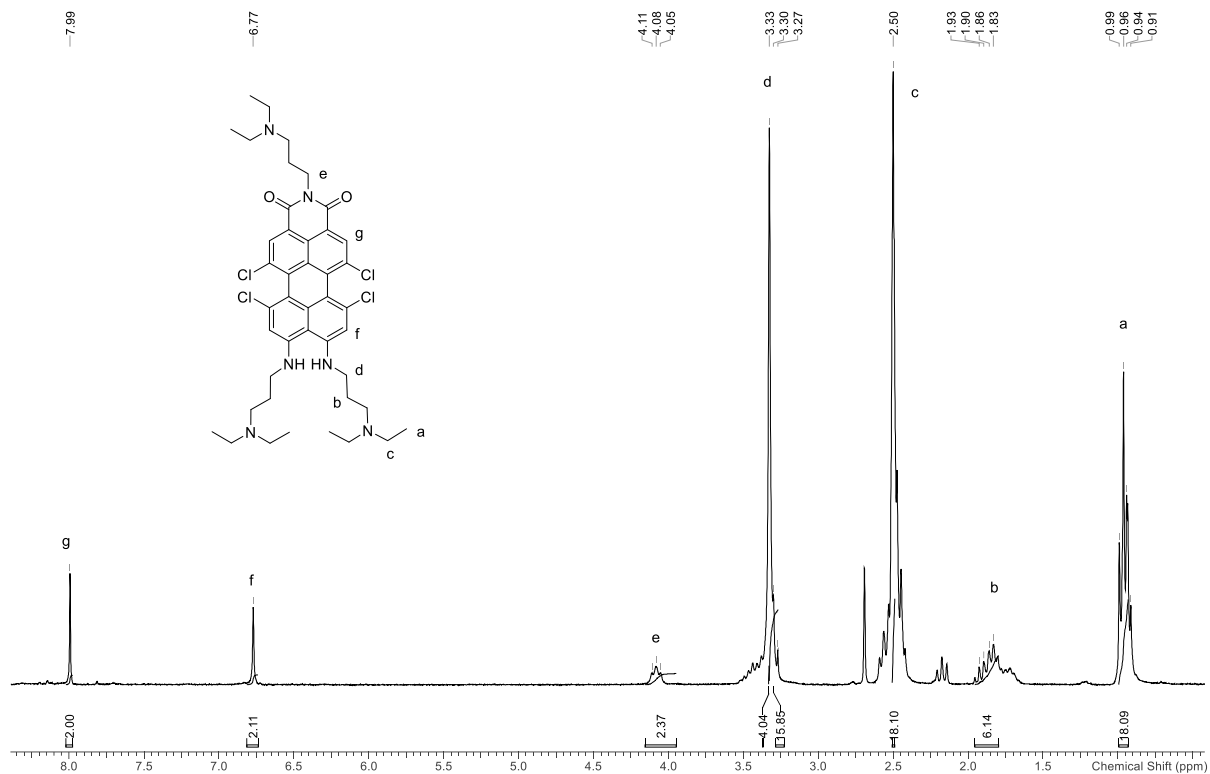
Figure 42 ^{1}H NMR spectrum of **3.34** in DMSO-d6 at room temperature (300 MHz)

Compounds **3.33** and **3.34** can be separated by column chromatography on silica gel using dichloromethane (DCM) and Triethylamine (TEA) 9,5:0,5 as mobile phase. **3.33** was further purified by precipitation in water and obtained as a solid from a saturated aqueous solution of sodium bicarbonate. The RP-HPLC profile shows a single peak chromatogram indicating that compound **3.33** has been obtained in pure form (Figure 43). **3.33** is soluble in water and possess the typical absorption profile of a push-pull dye with a broad absorption band at 660 nm with emission in the NIR (780 nm) in water (Figure 44) (Table 1).
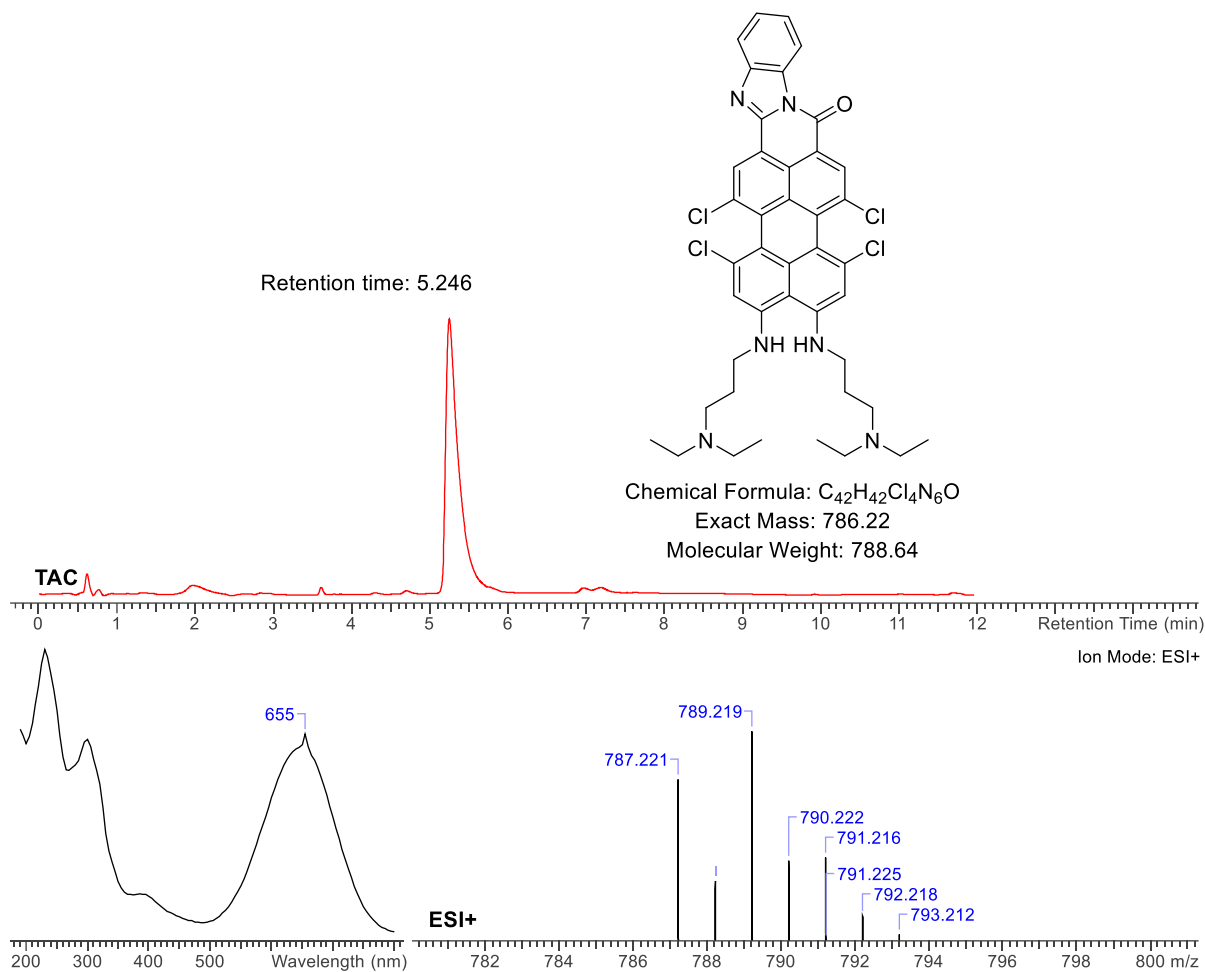
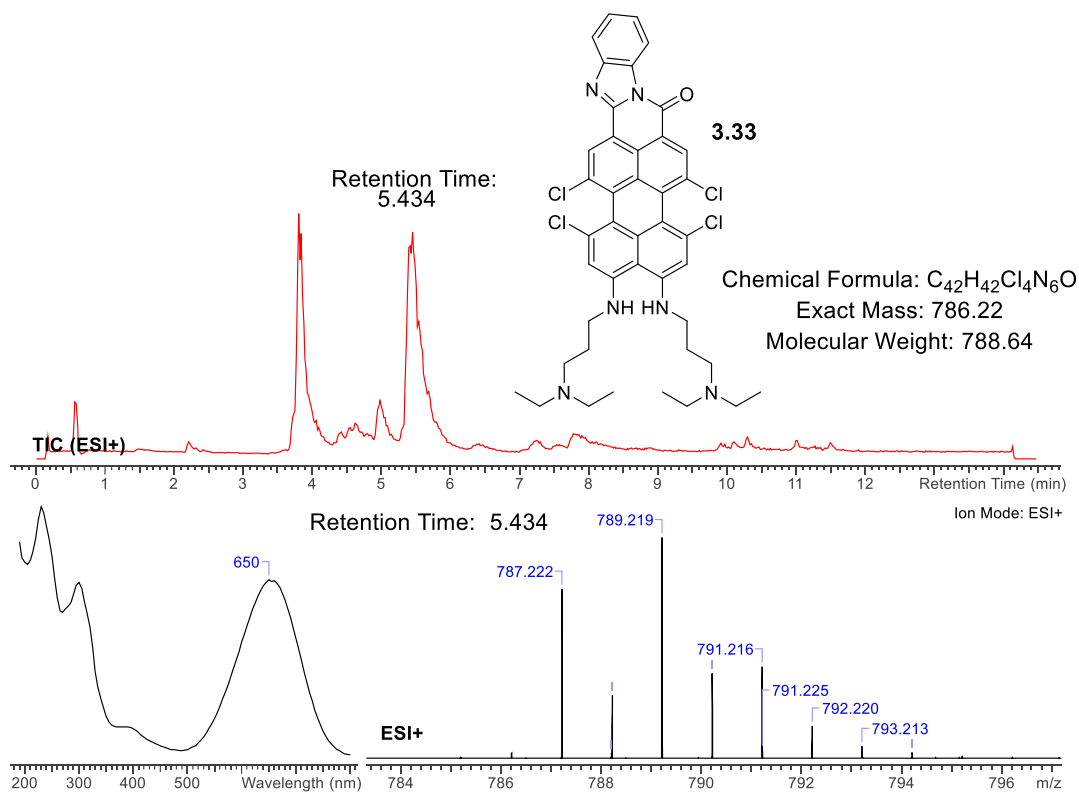

Figure 43 RP-HPLC-MS Chromatogram showing retention time of **3.33** at 5.2 minutes (top), the absorption profile (Bottom left) and high-resolution mass isotopic pattern (Bottom right).

Figure 44 Normalized absorption emission spectra of **3.33** (right) in water. Chemical structure, extinction coefficients, quantum yields and Stokes shift in water (left).

The fluorescence quantum yield of **3.33** in water was determined to be below 0.01% (Figure 44) (Table 1). To investigate the effect of the chemical modifications on the donor groups, **3.33** was modified further by the insertion of a chemical bridge between the *peri*-fused nitrogen atoms in form of aminal **3.35** and urea **3.36** bonds (Scheme 20).
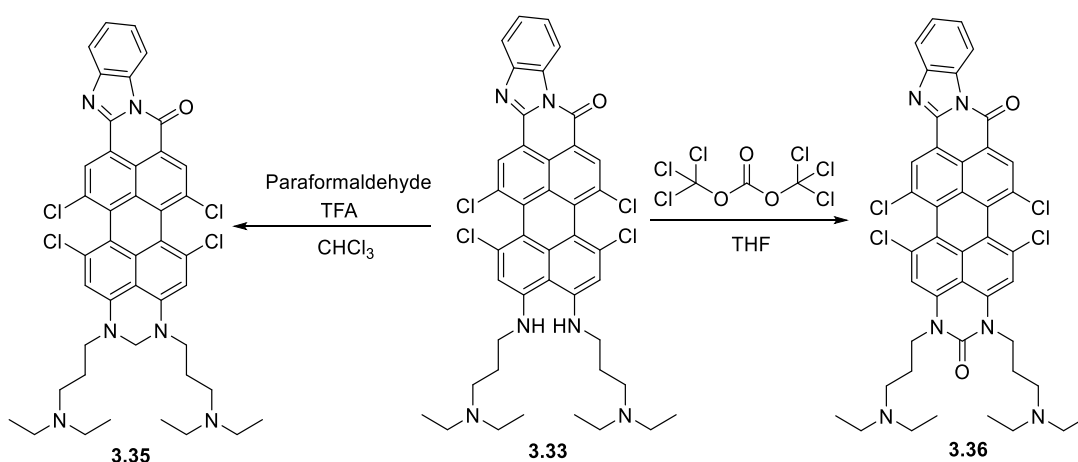
Scheme 20 Installation of aminal bridge on **3.33**, used as starting material, with paraformaldehyde to give **3.35** and with triphosgene to give **3.36**.

Compound **3.35** (Scheme 20) was obtained by the addition of paraformaldehyde to a solution of **3.33** in chloroform (CHCl$_3$) in the presence of trifluoroacetic acid (TFA). The reaction is an acid catalyzed aminal bond formation between the APMI *peri* nitrogen atoms. Compound **3.36** was synthesized by refluxing **3.33** in THF in the presence of triphosgene (Scheme 20) in this case the a carbonyl group is inserted between the *peri* nitrogens as an urea function. Photophysical properties of **3.35**, **3.33** and **3.36** in water are summarized in Table 1.

compound	$\lambda_{abs, max}$ / nm	$\varepsilon_{abs, max}$ / 10^4 Lmol^{-1}cm^{-1}	$\lambda_{em, max}$ / nm	Stokes Shift/nm	φ_{em}
3.33	700	0.89	780	80	<<0.01
3.35	640	1.50	770	130	0.01
3.36	595	2.14	725	130	0.14

Table 1 Photophysical properties of compound **3.33**, **3.35** and **3.36** in water

Compound **3.35** displayed an ipsochromically shifted absorption (λ_{abs}= 640 nm) in respect to **3.33** (λ_{abs}= 700 nm), the molar extinction coefficient raised to 15000 M^{-1} cm^{-1} and the quantum yield slightly increased to 0.01. (Table 1). Stokes shift were improved in respect to **3.33** reaching the value of 130 nm (Figure 45).
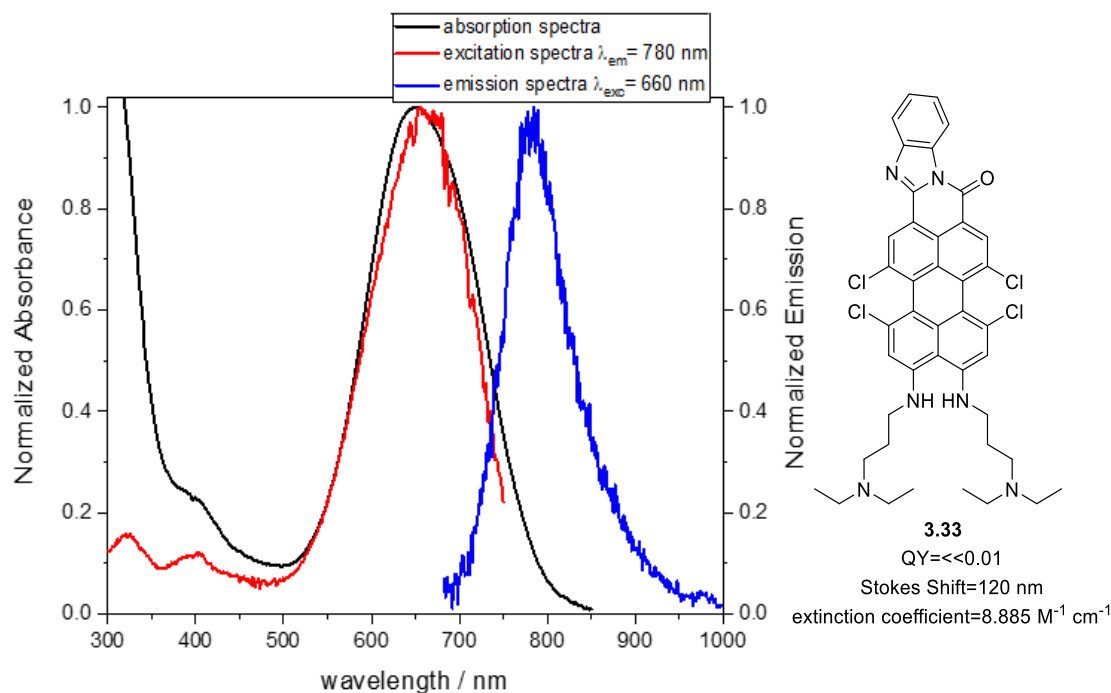

Figure 45 Normalized absorption and emission spectra of **3.33** in water (right). Chemical structure, extinction coefficients, Stokes shift and quantum yields in water (left).

Compound **3.36** displayed a markedly higher ipsochromic shift in the absorption (λ_{abs}= 595 nm) while keeping the same value of Stokes shift of Compound **3.35** in water (130 nm). The Quantum yield increased reaching the value of 0.14 (Table 1). Probably the urea bridge lead to a more rigid structure limiting the vibrational deactivation pathways of the excited state thus improving the chromophore emission properties (Figure 46).

3.36
QY=0.14
Stokes Shift=130 nm
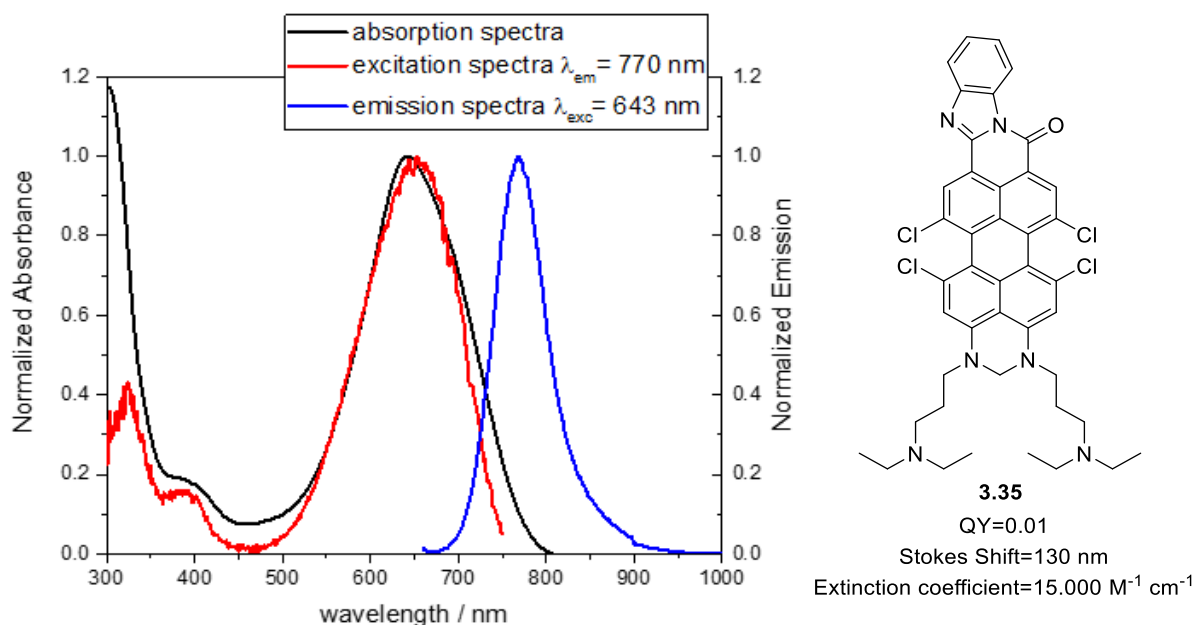Extinction coefficient=21.136 M^{-1} cm^{-1}
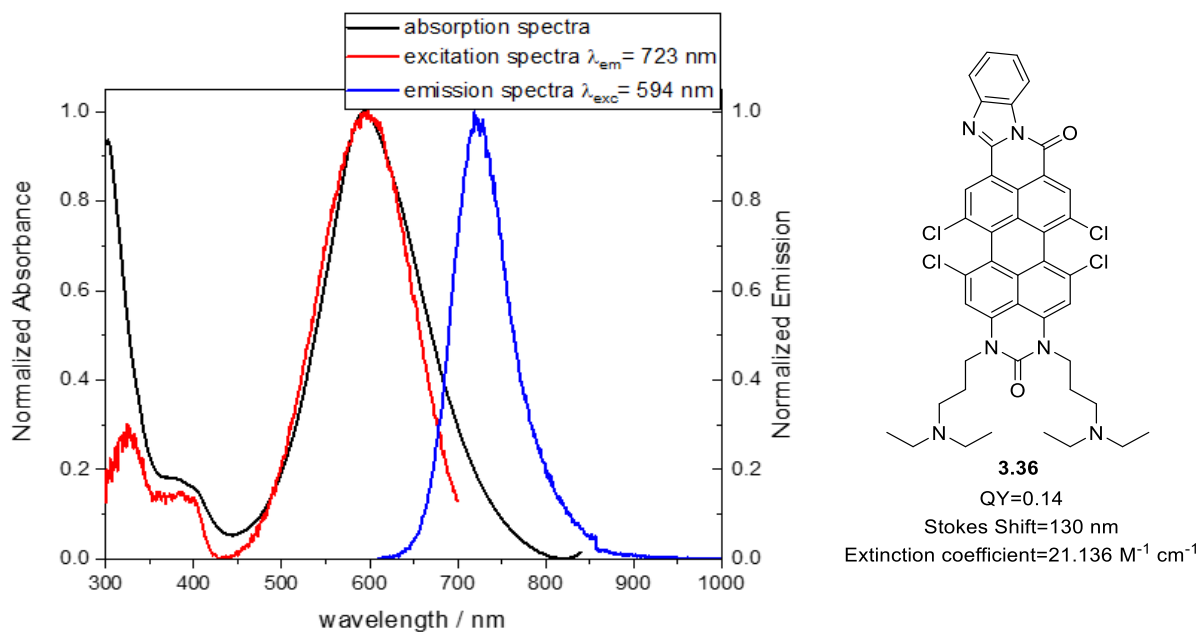
Figure 46 Normalized absorption and emission spectra of **3.36** in water (right). Chemical structure, extinction coefficients, Stokes shift and quantum yields in water (left).

In summary, chemical bridging shifts the absorbance to shorter wavelength and increase the molar absorptivity from 8885 M^{-1} cm^{-1} (Compound **3.33**) to 15000 M^{-1} cm^{-1} (Compound **3.35**) and 21.136 M^{-1} cm^{-1} (Compound **3.36**) (Figure 47). These results may indicate that the stabilization of the ground state of the molecule is occurring by modification of the fluorophore on the donor groups. This modification can be responsible for the absorption of more energetic photons (blue shift). (Figure 47).
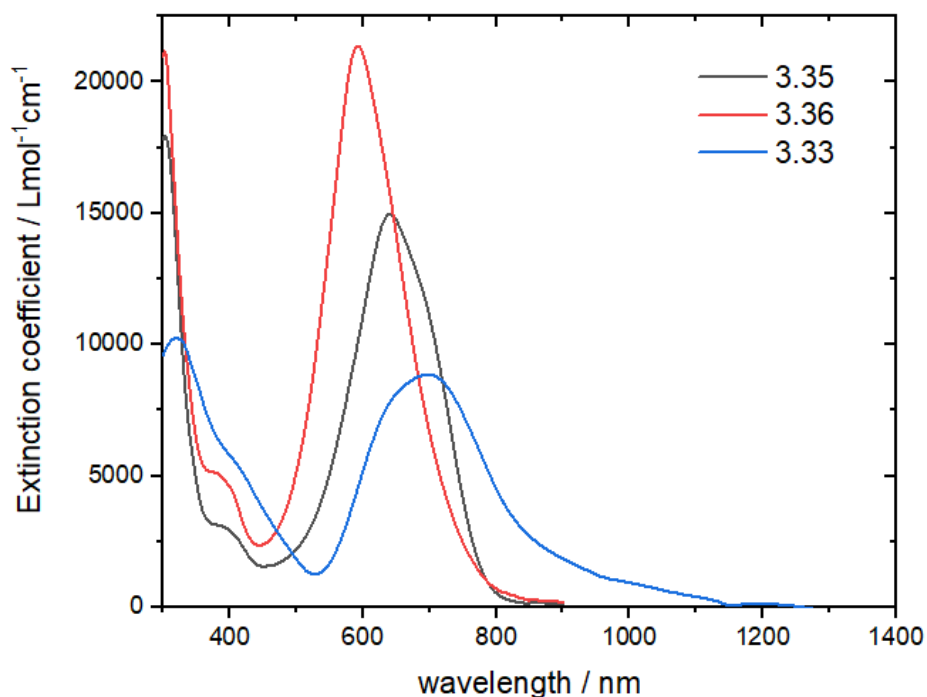
Figure 47 Extinction coefficients of **3.33**, **3.35** and **3.36** in water

Photostability study on **3.33**, **3.35** and **3.36** was performed by irradiating a sample solution in water and measuring the decrease in absorbance compared with ICG green in water under irradiation condition with UV light at 365 nm (Figure 48). After only 5 minutes, ICG starts to decrease the initial absorbance value by 2% and, after 1 hour, the value decrease by 20% (Figure 48). Compound **3.33** absorbance starts to decrease by 2% at 5 minutes, after 1 hour a decrease by 7% has been observed. Surprisingly, Compounds **3.36** and **3.35** shows no decrease in absorbance after 1 hour irradiation condition. (Figure 48). Probably the donor amino groups installed on the peri positions are responsible for the degradation of the fluorophore and their protection with stable groups like aminal and urea function may improve their photochemical inertia.
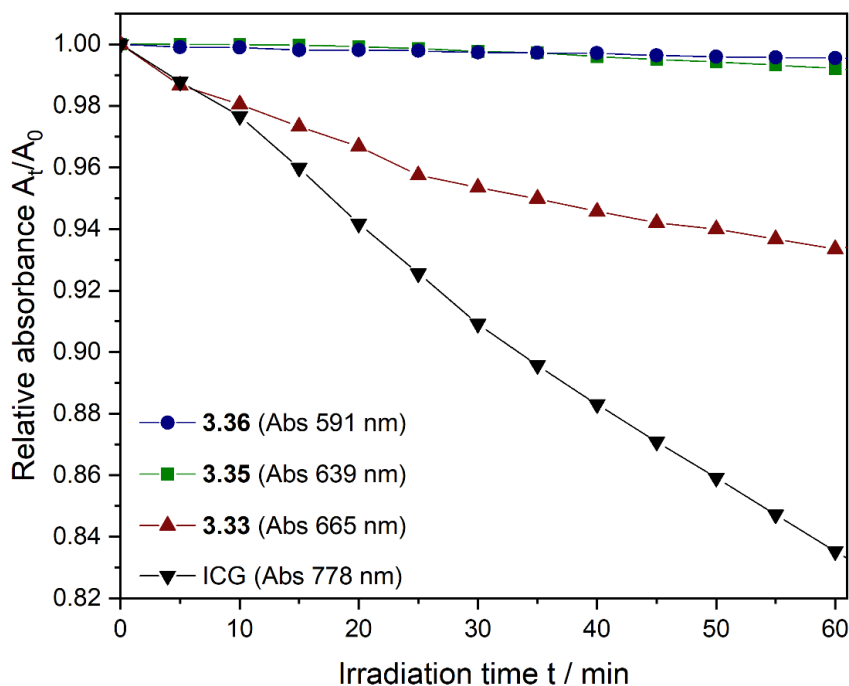
Figure 48 Absorbance (relative to $T_{0\ minutes}$) during one-hour irradiation with light (365 nm) for compounds **3.33**, **3.35**, **3.36** and ICG in H_2O at room temperature. Absorbance values were monitored at 591 nm (Compound **3.36**), 639 nm (Compound **3.35**), 665 nm (Compound **3.33**) and 778 nm (ICG).

These results indicate that Compounds **3.33**, **3.35** and **3.36** are more photostable than ICG green. I further observed that the chromophores that possess a chemical bridge between the nitrogen atoms installed on the *peri* positions, (Compound **3.35** and Compound **3.36**) do not decrease their absorption value under 1 hour irradiation conditions (Figure 48). These results are consistent with the hypothesis that the chemical bridge in form of urea and aminal bonds, improves the photostability of the fluorophore by protection of the donor groups. This evidence is also in agreement with the studies of Samanta et al[43]. and Song et al[102]. where it is demonstrated that electron withdrawing groups like acetyl or aliphatic protecting groups 7-Azabiciclo [2.2.1] heptane installed on donor moieties enhance the dye photostability and resistance to singlet oxygen promoted photodegradation[103].

3.1 Live cell staining properties of APMI dyes

To investigate the staining properties of **3.33**, **3.35** and **3.36**, we performed, in collaboration with Prof. Dr. Mark Vendrell, University of Edinburgh, a comparative intracellular localization study to assess the dye ability to concentrate in subcellular compartments of A549 cells. The dyes localize in different cellular regions, in particular, **3.33**, localizes mainly in the cell membrane, **3.35** gave mostly cytosolic staining and **3.36** can reach the cell nucleus in colocalization with Hoechst 33342 (Figure 49).
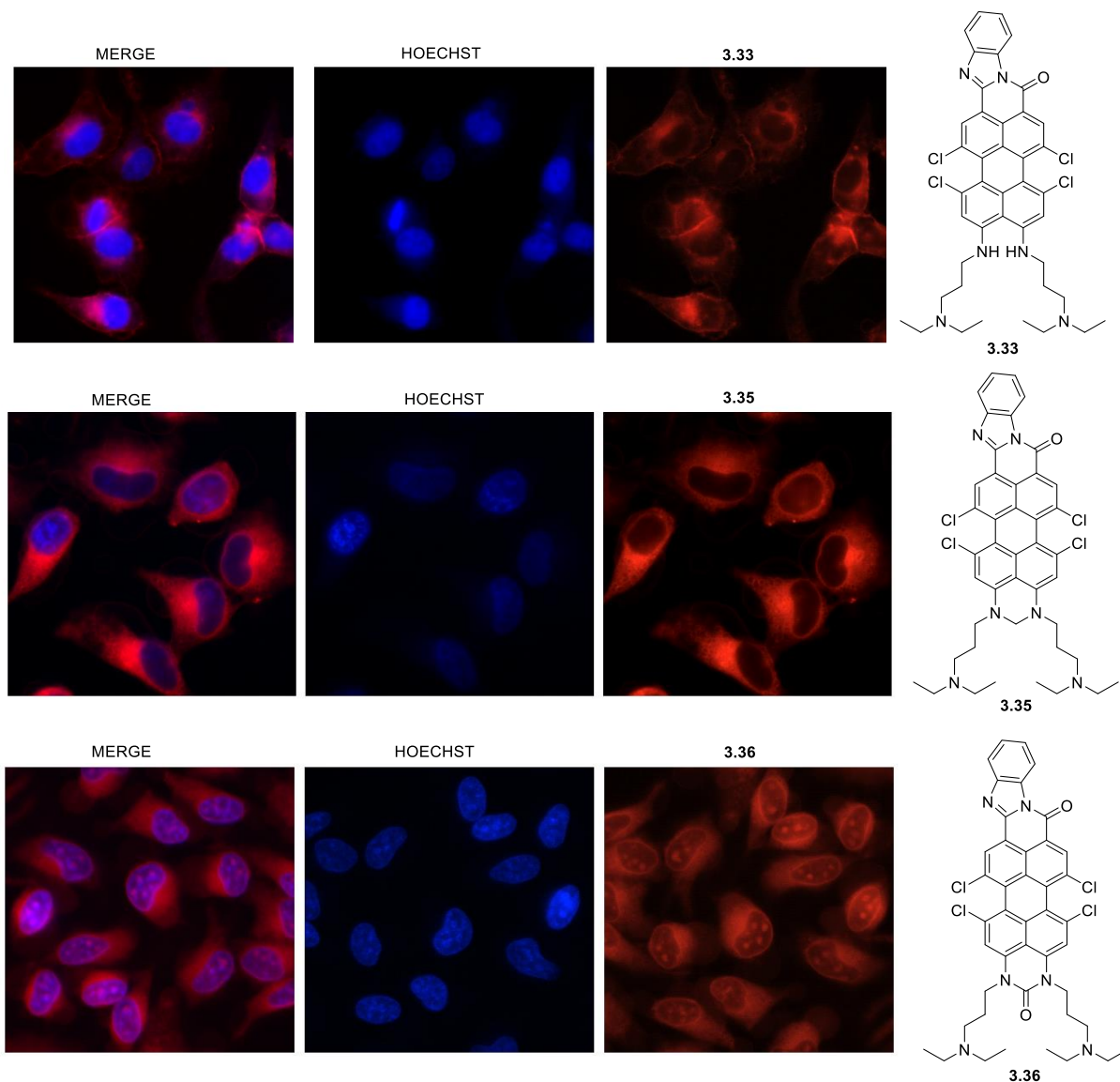
Figure 49 Selective staining of different cell compartments with compound **3.33** (top) **3.35** (center) and **3.36** (bottom)

Labelling kinetics studies were performed with **3.35** and **3.36** (Compound **3.33** was discarded due to weak emission) showing their gradual accumulation in cell compartments, reaching a plateau of emission after 30 minutes (Figure 50, Figure 51).
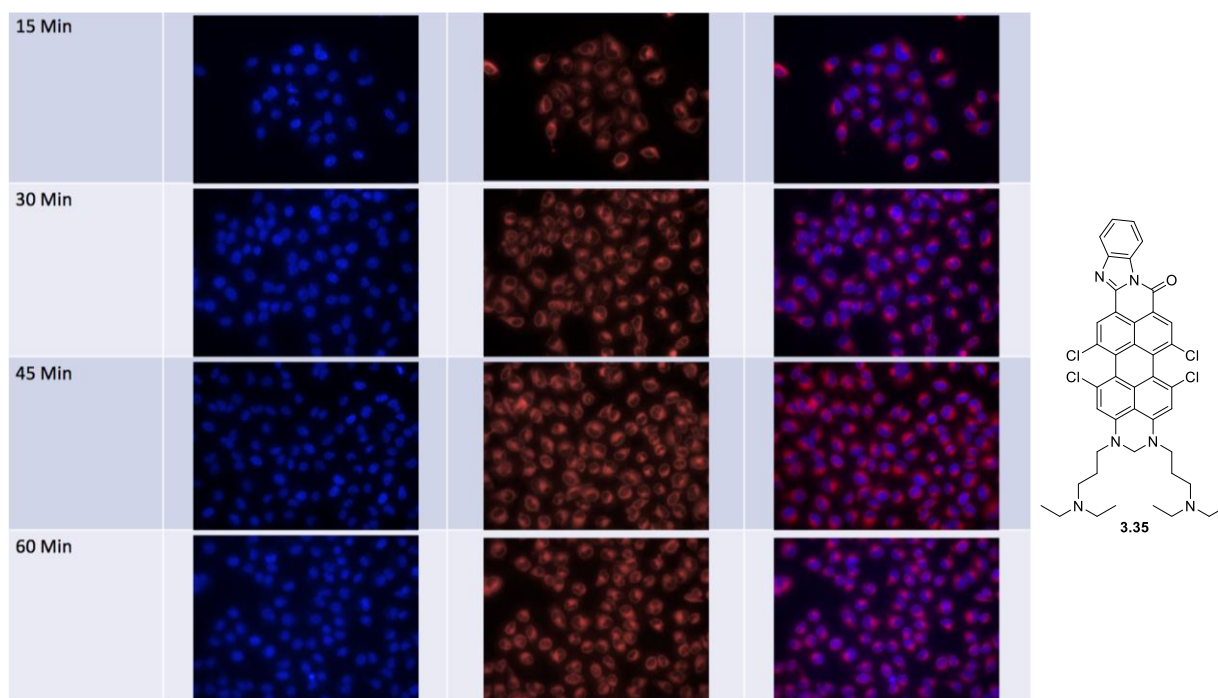
Figure 50 Kinetics of labelling in A549 cells showing accumulation in cytoplasm of **3.35** with plateau of emission after 30 minutes
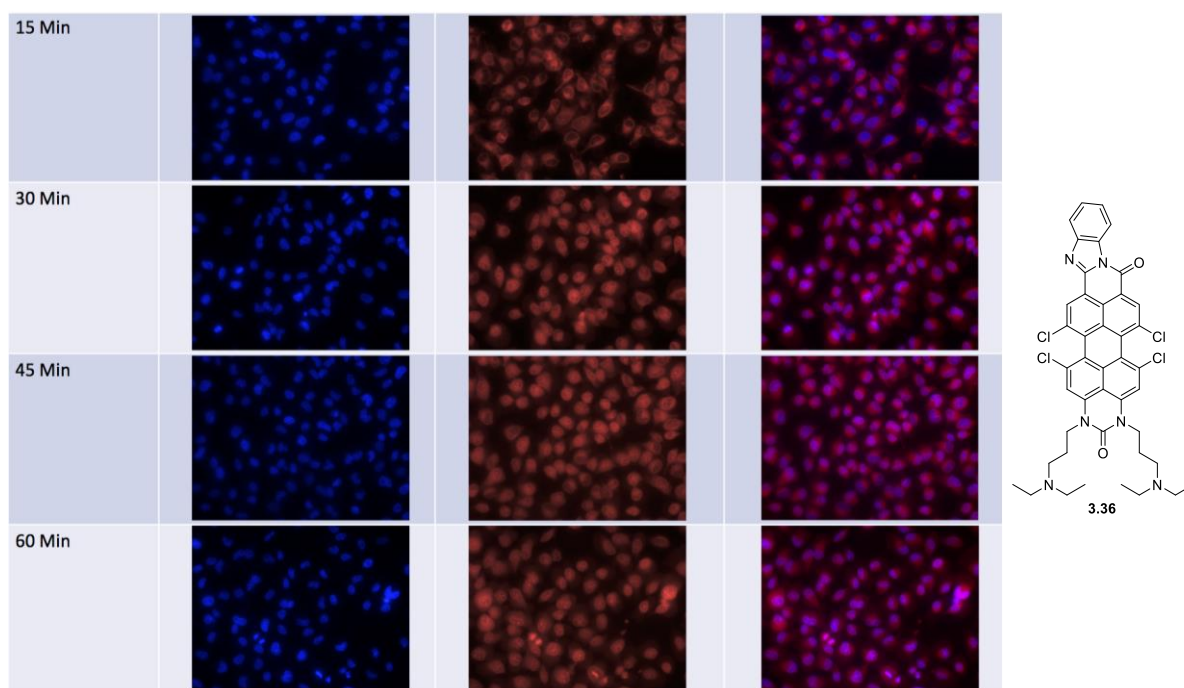
Figure 51 Kinetics of labelling in A549 cells showing accumulation in the nucleus of **3.36** with plateau of emission after 30 minutes

These results emphasize the ability of the chromophores **3.35** and **3.36** to achieve cell membrane penetration and accumulation in intracellular compartments in a short period of time without substantial decrease of fluorescence signal.

3.2 Staining of CD4+ T cells for live cell tracking *in vivo*

Immune cells like CD+ T cells, once isolated from patients and expanded *ex vivo,* can elicit antitumor response and this discovery set the basis of modern cellular immunotherapies[104-107].To track post transferred therapeutic T cells and their accumulation after infusions, cell labelling with NIR imaging contrasts have been developed[108]. Vendrell and coworkers, showed the ability to detect small population of cells (<10000) in longitudinal imaging studies with cyanine-based imaging reagents as cellular labels[109]. To evaluate the potential applications of APMI dyes in cell tracking experiments, we investigated their cytotoxicity and labelling efficacy with purified mouse CD4+ T cells. Viability tests have been performed to assess cell survival after 2 days while flow cytometry techniques have been used to confirm the dye retention after the same period of time. We observed that 80% of the cells survived after incubation with high retention profiles and minimal cytotoxicity. **3.36** showed the best profile for *in vivo* imaging studies (Figure 52).
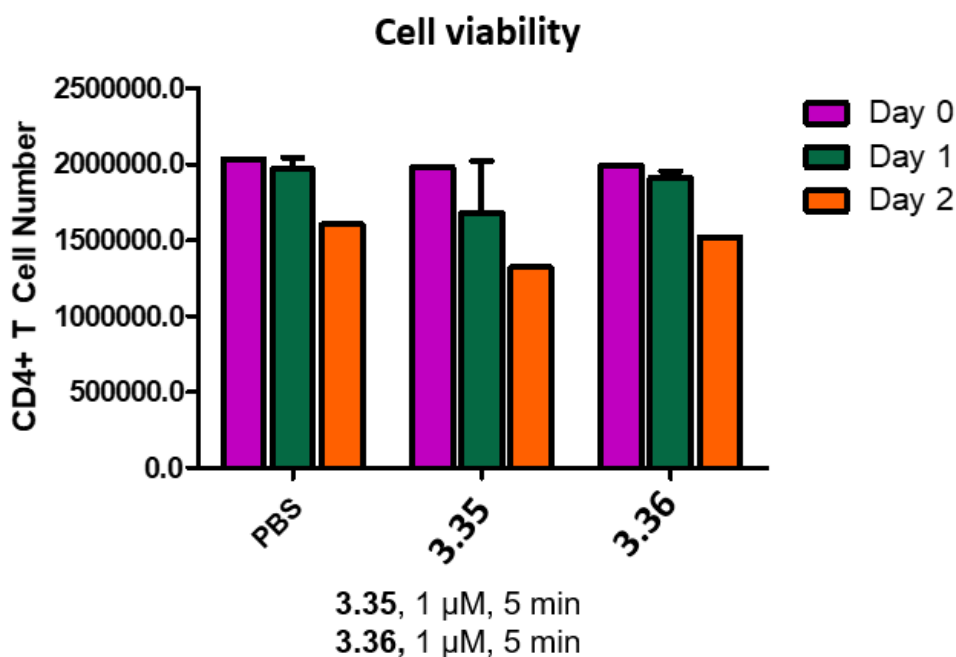
Figure 52 Cell viability assay showing CD4+ cells survival after 2 days with **3.35** and **3.36** in 1μM concentration (incubation time 5 minutes).

Through flow cytometry techniques, we confirmed that dyes **3.35** and **3.36** are retained in CD+ T cells without undergoing substantial fluorescence signal losses, (Figure 53, Figure 54).
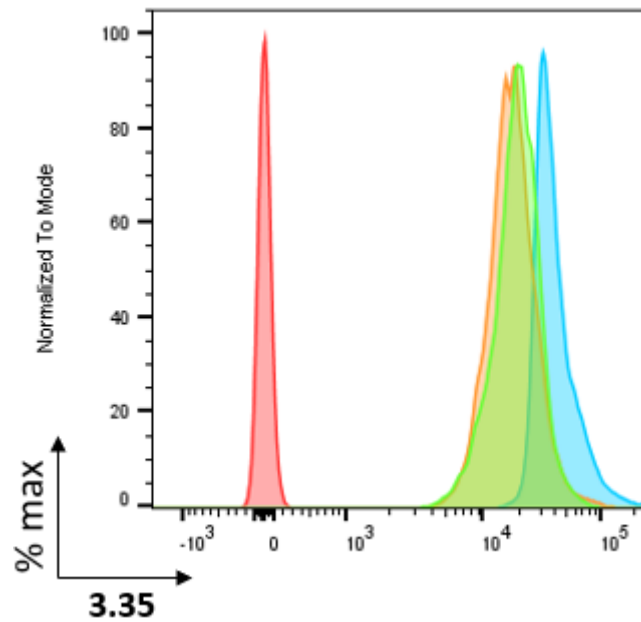
Figure 53 Flow cytometric analysis of CD4+cells with **3.35** in 1 μm concentration, incubation time 5 minutes. NIR fluorescence were recorded on day (0) blue, day 1 (Orange) day 2 (green), in comparison to unstained cells (red).
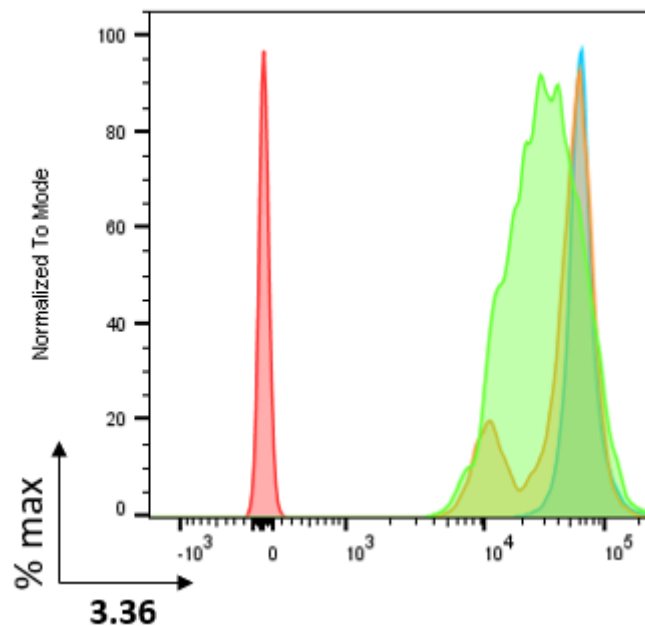
Figure 54 Flow cytometric analysis of CD4+cells with **3.36** in 1 μm concentration, incubation time 5 minutes. NIR fluorescence were recorded on day (0) blue, day 1 (Orange) day 2 (green), in comparison to unstained cells (red).

Based on cytotoxicity data, **3.36** (Figure 52) was selected for whole body imaging settings. CD4+ cells were labelled and injected in immunized mice. After 2 days, images were recorded with NIR camera showing accumulation of labelled T cells in lymph nodes. Control mice showed no signal in the same regions (Figure 55).
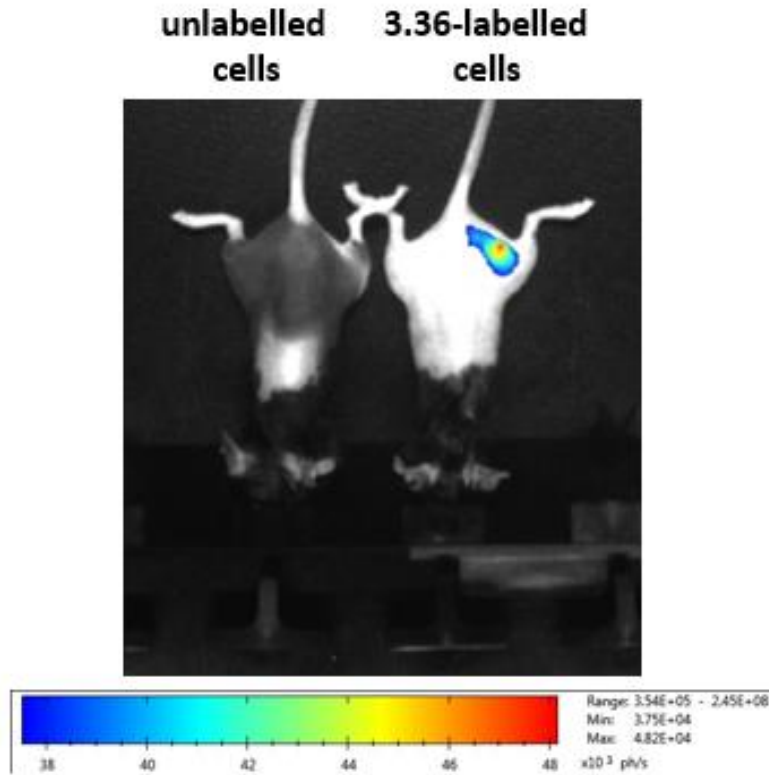
Figure 55 Accumulation of labelled cells with 3.36 in spleen. Colors from blue to red indicate the intensity of the signal in counts per second.

After dissection, spleen and lymph nodes resulted fluorescent indicating selective accumulation of NIR active CD+ cells in their internal compartments (Figure 56).
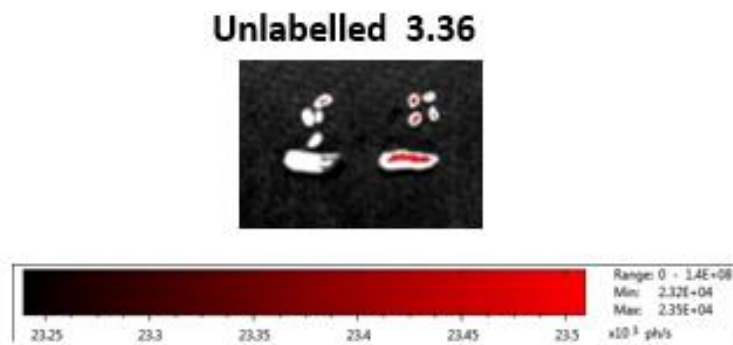
Figure 56 Selective accumulation of labelled cells in spleen and lymph nodes isolated after dissection. Colors from dark red to red represents the signal intensity.

3.3 *In vivo* NIR fluorescence angiography

Angiography or arteriography is a medical imaging technique that makes use of radiotracers or optical molecular contrasts to image the inside lumen of blood vessels, vein, and arteries. Angiographical analysis dates to 1927 when it was first developed by the Portuguese neurologist and physician Egas Monitz at the University of Lisbon. The first contrast used was a simple inorganic salt, sodium iodide. After injection through femoral arteries or jugular vein, the contrast resulted opaque to X-rays and gave the visualization of blood vessels distribution in brain[110]. The development of modern optical contrast agents followed the success gained in neurosurgery. Fluorescein, for example, was already known as a contrast in ophthalmology to give excellent visualization of the choroidal vascularization and in 1960, two medical students from Indiana University studied the first procedure entering in clinical practice for retinal angiography[111]. Moving to gastrointestinal surgery, the fluorescent contrast ICG green, was first used to shed light to the abdominal cavity organs with NIR light[112]. The advantage of the use ICG green in clinical settings lies not only on its emission in the NIR but also on the biodistribution and pharmacokinetic profiles[113]. ICG is an anionic dye and, when intravenously injected, binds to serum proteins like albumin, it is manly retained in the lumen of vessels giving insight to the vascular structure and organ capillary network. When accumulated in the liver, ICG is excreted through the bile duct into the small intestinal cavity. ICG is often used together with methylene blue (MB), a small molecule (319.85 g/mol) only partially bound to serum proteins. Contrary to ICG, most of the MB dose, follow the kidney excretion enlightening the ureters and bladder[112]. The use of ICG in combination with MB, is therefore, of great utility and help the surgeon to avoid damages to healthy tissues and the need of reoperation in patients[112]. ICG is used to study the presence of both metastases and primary liver cancers such as hepatocellular carcinoma and cholangiocarcinoma[114]. It has been shown for example that , this chromophore leaves the liver within a couple of hours in healthy tissues whereas it is retained in solid tumors, by compression of the bile ducts[112]. New imaging approaches of liver and gastrointestinal cancers also requires the visualization of the intestinal vascularization, in particular, the mesenteric artery as well as the tissue perfusion of the intestinal wall. This approach is useful not only to follow the correct revascularization after surgery but also provides in some cases, the access to the identification of specific anastomosis and junctions[114]. The rectosigmoid junction artery, for example, has a specific clinical relevance in patients affected by colorectal cancers[33]. As explained in chapter 1, ICG suffers, of several drawbacks like rapid photobleaching and aggregation phenomena in water[43]. ICG is

also unstable under visible light irradiation and start to degrade after few minutes thus losing its brightness and visibility by the surgeon[12]. Because of these disadvantages, research in FGS is moving toward the synthesis and use of new photostable NIR fluorophores. For this purpose, we demonstrated in section 3.3.1, that APMI fluorophores emits in the NIR up to 770 nm and does not undergoes degradation processes over one-hour irradiation conditions in water (Figure 48). As a result of our study, we advanced the use of water soluble APMI dyes as novel contrast agents for *in vivo* NIR fluorescence (NIRF) angiography in rats. In collaboration with Dr. Andrea Picchetto MD, surgeon from La Sapienza University of Rome, we evaluated NIR fluorescence angiography of the main splanchnic abdominal organs of 5 wild-type rats measuring the time needed for the chromophore to perfuse the small intestine and colon, vessels, the liver and the internal lumen of the duodenum. For this purpose, we injected a dose of 1,0-1,7 mg/kg of Compound **3.35** or Compound **3.36** dissolved in sterile saline physiological solution into the external jugular vein, and followed the fluorescence image angiograms using Quest® medical imaging device (Table 2).

Animal	Rat1, Compound **3.36** (1,1 mg)	Rat 2 Compound **3.36** * (1,3 mg)	Rat 3 Compound **3.36** (1,1 mg)	Rat 4 Compound **3.36** (1,7 mg)	Rat 5 Compound **3.35** (1,0 mg)
Splanchnic vessels	+/- 30 seconds	+/- 1:00 min	+/- 30 seconds	+/- 30 seconds	+++ 30 seconds
Splanchnic organs	+/- 1:00 min	+/- 2:00 min	+/- 1:00 min	+/- 1:00 min	++ 1 min
Liver	+ 2:00 min	+ 2:00 min	+ 2:00 min	+ 2:00 min	+++ 2 min,
Gut	+ 4:00 min	*	+ 4:00 min	+ 4:00 min	+++ 3 min
Bladder and/or Ureters	none	*	none	none	none

Table 2 Abdominal organs infusions after intravenous injection of APMI dye **3.36** or **3.35** solution in the jugular vein. The term + indicate positive to the organ infusion at the time it was observed with Quest Spectrum medical imaging® device. *Death due to anesthesia sequelae

3.36 was tested on rats 1-4 (Table 2), we observed a NIRF fluorescence angiography of the small bowel mesentery vessels and the big abdominal vessels (mesenteric, mesocolic and celiac vessels) after 30-60 seconds (Figure 57). In these regions, the signal lasted about 4 minutes (mean time).
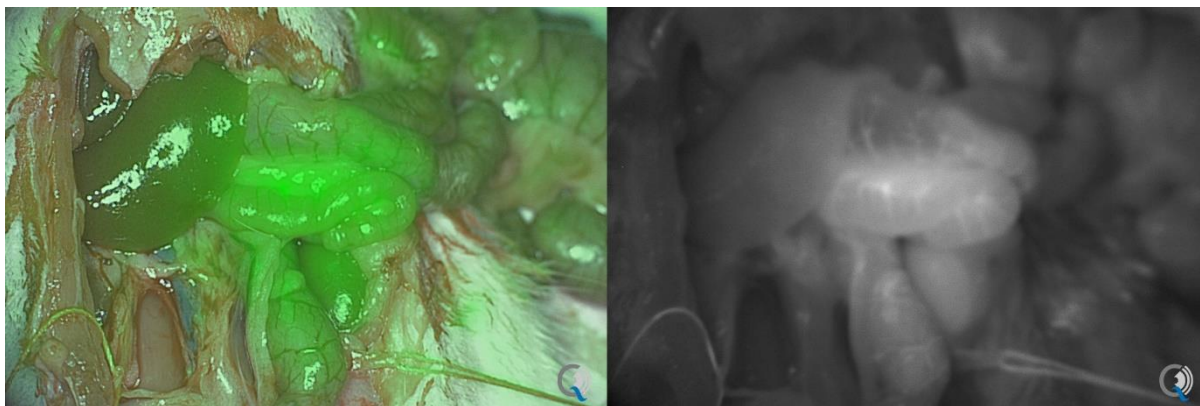
Figure 57 Splanchnic organ perfusion with **3.36** after 30-60 minutes

After 2 minutes, the liver showed a bright NIRF angiography that lasted for all the experiments a mean time of 20 minutes (Figure 58).
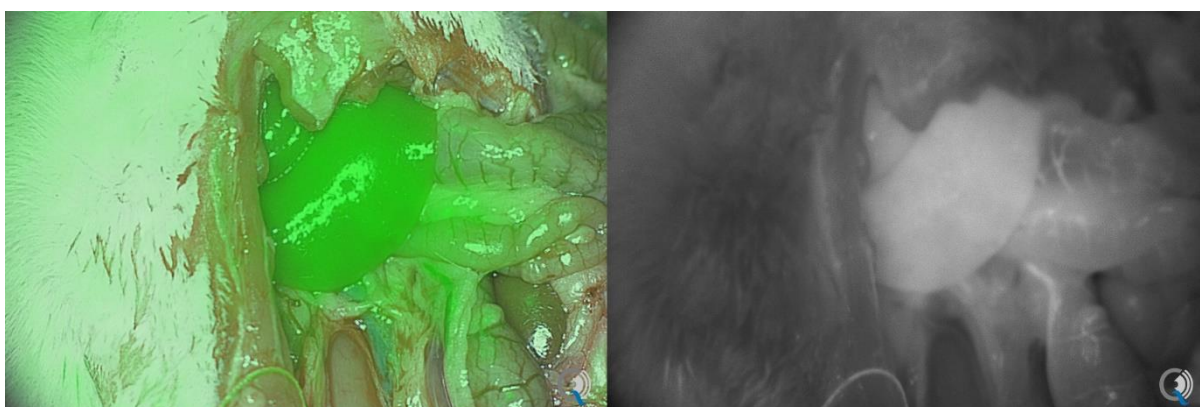
Figure 58 Liver fluorescence with **3.36** after 2 minutes

The duodenum and jejunum showed after 4 min a brighter endoluminal fluorescence rather than the ileum probably due to the biliary excretion of **3.36** (Figure 59).
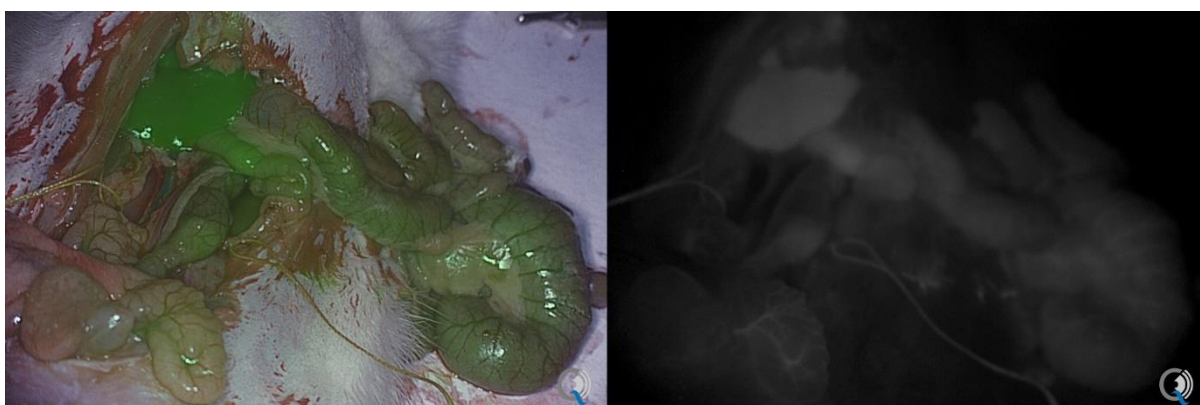
Figure 59 Fluorescence angiography of the duodenum and jejunum showing decrease in brightness in the ileal gut with **3.36**

Ureters and bladder did not show any fluorescence in the urine (Figure 60).
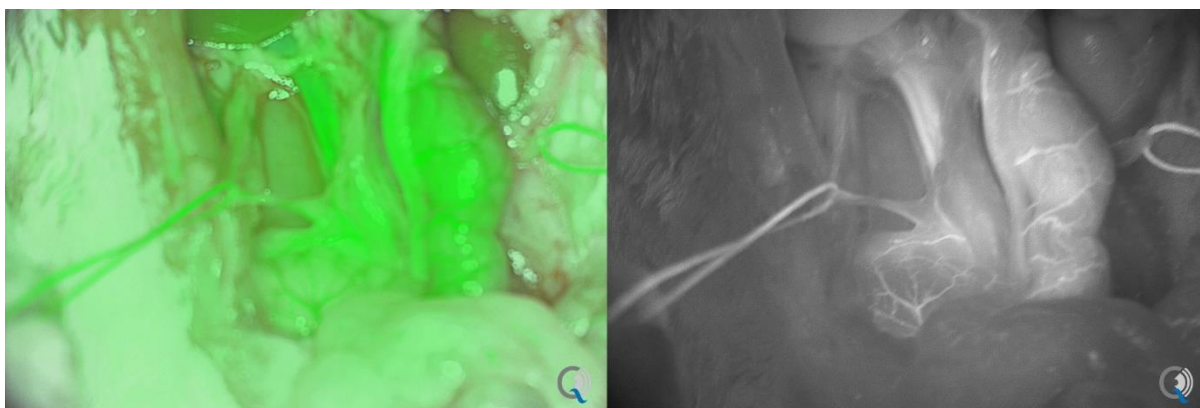
Figure 60 Image showing the ureters (silk threads) that did not appear to be fluorescent with **3.36**

3.35 was tested on rat 5. This compound was responsible for an unexpected ultrabright NIRF angiography of the splanchnic and retroperitoneal vessels (mesenteric mesocolic) and renal vein (Figure 61, Figure 62, Figure 63).
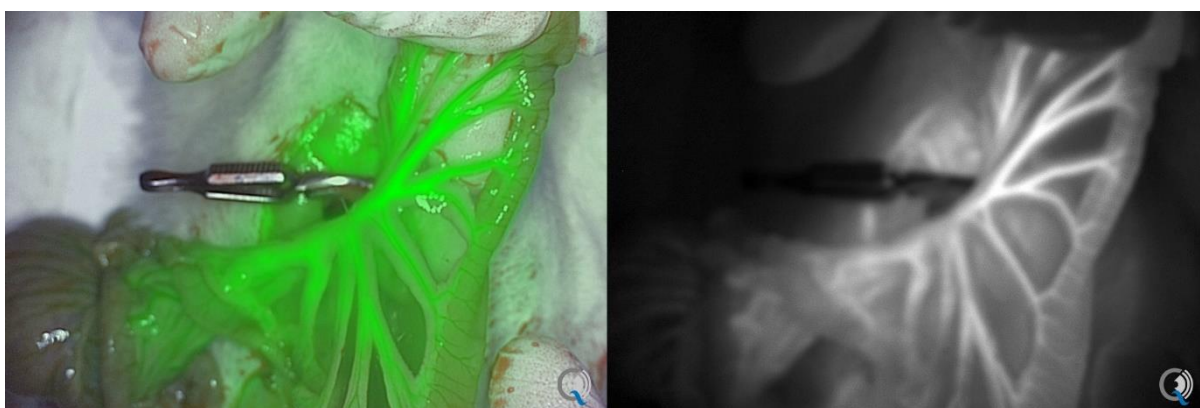
Figure 61 NIRF angiography of the mesenteric vessels with **3.35** after 30 seconds
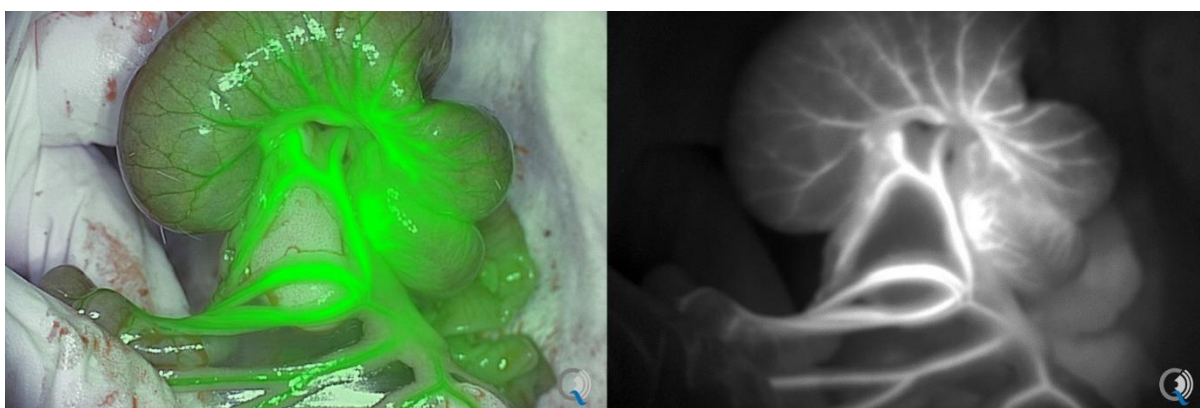
Figure 62 NIRF angiography of mesocolic vessels with **3.35** after 1 minute

Figure 63 Left kidney NIRF angiography showing renal vein and gonadal vessels with **3.35**

After 2 minutes, the liver showed an ultrabright NIR fluorescence angiography which lasted 20 minutes (Figure 64).
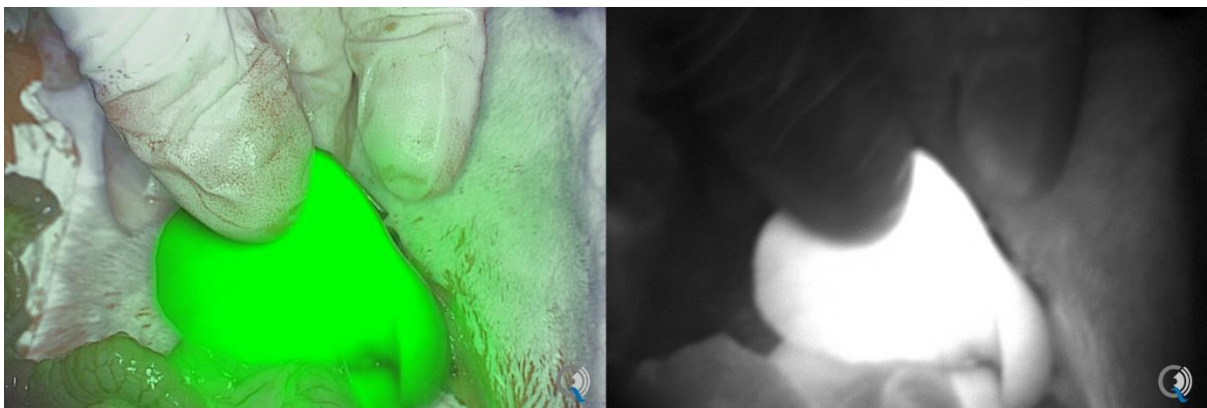
Figure 64 Ultrabright liver fluorescence with **3.35** after 2 minutes

After 3 minutes, the duodenum and jejunum showed an endoluminal fluorescence similar to the one obtained with **3.36** but the fluorescence intensity detectable on the screen was markedly higher (Figure 65). Also in this case, the ureters and the bladder did not show any fluorescence.
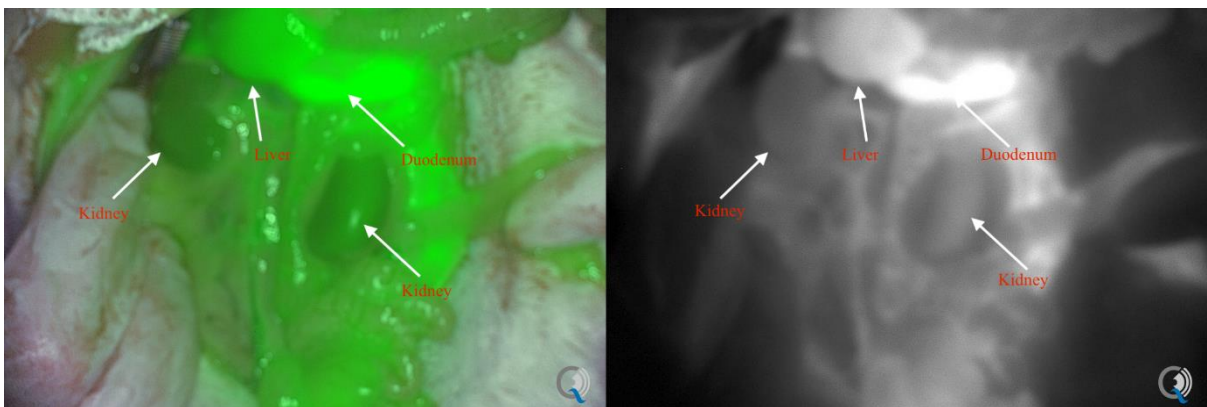
Figure 65 Liver and duodenum ultrabright NIRF angiography with **3.35**

Compound **3.36** and **3.35** exhibited a bright angiography of the main abdominal organs in particular the mesenteric, colic and ileocolic vessels. The signal of the NIR light didn't show any change in intensity during the time of the angiography over time, this result may suggest that the photostability of the dye play a significant role during the irradiation conditions used by the Quest imaging® device. Additionally, both compounds after 2 minutes accumulated in the liver and in the duodenum trough the bile after which time (3 minutes) the biliary ducts were detectable (Figure 59; Figure 65). Since the ureters didn't show any NIRF fluorescence, we concluded that the excretion of **3.36** and **3.35** was predominantly biliary. Unexpectedly, Compound **3.35** enlightened the biliary excretion pathway with an ultrabright angiography suggesting that the quantum yield of the dye may be significantly different in the biological medias encountered after the intravenous injection through jugular. Consequently, NIR angiography with APMI dyes may open new opportunities to improve the applications in FGS, in particular, they may be useful as valid alternatives to ICG green for the studies of the intestinal vascularization through angiographical techniques[115]. In this context they may be useful in gastrointestinal surgery not only for the identification of specific arteries like those of the mesenteric vessels but also vessels of specific clinical relevance like those associated to colic mesocolic arteries and the rectosigmoid junction[33]. NIR angiography with photostable APMI dyes may also have impact in reconstructive surgery after organ transplantation to help the surgeon to evaluate the location and state of reconstructed vessels including the identification of anastomosis and specific blockages[33]. In addition, the ultrabright liver angiography obtained with **3.35** (Figure 62) suggest that this dye may be used as photostable contrast in applications that require the visualization of the liver and the biliary tree for example cholecystectomy during hepatobiliary surgery[116]. In this context, hepatobiliary cancers are treated with the complete removal of the liver of affected patients, and it is very important that the surgeon detect in real time the position and state of the bile duct[116]. Therefore I propose **3.35** may be also used in alternative to ICG green to visualize the hampered biliary excretion through NIRF during surgery as reported in the work of Schaafsma et al.[11] where liver tumors of affected patients appears as fluorescent rims due to passive accumulation of the dye around the solid liver tumor[11]. In conclusions APMI dyes may be used as candidate to advance the use of novel photostable contrasts in FGS especially in those applications that require the visualization of the vascular networks of mesenteric arteries and those need the visualization of the hepatobiliary cancers in real time without the need of time expensive preoperative imaging treatments like MRI, PET and CT thus improving the quality if resection in during surgery and limiting the need of reoperation in patients[116].

3.4 Photoacoustic imaging

Photoacoustic (PA) imaging is a molecular and functional imaging modality that has been adopted to overcome the major drawbacks of the use of light as contrast in clinical settings and in FGS[117]. Visible and NIR Light is scattered and diffused by endogenous chromophores and cannot achieve penetration depth higher than 1-3 mm[118, 119]. Photoacustic imaging takes advantage from the absorption of NIR pulsed laser light from endogenous contrasts like hemoglobin, lipid, water and melanin but also from exogenous absorbers like organic dyes and nanoparticles[120]. Once reached the excited state, the chromophore release an high frequency acoustic wave (photoacoustic signal) (PA) that can be detected by commercially available ultrasound transducers reaching penetration depth up to 2.5 cm[120, 121, 122]. The release of photoacoustic signal upon light absorption has been observed in different class of dyes, between them, NIR absorbing squaraine and cyanine dyes has been widely employed *in vivo*[119]. Since APMI dyes, as described in the previous chapters, showed promising properties as NIR absorbing chromophores for *in vivo* applications, we tested their ability to produce photoacoustic (PA) signal in collaboration with Dr. Magdalena Steiner and Dr. Joost Holthof, from Fujifilm Visulasonics. In particular, we demonstrated the applicability of the chromophores with commercially available device Vevo®-LAZR-X from Fujifilm Visualsonics ® (Figure 66).

Figure 66 Commercially available device Vevo-LAZR X 8® Fujifilm Visualsonics, the Netherlands.

Dye solution in water was injected in the capillary tubing of the system Vevo®-LAZR-X and the device acquired a sequence of PA images in the wavelength range of 680-970 nm with a step size of 5 nm in the spectral mode. Photoacoustic signal (PA) was measured as signal intensity energy reaching the device in the region of interest. Vevo LAB ® software reports the total area of the defined contrast region. Quantification of the signal intensity is available for the average threshold signal power of each PA region measurement. (PA average) quantification values represent the average maximum intensity and applies only to the frame of which it appears (Figure 67) (Table 3). By comparing the signal intensity using the same amount of substance dissolved in distilled water, Compound **3.33** gave the best profile with an average PA signal of 30,435 in respect to **3.35** and **3.36** that gave 10.996 and 4.990 respectively (Table 3). Our results indicate that Compound **3.33** absorbs at 680 nm and generates a high intensity PA signal that is markedly higher than the signal produced by the homologues compounds **3.35** and **3.36** and ICG green (Figure 67) (Table 3). Compound **3.33** chemical structure lacks bridging units on the donor substituents (Figure 67) in respect to **3.35** and **3.36**. This structural change probably improves the release of the absorbed energy through ultrasound photoacoustic waves (Figure 67).
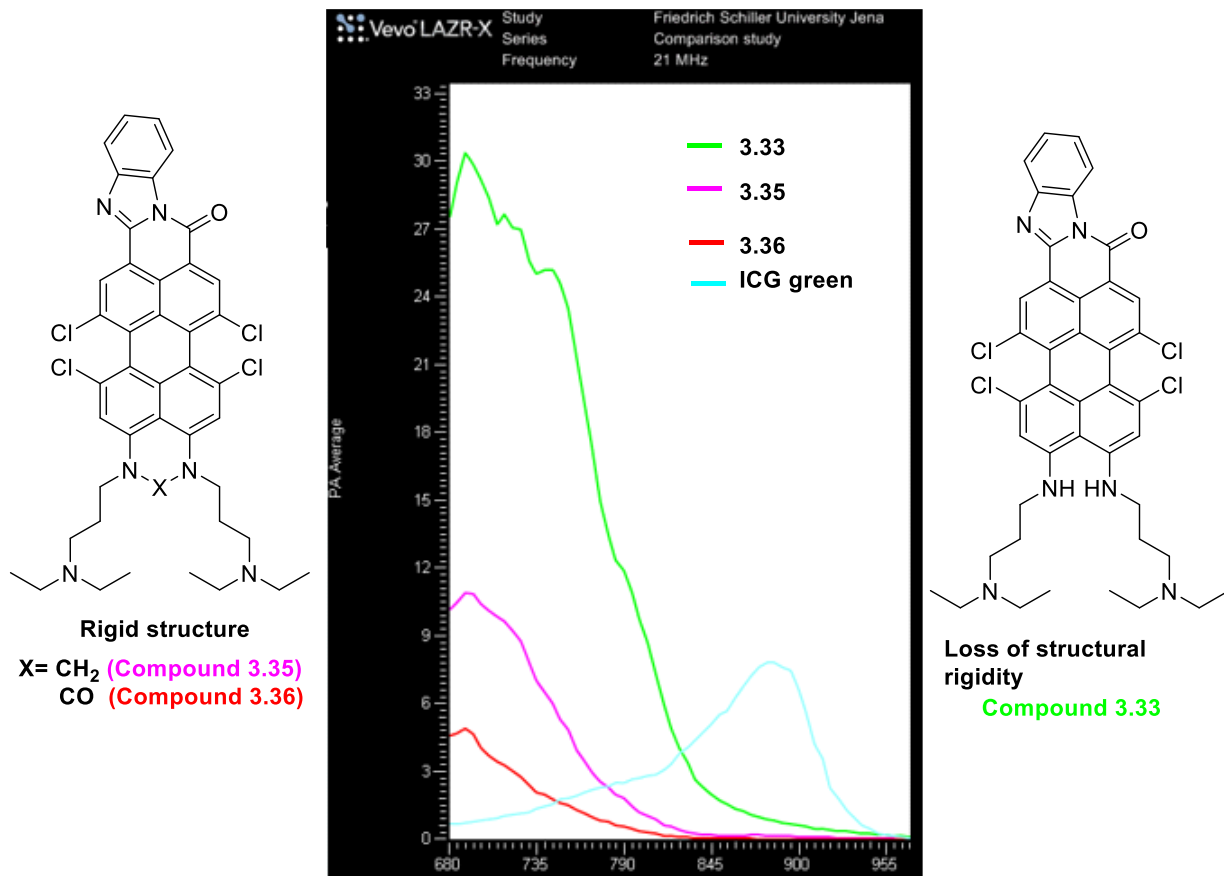
Figure 67 Photoacoustic signal (PA) is shown for **3.33** (green) **3.35** (violet) **3.36** (red) and **ICG** green (blue) (y axis) wavelength (x axis). The sample were dissolved in water and injected in the capillary tubing system of the device VEVO-LAZRX 8 Fujifilm Visualsonics. Chemical structures of **3.33** and **3.36** (left) and the chemical structure of **3.33** (right).

	Compound 3.33	Compound 3.35	Compound 3.36
Amount (mg)	4.3	4.2	4.5
Area (mm^2)	0.560	0.560	0.560
PA average (680 nm)	30.435	10.996	4.990
PA average threshold (680 nm)	76.729	22.652	7.699

Table 3 Parameters used in LAZR-X Vevo® device Amount of substance used, Area of detection of the signal measured in mm^2. PA (photoacoustic) signal refers to the average of the signal intensity reaching the device in the area of interest at the selected wavelength used as light excitation source in nm.

3.5 Results and Discussion of results obtained with APMI dyes

The goal of my research was to synthesize novel photostable NIR active contrast agents to be used in FGS. The installation of primary amines on the peri position of perylene monoimides bearing electron deficient amidine moieties give rise to APMI dye series with a light absorption profile in the NIR. This finding indicates that a push-pull system with donor (D) and acceptor (A) groups installed on the peri position of the perylene core, is responsible for the absorption band in the NIR (660 nm) and emission up to 770 nm in large Stokes shift (130 nm). This evidence is supported by the studies of Dessi et al.[123] and Bessho et al.[124] showing the red shifting effect in the absorption and emission of organic dyes bearing donor and a acceptor moieties at the terminal end of extended conjugated system[123]. According to the theoretical model of Chen et al.[125] the red shift is attributed to the electron density distribution that is mainly localized on the donor groups in the ground state of the molecule while the acceptor group host a the intramolecular charge transfer ICT in the excited state[125]. In addition, the modification of the donor groups in form of nitrogen atoms installed on the *peri* position showed to have a unique role in the improvements of photophysical properties of the chromophore. In particular, the installation of a chemical bridge in form of aminal and urea function between the *peri*-fused nitrogen atoms, improves extinction coefficients, quantum yields and Stokes shift of the chromophore (Table 1). This result indicates that the chemical motifs acting as chemical bridges in form of methylene or urea bridge not only improves the photophysical properties but also have a role as protecting functions against photobleaching.

This interpretation is confirmed by irradiation experiments of an aqueous solution of APMI dye with visible light (365 nm). In particular, we observed that the modified chromophore does not undergo a decrease of absorbance after one hour irradiation condition (Figure 48), therefore, we advanced the hypothesis that the *peri*-fused nitrogen atoms may be responsible for the photostability of the fluorophore. This hypothesis is consistent with the observations of Samanta et al.[43] reporting that the protection of an analog amine donor group with an electron withdrawing acetyl group in a cyanine dye scaffold improves the dye photostability[43, 109] also Mellanby et al.[109] showed that the delocalization of the electron density of donor N-substituted groups with electron deficient triazoles enhanced the light resistance of a cyanine dye by lowering photodegradation effects[109]. In addition, Large Stokes shifts can be attributed to the asymmetric structure of APMI chromophores achieved through the installation of the benzimidazole subunit as an acceptor unit. This observation is in agreement with the main findings of Ren et al.[126] suggesting that asymmetric fluorophores structures are responsible for large Stokes shift in the absorption and emission thus reducing self-quenching phenomena and inner filter effects[126]. We continued our investigations on APMI chromophores by studying the dye cellular permeability and distribution in intracellular compartments. In particular, we observed that **3.35** and **3.36** are cell permeable and mainly localize in cytoplasm and in the nucleus respectively where they are retained without substantial fluorescence losses (Figure 49). This result indicates that APMI dyes bearing basic positively charged protonated trialkyl amines in water are cell permeable and may pass the cell membrane by passive diffusion following an equilibrium distribution in intracellular compartments. I hypothesize this process may be driven by negative cell membrane potentials[127]. In particular, CD+ T cells retain **3.35** and **3.36** without cytotoxic effect after two days (Figure 52). We selected **3.36** as preferential candidate to label therapeutic CD+ T cells prior to be infused in mice. After infusion, we successfully visualized the accumulation of **3.36** labelled cells in spleen and lymph nodes (Figure 55, Figure 56). These findings indicate that APMI chromophores may find applications as non-cytotoxic cellular stains with high retention profile for longitudinal imaging studies in mice. Immune cells tracking *in vivo* can be used in cellular immunotherapies to detect small population of T cells in high sensitivity (4000 cells)[109]. For this purpose, we proposed APMI dyes as valuable candidates and cellular stains for therapeutic immune cells tracking in longitudinal imaging studies *in vivo*. Subsequently, to further investigate the applicability of the fluorophores as NIR contrast agents *in vivo*, we took advantage of the high-water solubility of **3.35** and **3.36** to observe their biodistribution profile *in vivo* in rats. We conducted a perspective monocentric study to evaluate the angiography of the main abdominal and

splanchnic organs and the dye preferential excretion pathway. Our findings showed ultrabright angiography of the main abdominal and splanchnic organs, in particular, the small bowel, mesentery vessels and big abdominal vessels (mesenteric mesocolic, celiac). Additionally, after 4 minutes, a fluorescent signal coming from the duodenum and jejunum endoluminal compartment was found to be brighter than the ileal gut in the fluorescence image (Figure 59). We hypothesize that the dye was partially excreted in the bile through the biliary duct in the first tract of the small intestine thus giving a first insight on the chromophore excretion pathway (Figure 59). To our surprise, **3.35** gave a better ultrabright angiography of the mesenteric, mesocolic vessels and the liver (Figure 60, Figure 61) indicating that probably an increase of quantum yields probably occurs after infusion in the bloodstream and excretion through the bile. The study may open new possibilities of the implications APMI dyes may have in gastrointestinal surgery in particular it may be used by the surgeon in real time to assess adequate blood perfusions and anastomotic leakages in both upper and lower gastrointestinal tract during surgical operations[128] or in the treatment of hepatobiliary cancer to assess liver function[11]. To conclude our studies on APMI properties, our curiosity brought us to investigate the performance of APMI dyes in photoacoustic imaging setups. Upon absorption of pulse NIR light, the generation of mechanical ultrasound signal was measured with commercially available Vevo® LAZR-X from Fujifilm Visualsonics thus giving insight on the role of APMI dyes in generating PA signals. The device measured a PA signal in the range of 680 nm in higher intensity for **3.33**, **3.35** and **3.36** in respect to ICG green, in particular **3.33**, gave a signal that was surprisingly higher in respect to the fluorophores presenting a chemical bridge between the nitrogen atoms in the peri positions (Table 3). These observations suggest that the bridging unit installed between the *peri*-nitrogen may limit the vibrational deactivation pathway after photon absorption, rigidifying the fluorophore structure. We suppose the rotation and vibration of the functional groups installed on the peri positions may promote the reduction of the dye quantum yield and the increase of vibrational energy release after-photon absorption. These considerations agree with the findings of Gao et al.[129] where it has been demonstrated that the PA signal is related to the intramolecular motions of the cromophore. Vibrational deactivation is associated to thermal to acoustic conversion resulting and in PA signal modulation. To summarize our findings, we synthesized APMI chromophores as NIR active contrast agents for *in vivo* applications thus demonstrating their utility as cellular stains for longitudinal imaging studies that may have a role in cellular immunotherapies. The chromophores also showed to be highly photostable and water soluble thus effective contrast for *in vivo* angiography. We successfully performed the *in vivo* angiography of the main

abdominal splanchnic organs and evaluated the possible implications and outcomes the chromophores may have in upper and lower gastrointestinal tract surgery, I propose APMI dyes as novel photostable candidates in fluorescence guided surgery for real time assessment of intestinal perfusions and hepatic function assessment in in hepatobiliary surgery. In addition, I evaluated the performance of APMI dyes in photoacoustic imaging devices as good sources of ultrasound signals and demonstrated the release of a photoacoustic signal. This evidence may have implications in photoacoustic imaging technology as APMI dye showed to be a performant PA signal emitter prior to modification of *peri* nitrogen atoms. In conclusion by taking advantages of the optical properties like red shifted emission in the NIR and large Stokes shift together with improved photostability, I propose APMI dyes as valid alternatives to cyanine-based contrast agents for *in vivo* applications in FGS ranging from cell tracking for cellular immunotherapies and contrasts for *in vivo* angiography and photoacoustic imaging devices.

Chapter 4 Preparation of NIR absorbing pH responsive activatable ON-OFF silicon rhodamine dyes

NIR always ON probes are the most used contrast agents in FGS clinical settings, nevertheless, their light signal cannot clearly define the tumor margins and boundaries on the fluorescence image as most of unbound probes on the tissue of interest are not completely cleared by bloodstream[52]. To improve the target to background signal and enlighten the boundaries between healthy and diseased tissue, activatable dyes have been developed[3]. Depending on their activation mechanism, activatable probes turn their state from an OFF non fluorescent to an ON-fluorescent state. Probes of this type are also called ON-OFF probes[45]. Signal activation in ON-OFF probes can be achieved in different ways as described in section 1.5, between them, photo induced electron transfer (PeT) is commonly used to improve the signal to background ratio at the specific probe accumulation site[54]. This mechanism has the advantage that it does not require the presence of a second molecule acting as a quencher. In short, a probe that works with PeT possess a functional group with a low oxidation potential that can transfer an electron to the fluorophore that generally possess a high reduction potential[54]. The photo induced electron transfer can be used to study the physiological pH and the dielectric constant of the media[130-136]. Once reached the target, the probe turns to be fluorescent and emit the fluorescence signal. Activatable probes outside the region of interest does not emit light and therefore they do not represent a limit in the detection of tumor margins. For this reason, activatable probes emitting in the far red (650-700 nm), offer a versatile option to be used simultaneously in the same operational set-up with commercially available 800 nm active NIR probes like those belonging to the cyanine family[112]. CypHer5E® (Compound **4.0**) (Figure 68), for example, is a well-known commercially available activatable cyanine ON-OFF probe that presents a fluorescent activation threshold associated with its pKa value in aqueous media. According with the specifications described by GE Healthcare® company, CypHer5E® pKa was designed to lie in the physiological range (pKa 7.3)[137, 138] (Figure 68).

Figure 68 Chemical structure of commercially available CypHer 5 ® and its protonation deprotonation equilibria showing a pKa in the physiological range (7.3)[138]

Silicon rhodamines are another class of activatable dyes emitting around 655-700 nm, they are highly water soluble, possess high extinction coefficients as well as high quantum yield in aqueous media[79]. The facile modification of the rhodamine scaffold give access to pH responsive probes based on photo induced electron transfer (PeT) with a fluorescence response based on protonation-deprotonation equilibria[79]. The dye pKa is therefore crucial to determine the fluorescence activation threshold (Figure 28)(Figure 69)[79].

Figure 69 Chemical structure of a pH responsive silicon rhodamine dye with fluorescence activation threshold dependent of protonation-deprotonation equilibria on the nitrogen atom.

Activatable pH responsive rhodamine dyes are widely used as pH indicators in cellular experiments, in particular they have been adopted to measure the pH value of the cytosol and functional cellular compartments like endosome and lysosomes without the needs of time consuming washing steps[130]. This approach has been mostly used to track antibody internalization once the fluorescent molecule has been conjugated with the macromolecule of interest, a particular range of activation threshold have been established close to the physiological range of pH 7.4. To design an activatable dye with a response in this range, the pKa of the probe has been evaluated in the ranges associated to every stage of cellular internalization process[130, 139]. In early endosomes, pH is still very close to the physiological range (7.0-6.9) but it takes more than 2 hours for the newly formed organelle to fuse with

lysosomes where the pH is close to 4[49, 91, 92]. One of the most used compounds that have been employed to study cellular internalization process, is pHrodo® dye (Figure 17). This rhodamine dye is a well-known commercially available compound used both in *in vitro* and *in vivo* research that can be easily modified to achieve the functionalization of vector macromolecules[130]. The fluorescence response is based on specific spatial arrangements of the dialkylamino substituents on the phenyl ring installed on position 9 (Figure 70) better known as "proton sponge" to give a pKa value extremely close to the physiological range (6.8-7.4). The pKa of the fluorophore conjugated with dextran was measured through fluorescence titration techniques showing the typical sigmoidal plot of an ON-OFF activatable probe (Figure 70).
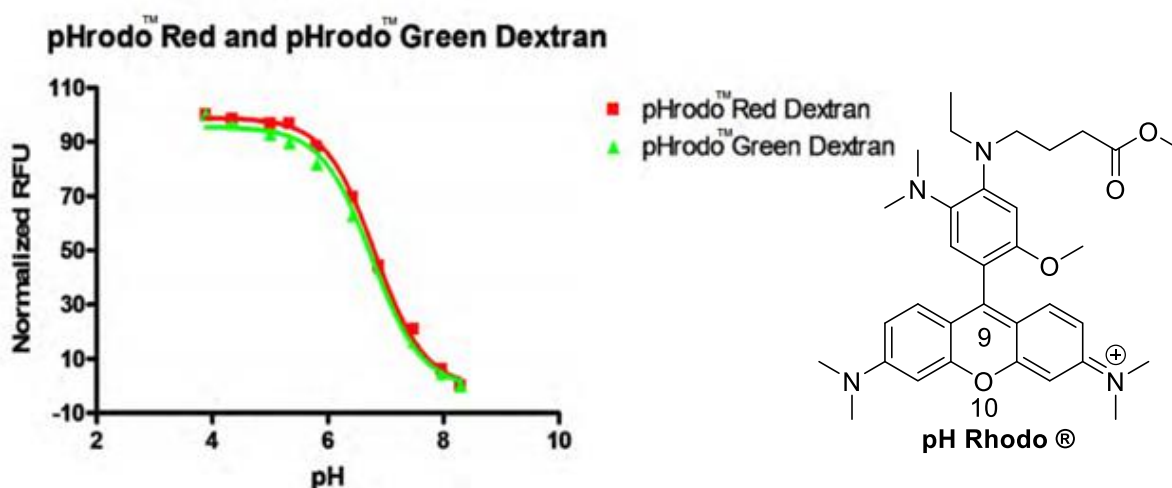

Figure 70 Sigmoidal plot showing decrease of fluorescence intensity in water of pH rodo® dye conjugated with dextran in water (pKa value measured was found to be approximately 7.0 in water). (www.thermofisher.com) (left) Chemical structure of pH rodo showing numbering system associated with the position of the oxygen atom (position 10) and the position of the phenyl ring (position 9)

Nevertheless, pHrodo®, is a rhodamine fluorophore that absorbs and emit in the visible range (585 nm) and does not present the same advantages of NIR probes such as high spatial resolution and high penetration depth in living tissues and presents limitations for in vivo imaging in FGS[57] as it is not compatible with commercially available dual imaging devices like those described in the work of Tanaka et al.[98] (Chapter 2) . In this work, the synthesis of a modified version of commercially available pHrodo® dye patented by Invitrogen® has been achieved. In particular, I kept the same spatial arrangement of substituents on the phenyl ring of the commercially available analog, and I installed a dimethyl silyl function on position 10 of the rhodamine scaffold (Figure 71). The fluorophore resulted fluorescent in the NIR with emission maxima on 675 nm. This result is of great importance as it is in accordance with the

data described by Fu et al[77]. (section 1.7)(Figure 27) where the substitution on position 10 with a silicon atom on a rhodamine dye scaffold, gives a bathochromic shift of 90 nm in the emission[77] (Figure 71) this value resulted close to the emission wavelength of FDA approved Methylene Blue (Figure 35). Subsequently, I evaluated the dye pKa by fluorescence titration techniques and I found it to be in the desired physiological range (7.4). I also modified the chemical structure to install bioconjugation linkers targeting primary thiols of cysteines, antibodies and small peptides. Cysteine modification on macromolecular vector molecules has been used for decades as the method of choice for site selective protein labelling thus, overcoming problems associated with the unwanted modification of the antibody binding regions[140]. Maleimide systems has been used in this context as useful terminal reactive moieties in antibody-drug conjugates and optical probes[141-143]. Maleimide systems presents anyway several associated drawbacks like the hydrolysis of the thiosuccinimide adduct in aqueous media[144]. I focused my attention on the installation of allyl linker to be used for UV-mediated click thiol-ene coupling reactions (TEC)[145, 146]. The installation of an allyl linker provides a functional group for the functionalization of antibodies or small cysteine containing peptides in mild aqueous conditions using UV light. The reaction proceed through a radical mechanism mediated by UV light and proton abstraction from a thiol functional group and further addition to the terminal double bond as explained in Scheme 21[145, 147, 148].

R_1= Cysteine containing peptide or antibody
R_2= Fluorphore containing an allyl linker
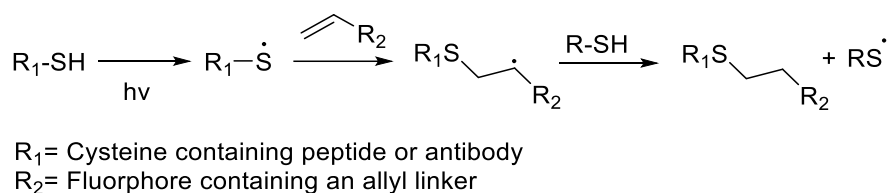
Scheme 21 Click Thiol-ene coupling radical mechanism in water used to perform fluorophore antibody conjugation.

In this chapter I provide the description of the synthesis of silicon rhodamine probe based on the selective modification of pH rodo® target structure on position 10 as described in Figure 71. And on the installation of the allyl linker toward the functionalization of cysteine containing macromolecules. (Figure 71).
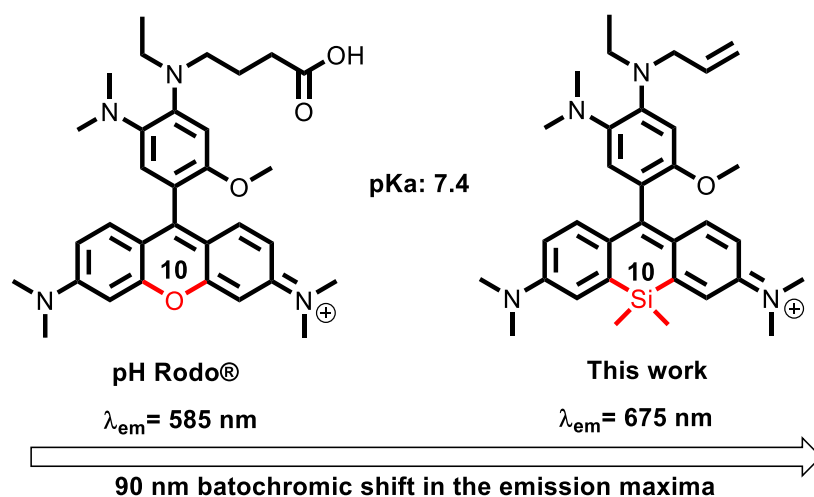
Figure 71 Modification of the pHrodo® target structure (right) on position 10 with a dimethyl silyl function giving the target structure (left) showing a bathochromic shift in the emission of 90 nm from the commercially available analog. The dye also possesses an allyl linker to be used in thiol-ene coupling reactions to label and functionalize antibodies and cysteine containing short peptides.

4.1 Synthetic design of NIR emitting pHrodo® analogs based on substitution of position 10 oxygen with a dimethyl silyl function.

4.1.1 Synthesis of pH responsive silicon rhodamine compounds

The target compound was designed as silicon rhodamine dye that mimic the structure of commercially available pHrodo® dye. Target Compound **4.33** is depicted in (Figure 72), it is designed to have a fluorescence activation threshold in the physiological range (pKa 7.4), it possess a proton sponge system and an allyl linker for suitable for UV mediated thiol-ene reactions in water for the functionalization of cysteine containing antibodies and small peptides (Figure 72).
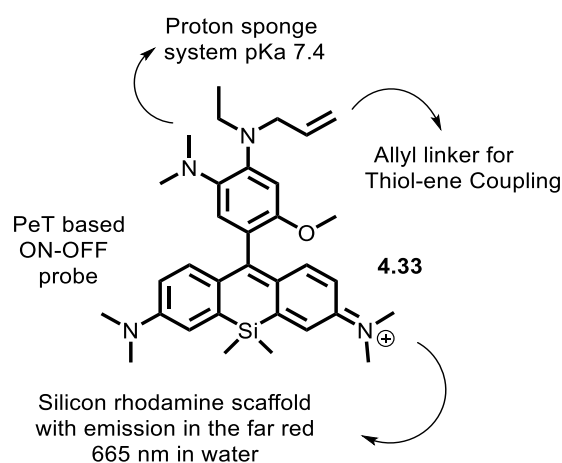

Figure 72 Target compound **4.33** with a description of the functional groups.

Retrosynthetic analysis of target Compound **4.33** (Scheme 22) is performed through the disconnection of the C9-C1' biaryl bond between the xanthene scaffold and the phenyl ring installed on position 9 (Scheme 22). Target tetrasubstituted bromo benzene **4.32** was identified as key synthetic intermediate bearing two N,N dialkyl amino groups ortho to each other (proton sponge) and, between them, an allyl linker to be used under TEC conditions was selected. Compound **4.34** was prepared from 4-methoxy-N,N-dimethylaniline Compound **4.32**. Silicon xanthone **4.10** was synthesized in 4 steps from biaryl silane **4.13** according to the procedure described by Butkevic et al.[89] (Scheme 15). The adopted synthetic route is depicted in Scheme 23
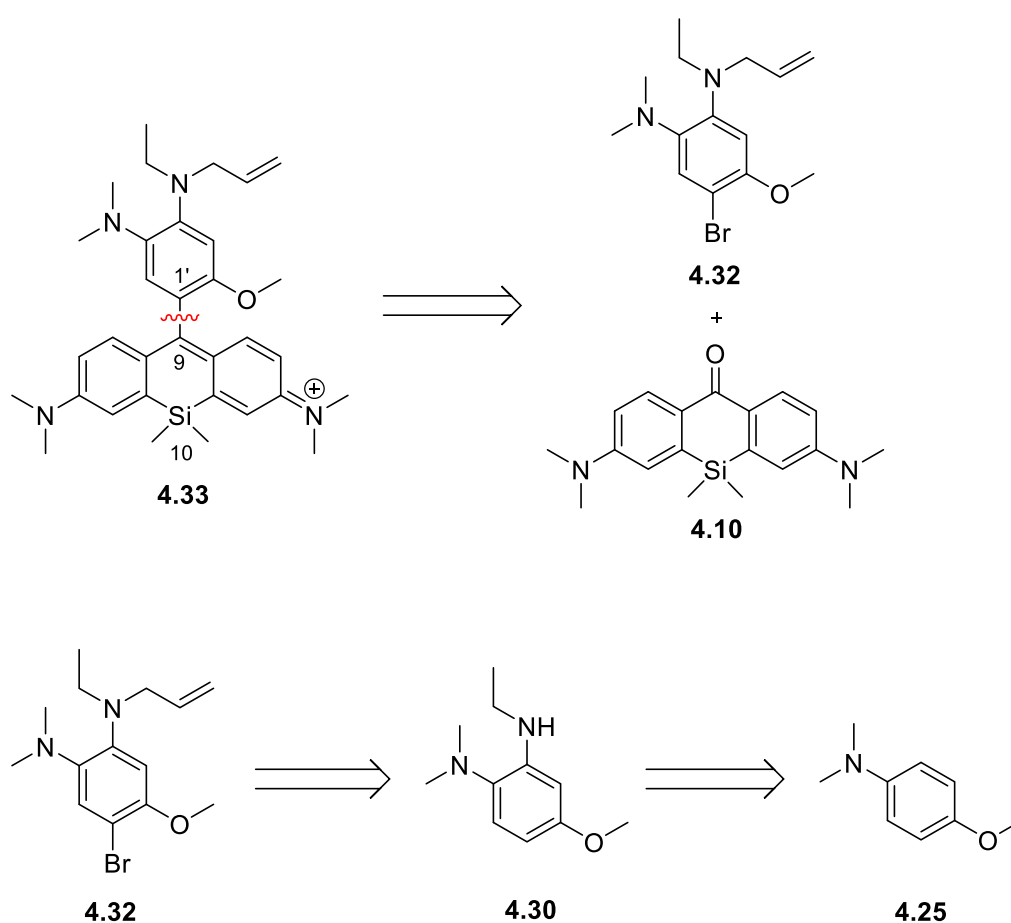

Scheme 22 Retrosynthetic analysis from disconnection of the biaryl bond C1'-C9 between the xanthene scaffold and phenyl ring installed on position 9.
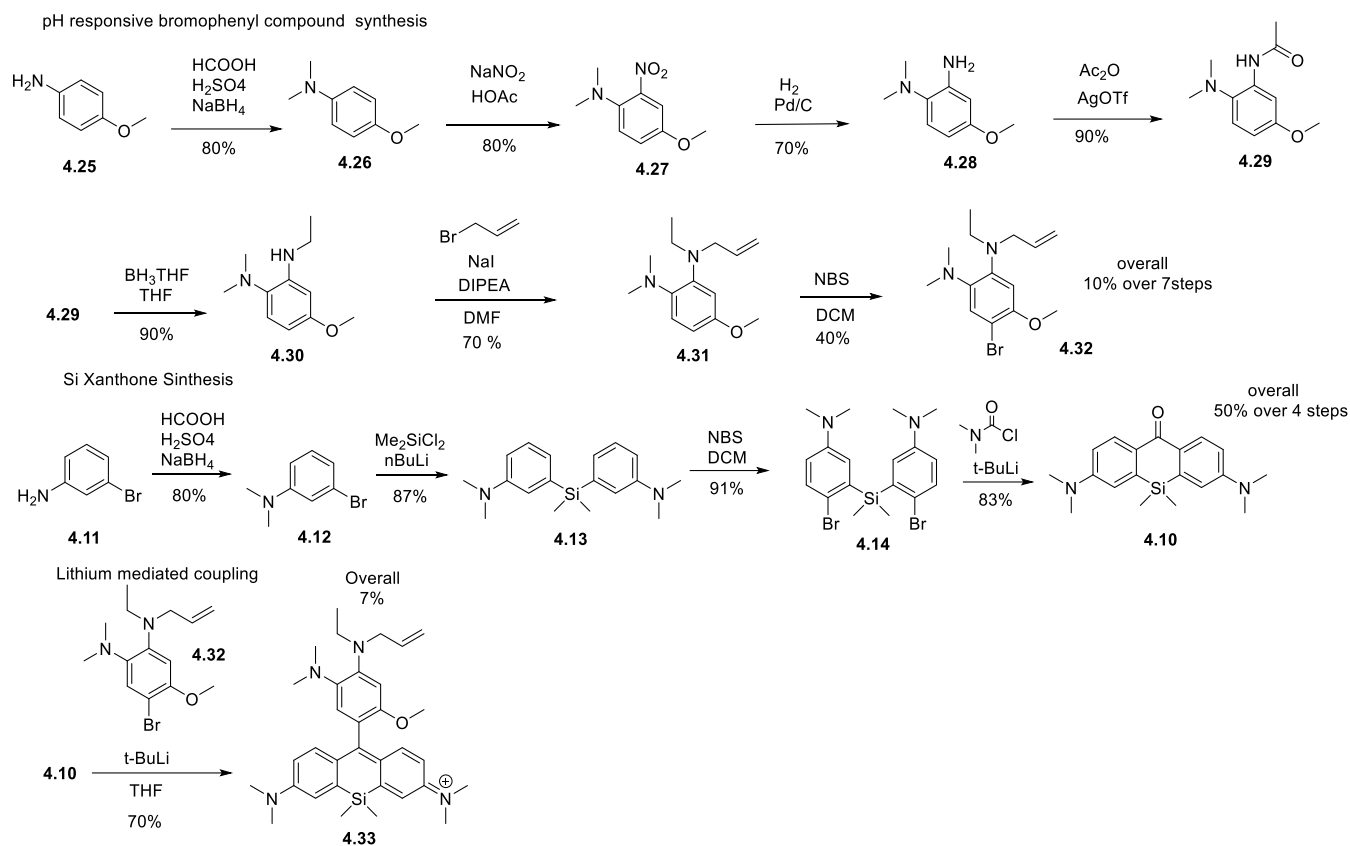
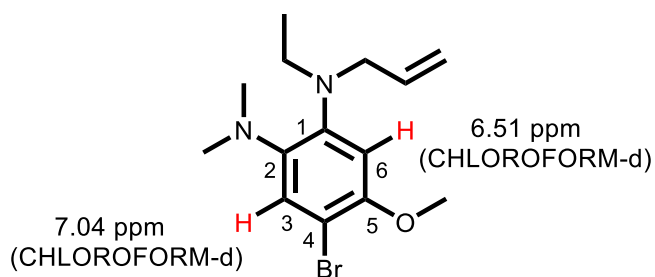Scheme 23 Adopted synthetic route providing silicon rhodamine **4.33**

Bromobenzene **4.32** (Scheme 23) was obtained in 7 steps (10% yield overall) from commercially available para anisidine **4.25**. The synthetic route starts with Compound **4.25** that undergoes reductive amination with sodium borohydride and formaldehyde in aqueous H_2SO_4 solution giving **4.26** in 80% yield[86]. Further nitration in water and acetic acid with sodium nitrite, gave **4.27**. Nitro group reduction in methanol under hydrogen atmosphere with palladium on supported carbon gave **4.28**. Mono alkylation of the free amino substituent was achieved in two steps, first, through acetylation with acetic anhydride in presence of catalytic amounts of AgOTf[149] giving **4.29** and subsequently through reduction with BH3 in THF under argon atmosphere giving **4.30**. A second order nucleophilic substitution reaction (SN_2) on the secondary amine of **4.30** with allyl bromide and sodium iodide in presence of DIPEA in DMF was performed to give **4.31**. In the next step, NBS was used to achieve regioselective bromination on position 5 of **4.31** giving **4.32** in 40% yield (Scheme 24).
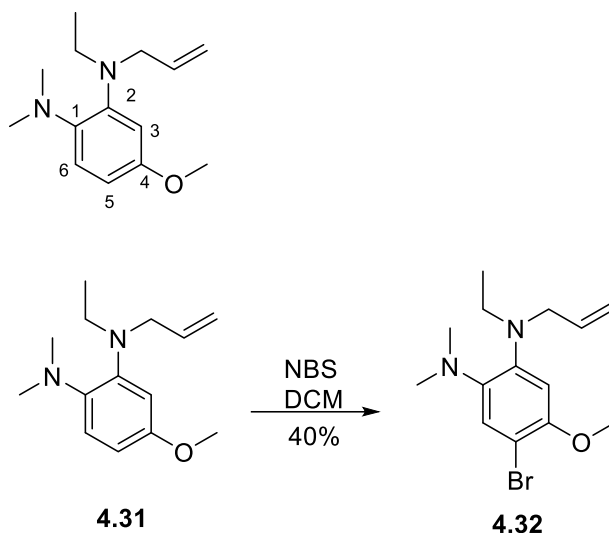
^{1}H NMR of Compound **4.33** shows the typical peaks of the aromatic protons para to each other of a tetrasubstituted aromatic compound on positions 1,3,4,5 (Figure 73; Figure 74).

Tetrasubstituded bromobenzene Compound 4.32

Chemical Formula: $C_{14}H_{21}BrN_2O$
Exact Mass: 312.08
Molecular Weight: 313.24

Figure 73 Chemical structure of tetrasubstituted bromobenzene Compound **4.32** with its numbering system. The protons para to each other are reported in red with their ppm value found in the ^{1}H spectrum in CHLOROFORM-d.
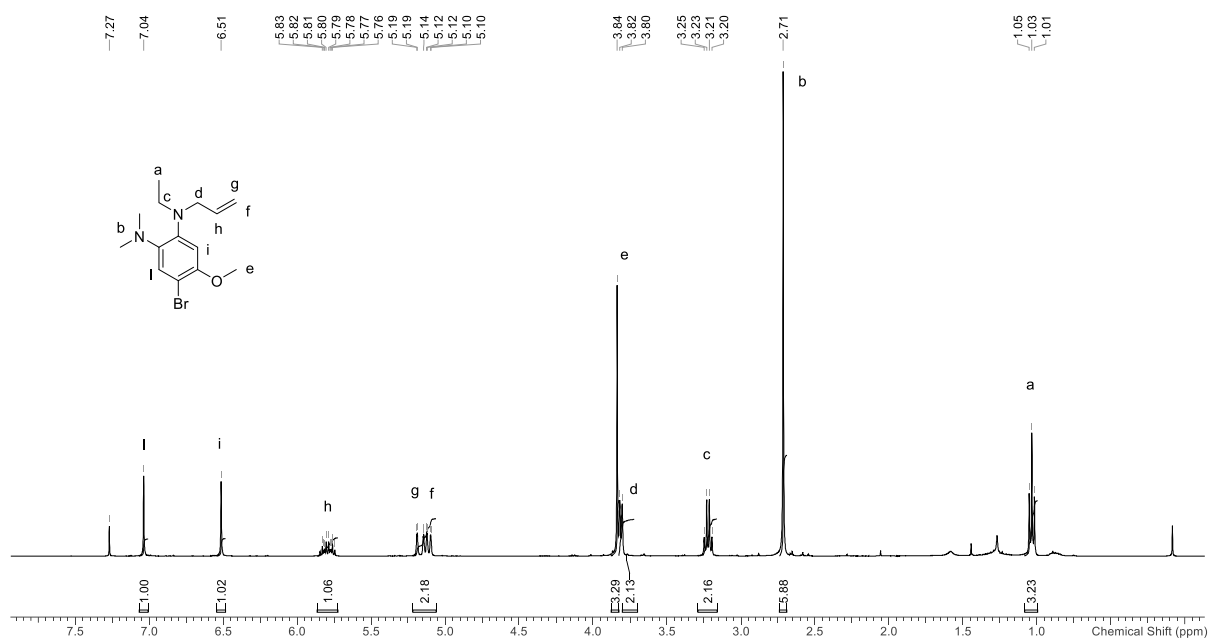
Figure 74 Experimental ^{1}H spectrum of **4.33** N1-allyl-4-bromo-N1-ethyl-5-methoxy-N2,N2-dimethylbenzene-1,2-diamine CHLOROFORM (400 MHz)

^{1}H-^{1}H COSY spectrum of Compound **4.32** show no coupling between the aromatic protons (Figure 75)
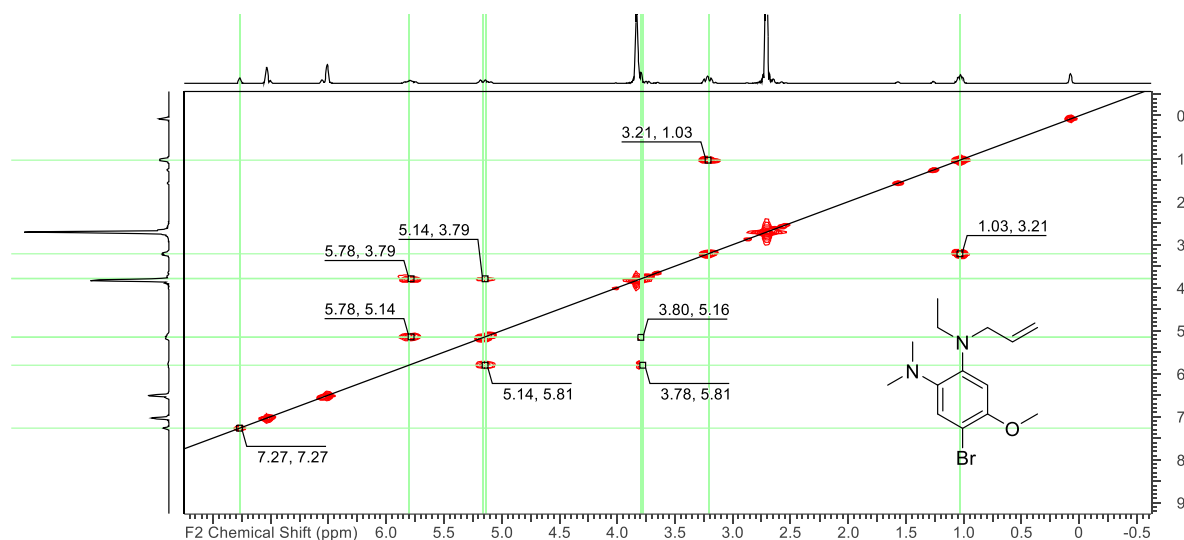

Figure 75 ^{1}H-^{1}H COSY spectrum of compound **4.32** in CHLOROFORM-d

Final coupling between phenyl lithium compound obtained from **4.32** and silicon xanthone **4.10** gave silicon rhodamine **4.33** in high yield (70%). The overall yield of the synthesis of **4.33** was calculated to be 7% over the longer linear sequence (Scheme 23). To explain the formation of compound **4.33**, I suppose that the phenyl lithium nucleophile is formed under lithium-halogen exchange conditions in THF at -78 °C and undergoes addition to the ketone function of xanthone compound **4.10**.
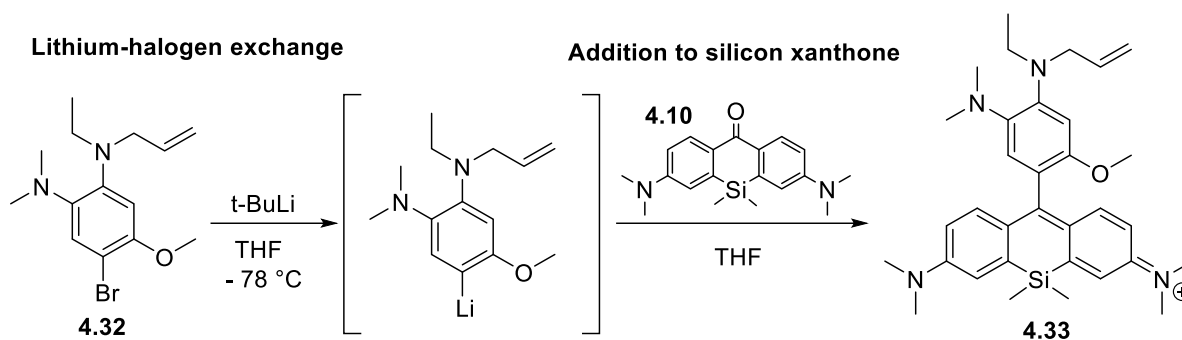
Scheme 25 *In situ* formation of a phenyl lithium nucleophile from lithium halogen exchange on substrate Compound **4.32** and further addition to the ketone function of silicon xanthone Compound **3.10.**

The molecular structure of **4.33** was confirmed by ^{1}H NMR spectroscopy, mass spectroscopy, and HPLC analysis (Chapter 6. Experimental section) ^{1}H NMR spectra of compound **4.33** is shown in Figure 76.
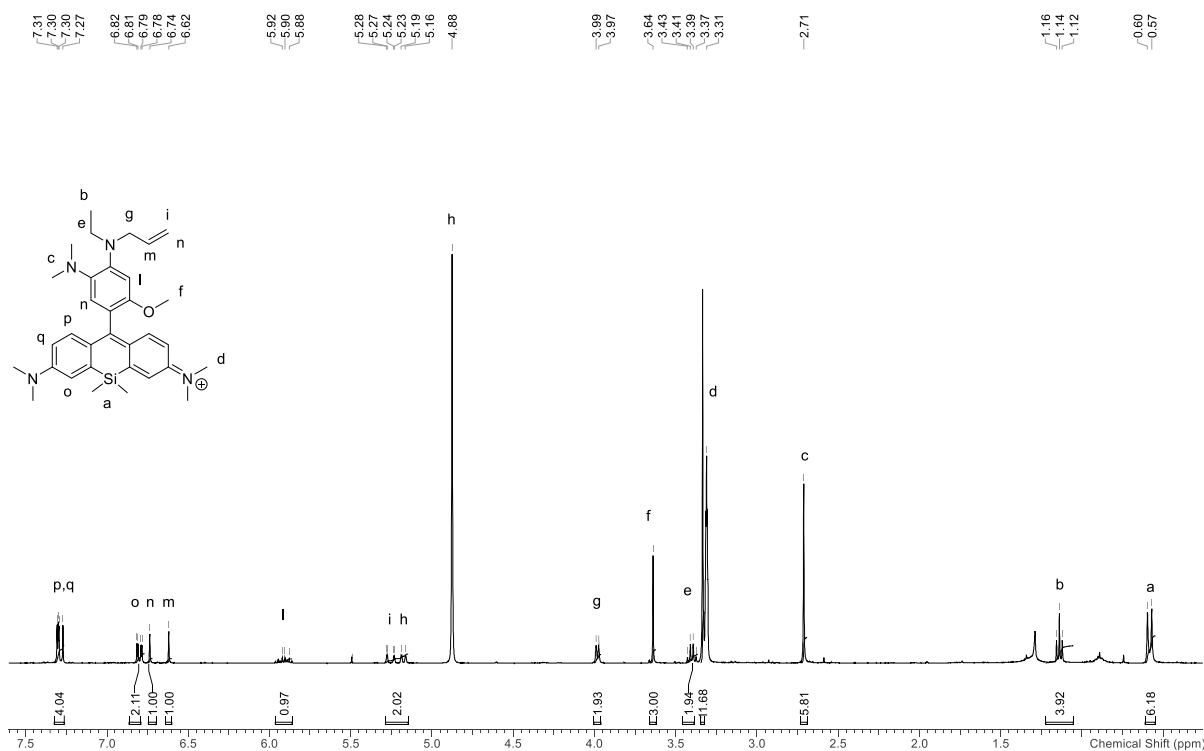

Figure 76 ^{1}H NMR spectrum of **4.33** at in methanol-d at room temperature (400 MHz)

RP-HPLC analysis shows a single peak chromatogram with absorption in the far red to NIR range (655 nm) and a mass spectrum showing the peaks associated to the protonated double charged species and those associated to the single charged free basic form (Figure 77).

Chemical Formula: $C_{33}H_{45}N_4OSi^+$
Exact Mass: 541.34
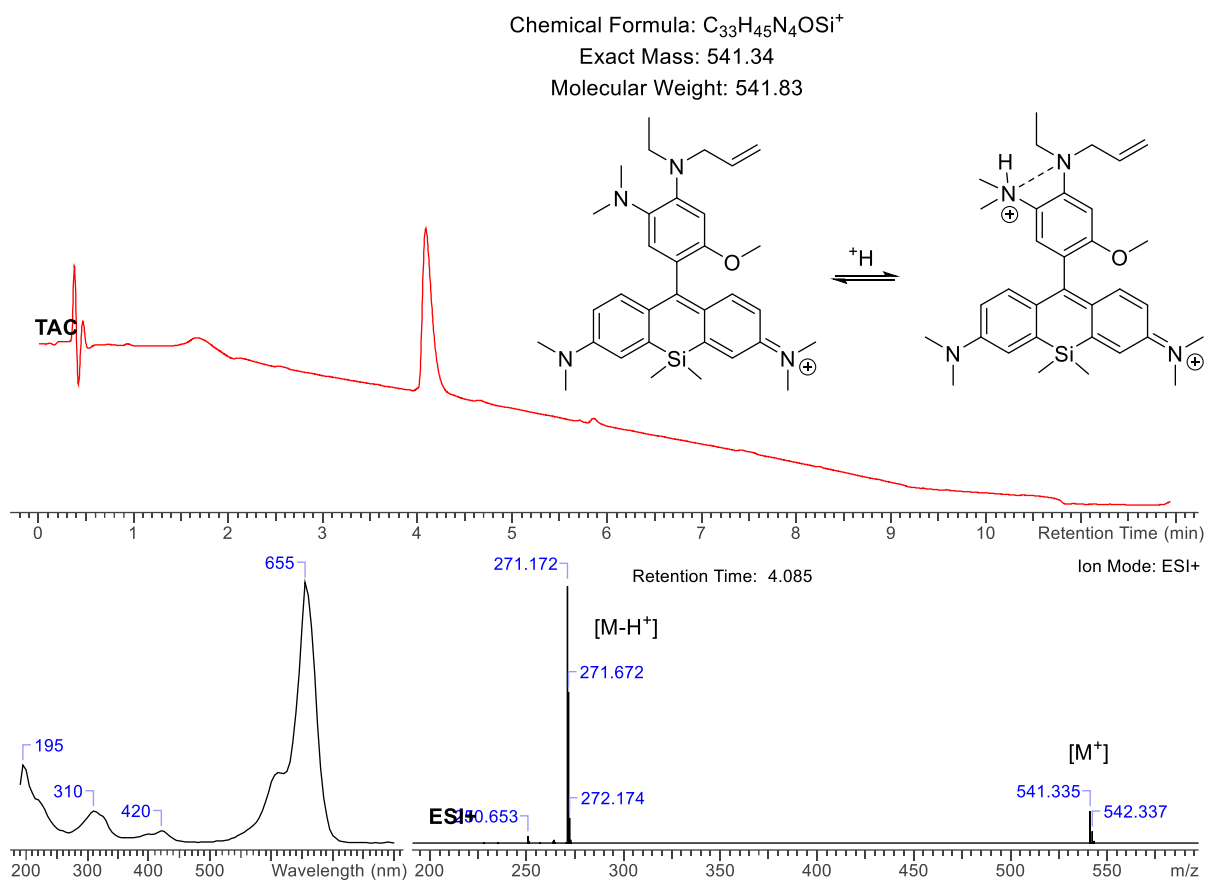Molecular Weight: 541.83

Figure 77 HPLC-chromatogram showing retention time of **4.33** (Top) UV vis absorption in the far red to NIR range (bottom left) and high-resolution mass spectrum showing the protonated double charged peak [M-H+] and the free base single charged form [M+] (bottom right). The chemical protonation-deprotonation equilibria is reported (Top right)

4.2 Spectral properties of pH responsive silicon rhodamine compound 4.33

Spectral properties of **4.33** were investigated in water in different pH buffers in water (Table 4). A slight shift of 5 nm to shorter wavelengths in the absorption has been observed for compound **4.33** from pH 1 (655 nm) to pH 10.2 (650 nm). The extinction coefficients also slightly decreased their values in basic environments (Figure 78; Table 4).

pH	$\lambda_{abs,max}$ /nm	$\lambda_{em,max}$/nm	$\varepsilon/10^4$	$\varphi_{em}(\%)$
1	655	675	3.5859	24.3
7.4	655	675	3.3314	16.09
9.2	650	675	3.0058	0
10.2	650	675	3.0000	0

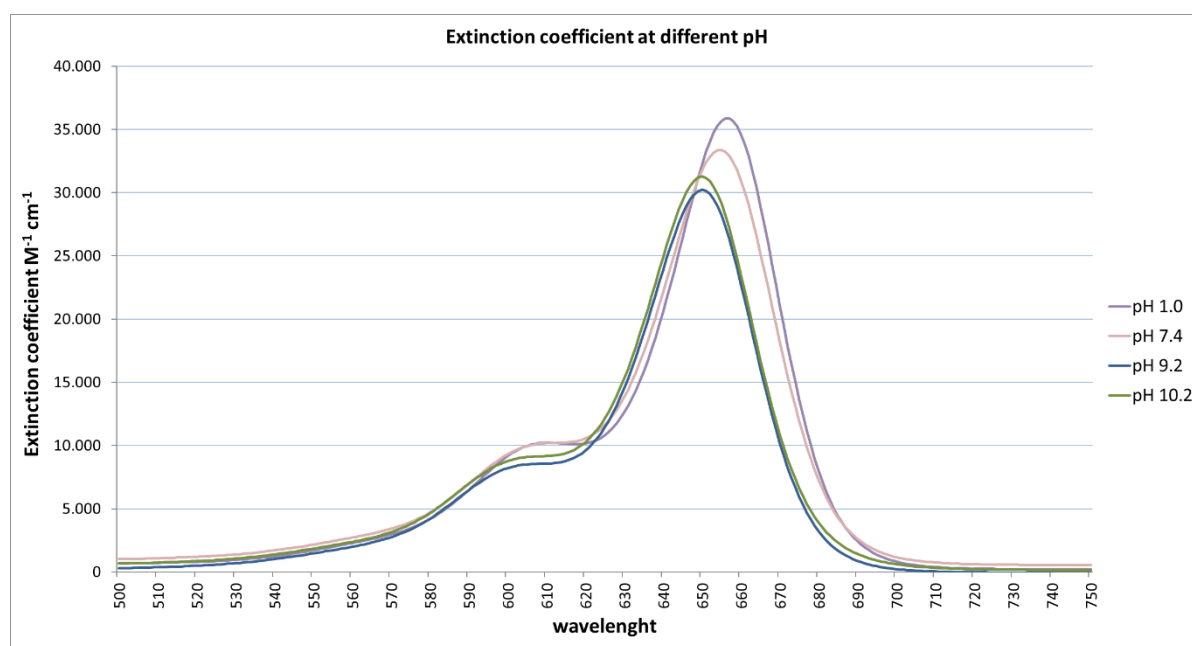Table 4 Photophysical properties of Compound **4.33** in water

Figure 78 pH dependency of the extinction coefficient of Compound **4.33** according to four different pH buffers pH **1**, pH **7.4,** pH **9.22** and pH **10.2** in water.

The emission maxima remained centered at 675 nm showing substantial decrease in emission intensity following increasing values of pH form 4 to 13 (Figure 79).
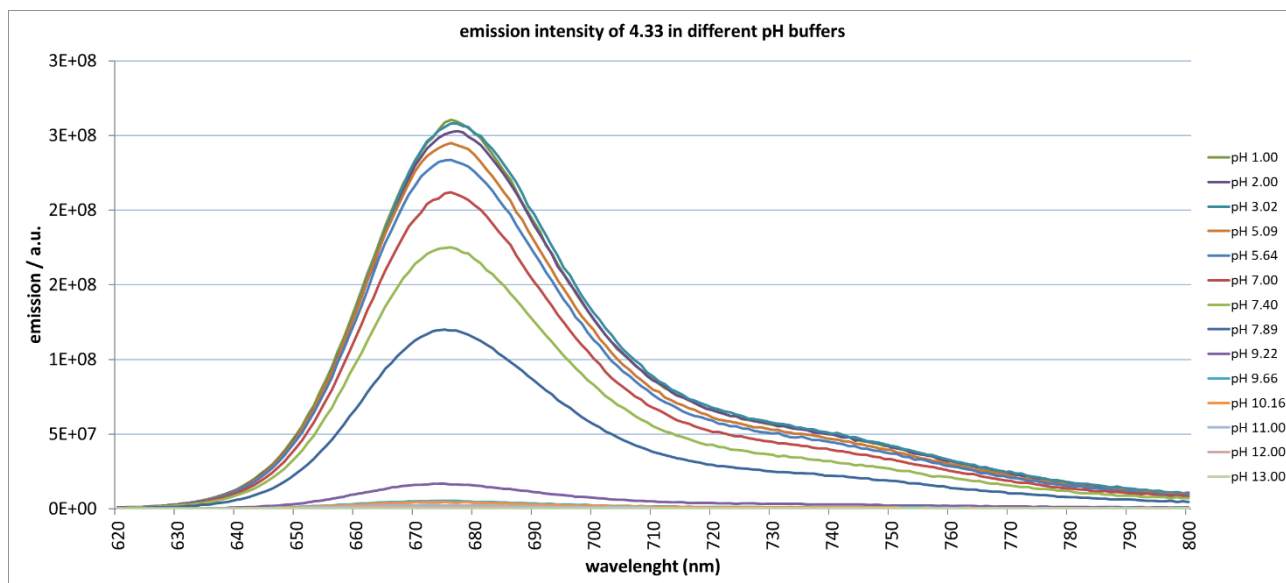

Figure 79 pH emission dependency of **4.33** in different pH buffers in water ranging from pH 1 to pH 13

Plotting the values of emission intensity versus the corresponding pH value, I obtained the expected sigmoidal plot similar to the one reported for the commercially available pHrodo® analog (Figure 70) predicting a pKa value of 7.4 (Figure 80).
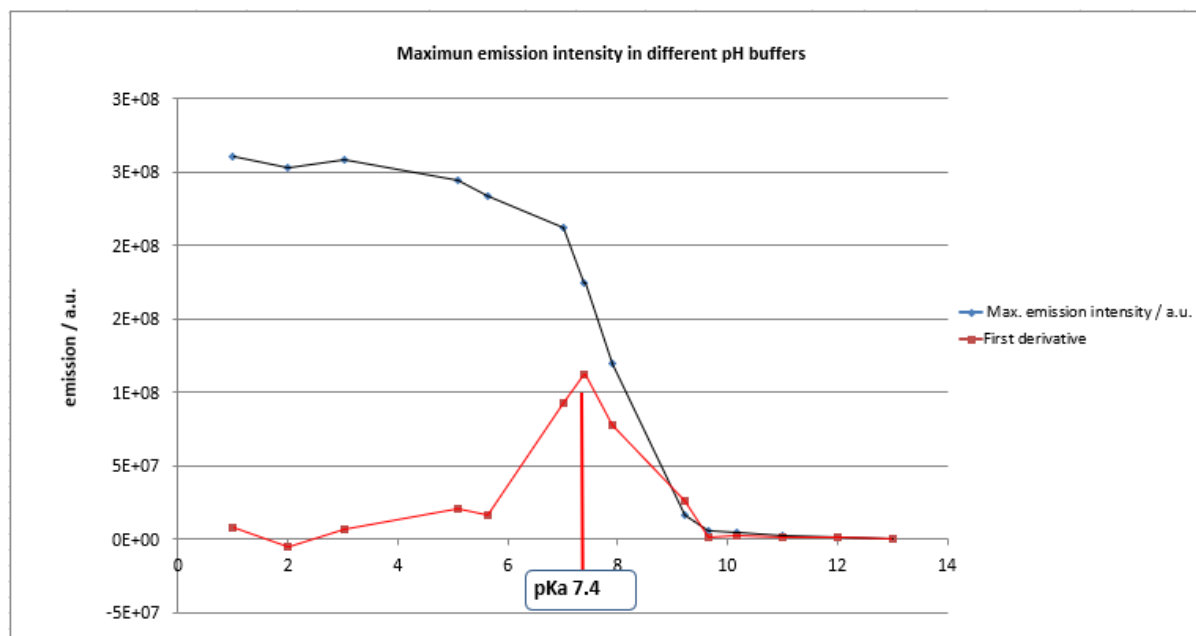

Figure 80 Sigmoidal plot of the emission intensity obtained with fluorescence titration techniques of **4.33** showing the calculated value of pKa 7.4 in the physiological range.

The emission quantum yields respect the behavior of a pH responsive activatable dye regulated by photo induced electron transfer mechanism. Emission QY start from from 24.3 % (pH 1) to 16% at physiological range (pH 7.4) and finally to 0% at pH 9.22 (Figure 81).
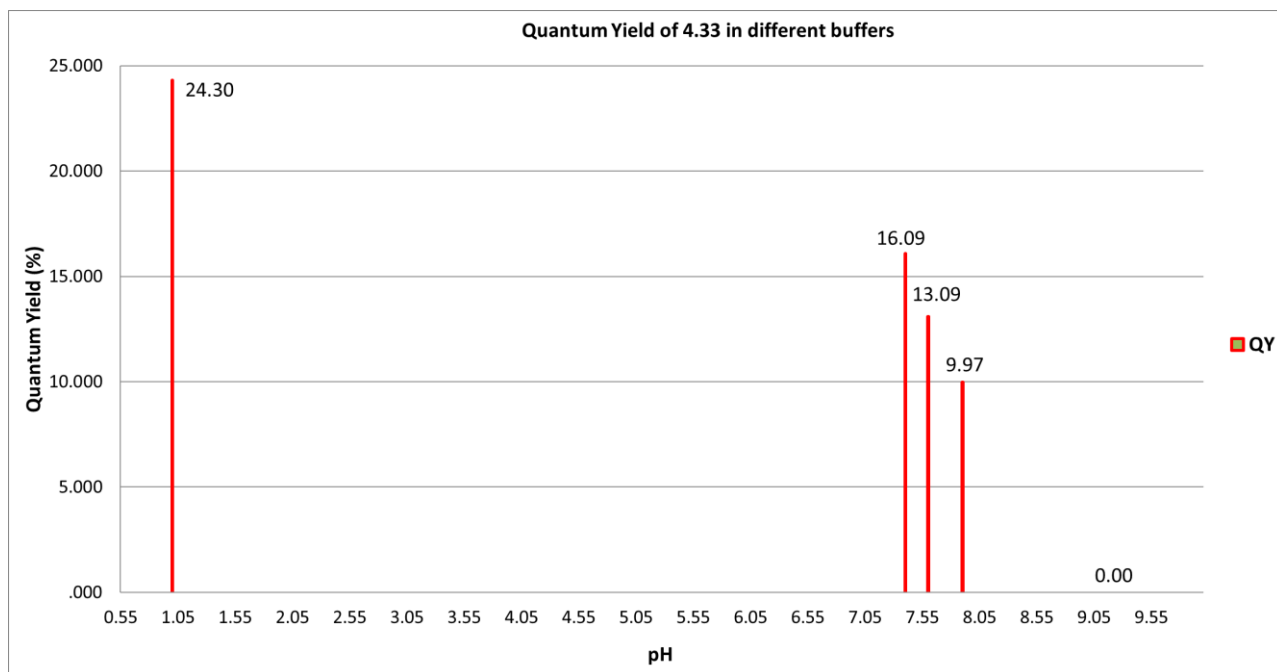

Figure 81 Quantum Yields of **4.33** in different pH buffers at pH 1.00 (24%), pH 7.40 (16.09%), pH 9.22 (0%).

4.2.2 Study on H-dimer formation

Commercially available dyes based on xanthene structure like OrgG® Alexa488® RhodG® R6G® TAMRA® Alexa568® ROX® TexRed® undergo H-dimer formation at a concentration range greater than 0.005 mM[150]. When conjugated to proteins, an increase in absorbance of the higher energy transition band and a decrease of the lowest energy transition band occurs (Figure 82). This phenomena has been ascribed to the formation of H-dimers after protein labelling that consists of dye pairing in dimers on the protein conjugation site[150] (Figure 82). Aggregation phenomena of fluorophores conjugated to proteins give the possibility to exploit the fluorescence quenching mechanism based on H-dimer formation at the concentration levels typically used for imaging experiments (10^{-6}M). H-Dimer formation has been used for the preparation of macromolecular activatable probes, as explained in section 1.5, based on dye dissociation equilibria upon protein denaturation or conformational change or in cellular internalization experiments[51].

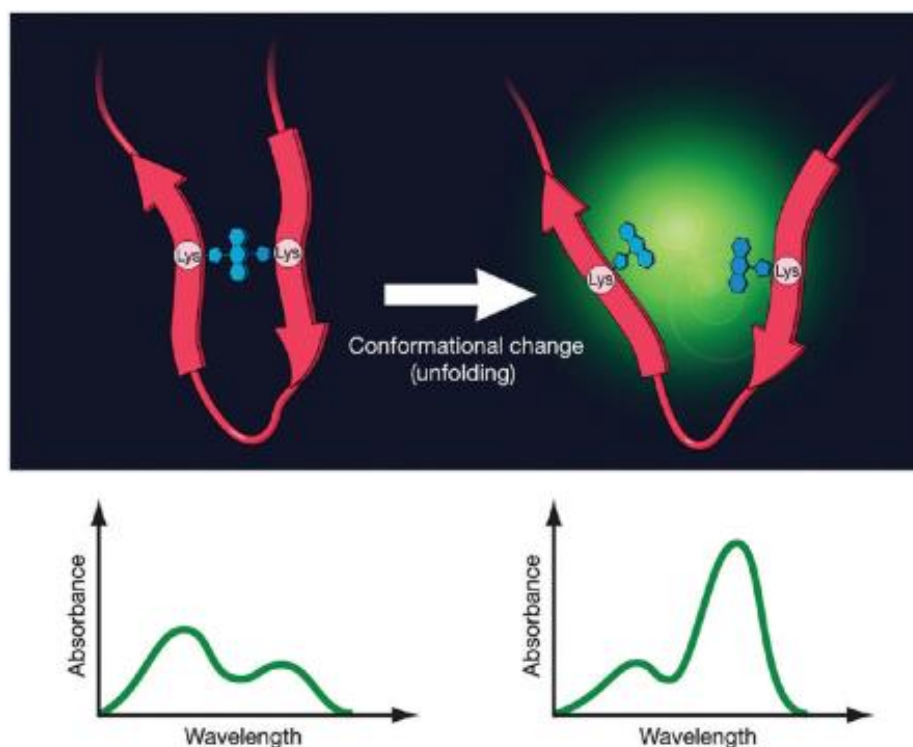Figure 82 Image showing proximate clustering of dyes on proteins conjugation site resulting in H-dimer formation (top) and effect of the formation of H-dimer on the dye absorption profile (bottom) When two dyes undergo association of the Head to head type (H-dimer) a decrease of the low energy peak (long perk) and an increase of the high energy peak (short peak) occur. Picture from the work of Ogawa et Al.[151]

The behaviour of **4.33** in concentrated aqueous solutions has been studied to test the capability of **4.33** to form H-dimers. This study has been conducted to set the basis for future tests on protein conjugates. I measured the absorption of **4.33** in concentrated aqueous solution (Figure 83) and plot the absorbance at the low energy peak 656 nm (Long peak) of **4.33** against the concentration values. I selected a range from 0.03 mM to 0.60 mM.
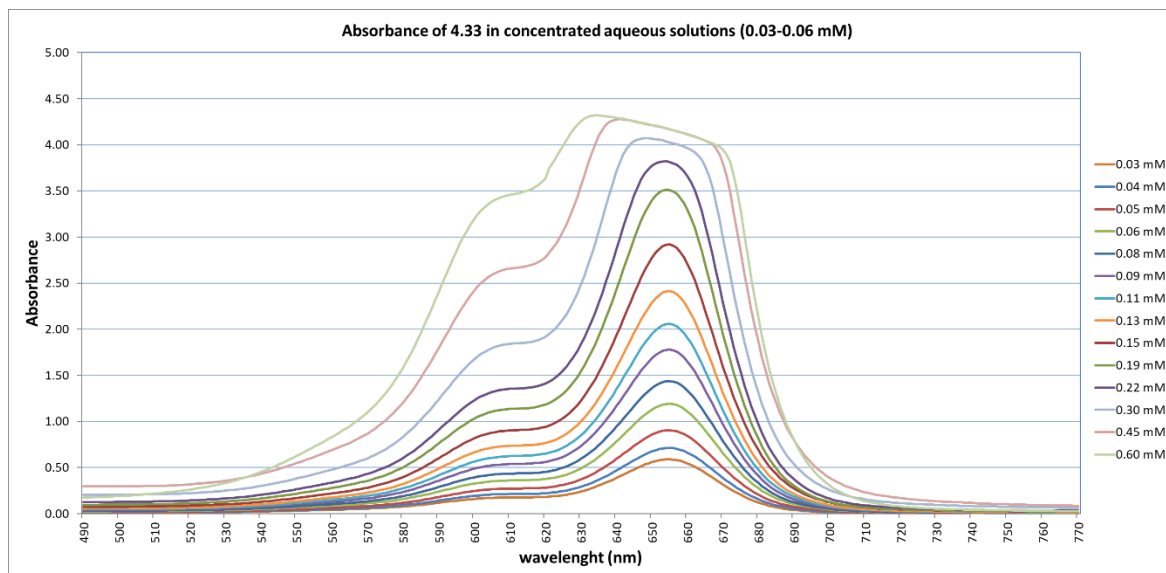

Figure 83 Absorbance of **4.33** in concentrated aqueous solution at pH 7.4. Concentration values are selected ranging from 0.03 to 0.60 mM.

I found that Lambert-Beer law was respected until the concentration range of 0.2 mM where a substantial deviation from the linearity was observed (Figure 84).
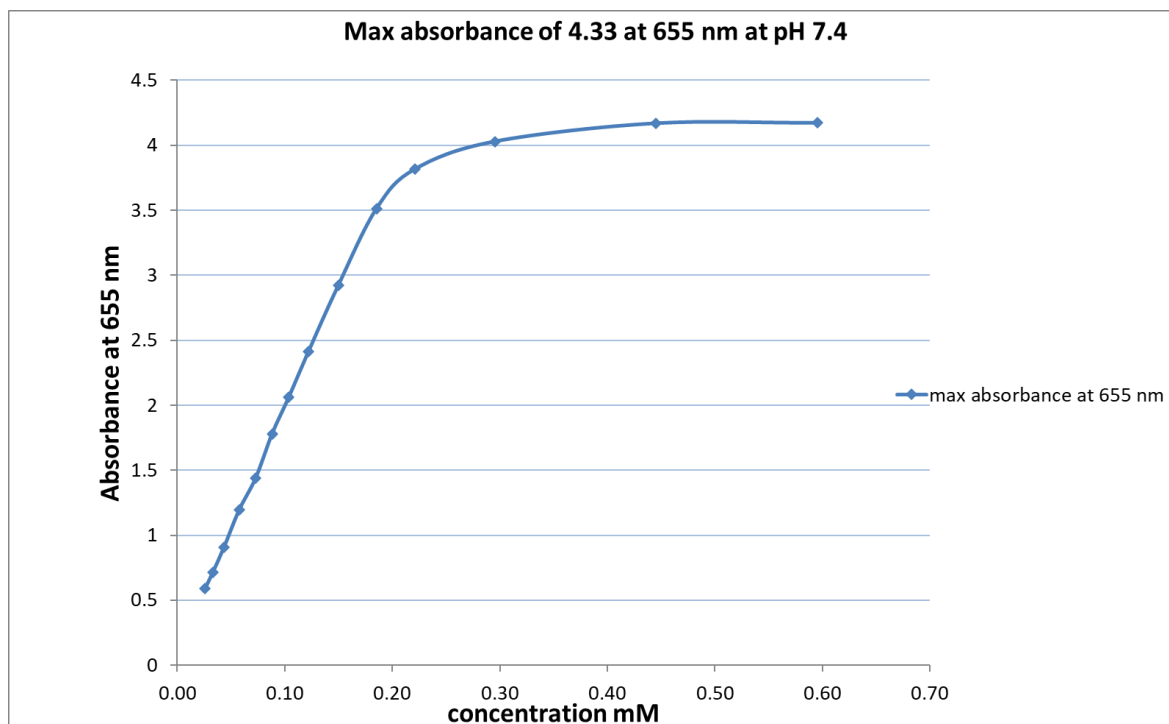

Figure 84 Maximum absorbance of **4.33** at 655 nm (long peak) in water pH 7.4 in concentration range from 0.004 mM to 0.7 mM showing a substantial deviation from the Lambert Beer law from concentration 0.2 mM.

Based on my observations, I also plotted the absorbance values corresponding to the high energy shoulder at 604 nm (short peak) against the same concentration range and I determined a linear correlation until the range of 0.66 mM (Figure 85). According to the literature, this behavior is typical of absorbers undergoing aggregation phenomena of the head to head type (H-dimers)[150, 152].
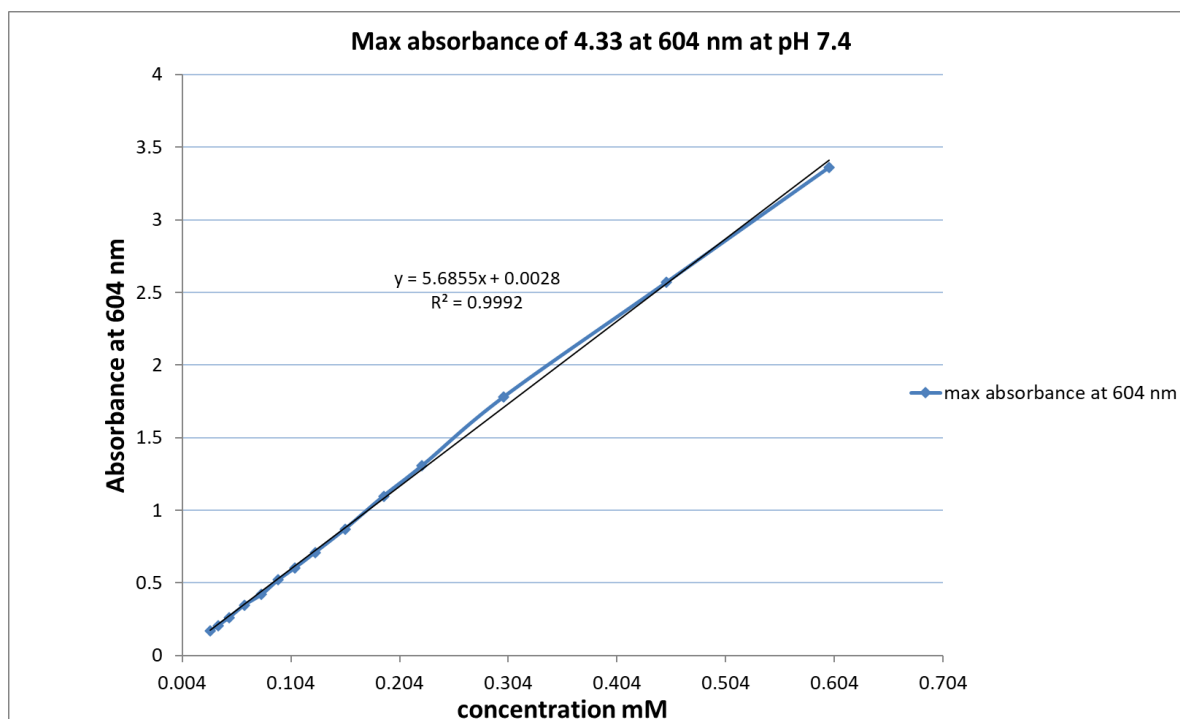

Figure 85 Maximum absorbance of **4.33** at 604 nm (short peak) measured in water at pH 7.4 in concentration range from 0.004 mM to 0,7 mM showing a linear correlation.

4.3 Results and discussion obtained with pH responsive silicon rhodamine dye 4.33

Compound **4.33** (Figure 72) has been designed as a pH responsive NIR active silicon rhodamine dye activatable in the physiological range working with photo induced electron transfer mechanism (PeT) for the labelling of vector macromolecules for solid tumors detection in high resolution. I based my research on the modification of commercially available pHrodo® dye structure on the 10th position. I hypothesized that a change with a dimethyl silyl function on this position could be responsible of an enhanced 90 nm red shifted absorption band in the far-red range (675 nm) (Figure 71) thus finding an application as contrast active on the methylene blue channel of commercially available dual imaging devices[98](Figure 34). The synthesis of Compound **4.33** confirmed the expected behavior of a NIR active probe with pH sensing properties and emphasizes the utility of the silicon atom insertion on rhodamine dye structure to shift the absorption in the NIR range of commercially available dye scaffold. In addition, the synthetic study I conducted define a robust approach for the preparation and functionalization of a silicon rhodamine dye with pH sensing properties. Measurements of the dye pKa value through fluorescence titration technique show a pKa value of 7.4 (Figure 86). This result is consistent with the findings of Vlasenko et al.[96] that reported the study of proton sponge systems on benzene and naphthalene structures[96]. The presence of two dimethyl amino function ortho to each other in benzene rings enhance the basicity of the phenyl ring in aqueous media and may find utility as proton acceptors in silicon rhodamine dyes with pH sensing properties in the physiological range. In particular, these findings has direct implications on the use of **4.33** not only in live cells imaging where it is possible to visualize internalization patterns of labeled macromolecules but also *in vivo* where it is possible to visualize tumor acidosis and acidic microenvironments thus allowing surgeons to detect narrow physiological differences between healthy and diseased tissues enlightening altered metabolism physiological state[17, 153].
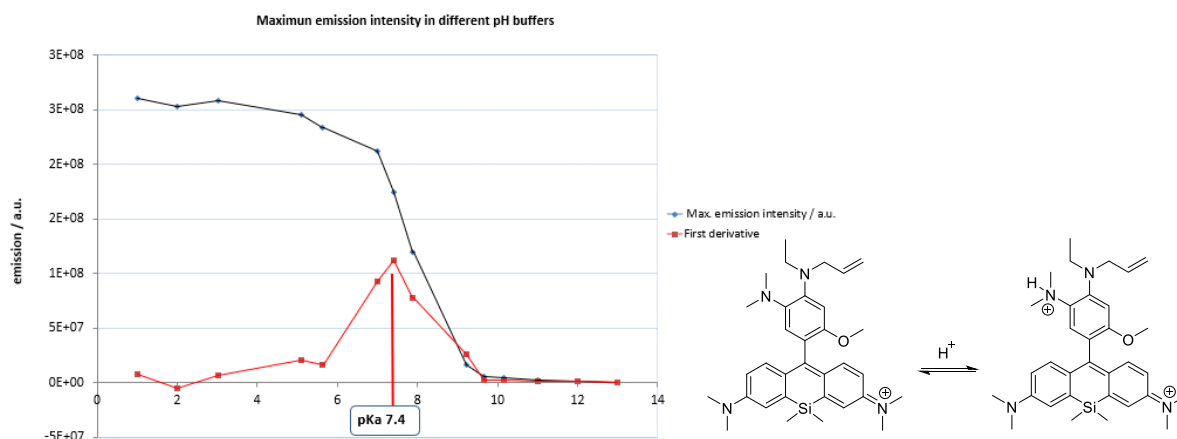
Figure 86 Protonation deprotonation equilibria of 4.33 (right) showing sigmoidal plot of emission intensity versus pH value showing calculated pKa value in physiological range 7.4 (left).

Further studies in concentrated aqueous solution demonstrates that Compound **4.33** undergoes aggregation phenomena in water forming dimers of the head-to-head type (H-dimers). In particular, I found a linear increase of the absorbance values at the high energy peak at 604 nm (short peak) giving insight on the mechanism of dye pairing in concentrated solution ranging from 0.2 to 0.7 mM. These findings may give a preliminary insight on the possibility to use **4.33** for future studies on H-dimer formation after being conjugated to proteins. In particular, this property may lead to improvements on the preparation of labeled vector conjugates with improved fluorescence quenching mechanism based on the synergy of photoinduced electron transfer and H-dimer formation. To extend the applicability of the dye to protein labelling applications, I designed **4.33** with an allyl linker for thiol-ene coupling (TEC) coupling reactions to label primary thiols on protein surface in water with the aid of UV light. As future perspective, I suggest the use of **4.33** as pH responsive dye active in 675 nm range to label cysteine containing vector molecules for the synthesis of bioconjugates targeting overexpressed antigens in solid tumors.

5. Summary, discussion, and future perspectives

Fluorophores active in the NIR are widely used in FGS as fluorescent contrast to provide real time imaging of diseased tissues and anatomical features otherwise difficult to discern like nerves, lymph nodes and vascular networks of abdominal organs[3]. Complementary fluorescent readouts are useful in precision surgery to improve tissue specific resection and to discern boundaries between healthy and diseased tissues[97]. These emission wavelengths can be used simultaneously in commercially available devices based on the detection and readout of two different detector channels[29] close to the emission wavelength of FDA approved ICG green and Methylene Blue (MB)[97]. The setting of a dual channel imager has been described in the work of Tanaka et al.[98] (Figure 34) (Chapter 2). For this reason, I worked on two different class of fluorophores perylene and silicon rhodamine dyes emitting in two different regions of the near infrared range, 770 nm and 675 nm respectively. In Chapter 3, the synthesis and application of new water-soluble push-pull perylene dyes is provided. The perylene fluorophores, named APMI dyes, were obtained with an NIR infrared emission up to up to 770 nm. The wavelength value resulted close to the ICG green channel and active on commercially available Quest medical imaging® device(Chapter 3.3). In addition, NIR emission was obtained in high quantum yield and large Stokes shift up to 130 nm in water. Large Stokes shifts are important parameters to be considered for the design of a NIR active contrast agents to improve the target to background ratio of the optical signal in diseased tissues thus, avoiding fluorophore self-quenching and inner filter effects[154-156]. In addition, it has been demonstrated that APMI chromophores possess a markedly higher resistance to photobleaching in respect to ICG green under visible light irradiation conditions. FDA approved ICG green is a well-known contrast agent used in FGS and starts to degrade after only 20 minutes showing short time resistance to degradation in clinical settings[12, 81, 157] (Figure 87) in contrast, APMI dyes combines high water solubility with the exceptional photostability of the perylene core showing resistance to degradation up to one hour. These properties make the chromophores ideal candidates for FGS applications where long irradiation conditions are needed especially during time consuming surgical operations[158]. APMI dyes were also tested on rats showing ultrabright angiography of the main abdominal cavity organs giving insight on their biodistribution through the vascular network of the mesenteric vessels and excretion profile through the bile ducts (Figure 87). In this context, an unexpected finding has also been reported using Compound **3.35**. After intravenous injection in the jugular vein, the contrast showed an ultrabright angiography of the liver and the bile ducts (Figure 61; Figure 62; Figure 63; Figure

64). These results may give insight on the role the protecting group on the *peri* nitrogen to improve the quantum yield in different biological media like the bile during excretion in the duodenum and open new possibilities for the use of the contrast in gastrointestinal surgery especially in cholangiography, cholecystectomy and in liver function assessment[11, 116, 159]. In addition to those experiments, cell permeability of APMI dyes has also been evaluated. The chromophores proved to be highly cell permeable and able to stain CD+ macrophages thus giving insight on the possible use of APMI dyes as contrast for *in vivo* live cell tracking[109]. This experiment shows APMI chromophores to have possible potential outcomes in cellular immunotherapies where the isolation of tumor responsive T cells from the peripheral blood of patients, their *ex vivo* expansion and direct infusion, is used to elicit antitumor response[109]. One of the main limitations in clinical translation of cellular immunotherapies, is the limited availability of non-cytotoxic NIR contrast agents to track cell movements in their natural environments in real time with high spatial and temporal resolution, for this reason, there is a constant need of NIR emitting dyes to track post transferred therapeutic cells[109]. NIR imaging has emerged as the most sensitive technology to track small population of labelled therapeutic cells (<10 000 cells)[109]. Contrast agents nowadays used in the clinics are based on heptamethine carbocyanine scaffold and possess negatively charged groups to limit the aggregation phenomena and improve water solubility. Anionic dyes cannot penetrate cell membrane in an energy independent manner therefore are not recommended as cellular staining agents[109]. Vendrell and coworkers proposed the first series of photostable cationic tricarbocyanine N-triazoles as potential label for therapeutic T cells[109]. This approach showed that positively charged fluorophores can efficiently penetrate cells membranes and can be used as labels for therapeutic T cells *in vivo*[109]. APMI dyes are basic water-soluble compounds bearing positively charged N,N diethyl amino groups, they resulted non cytotoxic cell permeable and optimal candidates to track therapeutic CD+ cells in mice. Therefore, they have been presented as a valuable alternative to cyanine dyes in this application field (Figure 87). Another potential application of APMI dyes has been evaluated in the field of photoacoustic imaging. This class of dyes showed the ability to absorb pulsed NIR light and release a photoacoustic PA signal active on commercially available ultrasound transducers. As a result, APMI dyes demonstrated to be successful candidates in photoacoustic imaging technology from Vevo®-LAZR-X from Fujifilm Visualsonics®. The performance of APMI dyes has direct implication and impact for the visualization of exogenous absorbers *in vivo* after intravenous injection. Photoacoustic technology is entering nowadays in the clinics because of higher penetration depth of the PA signal that may achieve centimeter depths[160]. In addition, acoustic signal scatters 100 times

lesser than optical signals thus allowing long term longitudinal monitoring of the imaging contrasts over time in high temporal and spatial resolution[160]. Therefore, APMI dyes can be used as absorbers not only in optical modalities but also with pulsed light with the duration of nanosecond[160]. This property makes APMI dyes more versatile in their applications as contrast agent *in vivo* especially, it has been demonstrated that the chromophores can provide signal of different types: optical with a NIR emission close to the ICG channel of Quest® medical imaging device and acoustic compatible with Vevo®-LAZR-X from Fujifilm Visualsonics® (Figure 87). These properties may satisfy the requirement of the modern real time imaging technologies used in the clinics such as multiple information acquisition from the imaging device and improved real time visualization of the diseased tissues or anatomical features otherwise difficult to discern by visual palpation and frozen section pathologic analysis[158].

NIR angiography of the main abdominal organs in rats

X=CH$_2$; CO

-Large Stokes shift up to 130nm
-Emission in the NIR up to 770 nm

Contrast in photoacustic imaging technology

Label for therapeutic immune CD$^+$ cells and live cell tracking in mice
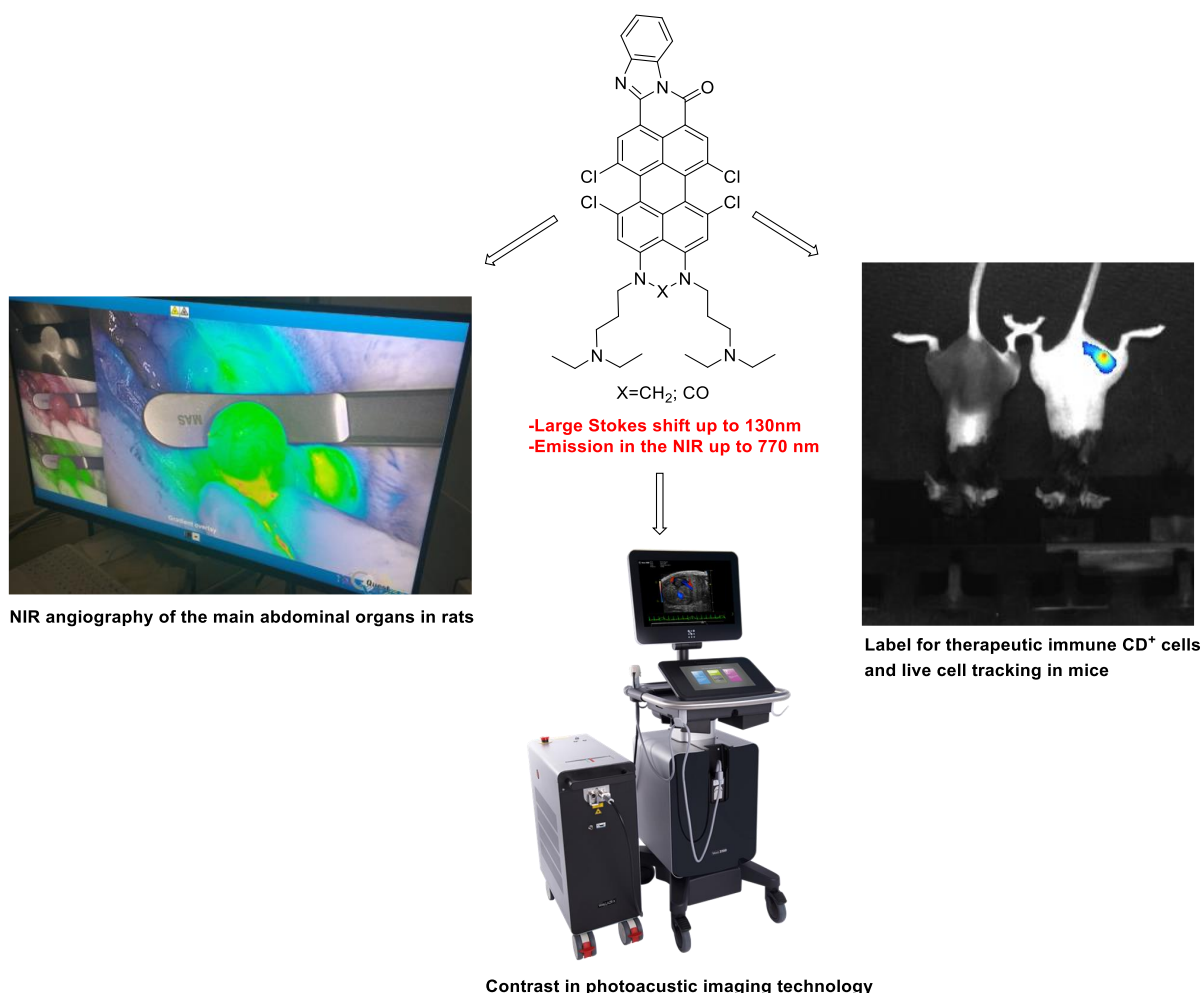
Figure 87 Applications of APMI dyes in NIR angiography of the abdominal organs in rats using Quest® medical imaging device (left) and as label for immune cells tracking in mice showing potential accumulation in lymph nodes (right) Contrast in photoacusti imaging technology using Vevo®-LAZR-X from Fujifilm Visulasonics®(bottom)

In parallel to this study, I also focused on the preparation of contrasts belonging to a different class of dyes to provide a second contrast active on the the far-red window 650-700 nm and to be used simultaneously in dual channel commercially available imagers (Figure 34). In particular, I selected silicon rhodamine dyes as they present an emission wavelength close to the emission of FDA approved Methylene blue (MB) in water (Chapter 2) (Figure 35). For this reason, in chapter 4, I provided the synthesis and characterization of an activatable silicon rhodamine dye with pH sensing properties (Figure 72). Compound **4.33** is water soluble and NIR emitting thanks to the installation of a silicon atom in position 10th of the rhodamine scaffold. This substitution gave a bathochromic shift of 90 nm in the emission in respect to commercially available pHrodo® dye achieving a value (675 nm) exceptionally close to the emission of Methylene Blue (MB) in water and thus compatible for this imaging channel. The pH dependent emission in the same emission range (675 nm) was observed in different pH buffers giving the typical sigmoidal plot of a pH dependent ON-OFF probe based on photo induced electron transfer (PeT) mechanism (Figure 86). The pKa value was found to be in the physiological range 7.0-7.4 thanks to the installation of a phenyl moiety bearing a pH responsive group (Figure 80). Probe **4.33** may be used for intraoperative navigation in FGS where more accurate detection of the boundaries between healthy and disease tissue is required. Current FDA approved dyes used in the clinics like ICG green, fluorescein and methylene blue and 5-Ala are defined as "always ON" non-targeted contrast agents[16]. These probes do not provide sufficient target to background ratio on the desired tissue, as an example, IRDyes® by LiCor® advancing in clinical trials, resulted highly specific to diseased tissues of interest but are not capable to clearly define the boundaries of the diseased tissues as the blood flow cannot completely clear the signal from unbound probes[16]. In the same way, also fluorescein based targeted probes containing folate moiety like folate FITC dye described by Mahalingham et al[159, 161] are highly specific toward ovarian cancers but lacks activatability on solid tumor surgical margins. Cancer cells that remain at the cut edge of the surgical specimen are part of the so-called positive margins and are responsible for cancer recurrence and metastasis[162]. It is well known that surgery based on visual palpation and time-consuming frozen section pathologic analysis is not able to clearly define and remove positive margins[163] (Figure 88).
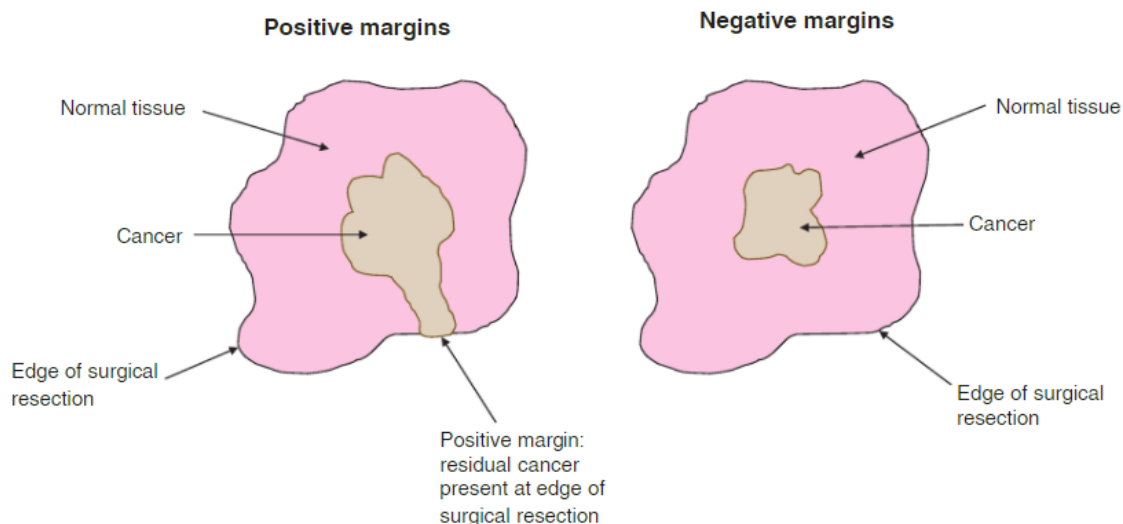
Figure 88 Picture taken from the work of Tringale et al.[163] showing the surgical margin when an incomplete surgical resection is performed (left) and when complete resection of the tumor mass has been accomplished (right). Positive margins are those associated with cancerous cells present at the edge of the surgical resection.[163]

Only activatable probes showed the ability to shed light on tumor boundaries in high target to background ratio[16]. Between them, probes that sense the presence of tumor specific enzyme metalloproteases are the most used[162, 163] additionally, probes based on PeT process to quench their fluorescence upon specific biological events associated tumor microenvironment, showed the ability to achieve activatability on positive margins[164]. This approach has been used to define the boundaries of small size metastatic tumors in high resolution. These results are shown in work of Urano et al.[49] showing accurate detection of submillimeter sized tumors using a visible range emitting BODIPY pH activatable probe.[49] (Figure 89)
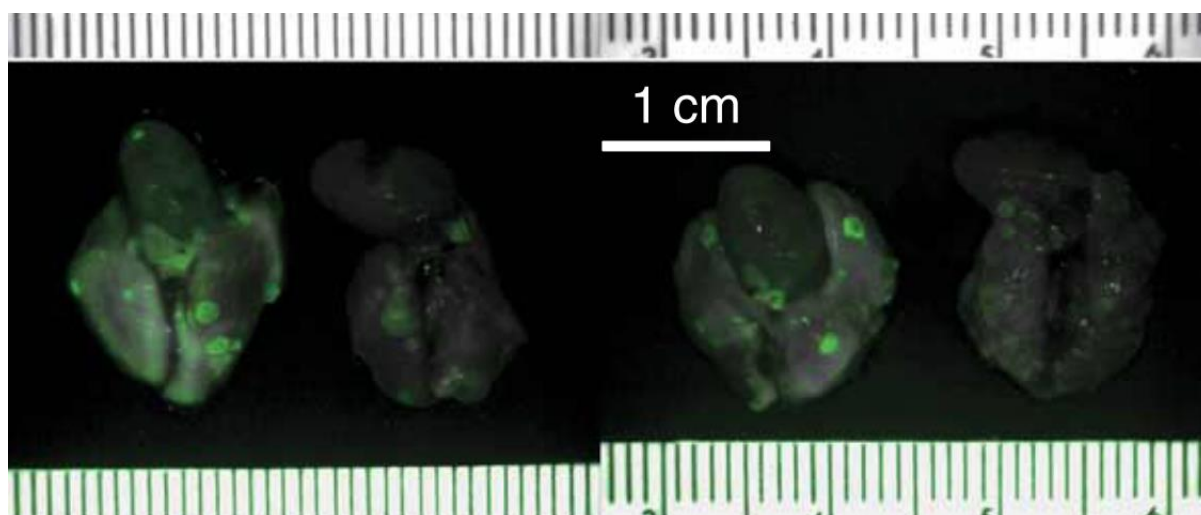

Figure 89 Detection of submillimeter size tumors on lungs with a BODIPY PeT probe from the work of Urano et al.[49]

To expand the use of PeT activatable probes in cancer diagnosis, Ogawa et al. proposed the use of pH Rodo® dye a rhodamine based red emitting probe that showed the ability to forms H-

dimer upon conjugation with tumor targeting macromolecules in water[57]. This effect combined with photoinduced electron transfer (PeT) mediated by the pH of the biological media, enhanced the target to background ratio in tumor bearing D-galactose positive peritoneal tumor bearing mice[57] (Figure 90). The probe was working with a dual quenching mechanism to switch off the fluorescence outside the diseased tissue thus increasing the spatial resolution on the tumor borders. From one side, pH Rodo® is a pH responsive probe and get fluorescent only when internalized in cancer cells, from the other, it can form H-dimers upon protein conjugation. This is considered a concomitant effect that enhance the fluorescence quenching outside the region of interest thus improving the fluorescence image contrast[57] (Figure 90).
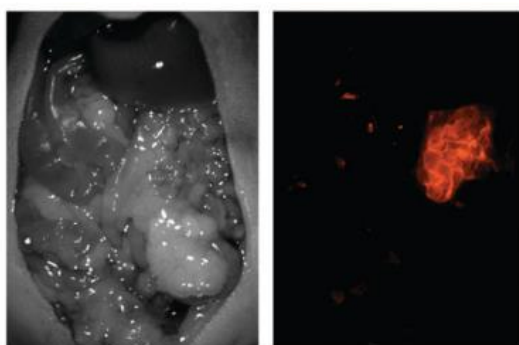

Figure 90 D-galactose positive peritoneal tumor bearing mice showing enhanced signal on D-galactose positive tumors (left) taken from the work of Ogawa et al.[165]

To date, there are no activatable pH responsive probes with dual quenching modalities based on H-dimer formation with an emission close to Methylene Blue (MB) (Figure 35) to be used in commercially available dual imager devices like those described In the work of Tanaka et al .[98] (Figure 34) Probe **4.33** I synthesized, is emitting in the far-red range with a wavelength value (675 nm) extremely close to the one of FDA approved Methylene blue (Figure 35) and it is activatable working with a dual quenching mechanism based on H-dimer formation and photo induced electron transfer modulated by the pH of the media, therefore, represent a valuable improvement in respect to the commercially available analog pHrodo®. For those reasons, as a future perspective, my intention is to continue to work on activatable silicon rhodamine dye **4.33** by studying cell permeability properties and biodistribution profile *in vivo*. I will also focus on the reactivity of the allyl linker installed on the phenyl moiety using UV mediated click thiol-ene coupling reactions in water for the functionalization of small cysteine containing peptides and antibodies[145, 146, 148, 166]. I am planning to use the linker toward the labelling of tumor specific vector macromolecules like monoclonal antibodies Trastuzumab (Herceptin®) and Bevacizumab (Avastin®). In addition, I propose to study the absorption profile of the dye-protein conjugate to assess de dye ability to form conjugate pairs H-dimers.

The experimental setup will follow the approach described in the work of Ogawa et al.[151](Figure 82) (Figure 91). This study may find an outcome in live cell imaging experiments to enlighten internalization patterns of vector macromolecules in cancer cells. Future perspective may be focused on the intravenous injection of the macromolecular probe in tumor bearing mice to assess the concentration and fluorescence activation of the probe on the desired tissues of interest.
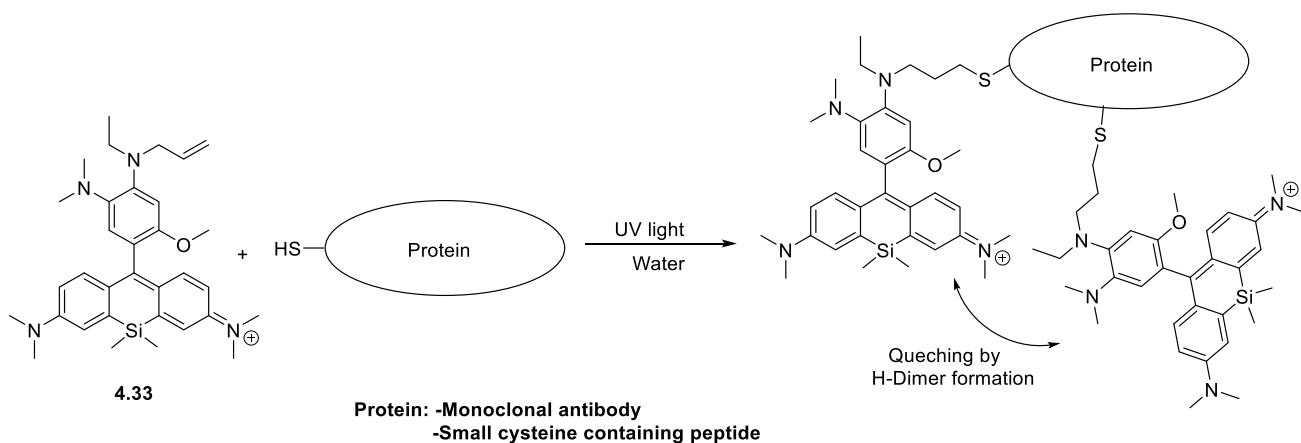

Figure 91 Future perspective on the study of H-dimer formation on proteins after labelling through UV mediated Click thiol-ene reactions in water. Following the approach of Ogawa et al.[151]

In conclusion, to summarize my findings, I provided valuable alternatives in the field of NIR emitting probes in FGS and evaluate the potential of perylene and silicon rhodamine class of dyes, in particular, I focused on the NIR emission that can be used simultaneously in the same operational setup with commercially available dual channel imagers (Figure 34)[97]. Perylene shows emission at 770 nm while silicon rhodamines at 675 nm. Perylene dyes can be used as always ON probes for *in vivo* angiography applications and evaluation of abdominal organs perfusion during surgery. They are designed to be active on Quest® medical imaging device thus demonstrating the potential implication in the field of fluorescence guided navigation technologies nowadays entering in operational rooms[97]. This result has direct outcomes in gastrointestinal reconstructive surgery. APMI dyes may be intraoperatively used to assess liver function and the quality of intestinal blood perfusions. In particular, I propose to use the contrast to evaluate anastomotic leakages in upper and lower gastrointestinal tract in laparoscopic and colorectal surgery[128]. It is also possible to visualize the biliary tree and the biliary excretion pathway in high resolution through the enhanced emission intensity found in the bile[11]. This property may have direct implications in cholangiography, cholecystectomy[116] and in the treatment of hepatobiliary cancer through hepatic function assessment[11]. At the same time, APMI dyes are cell permeable and may be used in cellular immunotherapies as valid

candidates in alternative to tricarbocyanines N-amines and N triazoles described in the work of Mellanby et al.[109] APMI dyes belong to the class of perylene push-pull dyes and they present an improved photostability in water also thanks to the protection of the electron donor N-amine groups on the *peri* positions that have been protected through electron withdrawing chemical functions[43]. The availability of new photostable cell permeable NIR contrast has direct implications in cellular immunotherapies to treat disorders driven by ineffective immune responses. This may include chronic infections and cancer[109]. APMI dyes demonstrated not only to be effective in labelling of CD+ macrophages but also as contrast for photoacoustic imaging devices upon absorption of pulsed NIR light and release of photoacoustic signal. This function is compatible with commercially available ultrasound transducers from Vevo®-LAZR-X from Fujifilm Visualsonics® thus demonstrating the versatility of the chromophore as absorbers of different types of excitation sources in optical and photoacoustic imaging settings. APMI dyes are active on the ICG green channel of commercially available devices and have an emission reaching 770 nm. On the other hand, silicon rhodamine **4.33** I synthesize, showed to be emissive at 675 nm a value close to the emission of FDA approved Methylene blue. This property has direct implications in dual imaging settings as second contrast to be used in conjunction with NIR emitting probes active on the ICG green channel[97]. Additionally, **4.33** is a cationic water-soluble compound with pH sensing properties based on photo induced electron transfer[167]. The proton sponge system Installed in the act as a quencher in basic media according to the protonation deprotonation equilibria in the physiological range (pKa 7.4) and therefore may be used to sense acidic environment in tumor microenvironments[17]. This property may be used *in vivo* to detect the enhanced metabolism of cancer cells in solid tumors[153]. It is well known that the extracellular matrix of solid tumors present strong pH differences from normal tissues therefore it can help to display boundaries between normal and diseased tissues[17]. At the same time, probe **4.33** has been designed with a terminal allyl linker that may be used in UV mediated click thiol-ene reactions toward the modification of primary cysteine containing peptides or antibodies for the preparation of targeted macromolecular probes (Figure 91). Compound **4.33** also demonstrated to form H-dimers in aqueous solution thus giving a first insight on the possibility to use this effect as a second fluorescence quenching modality together with the pH dependency to quench the light signal outside the tumor acidic microenvironment[17]. This strategy will allow fluorescence activation only after internalization in cancer cells. Considering together APMI dyes and silicon rhodamine dyes **4.33** are two class of dyes that can find applications in fluorescence guided surgery, to answer to the needs of photostable contrast to be used as alternative of cyanine-based contrast agents. Their

simultaneous use together with commercially available dual channel imagers may help the development of precision surgery in real time specially to visualize the differences between healthy and diseased tissues to improve the quality of resections thus avoiding disease recurrence and the need of reoperation in patients. With my dissertation, I would like to give a contribution to this important filed of surgical oncology to help surgeon to light up critical structures otherwise difficult to discern like ureters, bile ducts the gastrointestinal vascularity and capillary networks and help medical research to achieve the goal of precision surgery to improve post operative patient assessment and quality of life.

6. Experimental section

6.1 Chemicals and solvents

All solvents and chemicals were purchased in commercial grade (Sigma Aldrich, Acros Organics, Fisher Scientific, Fluka and Merck) and unless otherwise stated, used as obtained.

6.2 Analytical techniques

6.2.1 Chromathography and Mass Spectrometry

The progress of all reactions was monitored by thin layer chromatography (Macherey-Nagel F 254 silica gel sheet) with appropriate solvents described for each compound in the synthetic procedures. Column chromatography was performed on silica gel from Macherey Nagel (0.063 mm – 0.200 mm). Ultra-high performance liquid chromatography coupled with high resolution mass spectrometry was carried out using a THERMO (Bremen, Germany) UltiMate HPG-3400 RS binary pump, WPS-3000 auto sampler which was set to 10 °C and which was equipped with a 25 μL injection syringe and a 100 μL sample loop. The column was kept at 25 °C within the column compartment TCC-3200. Chromatography column was used THERMO Accucore® C-18 RP (100 × 2.1 mm; 2.6 μm) using the gradient in Error! Reference source not found. at a constant flowrate of 0.4 mL/min. Eluent A was water, with 2% acetonitrile and 0.1% formic acid. Eluent B was acetonitrile with 0.1% formic acid. Mass spectra were recorded with THERMO QExactive plus orbitrap mass spectrometer coupled to a heated electrospray source (HESI). Column flow was switched at 0.5 min from waste to the MS and at 11.5 min again back to the waste, to prevent source contamination. For monitoring a full scan mode was selected with the following parameters. Polarity: positive; scan range: 100 to 1500 m/z; resolution: 280,000; AGC target: 3 × 106; maximum IT: 200 ms. General settings: sheath gas flow rate: 60; auxiliary gas flow rate 20; sweep gas flow rate: 5; spray voltage: 3.0 kV; capillary temperature: 360 °C; S-lens RF level: 50; auxiliary gas heater temperature: 400 °C; acquisition time frame: 0.5 - 11.5 min. For negative ionization mode all values were kept instead of the spray voltage which was set to 3.3 kV.

| Time [min]	Solvent B [%]
0	0
0.2	0
8.0	100
11.0	100
11.1	0
12.0	0

Table S 1 HPLC gradient for UHPLC/HRMS

6.3.2 NMR spectroscopy

^{1}H NMR spectra were recorded on Bruker Avance 250MHz, Bruker Avance 300MHz and Bruker Avance 700MHz instruments.

6.3.2 Uv-visible absorption ad emission spectroscopy

UV vis absorption spectra were recorded on a Jasco V780 UVvis/NIR spectrophotometer in 1 cm quartz cuvettes using a cuvette filled with blank solvent as reference. Photostability tests were carried out in 1cm quartz cuvettes in O_2-saturated H_2O irradiated with a 365 nm LED (P = 85 mW). The UV-vis absorption spectra were collected on a Jasco V530 spectrophotometer. Steady-state emission spectra were recorded on a FLS 980 emission spectrometer (Edinburgh Instruments). Quantum were determined *via* relative method, using ICG in EtOH ($\phi_F = 0.13$) (B. Valeur, M. N. Berberan-Santos, Molecular Fluorescence, Wiley-VCH Verlag GmbH & Co. KGaA, Weinheim, Germany, **2012**., 10.1021/ac101329h) as standard.

Synthesis of 1,17-dibromo-3,4,14,15-tetrachloro-6H-benzo[10,5]anthra[2,1,9-def]benzo[4,5]imidazo[2,1-a]isoquinolin-6-one (3)
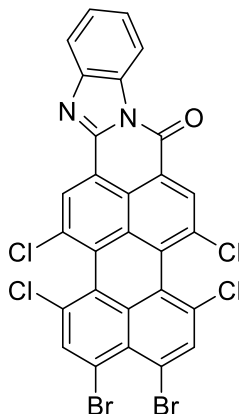
Chemical Formula: $C_{28}H_8Br_2Cl_4N_2O$
Exact Mass: 685.78
Molecular Weight: 689.99

8,9-dibromo-5,6,11,12-tetrachloro-1H,3H-benzo[10,5]anthra[2,1,9-def]isochromene-1,3-dione (**2**) (1 g, 1.62 mmol) and benzene-1,2-diamine (1.75 g, 16.18 mmol) were dissolved in a mixture of NMP and acetic acid (40 ml, 1:1). The reaction mixture was stirred and heated at 140 °C for 1.5 hrs. The mixture was cooled down to room temperature and poured into water (100 ml). The precipitate (900 mg, 1.30 mmol) was filtered, washed with water and methanol and dried.

Yield: 900 mg (80%)

ESI-MS m/z (%): 687.77 [M$^+$] calcd 685.78.

Synthesis of 3,4,14,15-tetrachloro-1,17-bis((3-(diethylamino)propyl)amino)-6H-benzo[10,5]anthra [2,1,9-def]benzo[4,5]imidazo[2,1-a]isoquinolin-6-one (4)
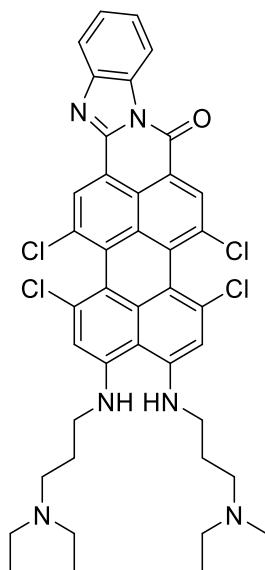
Chemical Formula: $C_{42}H_{42}Cl_4N_6O$
Exact Mass: 786.22
Molecular Weight: 788.64

1,17-dibromo-3,4,14,15-tetrachloro-6H-benzo[10,5]anthra[2,1,9-def]benzo[4,5]imidazo[2,1-a]isoquinolin-6-one (**3**) (500 mg, 0.72 mmol) was suspended in NMP (12 ml). Triethylamine (145.71 mg) and 3-(diethylamino) propylamine 313 mg (2.53 mmol) were added. The resulting mixture was heated to 110 °C under argon atmosphere and stirred for 1.5 h. After cooling to room temperature, the reaction mixture was poured into water and the precipitate was filtered off, dried and purified by column chromatography (DCM: TEA 95:5) as eluent. The product was dried and dissolved 10% aqueous hydrochloric acid. The product was isolated by dropwise addition of a saturated solution of sodium carbonate until precipitation occurs. The product was filtered washed with water and dried (175 mg, 0.22 mmol)

Yield: 180 mg, 30%.

^{1}H NMR (DMSO-d$_6$, 400 MHz): δ = 8.60 (d, J = 7.9 Hz, 1H), 8.54 (s, 1H), 8.36 (s, 1H), 7.87 (d, J = 7.9 Hz, 1H), 7.46-7.53 (m, 1H), 7.39-7.46 (m, 1H), 6.94 (s, 1H), 6.90 (s, 1H), 3.35-3.61 (m, 4H), 2.60-2.87 (m, 12H), 1.92 (dt, J = 14.0, 7.0 Hz, 4H), 1.06 (q, J = 7.3 Hz, 12H) ppm.

^{13}C NMR (DMSO-d$_6$, 126 MHz): δ = 158.5, 150.7, 150.0, 146.6, 142.5, 138.8, 137.6, 134.3, 132.5, 131.5, 130.6, 129.3, 128.6, 127.9, 127.3, 125.8, 124.8, 121.9, 119.2, 117.3, 115.0, 112.5, 111.7, 110.2, 109.5, 108.7, 49.4, 46.7, 41.6, 22.9, 8.9 ppm.

ESI-HRMS m/z (%): found 789.221 [M⁺] calcd. 788.64.

Synthesis of 5,6,16,17-tetrachloro-1,3-bis(3-(diethylamino)propyl)-2,3-dihydrobenzo[4'',5'']imidazo[1'',2'':1',2']pyrido[3',4',5':6,7]phenaleno[1,2,3-gh]perimidin-8(1H)-one (5)
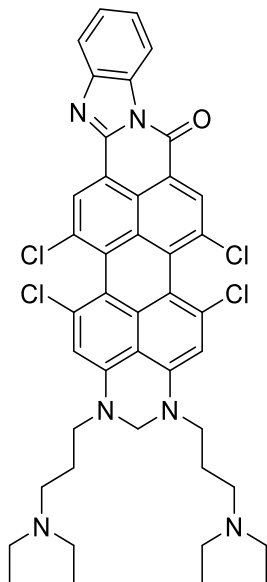
Chemical Formula: $C_{43}H_{42}Cl_4N_6O$
Exact Mass: 798.22
Molecular Weight: 800.65

3,4,14,15-tetrachloro-1,17-bis((3-(diethylamino)propyl)amino)-6H-benzo[10,5]anthra[2,1,9-def]benzo[4,5]imidazo[2,1-a]isoquinolin-6-one (**4**) (200 mg, 0.253 mmol) and paraformaldehyde (22.8 mg, 0.76 mmol) were suspended in chloroform (19 ml). Trifluoroacetic acid (28.16 mg, 0.25 mmol) was added. The resulting mixture was stirred under reflux and argon atmosphere for 1.5 h. After cooling the reaction mixture to room temperature, the solvent was evaporated under reduced pressure. The product (160 mg, 0.20 mmol) was obtained as a solid without purification.

Yield: 160 mg, 76 %.

¹H NMR (DMSO-d₆, 300 MHz): δ = 9.56 (s, 1H), 8.61(s, 1H), 8.53 (s, 1H), 8.44-8.42 (m, 1H), 7.85-7.84 (m, 1H), 7.47-7.46 (m, 2H), 7.18 (s, 1H), 7.17 (s, 1H) 4.86 (s, 2H), 3.70-3.69 (m, 3H), 3.22-3.17 (m, 12H), 2.08 (m, 4H), 1.24-1.22 (br t, J = 7.2 Hz, 12H) ppm.

¹³C NMR (DMSO-d₆, 126 MHz): δ = 159.51, 148.40, 146.79, 146.27, 143.97, 139.08, 138.55, 133.30, 132.26, 132.09, 131.83, 129.08, 128.74, 128.29, 127.64, 126.07, 125.42, 123.11, 120.12, 119.22, 117.09, 115.71, 112.05, 111.75, 108.06, 107.41, 107.4, 64.04, 48.73, 46.99, 46.35, 21.05, 21.1, 9.09, ppm.

ESI-HRMS m/z (%): 800.221 [M$^+$] calcd 800.65.

Synthesis of 5,6,16,17-tetrachloro-1,3-bis(3-(diethylamino)propyl)benzo [4'',5'']imidazo[1'',2'':1',2']pyrido[3',4',5':6,7]phenaleno[1,2,3-gh]perimidine-2,8(1H,3H)-dione (6)
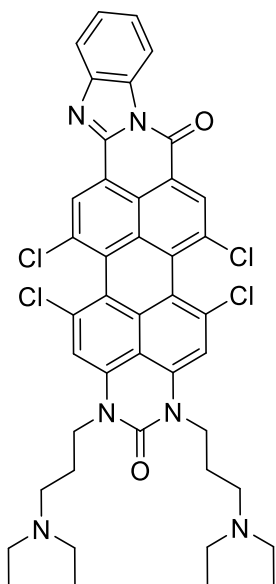
Chemical Formula: $C_{43}H_{40}Cl_4N_6O_2$
Exact Mass: 812.20
Molecular Weight: 814.63

3,4,14,15-tetrachloro-1,17-bis((3-(diethylamino)propyl)amino)-6H-benzo[10,5]anthra[2,1,9-def] benzo[4,5]imidazo[2,1-a]isoquinolin-6-one (**4**) (300 mg, 0.38 mmol) was dissolved in anhydrous THF (19 ml). Triphosgene 135 mg (0.45 mmol) was dissolved in anhydrous THF (2 ml) and added dropwise. The resulting mixture was refluxed for 2 h. After cooling the reaction mixture to room temperature, the solvent was evaporated under reduced pressure. The product was obtained by precipitation from THF and hexane (244 mg, 0.29 mmol).

Yield: 244mg (79%).

^{1}H NMR (600 MHz, DMSO-d_6) δ ppm 1.24 - 1.26 (m, 13 H) 2.16 (dt, J=15.36, 7.45 Hz, 4 H) 3.09 - 3.19 (m, 12 H) 3.27 (br dd, J=10.27, 5.32 Hz, 4 H) 3.33 - 3.46 (m, 141 H) 4.21 - 4.38 (m, 4 H) 7.50 - 7.53 (m, 2 H) 7.55 - 7.58 (m, 2 H) 7.89 - 7.91 (m, 1 H) 8.17 - 8.23 (m, 1 H) 8.44 - 8.47 (m, 1 H) 8.60 - 8.64 (m, 1 H) 8.69 - 8.73 (m, 1 H)

^{13}C NMR (DMSO-d$_6$, 126 MHz): δ = 162.52, 158.94, 149.36, 147.76, 143.44, 140.37, 140.23, 139.78, 138.27, 137.72, 133.88, 131.78, 131.41, 130.42, 130.29, 129.89, 127.30, 125.81, 125.46, 122.56, 120.63, 119.94, 118.36, 115.27, 115.00, 109.49, 108.95, 48.45, 46.14, 41.34, 34.17, 20.92, 8.47 ppm.

ESI-MS m/z (%): 815.200 [M$^+$] calcd. 812.20.

4-methoxy-N,N-dimethylaniline
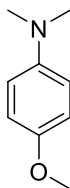
Chemical Formula: C$_9$H$_{13}$NO
Exact Mass: 151.10
Molecular Weight: 151.21

Aqueous H$_2$SO$_4$ (3 M, 19,2 ml) was added to a stirred solution of aq. formaldehyde (37% 8 ml mmol) in tetrahydrofuran (86,02 ml) the mixture was cooled to 0°C and stirred for another 10 min, p-anisidine (4 g, 32 mmol) was dissolved in the reaction mixture than stirred for additional 10 min. Solid NaBH$_4$ (g, mmol) was slowly added portionwise within 30 min while the temperature was maintained at 0°C. The resulting mixture was allowed to warm and stirred for 1 hour at 20°C Saturated aq. NaHCO3 (350 mL) was then added, and the reaction mixture was extracted with Ethyl acetate (3 × 100 mL). The combined organic layers were dried over anhydrous MgSO4 and filtered, and solvents were evaporated under reduced pressure. The crude product was of sufficient purity for the next step. 4.1 g (85% yield).

Analytical data are in agreement with the work of Randt et Al (**Randt2019**).

4-methoxy-N,N-dimethyl-2-nitroaniline
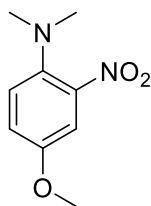
4-methoxy-*N,N*-dimethyl-2-nitroaniline
Chemical Formula: $C_9H_{12}N_2O_3$
Exact Mass: 196.08
Molecular Weight: 196.21

To a solution of 4-methoxy-N,N-dimethylaniline (4.04 g, 26.72 mmol) in water (534 ml) and acetic acid (49 ml) was added a solution of NaNO2 (3.69 g, 53.43 mmol) in water (10ml) dropwise within 30 min at room temperature .The reaction mixture was stirred at room temperature for 3 hours. The product was extracted by ethyl acetate (150 ml x 3). The combined organic layers were dried over anhydrous sodium sulfate. 4-methoxy-N,N-dimethyl-2-nitroaniline was obtained as a red oil 4.71 g (90% yield). The crude product was of sufficient purity for the next step

Analytical data are in agreement with the work of Yang et Al (**Yang2007**)

4-methoxy-N^1,N^1-dimethylbenzene-1,2-diamine
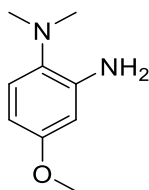
Chemical Formula: C$_9$H$_{14}$N$_2$O
Exact Mass: 166.11
Molecular Weight: 166.22

To palladium on activated charcoal (648 mg) was added methanol (10 ml) under argon carefully. A solution of 4-methoxy-N,N-dimethyl-2-nitroaniline (4.78 g, 24.36 mmol) in methanol (57 ml) was treated with the palladium suspension by a pipet. The solution was equipped with a 3-way stopcock attached by a 3 l balloon filled with hydrogen. The solution was evacuated and refilled with hydrogen carefully three times. The solution was stirred under hydrogen atmosphere 18 hours. Filtration through a celite pad was performed to remove palladium, the filtrate was concentrated to dryness to get crude product. The crude product was purified by chromatography on silica gel hexane: ethyl acetate 7:3 to give 4-methoxy-N^1,N^1-dimethylbenzene-1,2-diamine 2.83 g (70% yield).

Analytical data are protected by patent WO2013180813[168]

^{1}H NMR (400 MHz, Chloroform-*d*) δ ppm 2.64 (s, 6 H) 3.68 - 3.80 (m, 3 H) 4.09 (br s, 2 H) 6.25 - 6.39 (m, 2 H) 6.97 (d, *J*=8.48 Hz, 1 H)

^{13}C NMR (101 MHz, Chloroform-*d*) δ ppm 44.30 (s, 1 C) 55.21 (s, 1 C) 101.05 (s, 1 C) 102.88 (s, 1 C) 120.22 (s, 1 C) 134.25 (s, 1 C) 142.69 (s, 1 C) 156.79 (s, 1 C)

EI-MS (m/z %): [M+] Calcd 166.22 Found 166

N-(2-(dimethylamino)-5-methoxyphenyl)acetamide
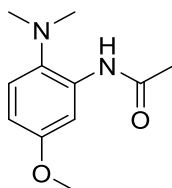
Chemical Formula: $C_{11}H_{16}N_2O_2$
Exact Mass: 208.12
Molecular Weight: 208.26

To a stirred mixture of 4-methoxy-N^1,N^1-dimethylbenzene-1,2-diamine (2.7 g, 16.24 mmol) and Ac_2O (2,4 g, 23.51 mmol) was added AgOTf (41.72 mg, 0.16 mmol). The reaction mixture was heated to 60°C and the progress monitored by TLC until all the starting material was found to be consumed. After completion, the reaction mixture was washed with saturated aqueous $NaHCO_3$ (15 ml) and extracted with EtOAc. The combined organic layers were evaporated under reduced pressure. The product obtained as a solid. Purification were performed on silica gel Hex:EtOAc 1:1. 2.87 g (84% yield)

Analytical data are protected by patent WO2013180813[168]

^{1}H NMR (400 MHz, Chloroform -*d*) δ ppm 2.19 - 2.25 (m, 3 H) 2.61 (br s, 6 H) 3.80 (s, 3 H) 6.54 - 6.65 (m, 1 H) 7.11 (d, *J*=8.77 Hz, 1 H) 7.98 - 8.18 (m, 1 H) 8.66 (br s, 1 H).

^{13}C NMR (101 MHz, Chloroform-*d*) δ ppm 45.37 (s, 2 C) 55.51 (s, 1 C) 104.45 (s, 1 C) 109.31 (s, 1C) 120.85 (s, 1C) 134.34 (s, 1C) 135.34 (s, 1C) 157.00 (s, 1C) 168.41 (s, 1C).

EI-MS (m/z %): [M+] Calcd. 208.26 Found. 208

N²-ethyl-4-methoxy-N¹,N¹-dimethylbenzene-1,2-diamine
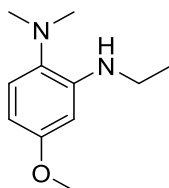
Chemical Formula: $C_{11}H_{18}N_2O$
Exact Mass: 194.14
Molecular Weight: 194.28

A solution of N-(2-(dimethylamino)-5-methoxyphenyl)acetamide (2.68 g, 12.8 mmol) in anhydrous THF (9.84 ml) was treated with BH3-THF (38.4 ml of 1M solution in THF) carefully. The mixture was heated to reflux for 2 hrs and cooled down to r.t. MeOH (10 ml) was added to the solution slowly to quench extra amount of borane complex at r.t. and the mixture was heated to reflux for 10 min. The solution was cooled to room temperature and evaporated to dryness. The residue was dissolved in 300 ml of ethyl acetate and washed by saturated solution of sodium bicarbonate and dried over anhydrous sodium sulfate. Evaporation gave pure product N²-ethyl-4-methoxy-N¹,N¹-dimethylbenzene-1,2-diamine, no further purification was required. 2.24 g (90% yield)

^{1}H NMR (300 MHz, Chloroform-d) δ ppm 1.31 (t, J=7.17 Hz, 3 H) 2.61 (s, 6 H) 3.11 - 3.22 (m, 2 H) 3.79 (s, 2 H) 4.72 (br s, 1 H) 6.17 - 6.24 (m, 2 H) 6.92 - 6.99 (m, 1 H)

^{13}C NMR (63 MHz, Chloroform-d) δ ppm 14.84 (s, 1 C) 38.17 (s, 1 C) 44.49 (s, 1 C) 55.18 (s, 1 C) 97.04 (s, 1 C) 99.36 (s, 1 C) 119.55 (s, 1 C) 133.87 (s, 1 C) 144.56 (s, 1 C) 157.38 (s, 1 C)

EI-MS m/z: calcd 194.28 Found 194

1-(3-bromopropyl)-1H-pyrrole-2,5-dione
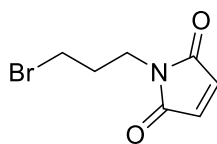
Chemical Formula: $C_7H_8BrNO_2$
Exact Mass: 216.97
Molecular Weight: 218.05

PPh$_3$ (3.75 g, 0.0143 mmol) was dissolved in 55 ml dry THF and the temperature of the mixture was kept at -78°C with a dry ice/ acetone bath. Diethyl azodicarboxylate (DEAD) (2.489 g; 0.0143 mmol) was added dropwise to the reaction mixture over 2 minutes. The reaction was stirred for 10 minutes followed by addition of 3-bromopropanol (3.18 g, 0.023 mmol) for over 2 min. After 5 min of stirring, maleimide (1.39 g, 0.0143 mmol) was added in solid form at -78°C. The reaction was then brought to room temperature and allowed to stir at room temperature for 10 hours. The reaction mixture was concentrated under rotary evaporator and the raw material purified on silica gel Hexane ethyl acetate 7:3. Pure product was obtained as a colorless oil 1.5 g (52% yield).

Analytical data are in agreement with the work of Perera et al[169].

1-(3-((2-(dimethylamino)-5-methoxyphenyl)(ethyl)amino)propyl)-1H-pyrrole-2,5-dione
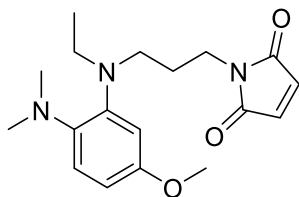
Chemical Formula: $C_{18}H_{25}N_3O_3$
Exact Mass: 331.19
Molecular Weight: 331.42

A solution of N^2-ethyl-4-methoxy-N^1,N^1-dimethylbenzene-1,2-diamine (380 mg, 2 mmol) in 4 ml of DMF was treated with 1-(3-bromopropyl)-1H-pyrrole-2,5-dione (1.7 g, 8 mmol), NaI (149 mg, 1 mmol) DIPEA (1 ml, 6 mmol) and the mixture was heated to 100 °C for 22 hours. The reaction was cooled to room temperature, DMF was removed by cold distillation under reduced pressure. The solid residue was dissolved in ethyl acetate, washed with a saturated solution of $NaHCO_3$. The organic layer was dried over anhydrous sodium sulfate and evaporated to give crude product. The crude product was purified by gradient column chromatography on silica gel gradient DCM 100% → DCM: iPr 5% . Pure product was obtained as a colorless oil 130 mg (20% yield).

^{1}H NMR (250 MHz, Chloroform-*d*) δ ppm 1.01 (t, *J*=7.04 Hz, 3 H) 1.78 (quin, *J*=7.32 Hz, 2 H) 2.63 - 2.76 (m, 6 H) 3.08 - 3.29 (m, 4 H) 3.52 (t, *J*=7.23 Hz, 2 H) 3.76 (s, 3 H) 6.41 - 6.55 (m, 2 H) 6.67 (s, 2 H) 6.84 (d, *J*=8.42 Hz, 1 H)

^{13}C NMR (101 MHz, Chloroform-*d*) δ ppm 11.99 (s, 1 C) 26.19 (s, 1 C) 36.24 (s, 1 C) 42.72 (s, 1 C) 44.53 (s, 1 C) 48.08 (s, 1 C) 55.30 (s, 1 C) 105.20 (s, 1 C) 107.95 (s, 1 C) 118.80 (s, 1 C) 133.97 (s, 1 C) 140.79 (s, 1 C) 144.20 (s, 1 C) 154.91 (s, 1 C) 170.69 (s, 1 C)

ESI-HRMS: calcd: 331.42 found: 332.196

N²-allyl-N²-ethyl-4-methoxy-N¹,N¹-dimethylbenzene-1,2-diamine
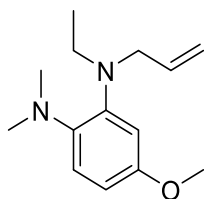
Chemical Formula: $C_{14}H_{22}N_2O$
Exact Mass: 234.17
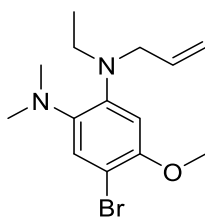Molecular Weight: 234.34

A solution of N²-ethyl-4-methoxy-N¹,N¹-dimethylbenzene-1,2-diamine (1.15 g, 5.92 mmol) in 16.6 ml of DMF was treated with allyl bromide (0.614 ml, 7.1 mmol), NaI (1.1 g, 7.34 mmol) DIPEA (3.1 ml, 17.76 mmol) and the mixture was heated to 100 °C for 22 hours. The reaction was cooled to room temperature, DMF was removed by cold distillation under reduced pressure. The solid residue was dissolved in ethyl acetate, washed with a saturated solution of $NaHCO_3$. The organic layer was dried over anhydrous sodium sulfate and evaporated to give crude product. The crude product was purified by column chromatography Hex: Et_2O 9:1. The product was obtained as a colorless oil 1.033g (90% yield).

^{1}H NMR (400 MHz, Chloroform-d) δ ppm 1.05 (t, J=7.02 Hz, 3 H) 2.74 (s, 6 H) 3.23 (q, J=7.02 Hz, 2 H) 3.78 (s, 3 H) 3.83 (dt, J=6.36, 1.21 Hz, 2 H) 5.05 - 5.23 (m, 2 H) 5.85 (ddt, J=17.06, 10.34, 6.32, 6.32 Hz, 1 H) 6.48 (dd, J=8.62, 2.78 Hz, 1 H) 6.53 (d, J=2.92 Hz, 1 H) 6.87 (d, J=8.48 Hz, 1 H)

^{13}C NMR (101 MHz, Chloroform-d) δ ppm 12.01 (s, 1 C) 42.57 (s, 1 C) 43.62 (s, 1 C) 53.95 (s, 1 C) 55.33 (s, 1 C) 105.08 (s, 1 C) 108.24 (s, 1 C) 116.28 (s, 1 C) 118.62 (s, 1 C) 136.25 (s, 1 C) 140.56 (s, 1 C) 144.33 (s, 1 C) 154.89 (s, 1 C).

EI-MS m/z: Calcd: 234.34 Found: 234.173

N1-allyl-4-bromo-N1-ethyl-5-methoxy-N2,N2-dimethylbenzene-1,2-diamine

Chemical Formula: $C_{14}H_{21}BrN_2O$
Exact Mass: 312.08
Molecular Weight: 313.24

N^2-allyl-N^2-ethyl-4-methoxy-N^1,N^1-dimethylbenzene-1,2-diamine (665 mg, 2.84 mmol) was dissolved in DCM 28 ml. N-Bromo Succinimide NBS (556 mg, 3.124 mmol) was added at room temperature to the reaction mixture and the resulting solution was stirred overnight. The solvent was evaporated under reduced pressure and the solid residue was absorbed on silica and purified by column chromathography on silica gel Hex : Et$_2$O 9:1. Product was obtained as a colorless oil 345 mg (38% yield)

^{1}H NMR (400 MHz, Chloroform-d) δ ppm 1.03 (t, J=7.16 Hz, 3 H) 2.71 (s, 6 H) 3.22 (q, J=7.02 Hz, 2 H) 3.81 (d, J=6.43 Hz, 2 H) 3.84 (s, 3 H) 5.06 - 5.22 (m, 2 H) 5.72 - 5.86 (m, 1 H) 6.51 (s, 1 H) 7.04 (s, 1 H)

^{13}C NMR (101 MHz, Chloroform-d) δ ppm 11.93 (s, 1 C) 42.28 (s, 1 C) 43.71 (s, 1 C) 53.71 (s, 1 C) 56.74 (s, 1 C) 102.92 (s, 1 C) 106.45 (s, 1 C) 116.73 (s, 1 C) 122.90 (s, 1 C) 135.78 (s, 1 C) 141.26 (s, 1 C) 143.17 (s, 1 C) 150.79 (s, 1 C)

EI-MS m/z: Calcd: 313.24 Found: 312.151

5-bromo-4-methoxy-N1, N1-dimethylbenzene-1,2-diamine
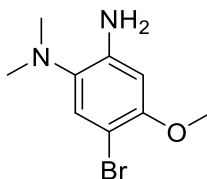
Chemical Formula: $C_9H_{13}BrN_2O$
Exact Mass: 244.02
Molecular Weight: 245.12

4-methoxy-N^1,N^1-dimethylbenzene-1,2-diamine (440 mg, 2.65 mmol) was dissolved in DCM 10 ml, AlCl3 was added (35.33 mg, 0.26 mmol) and the temperature was kept at 0°C. After complete dissolution of the solids, Br_2 (508 mg, 3.18 mmol) was added in one portion. The resulting solution was left stirring overnight at rt. The solvent was removed in vacuo and the solid residues dissolved in water 10 ml and treated with NaOH (127 mg in 5 ml H_2O). The resulting aqueous solution was extracted with EtOAc. The collected organic layers were dried over anhydrous sodium sulfate and evaporated to give a yellow solid. 450 mg (70% yield).

^{1}H NMR (400 MHz, Chloroform-*d*) δ ppm 2.61 (s, 6 H) 3.82 (s, 3 H) 4.10 (br s, 2 H) 6.34 (s, 1 H) 7.15 (s, 1 H)

^{13}C NMR (101 MHz, Chloroform-*d*) δ ppm 44.22 (s, 1 C) 56.36 (s, 1 C) 98.27 (s, 1 C) 99.59 (s, 1 C) 124.58 (s, 1 C) 142.03 (s, 1 C)

EI-HRMS: calcd: 245.12 found 244.021

N-(4-bromo-2-(dimethylamino)-5-methoxyphenyl)acetamide
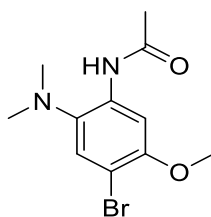
Chemical Formula: $C_{11}H_{15}BrN_2O_2$
Exact Mass: 286.03
Molecular Weight: 287.16

To a stirred mixture of 5-bromo-4-methoxy-N1, N1-dimethylbenzene-1,2-diamine (654 mg, 2.27 mmol) and Ac2O (585 mg, 2.27 mmol) was added AgOTf (2.3 mg, 0.02 mmol). The reaction mixture was heated to 60°C and the progress monitored by TLC until all the starting material was found to be consumed. After completion, the reaction mixture was washed with saturated aqueous $NaHCO_3$ (15 ml) and extracted with EtOAc. The combined organic layers were evaporated under reduced pressure. The crude product was purified on silica gel hexane : Ethylacetate 1:1 to give the pure product as a brown solid 640 mg (98% yield).

^{1}H NMR (250 MHz, Chloroform-d) δ ppm 2.19 - 2.33 (m, 4 H) 2.60 (s, 6 H) 3.78 - 4.00 (m, 4 H) 7.30 - 7.37 (m, 1 H) 8.20 (s, 1 H) 8.57 (br s, 1 H)

^{13}C NMR (101 MHz, , Chloroform-d) δ ppm 25.09 (s, 1 C) 45.30 (s, 1 C) 56.48 (s, 1 C), 103.37 (s, 1C), 104.25 (s, 1C), 125.12 (s, 1 C), 134.08 (s, 1 C) 135.92 (s, 1C) 153.24 (s, 1C) 168.47 (s, 1C).

EI-HRMS m/z (%) Calcd. 287.16 Found: 288.023

4-bromo-N1-ethyl-5-methoxy-N2,N2-dimethylbenzene-1,2-diamine
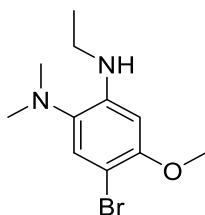
Chemical Formula: $C_{11}H_{17}BrN_2O$
Exact Mass: 272.05
Molecular Weight: 273.17

A solution of N-(4-bromo-2-(dimethylamino)-5-methoxyphenyl)acetamide (510 mg, 1.78 mmol) in anhydrous THF (1.4 ml) was treated with BH3-THF (5.34 ml of 1M solution in THF, 38.4 ml) carefully. The mixture was heated to reflux for 2 hrs and cooled down to room temperature. MeOH (5 ml) was added to the solution slowly to quench extra amount of borane complex at room temperature and the mixture was heated to reflux for 10 min. The solution was cooled to room temperature and evaporated to dryness. The residue was dissolved in 300 ml of ethyl acetate and washed by saturated solution of sodium bicarbonate and dried over anhydrous sodium sulfate. Evaporation gave pure product N^2-ethyl-4-methoxy-N^1,N^1-dimethylbenzene-1,2-diamine no further purification was required. 370 mg (76% yield)

^{1}H NMR (500 MHz, , Chloroform-*d*) δ ppm 1.31 (t, *J*=7.17 Hz, 3 H) 2.58 (s, 6 H) 3.17 (q, *J*=6.92 Hz, 2 H) 3.87 (s, 3 H) 4.69 (br s, 1 H) 6.20 (s, 1 H) 7.12 (s, 1 H)

^{13}C NMR (126 MHz, , Chloroform-*d*) δ ppm 14.75 (s, 1 C) 38.30 (s, 1 C) 44.39 (s, 1 C) 56.43 (s, 1 C) 95.22 (s, 1 C) 95.80 (s, 1 C) 124.01 (s, 1 C) 134.25 (s, 1 C) 143.95 (s, 1 C) 153.33 (s, 1 C)

EI-MS (%) Calcd 273.17 Found 272.052

1-(3-((4-bromo-2-(dimethylamino)-5-methoxyphenyl)(ethyl)amino)propyl)-1H-pyrrole-2,5-dione
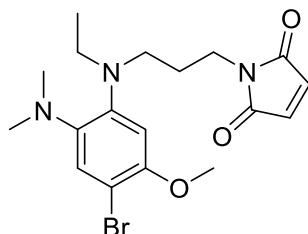
Chemical Formula: $C_{18}H_{24}BrN_3O_3$
Exact Mass: 409.10
Molecular Weight: 410.31

A solution of 4-bromo-N^1-ethyl-5-methoxy-N^2, N^2-dimethylbenzene-1,2-diamine (20 mg, 0.073 mmol) in 0.244 ml of DMF was treated with 1-(3-bromopropyl)-1H-pyrrole-2,5-dione (63 mg , 0.289 mmol), NaI (10 mg, 0.067 mmol) DIPEA (28 mg, 0.22 mmol) and the mixture was heated to 100 °C for 22 hours. The reaction was cooled to room temperature, DMF was removed by cold distillation under reduced pressure. The solid residue was dissolved in ethyl acetate, washed with a saturated solution of NaHCO₃. The organic layer was dried over anhydrous sodium sulfate and evaporated to give crude product. The crude product was purified by gradient column chromatography on silica gel gradient DCM 100% → DCM: iPr 5%. Pure product was obtained as a brown solid 10 mg (33% yield).

^{1}H NMR (400 MHz, Chloroform-*d*) δ ppm 1.02 (t, *J*=7.02 Hz, 3 H) 1.57 (br s, 6 H) 1.74 - 1.81 (m, 2 H) 2.18 (s, 1 H) 2.66 - 2.71 (m, 6 H) 3.11 - 3.19 (m, 2 H) 3.21 - 3.27 (m, 2 H) 3.51 (t, *J*=7.31 Hz, 2 H) 3.84 (s, 3 H) 6.51 (s, 1 H) 6.67 (s, 2 H) 7.03 (s, 1 H)

^{13}C NMR (101 MHz, Chloroform-*d*) δ ppm 12.01 (s, 1C) 26.16 (s, 1C) 36.20 (s, 1C) 42.44 (s, 1C) 44.61(s, 1C) 47.88(s, 1C) 56.78(s, 1C) 103.24 (s, 1C) 106.21(s, 1C) 123.17 (s, 1C) 134.03 (s, 1C) 141.59 (s, 1C) 143.11 (s, 1C) 150.95 (s, 1C) 170.70 (s, 1C).

ESI-HRMS m/z (%) Calcd 410.31 Found: 410.108

3-bromo-N,N-dimethylaniline
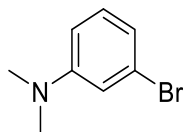
Chemical Formula: $C_8H_{10}BrN$
Exact Mass: 199.00
Molecular Weight: 200.08

Aqueous H_2SO_4 (3 M, 12 ml) was added to a stirred solution of aq. formaldehyde (37% 5ml mmol) in tetrahydrofuran (62 ml) the mixture was cooled to 0°C and stirred for another 10 min, 3-bromo aniline (3.44 g, 20 mmol) was dissolved in the reaction mixture than stirred for additional 10 min. Solid $NaBH_4$ (3.026 g, 8.68 mmol) was slowly added portion wise within 30 min while the temperature was maintained at 0°C. The resulting mixture was allowed to warm and stirred for 1 hour at 20°C. Saturated aq. NaHCO3 (350 mL) was then added, and the reaction mixture was extracted with Ethyl acetate (3 × 100 mL). The combined organic layers were dried over anhydrous MgSO4 and filtered, and solvents were evaporated under reduced pressure. The crude product was purified over silica gel hexane: ethyl acetate 8:2. The product was obtained as a yellow oil 3.9 g (97% yield).

Analytical data agree with the work of Pastierik et al[86].

3,3'-(dimethylsilanediyl)bis(N,N-dimethylaniline)
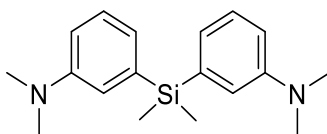
Chemical Formula: $C_{18}H_{26}N_2Si$
Exact Mass: 298.19
Molecular Weight: 298.51

A solution of 3-bromo-N,N-dimethylaniline (3.89 g, 19.4 mmol,) in THF (38.88 ml) was cooled to -78 °C under nitrogen. n-Butyllithium (2.65 M in hexanes, 7.76 mL, 20.56 mmol) was added, and the reaction was stirred at -78 °C for 30 min. Dichlorodimethylsilane (0.97 µl, 31.4 mmol) was then added. The dry ice bath was removed, and the reaction was stirred at room temperature for 3 h. It was subsequently quenched with saturated NH₄Cl, diluted with water, and extracted with EtOAc (2×). The combined organic extracts were washed with brine, dried over anhydrous MgSO4, filtered, and concentrated in vacuo. Purification by flash chromatography on silica gel Hex: EtOAc (5%) giving pure product as a colorless oil 1.95 g (80% yield)

Analytical data are in agreement with the work of Grimm et Al. and Butkevich et Al.

Published[170] yield (97%)

3,3'-(dimethylsilanediyl)bis(4-bromo-N,N-dimethylaniline)
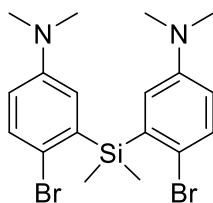
Chemical Formula: $C_{18}H_{24}Br_2N_2Si$
Exact Mass: 454.01
Molecular Weight: 456.30

N-Bromosuccinimide NBS (2.44 g, 13.7 mmol) was added in small portions to a solution of 3,3'-(dimethylsilanediyl)bis(N,N-dimethylaniline) (1.95 g, 6.5 mmol) in acetonitrile (40 mL), cooled in ice-water bath. The mixture was stirred for further 1 h at 0 °C. Sat. aq. NaHCO3 (40 mL) was then added, and the reaction mixture was extracted with CH2Cl2 (3×40 mL), the combined extracts were washed with brine and dried over Na2SO4. The product was isolated by flash column chromatography on silica gel in DCM to give light yellow solid. Yield 2.72 g (91% yield).

Analytical data are in agreement with the work of Butkevich et Al[90].

3,7-bis(dimethylamino)-5,5-dimethyldibenzo[b,e]silin-10(5H)-one
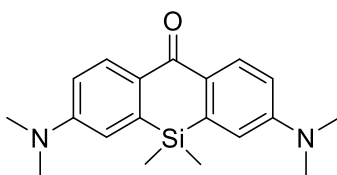
Chemical Formula: $C_{19}H_{24}N_2OSi$
Exact Mass: 324.17
Molecular Weight: 324.50

tert-Butyllithium (10.8 mL of 1.7 M in pentane, 18.36 mmol) was added quickly dropwise to a cold (-78 °C) solution of 3,3'-(dimethylsilanediyl)bis(4-bromo-N,N-dimethylaniline) (2.48 g, 5.44 mmol) in anhydrous THF (100 mL). The resulting dark yellow solution was stirred at -78 °C for 1.5 h. N,N-dimethylcarbamoyl chloride (0.55 mL, 5.98 mmol, 1.1 eq) was then injected dropwise. The resulting mixture was stirred at -78 °C for 30 min, then allowed to warm up to rt and left stirring overnight. It was then quenched with sat. aq. NH4Cl (50 mL), water was added to dissolve solids, and the mixture was extracted with ethyl acetate (3×40 mL). The combined extracts were washed with brine, dried over Na2SO4, filtered, and the product was isolated by flash column chromatography DCM: EtOAc (5%) to give 1.11 g (71 % yield) of the ketone as bright green crystalline solid.

Analytical data are in agreement with the work of Butkevich et Al[90].

N-(10-(4-(allyl(ethyl)amino)-5-(dimethylamino)-2-methoxyphenyl)-7-(dimethylamino)-5,5-dimethyldibenzo[b,e]silin-3(5H)-ylidene)-N-methylmethanaminium
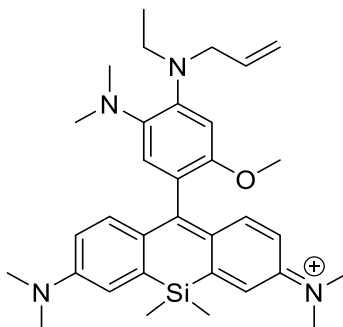
Chemical Formula: $C_{33}H_{45}N_4OSi^+$
Exact Mass: 541.34
Molecular Weight: 541.83

N1-allyl-4-bromo-N1-ethyl-5-methoxy-N2, N2-dimethylbenzene-1,2-diamine (200 mg, 0.64 mmol) was dissolved in THF 2 ml under argon atmosphere. Tert-Butyl lithium 1.7 M in pentane (0.41 ml, 0.697 mmol) was slowly added to the solution at -78 °C with a dry ice /acetone bath. The reaction was stirred for 10 min then a solution of 3,7-bis(dimethylamino)-5,5-dimethyldibenzo[b,e]silin-10(5H)-one (98.6 mg, 0.32 mmol) in THF (8 ml) was added dropwise carefully under argon atmosphere. The solution was left at -78 °C for 10 min then the dry ice/ acetone bath was removed, and the solution was left under stirring for one hour until the temperature reached room temperature. The solution resulted orange /red in color. When Acetic acid was added the solution turned dark blue indicating the formation of the product. The dye was isolated by column chromathography on silica gel DCM:MeOH 9:1 to give the pure product as a blue solid. 184 mg (94% yield)

^{1}H NMR (400 MHz, Methanol-d) δ ppm 0.55 - 0.61 (m, 6 H) 1.14 (t, J=7.02 Hz, 4 H) 2.71 (s, 6 H) 3.32 - 3.35 (m, 1 H) 3.33 (s, 10 H) 3.36 - 3.43 (m, 2 H) 3.64 (s, 3 H) 3.98 (d, J=6.14 Hz, 2 H) 4.84 - 4.85 (m, 1 H) 4.85 - 4.94 (m, 1 H) 4.88 (s, 15 H) 4.87 - 4.89 (m, 1 H) 5.15 - 5.29 (m, 2 H) 5.86 - 5.96 (m, 1 H) 6.62 (s, 1 H) 6.74 (s, 1 H) 6.80 (dd, J=9.65, 2.63 Hz, 2 H) 7.26 - 7.33 (m, 4 H)

^{13}C NMR (101 MHz, Methanol-d) δ ppm 12.46 (s, 1C) 30.69 (s, 1C) 40.82 (s, 1 C) 42.82 (s, 1 C) 44.98 (s, 1C) 54.82 (s, 1C) 56.45 (s, 1C) 106.04 (s, 1C) 114.87 (s, 1C) 117.43 (s, 1C) 121.59 (s, 1 C) 129.59 (s, 1C) 137.00 (s, 1C) 140.61 (s, 1C), 143.14 (s, 1C) 146.25 (s, 1C) 149.33 (s, 1C) 153.42 (s, 1C), 155.66 (s, 1C), 170.70 (s, 1C).

EI-HRMS m/z (%) Calcd. 541.83 Found. 541.336

10-(5-(dimethylamino)-4-(ethylamino)-2-methoxyphenyl)-N3,N3,N7,N7,5,5-hexamethyl-5,10-dihydrodibenzo[b,e]siline-3,7-diamine
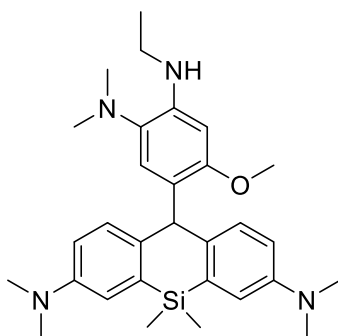
Chemical Formula: $C_{30}H_{42}N_4OSi$
Exact Mass: 502.31
Molecular Weight: 502.78

N-(10-(4-(allyl(ethyl)amino)-5-(dimethylamino)-2-methoxyphenyl)-7-(dimethylamino)-5,5-dimethyldibenzo[b,e]silin-3(5H)-ylidene)-N-methylmethanaminium (40 mg, 0.074 mmol) was dissolved in MeOH (4 ml), NaBH4 (11.18 mg, 0.29 mmol) was added and the system was stirred for 5 minutes at rt. The solvent was distilled away under reduced pressure, water was added, the mixture extracted using dichloromethane. The organic layer was washed using a saline solution and dried using Na2SO4 and the solvent was distilled away under reduced pressure. The residue was dissolved in dichloromethane (5 ml) 1,3-dimethylbarbituric acid (46.21 mg, 0.29 mmol) and tetrakis triphenylphosphine palladium (9 mg, 0.0078 mmol) were added and the system was stirred for 11 hours in argon atmosphere at 35 °C. A saturated aqueous solution of sodium hydrogen carbonate was added, the mixture was extracted using dichloromethane, the organic layers was dried using NaSO4, the solvent was distilled away under reduced pressure, and the residue was then purified using column chromatography Hex:Et2O 1:1 to obtain pure product 10 mg (27% yield).

^{1}H NMR (600 MHz, Chloroform-*d*) δ ppm 0.07 - 0.09 (m, 2 H) 0.48 - 0.52 (m, 1 H) 0.50 (s, 2 H) 0.57 (s, 2 H) 0.55 - 0.59 (m, 1 H) 0.90 (t, *J*=7.06 Hz, 2 H) 1.26 - 1.28 (m, 4 H) 1.51 - 1.64 (m, 3 H) 2.38 (s, 6 H) 2.93 (s, 12 H) 3.13 (q, *J*=7.15 Hz, 2 H) 3.88 (s, 3 H) 5.85 (s, 1 H) 6.18 (s, 1 H) 6.47 (s, 1 H) 6.71 (dd, *J*=8.62, 2.93 Hz, 2 H) 6.94 (d, *J*=2.75 Hz, 2 H) 7.25 (d, *J*=8.80 Hz, 2 H)

^{13}C NMR (151 MHz, Chloroform-*d*) δ ppm 0.71 (s, 1 C), 0.63 (s, 1C), 1.22 (s, 1 C), 14.32 (s, 1 C), 15.25 (s, 1 C) 22.86 (s, 1 C) 31.79 (s, 1 C) 38.72 (s, 1C) 41.23 (s, 1C) 44.54 (s, 1C) 45.59 (s, 1C) 56.18 (s, 1C), 94.88 (s, 1 C) 115.13 (s, 1 C) 116.99 (s, 1 C) 121.34 (s, 1C) 124.09 (s, 1C) 130.48 (s, 1C) 133.25 (s, 1C) 134.45 (s, 1C) 139.56 (s, 1C) 142.25 (s, 1C) 148.16 (s, 1C), 153.84 (s, 1C)

ESI-MS (%) Oxidized form calcd. 501.30 found. 501.303
ESI-MS (%) Reduced form calcd. 502.78 found. 503.318
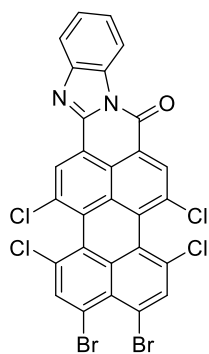
Chemical Formula: $C_{28}H_8Br_2Cl_4N_2O$
Exact Mass: 685.78
Molecular Weight: 689.99

Retention Time: 0.802

Ion Mode: APCI-

APCI-
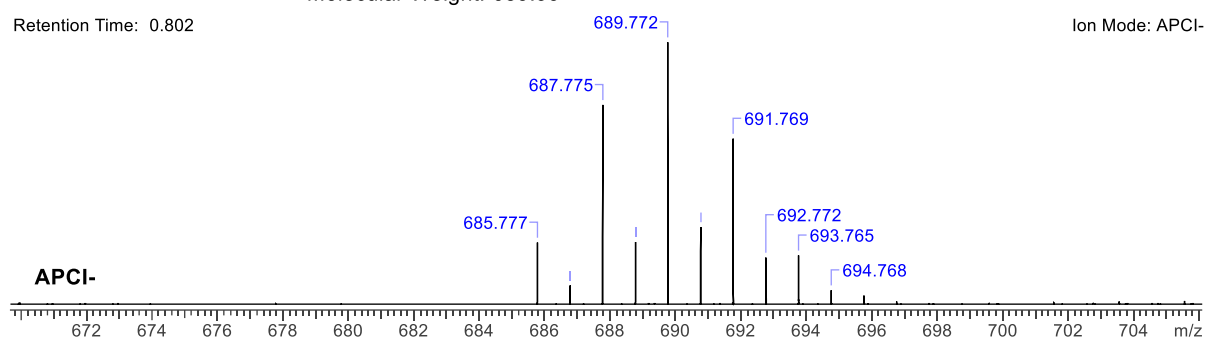
Figure 92 ESI HRMS of 1,17-dibromo-3,4,14,15-tetrachloro-6H-benzo[10,5]anthra[2,1,9-def]benzo[4,5]imidazo[2,1-a]isoquinolin-6-one.
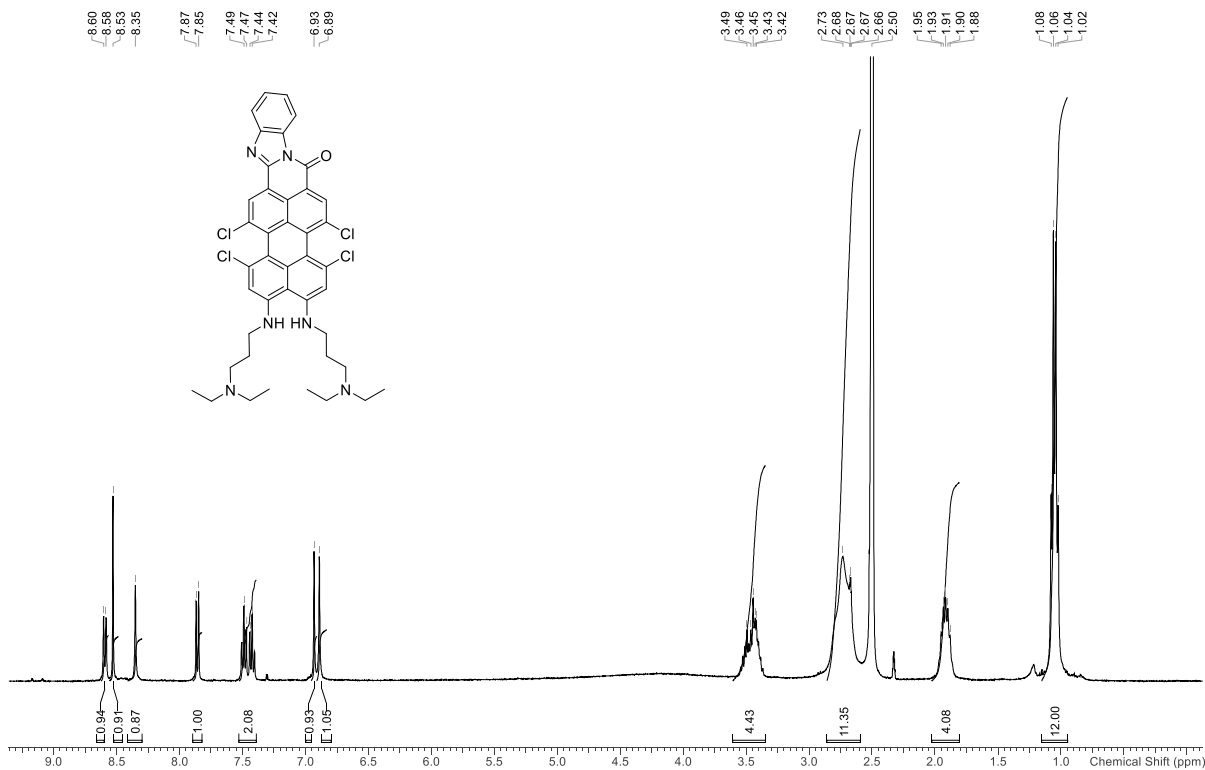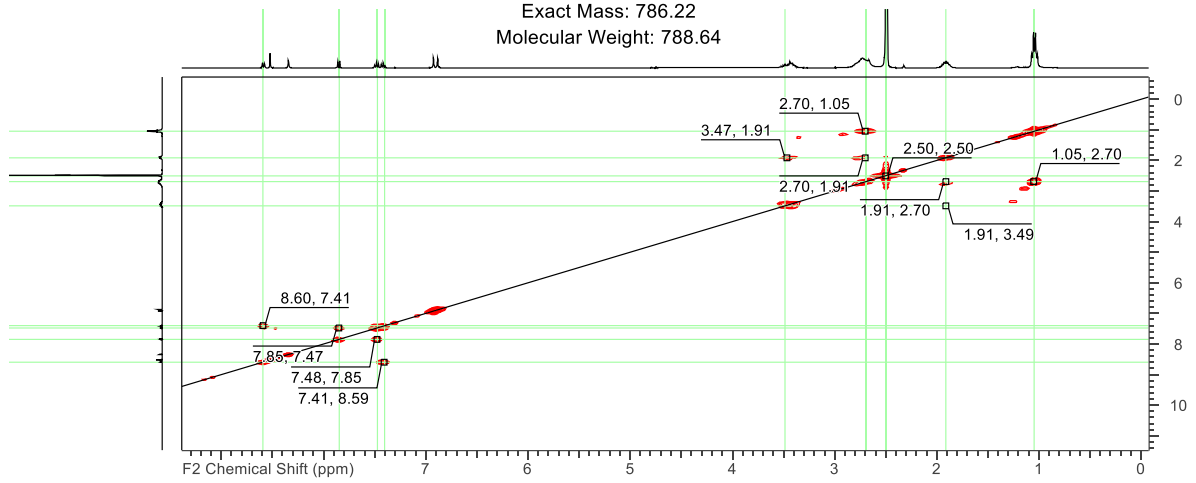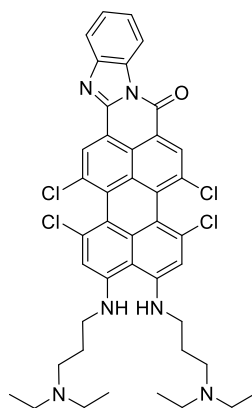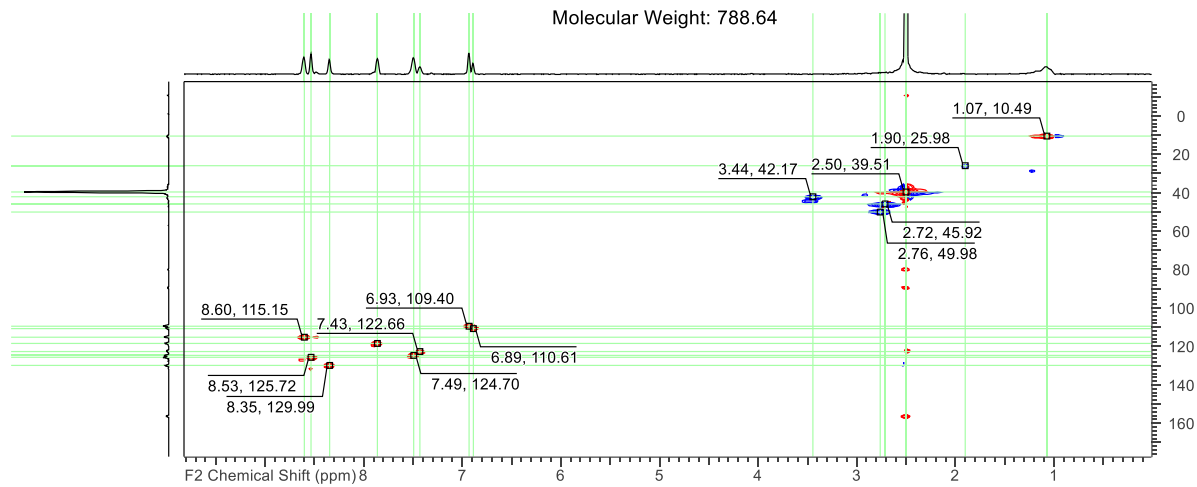
Figure 93 ¹H NMR spectrum of 3,4,14,15-tetrachloro-1,17-bis((3-(diethylamino)propyl)amino)-6H-benzo[10,5]anthra[2,1,9-def]benzo[4,5]imidazo[2,1-a]isoquinolin-6-one (400 MHz, DMSO-d6)
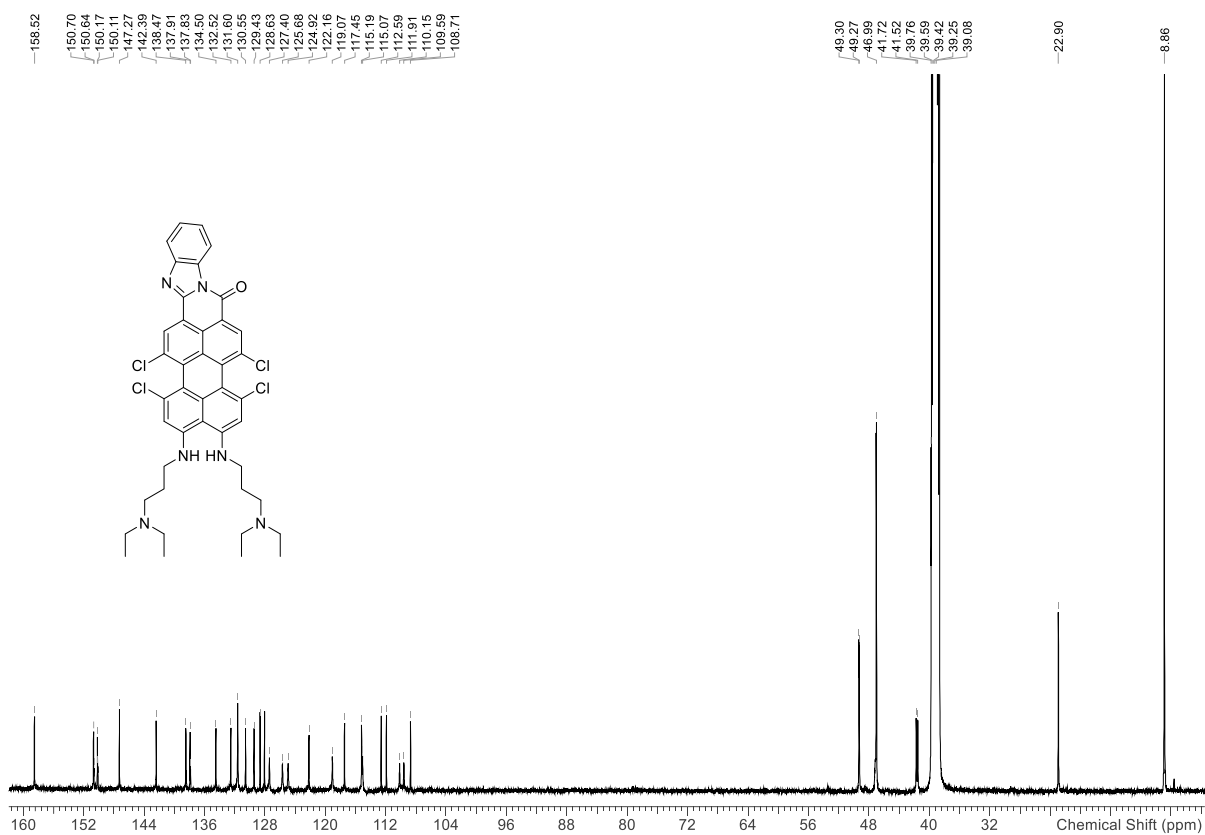
Figure 94 ¹³C NMR spectrum of 3,4,14,15-tetrachloro-1,17-bis((3-(diethylamino)propyl)amino)-6H-benzo[10,5]anthra[2,1,9-def]benzo[4,5]imidazo[2,1-a]isoquinolin-6-one (126 MHZ, DMSO-d6)
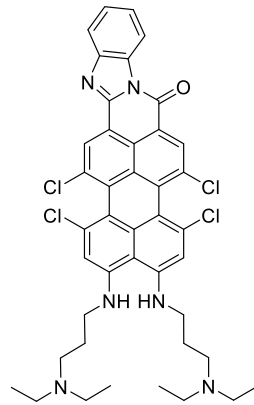
Chemical Formula: $C_{42}H_{42}Cl_4N_6O$
Exact Mass: 786.22
Molecular Weight: 788.64

Figure 95 1H-1H spectrum of 3,4,14,15-tetrachloro-1,17-bis((3-(diethylamino)propyl)amino)-6H-benzo[10,5]anthra[2,1,9-def]benzo[4,5]imidazo[2,1-a]isoquinolin-6-one (DMSO-d6)

Chemical Formula: $C_{42}H_{42}Cl_4N_6O$
Exact Mass: 786.22
Molecular Weight: 788.64

Figure 96 ^{1}H-^{13}C spectrum of 3,4,14,15-tetrachloro-1,17-bis((3-(diethylamino)propyl)amino)-6H-benzo[10,5]anthra[2,1,9-def]benzo[4,5]imidazo[2,1-a]isoquinolin-6-one (DMSO-d6)
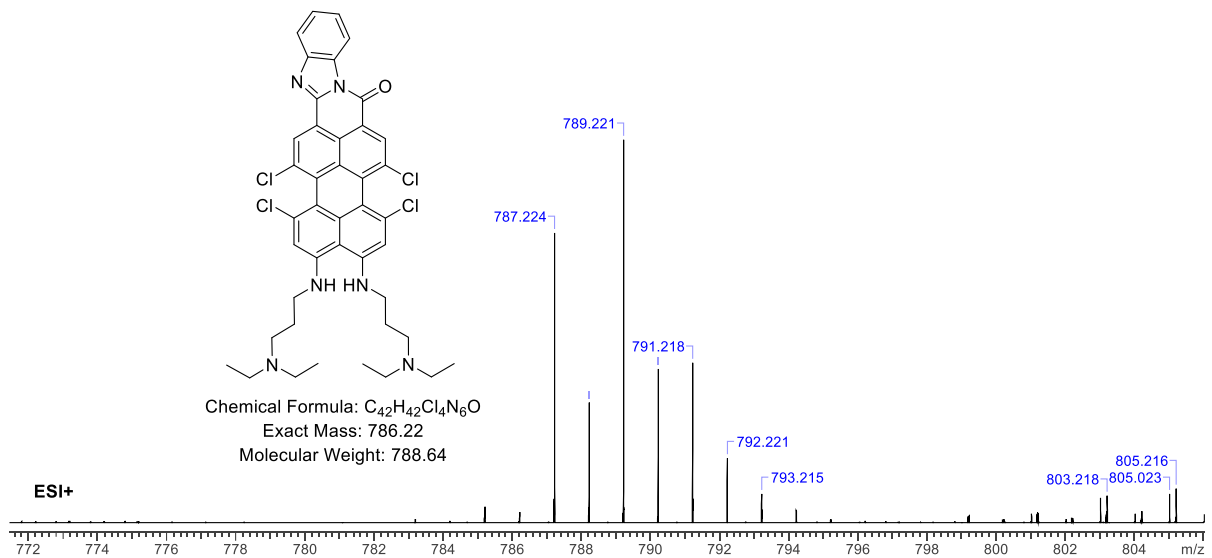
Figure 97 ESI-HRMS of 3,4,14,15-tetrachloro-1,17-bis((3-(diethylamino)propyl)amino)-6H-benzo[10,5]anthra[2,1,9-def]benzo[4,5]imidazo[2,1-a]isoquinolin-6-one
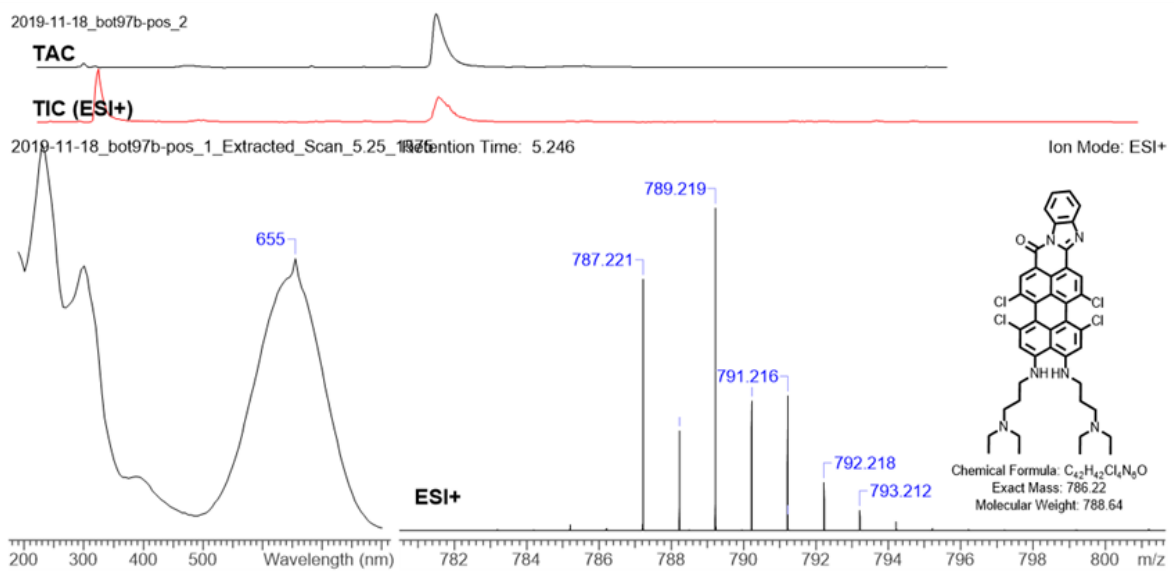
Figure 98 Chromatogram peak of 3,4,14,15-tetrachloro-1,17-bis((3-(diethylamino)propyl)amino)-6H-benzo[10,5]anthra[2,1,9-def]benzo[4,5]imidazo[2,1-a]isoquinolin-6-one at retention time 5.2 minutes (top), absorption profile (bottom left), ESI mass isotopic pattern (bottom right).
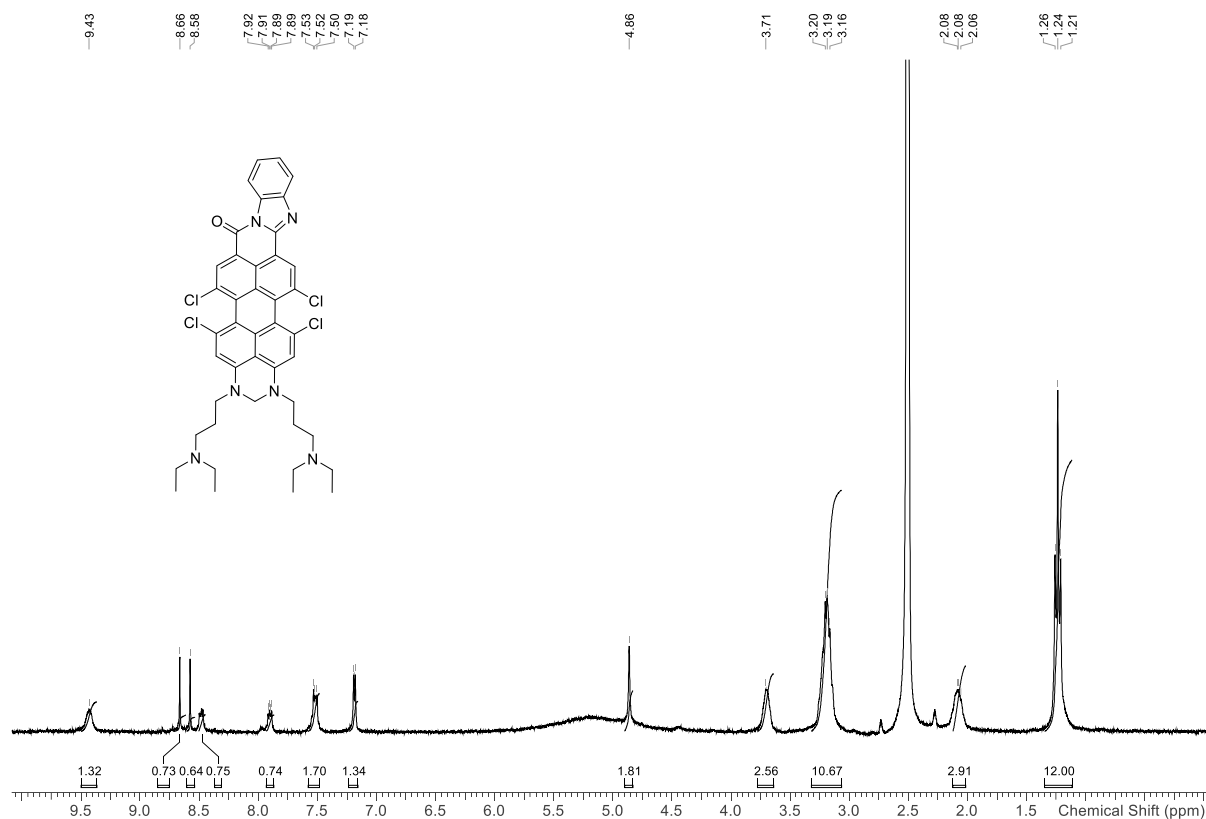
Figure 99 ¹H NMR spectrum of 5,6,16,17-tetrachloro-1,3-bis(3-(diethylamino)propyl)-2,3-dihydrobenzo[4'',5'']imidazo[1'',2'':1',2']pyrido[3',4',5':6,7]phenaleno[1,2,3-gh]perimidin-8(1H)-one (300 MHz, DMSO-d6)
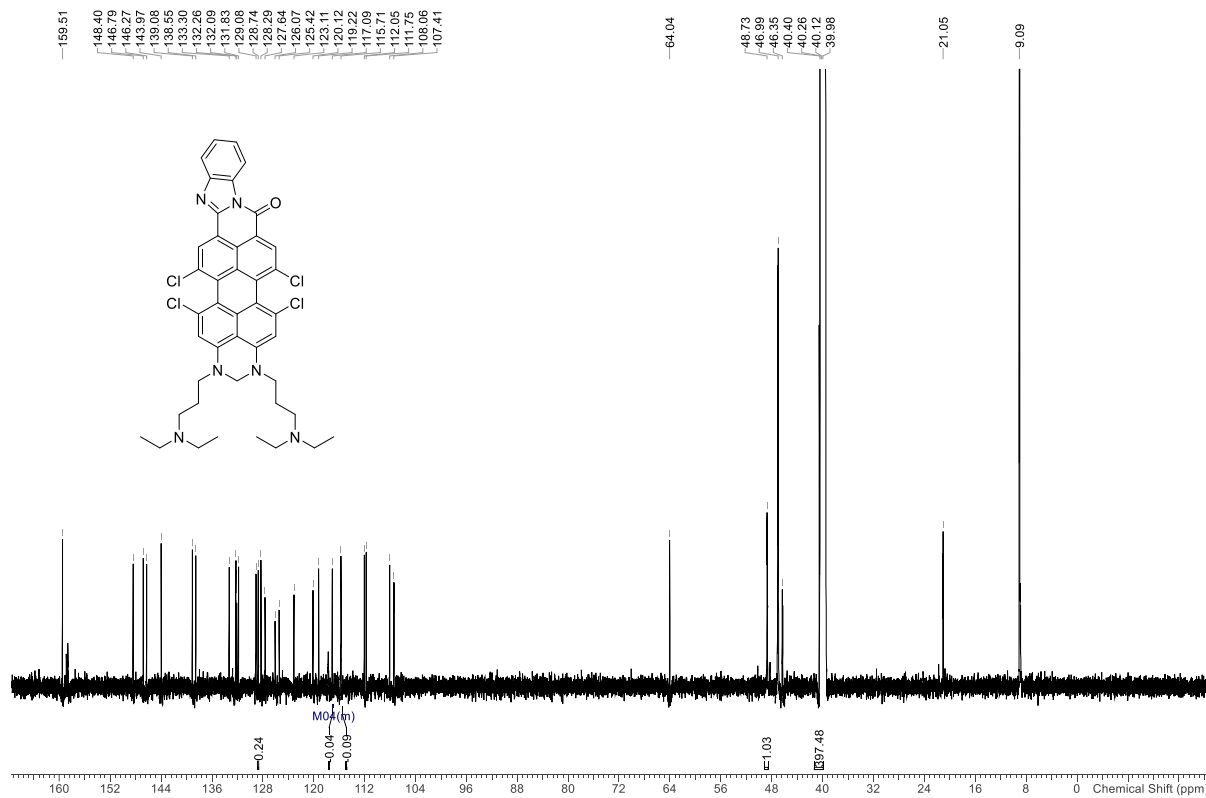

Figure 100 ¹³C spectrum of 5,6,16,17-tetrachloro-1,3-bis(3-(diethylamino)propyl)-2,3-dihydrobenzo[4'',5'']imidazo[1'',2'':1',2']pyrido[3',4',5':6,7]phenaleno[1,2,3-gh]perimidin-8(1H)-one (126 MHz, DMSO-d6)
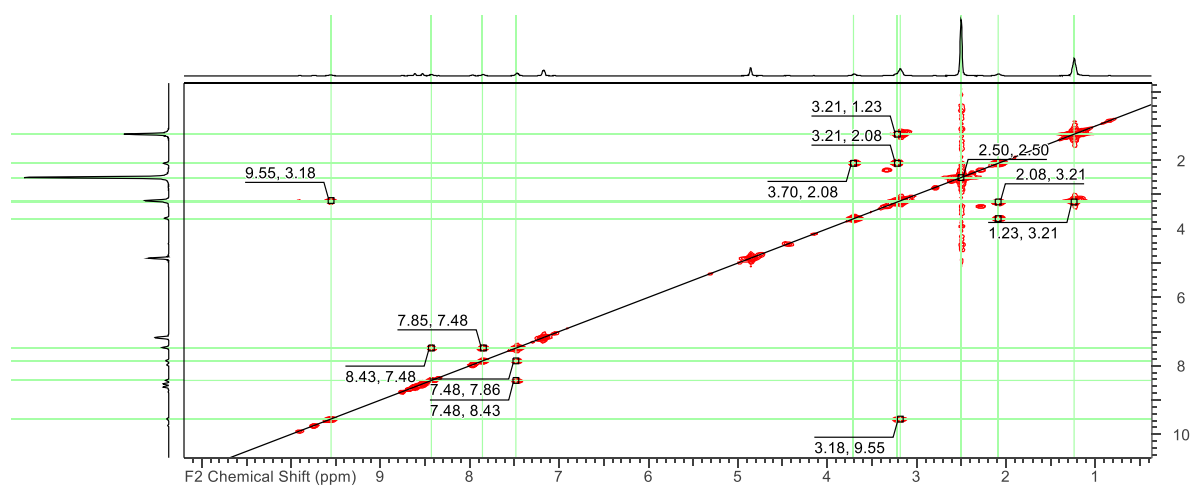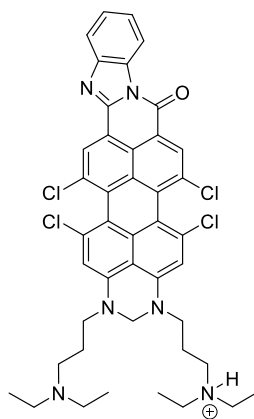
Figure 101 ^{1}H-^{1}H COSY spectrum of 5,6,16,17-tetrachloro-1,3-bis(3-(diethylamino)propyl)-2,3-dihydrobenzo[4'',5'']imidazo[1'',2'':1',2']pyrido[3',4',5':6,7]phenaleno[1,2,3-gh]perimidin-8(1H)-one (DMSO-d6)

Figure 102 ¹H-¹³C HSQC spectrum of 5,6,16,17-tetrachloro-1,3-bis(3-(diethylamino)propyl)-2,3-dihydrobenzo[4'',5'']imidazo[1'',2'':1',2']pyrido[3',4',5':6,7]phenaleno[1,2,3-gh]perimidin-8(1H)-one (DMSO-d6).
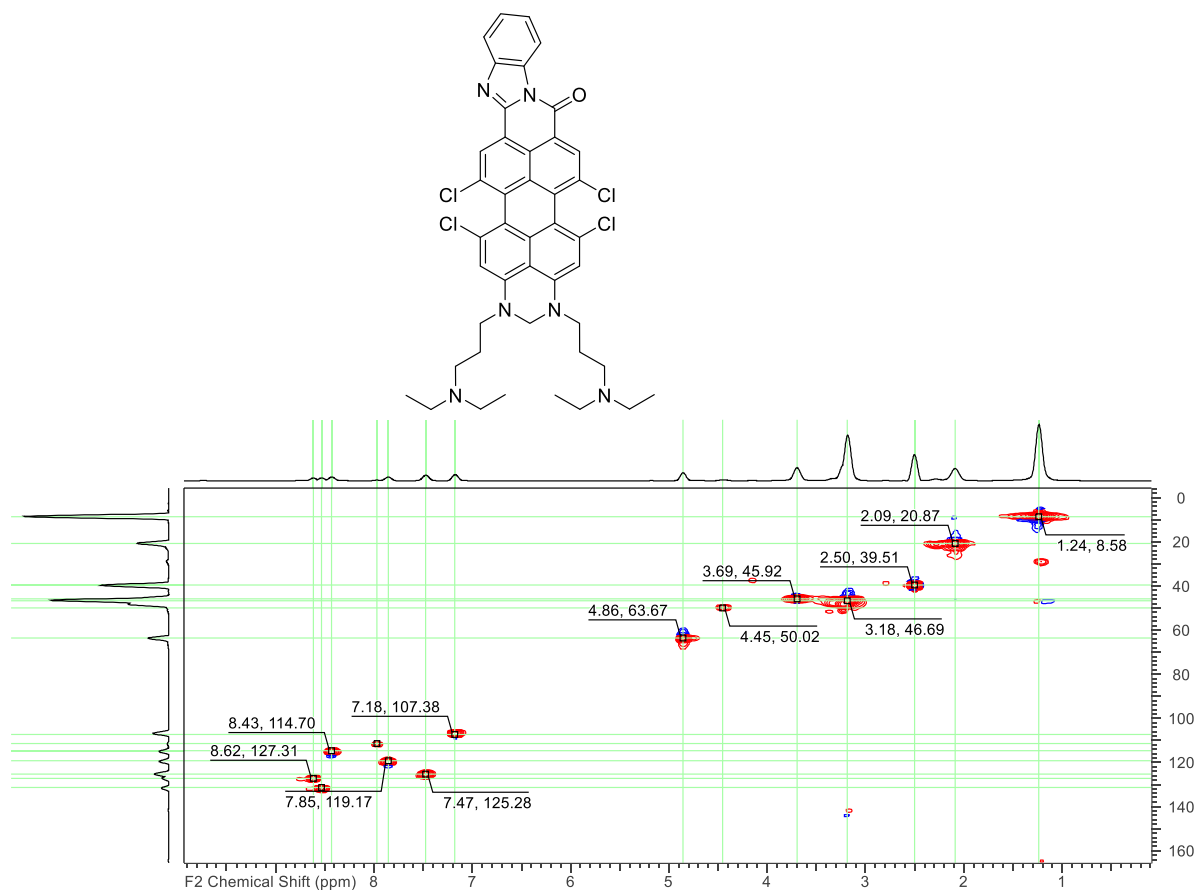

Chemical Formula: $C_{43}H_{42}Cl_4N_6O$
Exact Mass: 798.22
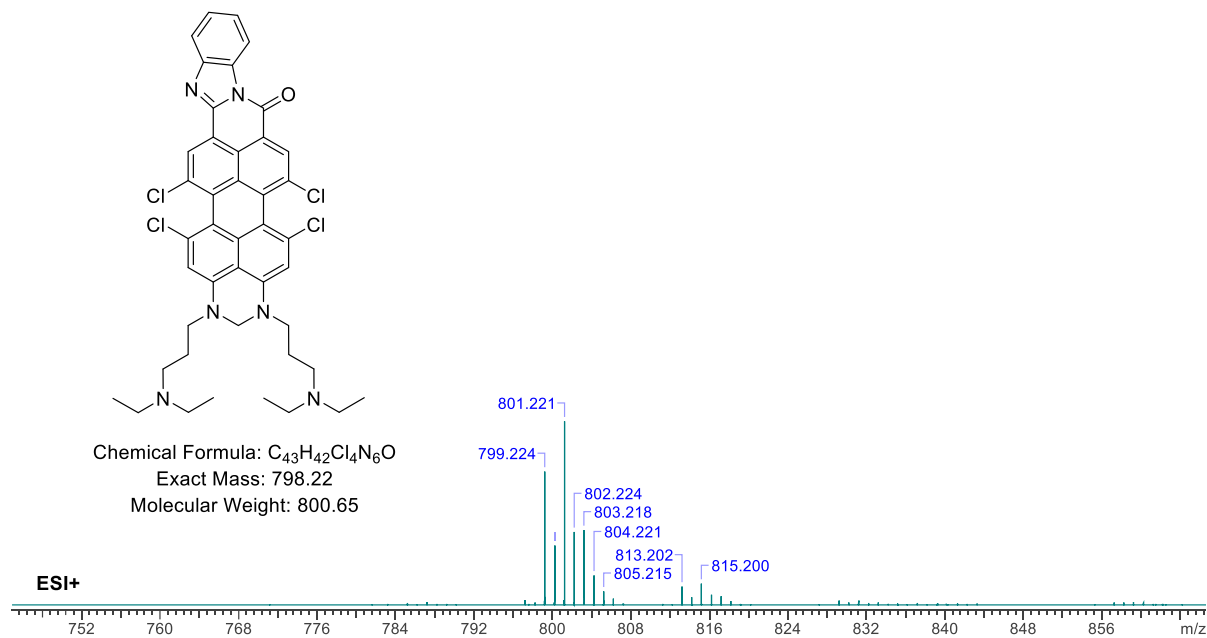Molecular Weight: 800.65

ESI+

Figure 103 ESI-HRMS 5,6,16,17-tetrachloro-1,3-bis(3-(diethylamino)propyl)-2,3-dihydrobenzo[4'',5'']imidazo[1'',2'':1',2']pyrido[3',4',5':6,7]phenaleno[1,2,3-gh]perimidin-8(1H)-one

2020-06-22_bf157b_2_2_01_2068_1_MS1_Positive

TIC (Positive)

6.79 6.80 6.81 6.82 6.83 6.84 6.85 6.86 6.87 6.88 6.89 6.90 6.91 6.92   Retention Time (min)

Retention Time: 6.879

Ion Mode: Positive

Chemical Formula: $C_{43}H_{42}Cl_4N_6O$
Exact Mass: 798.22
Molecular Weight: 800.65

Positive

799.223
801.221
802.224
803.219
804.221
805.217
813.202
815.202
817.200

788 790 792 794 796 798 800 802 804 806 808 810 812 814 816 818 820 m/z
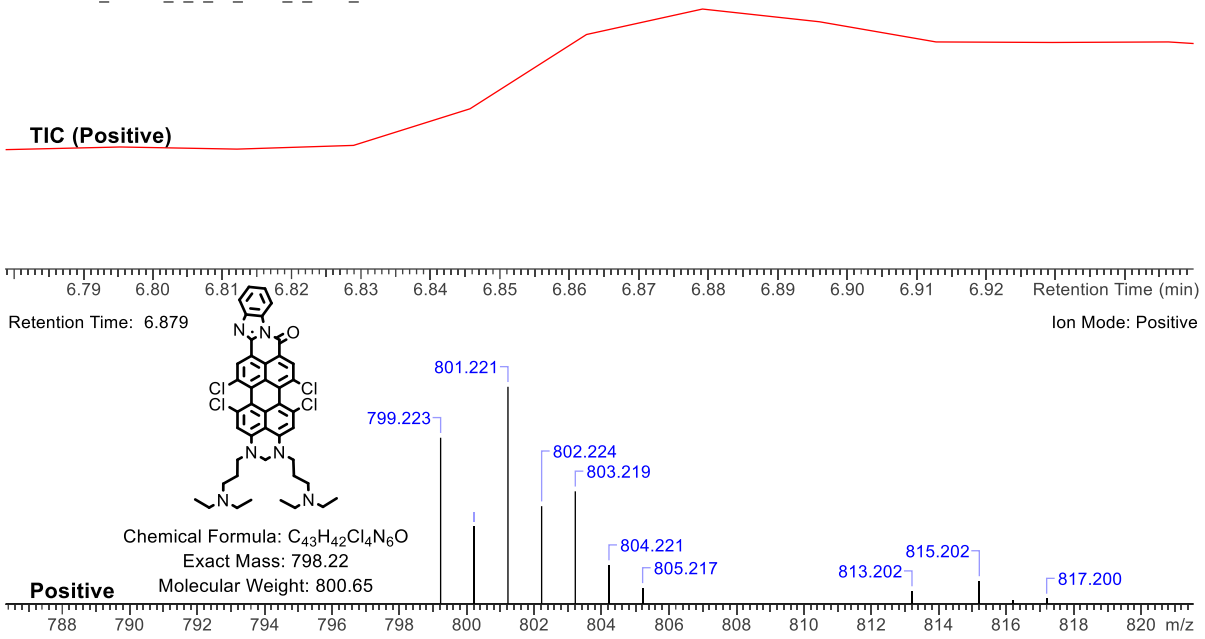
Figure 104 Chromatogram peak of 5,6,16,17-tetrachloro-1,3-bis(3-(diethylamino)propyl)-2,3-dihydrobenzo[4'',5'']imidazo[1'',2'':1',2']pyrido[3',4',5':6,7]phenaleno[1,2,3-gh]perimidin-8(1H)-one at retention time 6.879 minutes (top), far red absorption profile (bottom left), ESI mass isotopic pattern (bottom right)
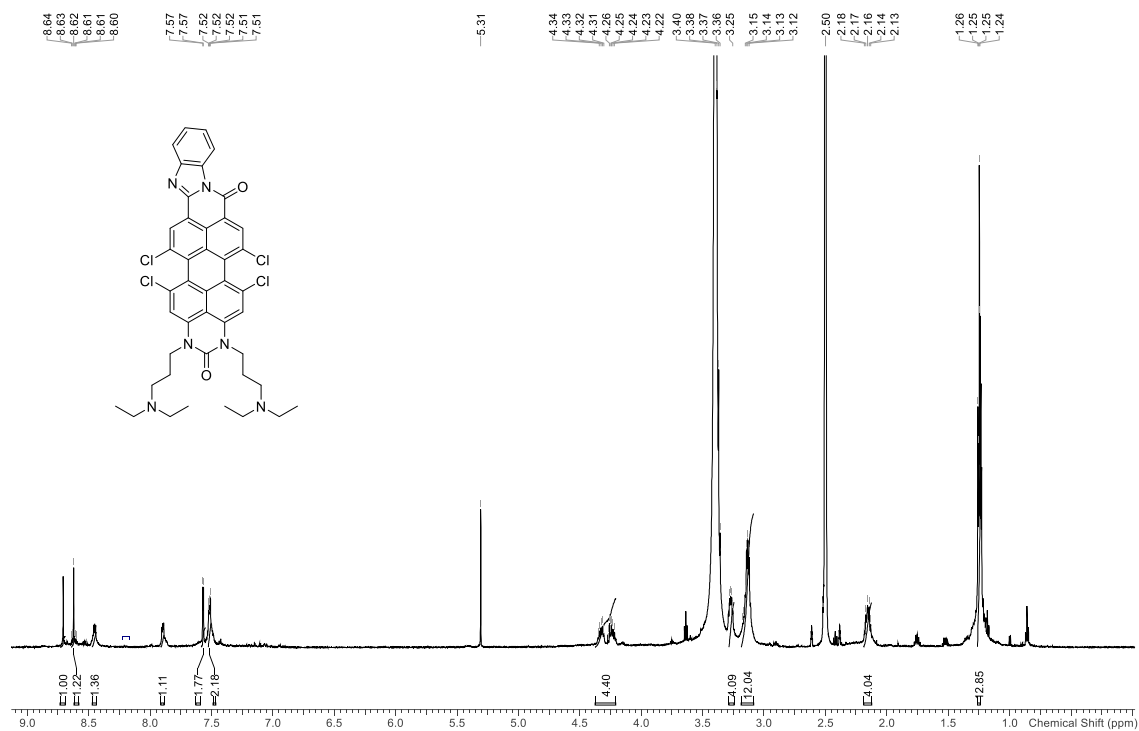
Figure 105 ¹H NMR spectrum of 5,6,16,17-tetrachloro-1,3-bis(3-(diethylamino)propyl)benzo[4'',5'']imidazo[1'',2'':1',2']pyrido[3',4',5':6,7]phenaleno[1,2,3-gh]perimidine-2,8(1H,3H)-dione (DMSO-d6, 400 MHz)
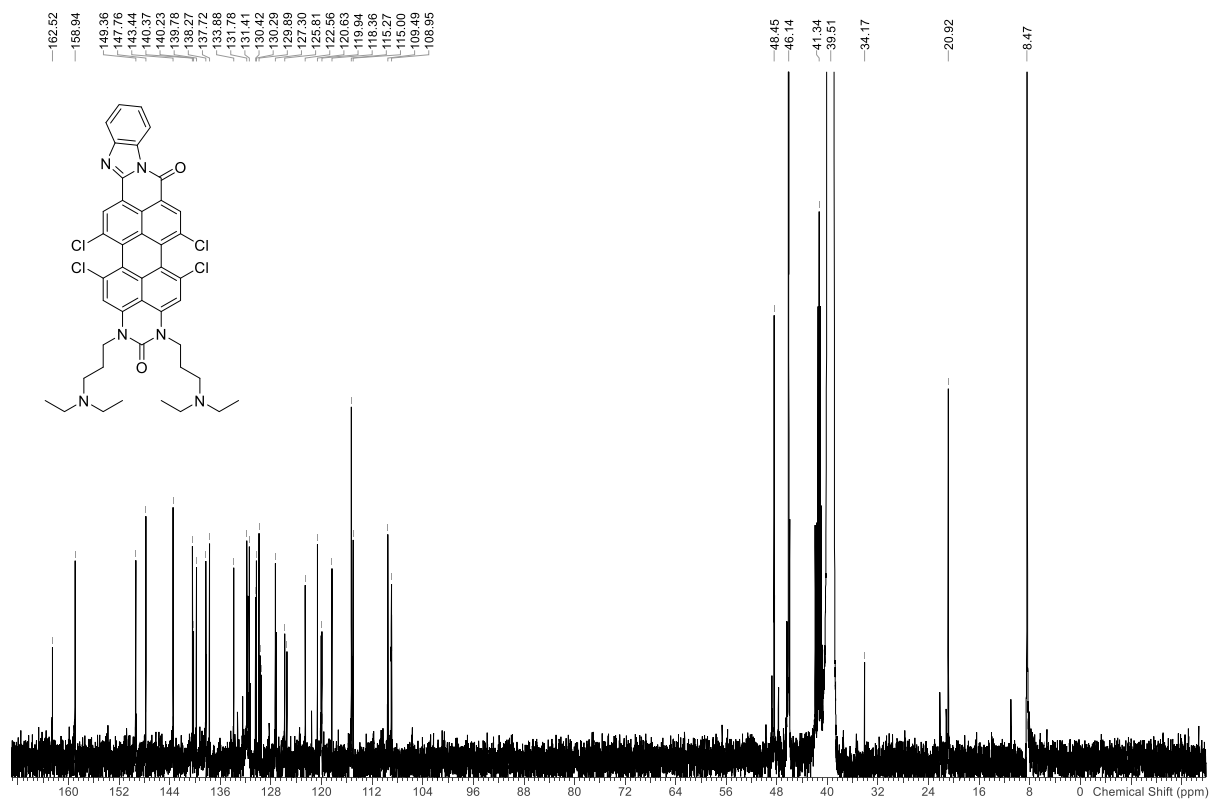

Figure 106 ¹³C NMR spectrum of 5,6,16,17-tetrachloro-1,3-bis(3-(diethylamino)propyl)benzo[4'',5'']imidazo[1'',2'':1',2']pyrido[3',4',5':6,7]phenaleno[1,2,3-gh]perimidine-2,8(1H,3H)-dione (DMSO-d6, 126 MHz)

Figure 107 ¹H-¹H COSY spectrum of 5,6,16,17-tetrachloro-1,3-bis(3-(diethylamino)propyl)benzo[4'',5'']imidazo[1'',2'':1',2']pyrido[3',4',5':6,7]phenaleno[1,2,3-gh]perimidine-2,8(1H,3H)-dione (DMSO-d6)

Figure 108 ¹H-¹³C HSQC spectrum of 5,6,16,17-tetrachloro-1,3-bis(3-(diethylamino)propyl)benzo[4'',5'']imidazo[1'',2'':1',2']pyrido[3',4',5':6,7]phenaleno[1,2,3-gh]perimidine-2,8(1H,3H)-dione (DMSO-d6)

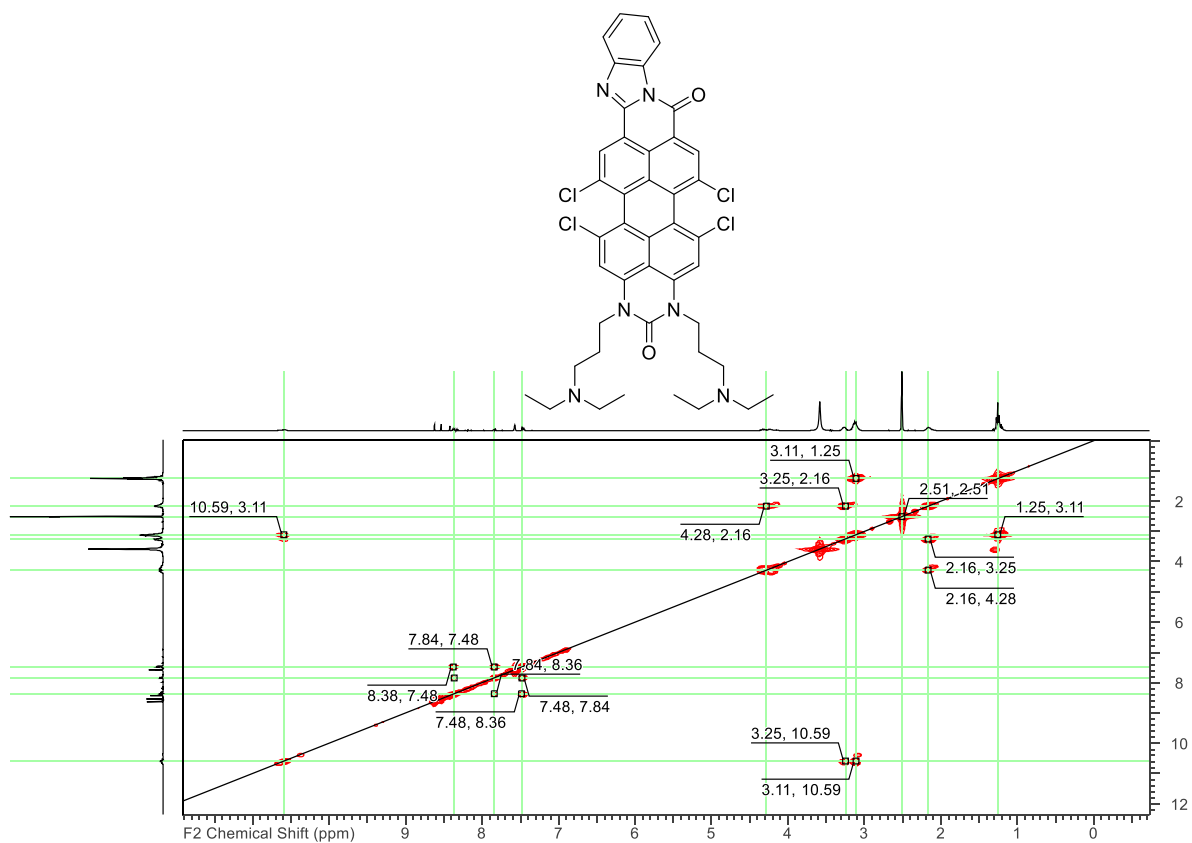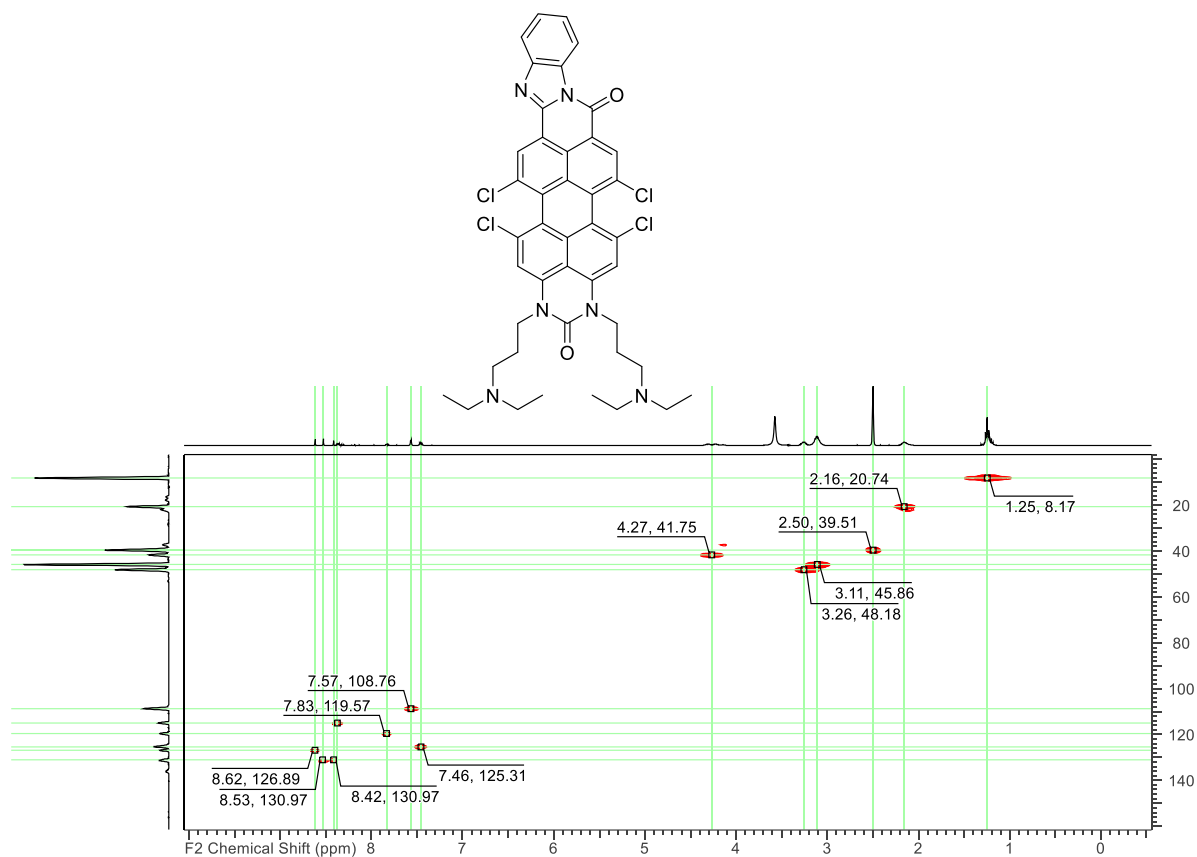Chemical Formula: $C_{43}H_{40}Cl_4N_6O_2$
Exact Mass: 812.20
Molecular Weight: 814.63

ESI+

Figure 109 ESI-HRMS of 5,6,16,17-tetrachloro-1,3-bis(3-(diethylamino)propyl)benzo[4'',5'']imidazo[1'',2'':1',2']pyrido[3',4',5':6,7]phenaleno[1,2,3-gh]perimidine-2,8(1H,3H)-dione

Figure 110 Chromatogram showing peak of 5,6,16,17-tetrachloro-1,3-bis(3-(diethylamino)propyl)benzo[4'',5'']imidazo[1'',2'':1',2']pyrido[3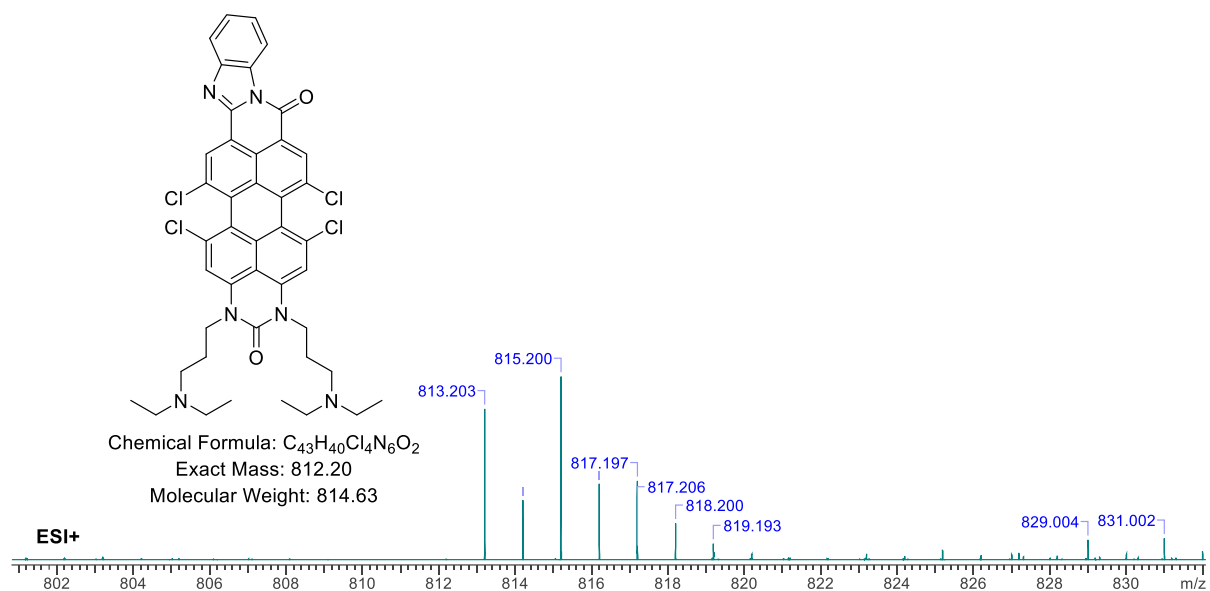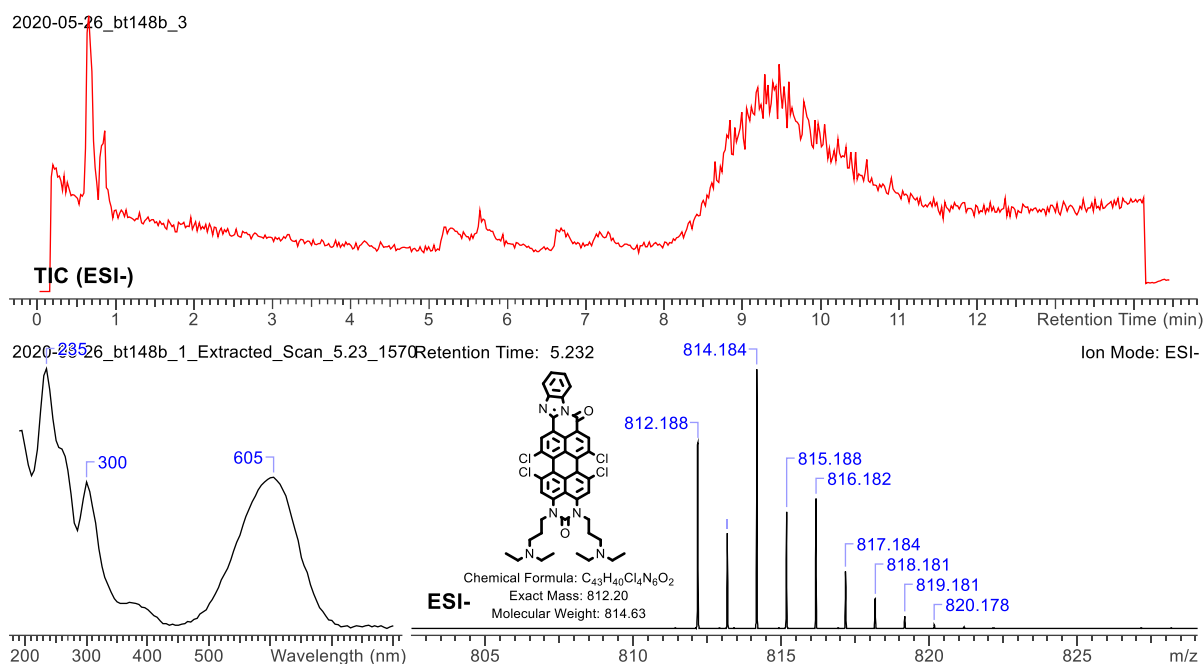',4',5':6,7]phenaleno[1,2,3-gh]perimidine-2,8(1H,3H)-dione at retention time 5.23 minutes (top), absorption profile (bottom-left), ESI isotopic pattern (bottom right).
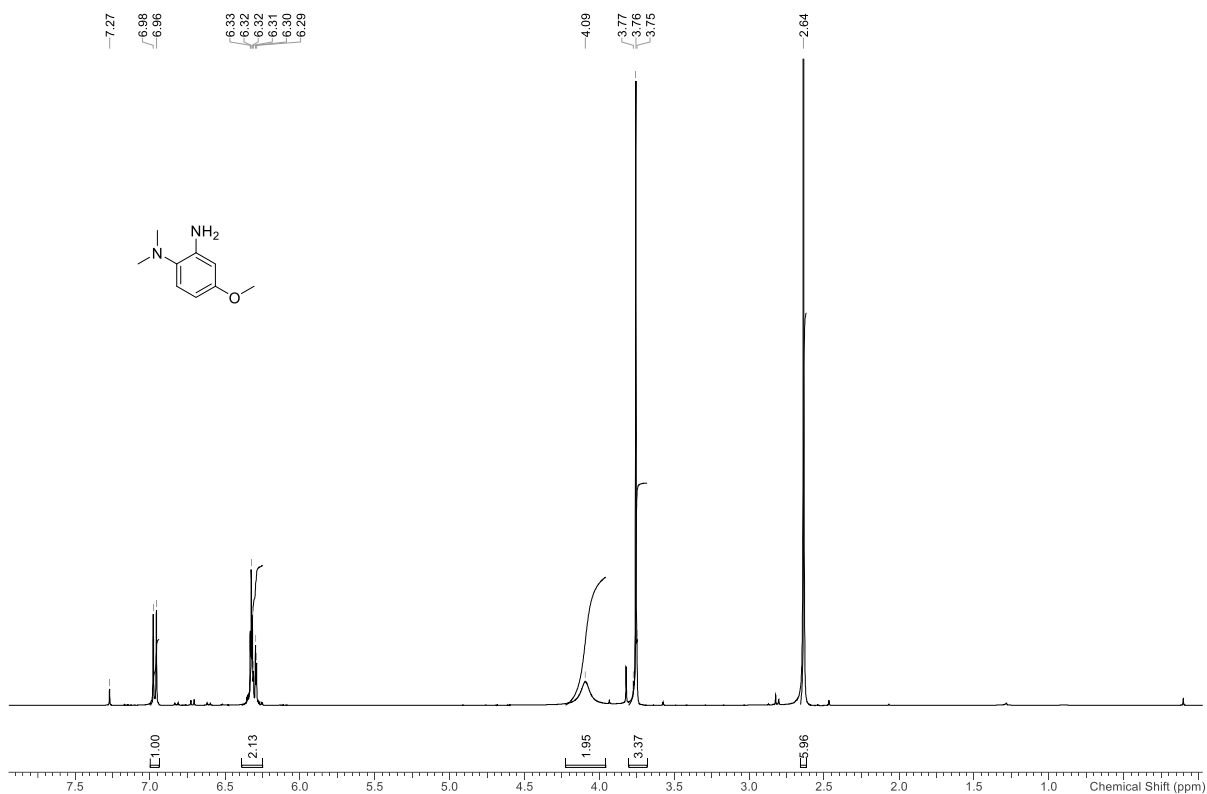
Figure 111 ^{1}H spectrum of 4-methoxy-N^1,N^1-dimethylbenzene-1,2-diamine (250 MHz Chloroform-d)
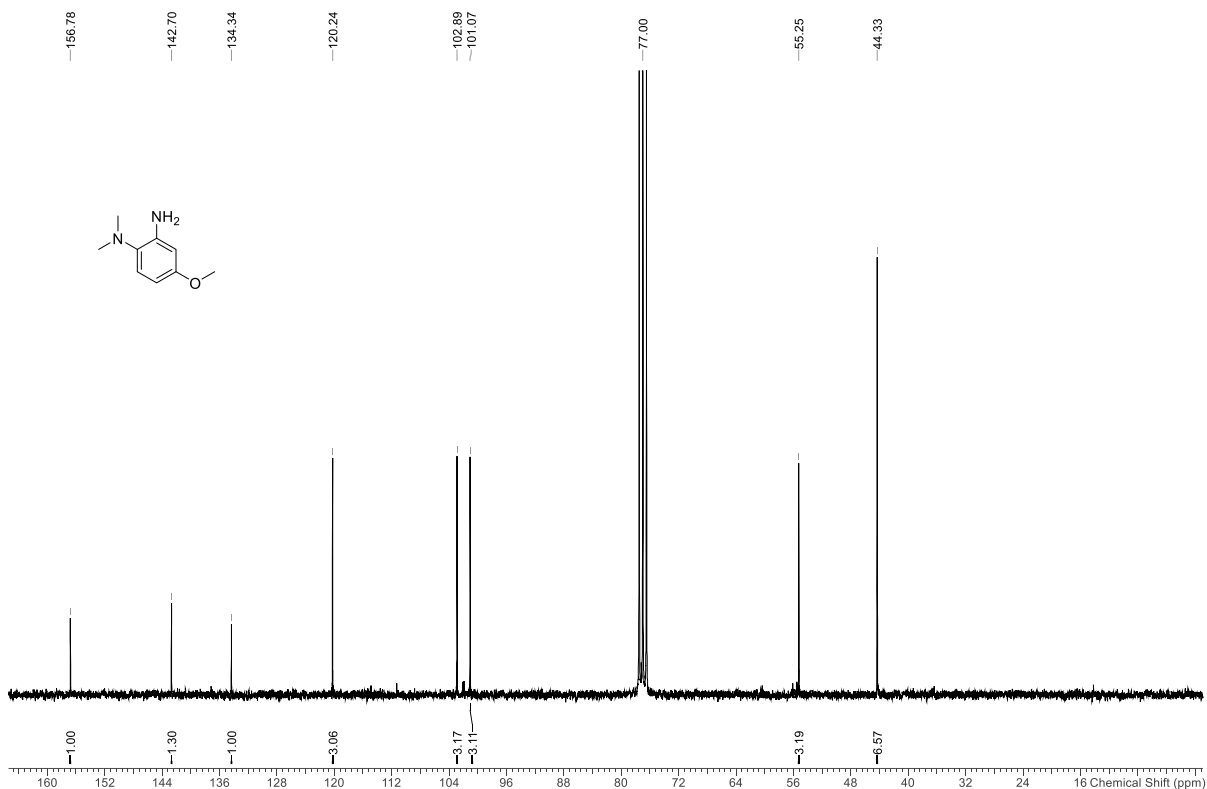
Figure 112 ^{13}C NMR spectrum 4-methoxy-N^1,N^1-dimethylbenzene-1,2-diamine (63 MHz Chloroform-d)
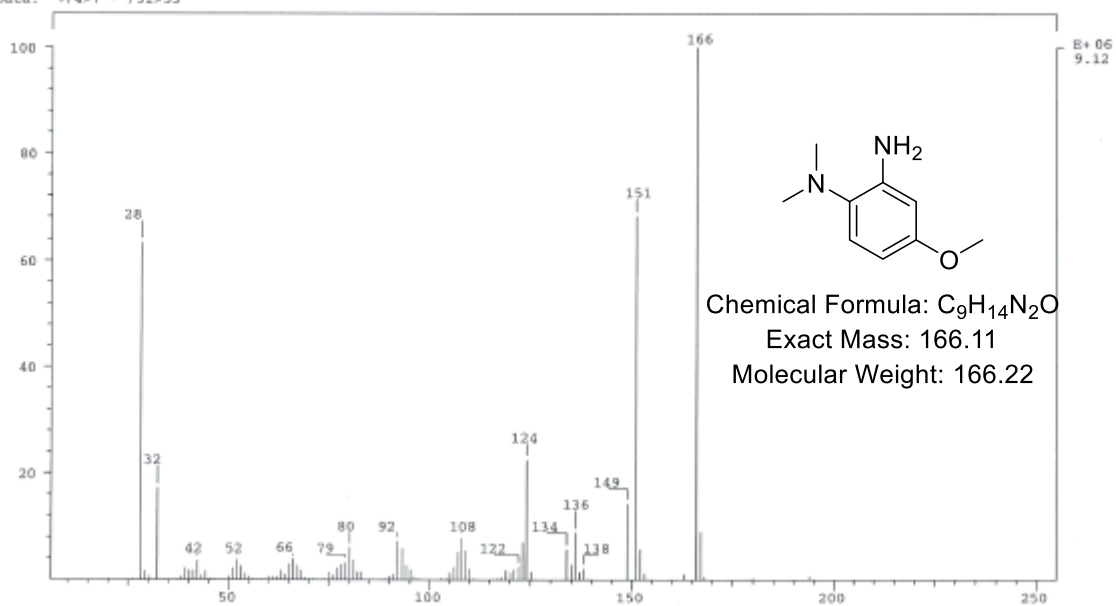
Figure 113 EI-MS spectrum of 4-methoxy-N[1],N[1]-dimethylbenzene-1,2-diamine
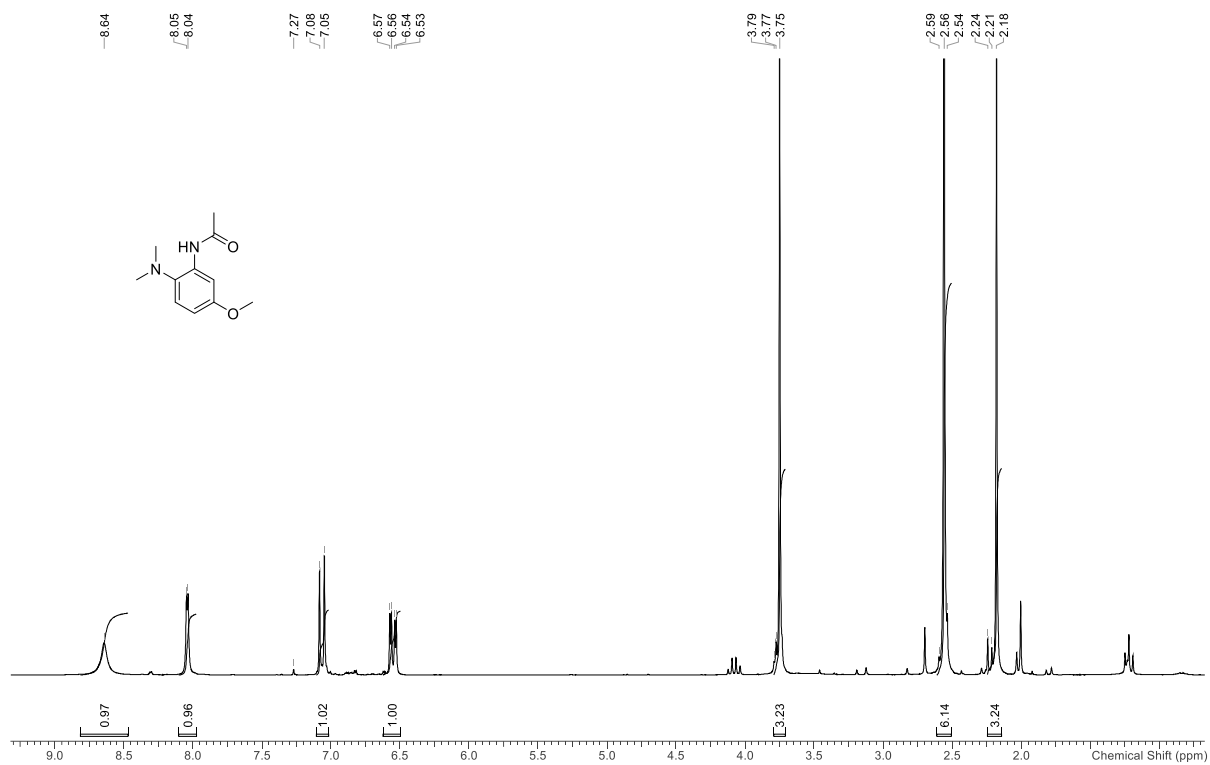
Figure 114 ¹H NMR spectrum of N-(2-(dimethylamino)-5-methoxyphenyl)acetamide (400 MHz, Chloroform-d)
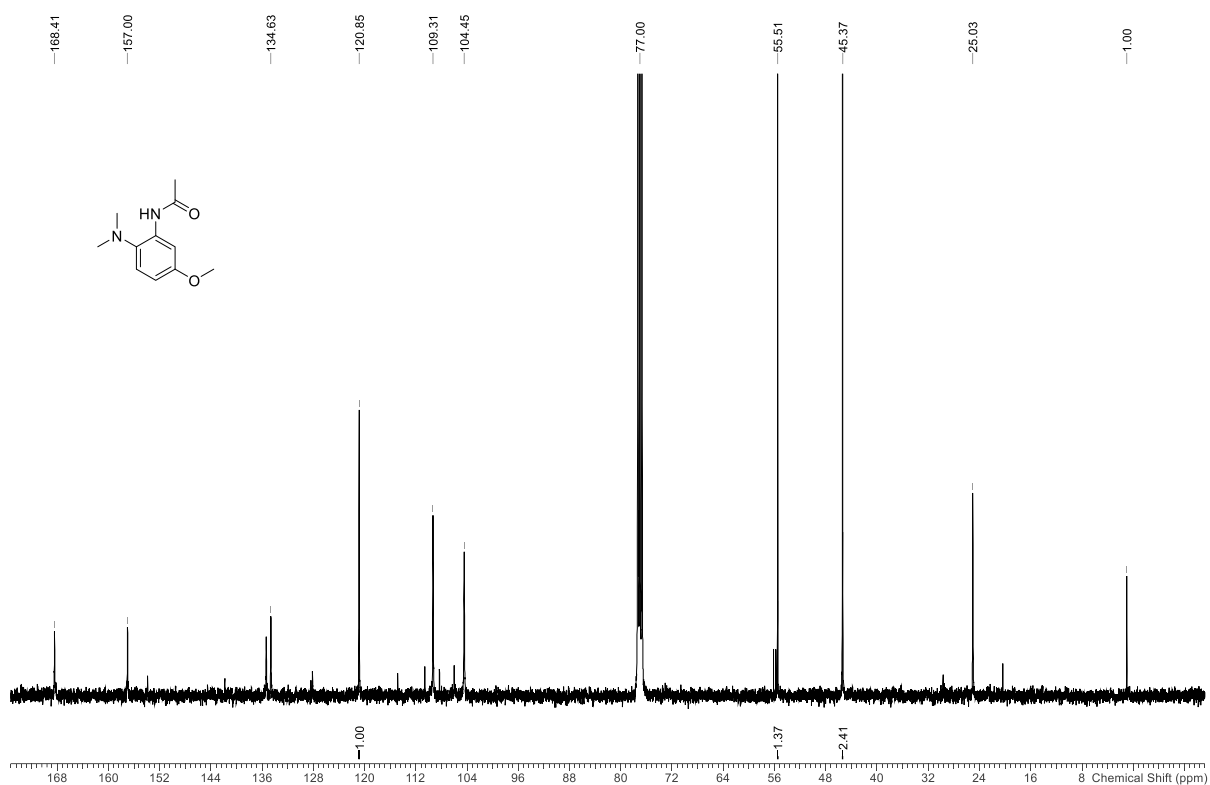
Figure 115 ¹³C NMR spectrum of N-(2-(dimethylamino)-5-methoxyphenyl)acetamide (101 MHZ, Chloroform-d)
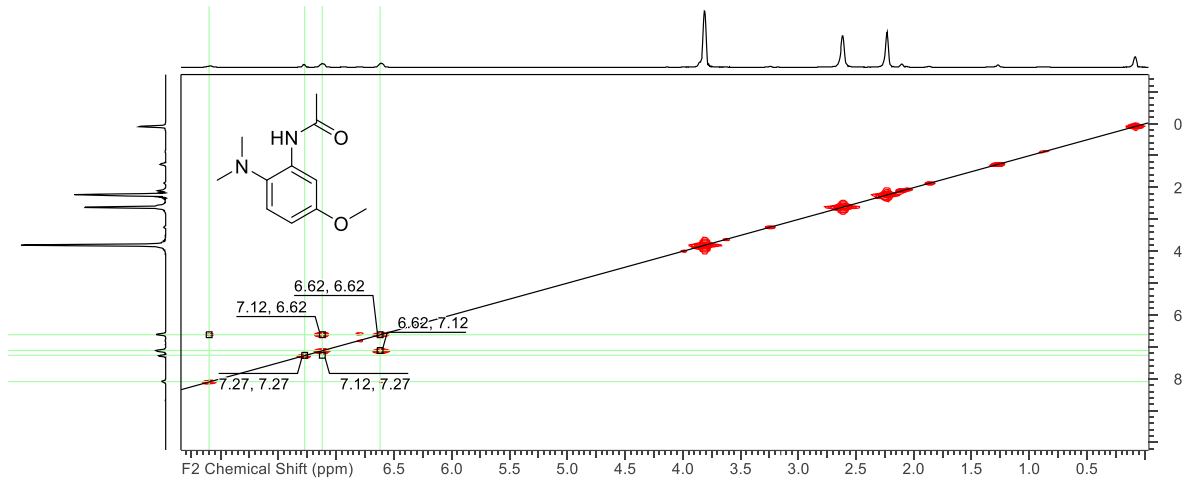
Figure 116 ¹H-¹H COSY spectrum of N-(2-(dimethylamino)-5-methoxyphenyl)acetamide (Chloroform-d)
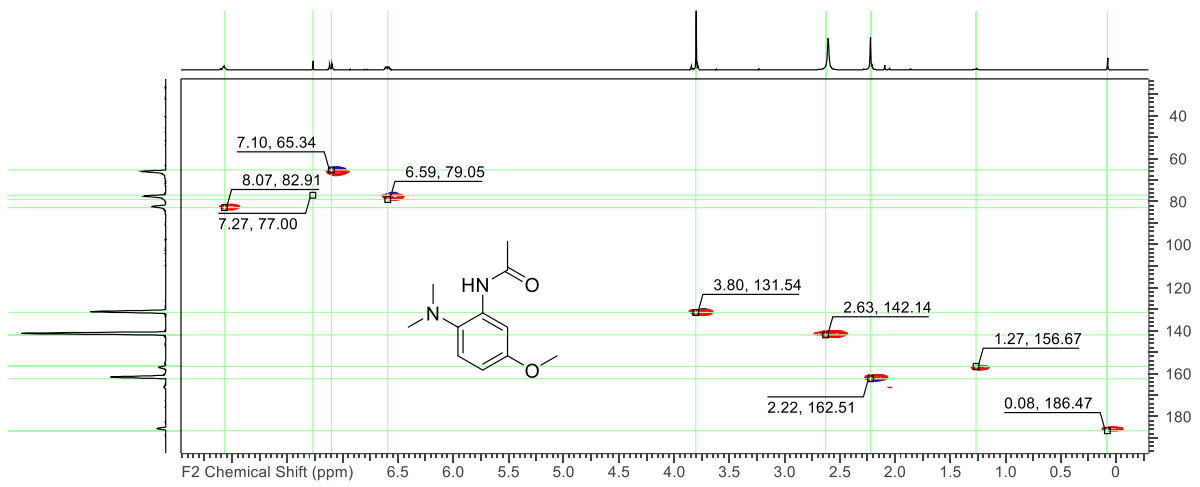
Figure 117 ¹H-¹³C HSQC spectrum of N-(2-(dimethylamino)-5-methoxyphenyl)acetamide (Chloroform-d)
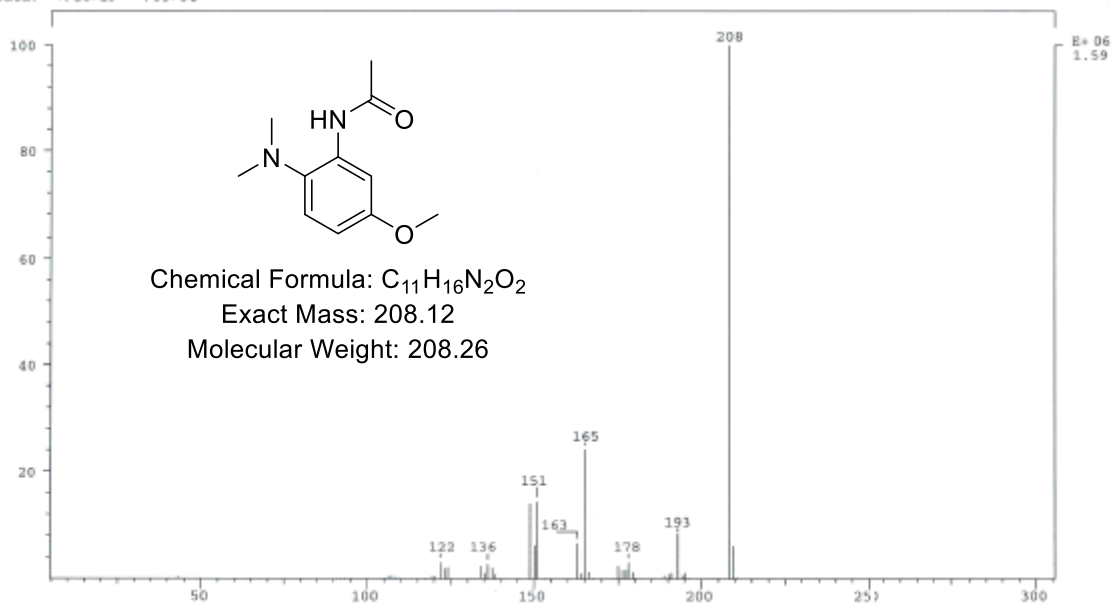
Figure 118 EI-MS spectrum of N-(2-(dimethylamino)-5-methoxyphenyl)acetamide
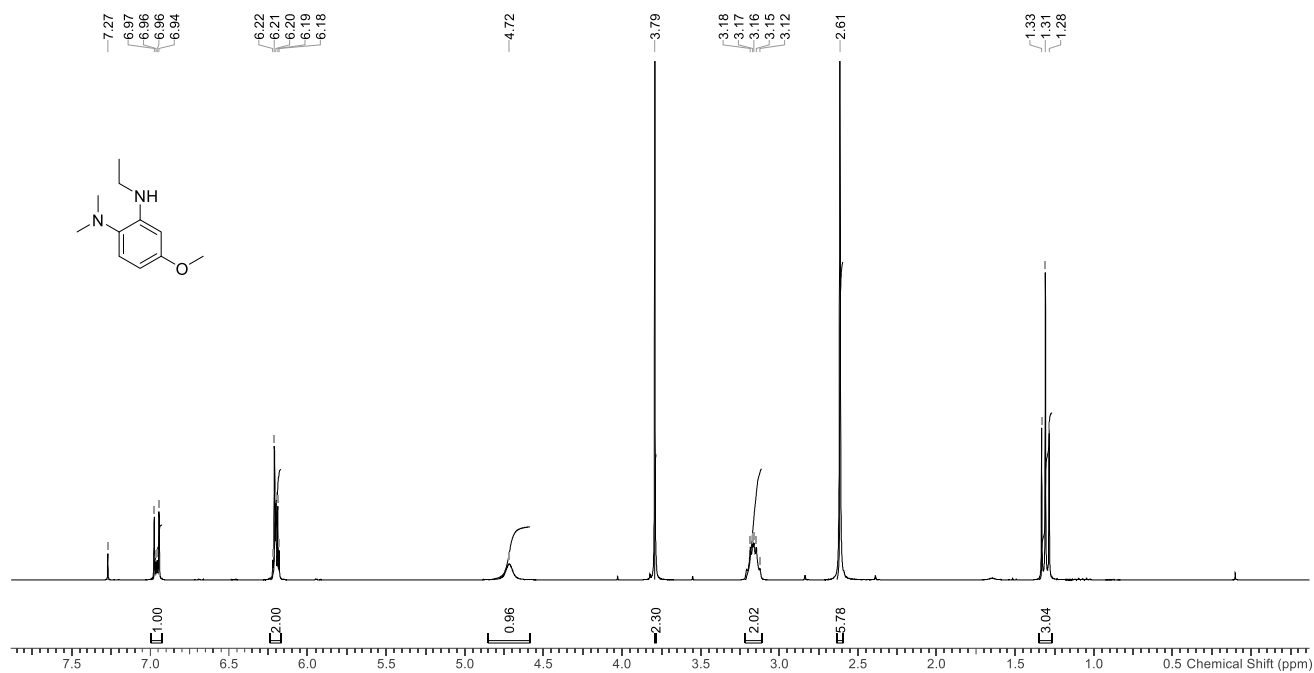
Figure 119 ¹H spectrum of N²-ethyl-4-methoxy-N¹,N¹-dimethylbenzene-1,2-diamine (300 MHz, Chloroform-d)
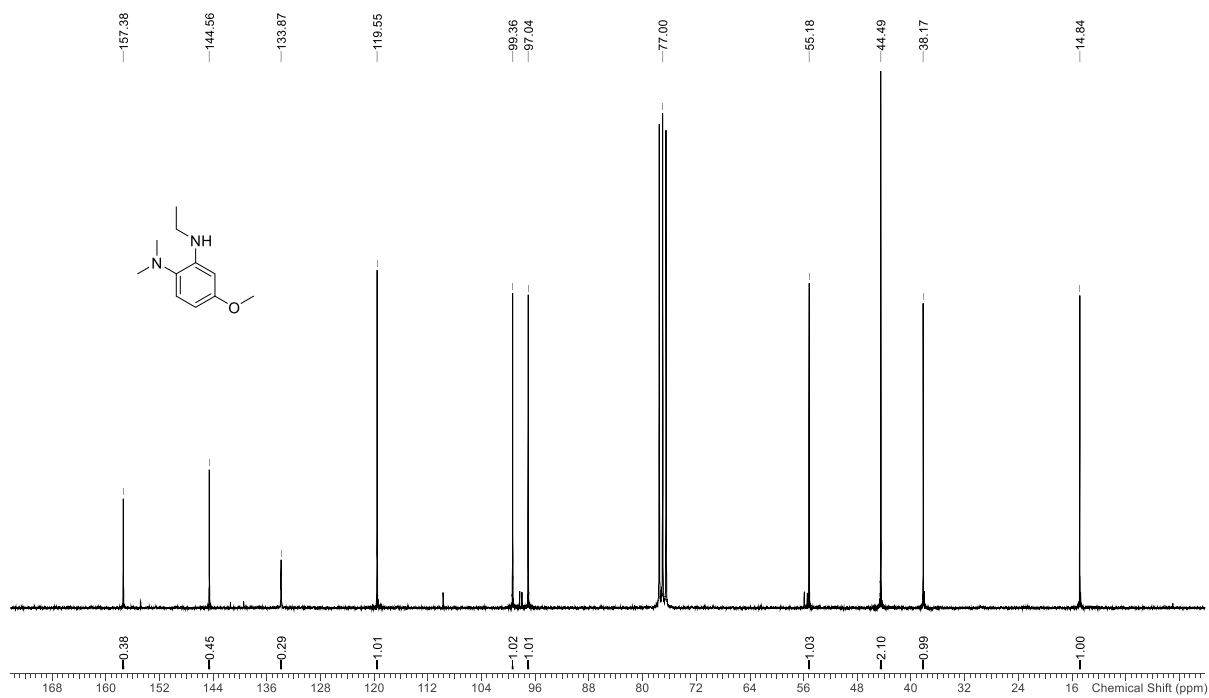
Figure 120 ¹³C spectrum of N2-ethyl-4-methoxy-N1,N1-dimethylbenzene-1,2-diamine (101 MHz, Chloroform-d)

Figure 121 ^{1}H-^{1}H COSY spectrum of N^2-ethyl-4-methoxy-N^1,N^1-dimethylbenzene-1,2-diamine (Chloroform-d)

Figure 122 ^{1}H-^{13}C HSQC spectrum of N^2-ethyl-4-methoxy-N^1,N^1-dimethylbenzene-1,2-diamine (Chloroform-d)

Chemical Formula: $C_{11}H_{18}N_2O$
Exact Mass: 194.14
Molecular Weight: 194.28

Figure 123 EI-MS Spectrum of N^2-ethyl-4-methoxy-N^1,N^1-dimethylbenzene-1,2-diamine
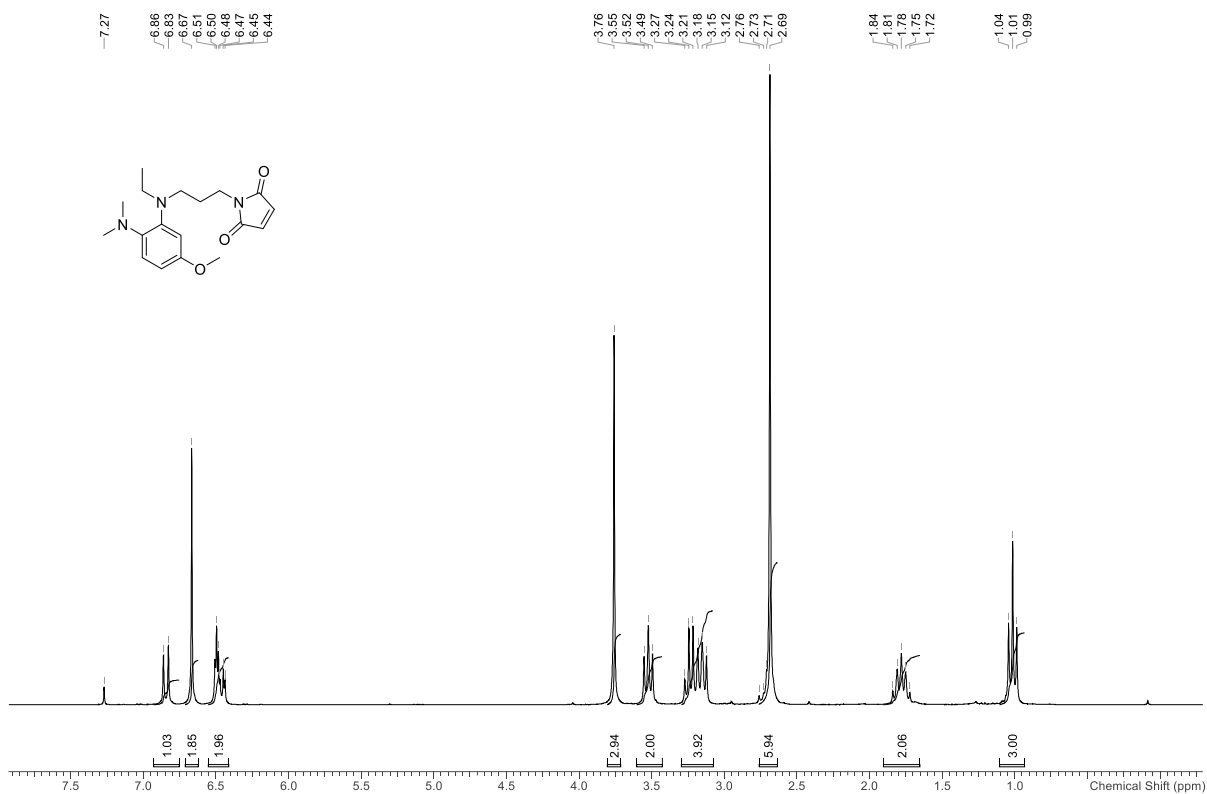
Figure 124 ¹H spectrum of 1-(3-((2-(dimethylamino)-5-methoxyphenyl)(ethyl)amino)propyl)-1H-pyrrole-2,5-dione (300 MHz, Chloroform-d)
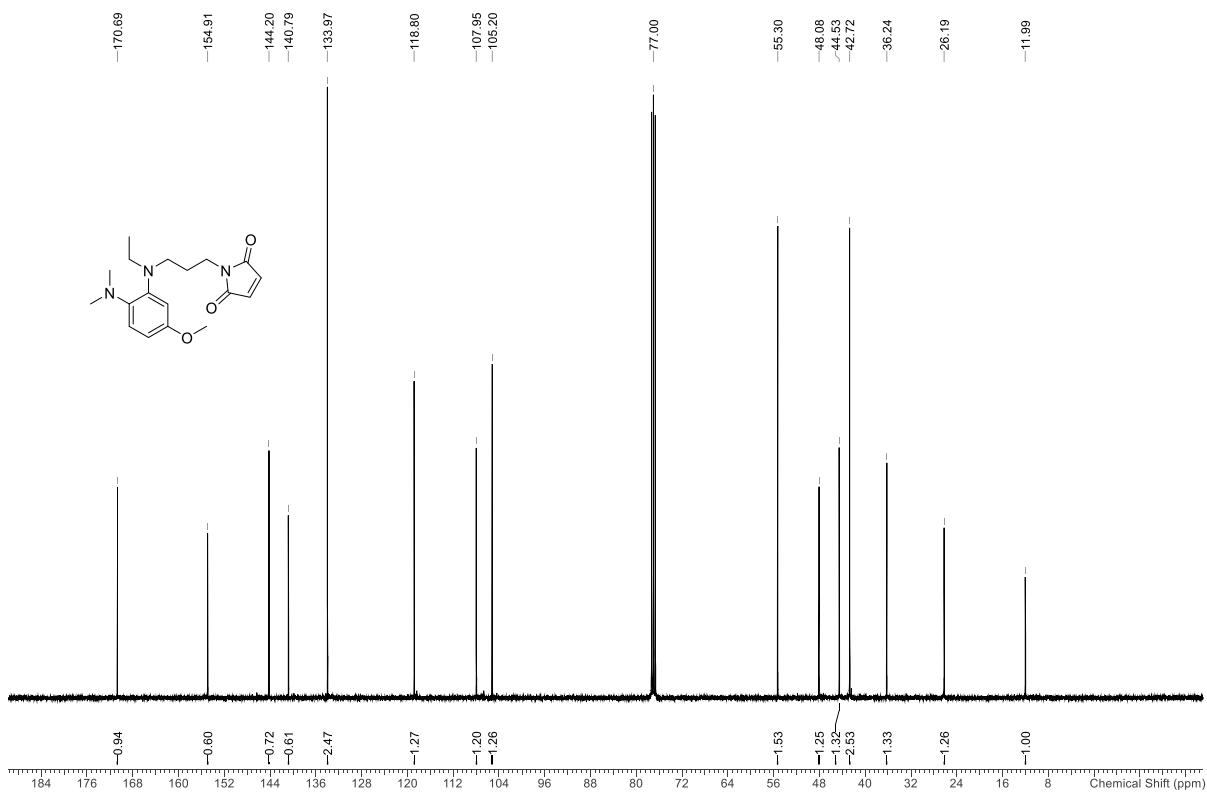
Figure 125 ¹³C spectrum of 1-(3-((2-(dimethylamino)-5-methoxyphenyl)(ethyl)amino)propyl)-1H-pyrrole-2,5-dione (Chloroform-d, 126 MHz)

Figure 126 ¹H ¹H COSY spectrum of 1-(3-((2-(dimethylamino)-5-methoxyphenyl)(ethyl)amino)propyl)-1H-pyrrole-2,5-dione (Chloroform-d)

Figure 127 ¹H-¹³C spectrum of 1-(3-((2-(dimethylamino)-5-methoxyphenyl)(ethyl)amino)propyl)-1H-pyrrole-2,5-dione (Chloroform-d)
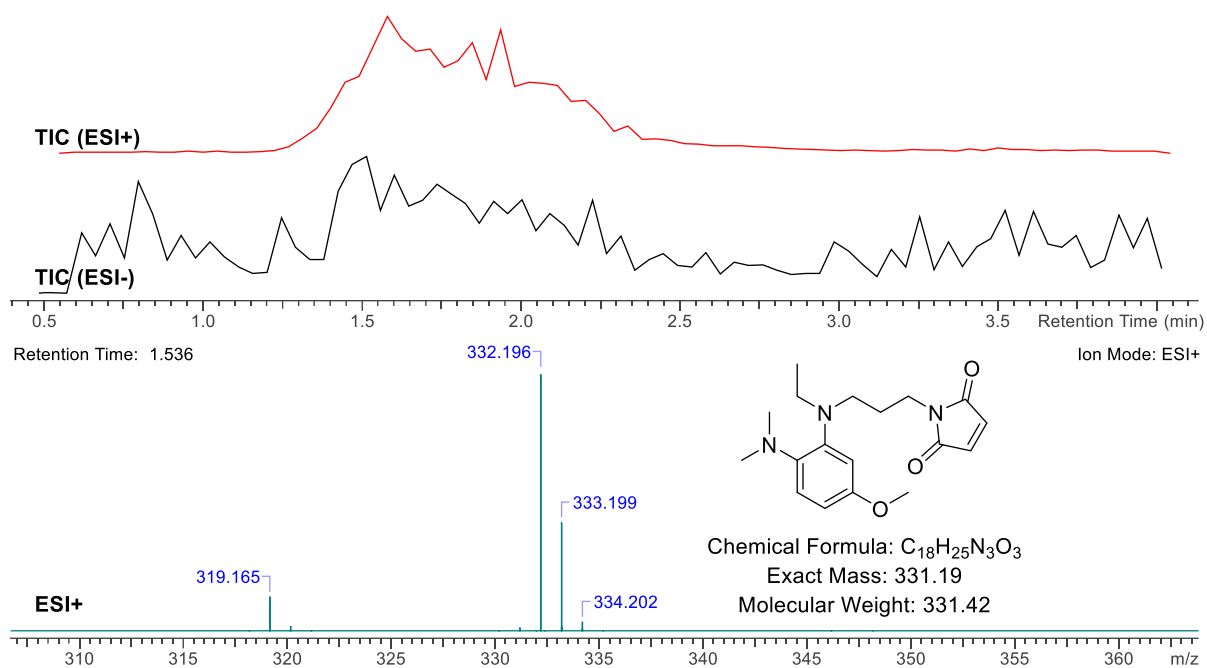
Figure 128 ESI-HRMS spectrum of 1-(3-((2-(dimethylamino)-5-methoxyphenyl)(ethyl)amino)propyl)-1H-pyrrole-2,5-dione
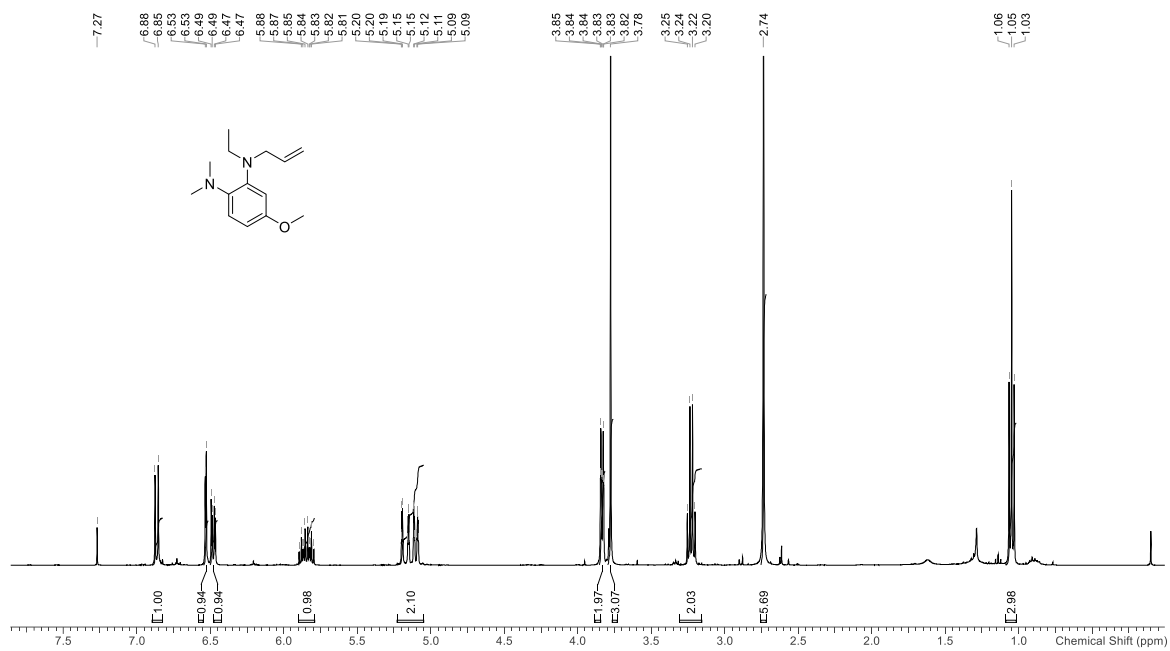
Figure 129 ^{1}H NMR spectrum ofN^2-allyl-N^2-ethyl-4-methoxy-N^1,N^1-dimethylbenzene-1,2-diamine (400 MHz, Chloroform-d)
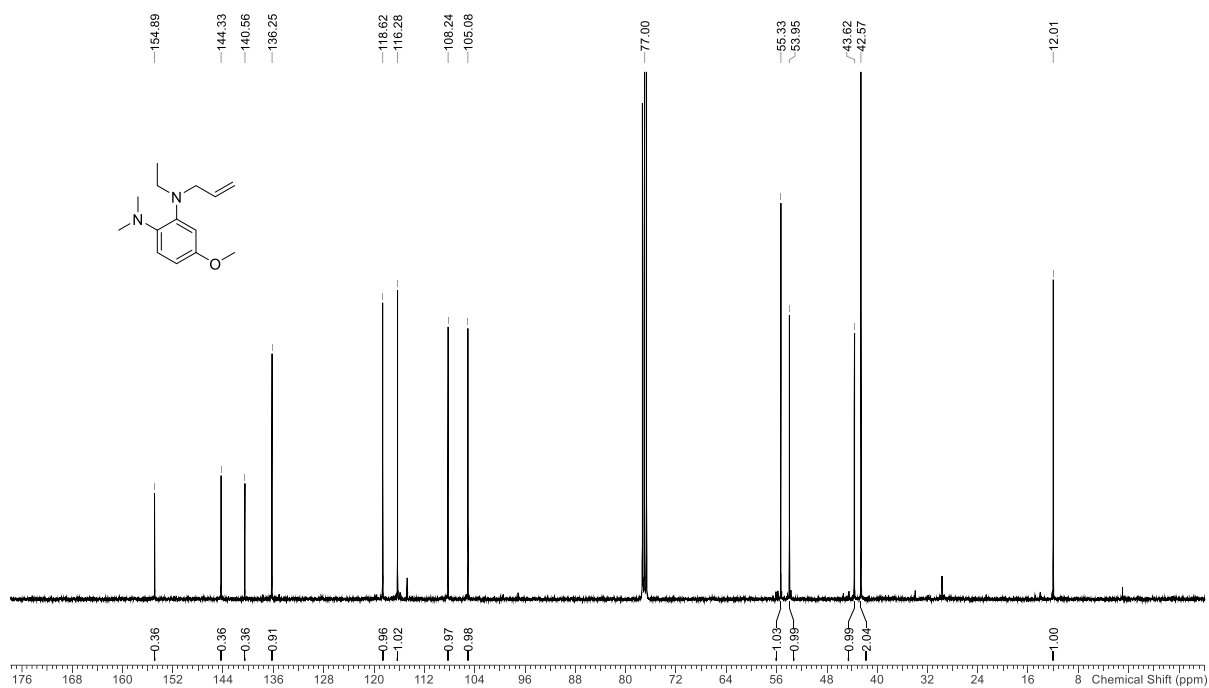
Figure 130 ^{13}C spectrum of N^2-allyl-N^2-ethyl-4-methoxy-N1,N1-dimethylbenzene-1,2-diamine (101 MHz, Chloroform-d)

Figure 131 ¹H-¹H COSY spectrum of N²-allyl-N²-ethyl-4-methoxy-N¹,N¹-dimethylbenzene-1,2-diamine (Chloroform-d)

Figure 132 ¹H-¹³C HSQC spectrum of N²-allyl-N²-ethyl-4-methoxy-N¹,N¹-dimethylbenzene-1,2-diamine (Chloroform-d)
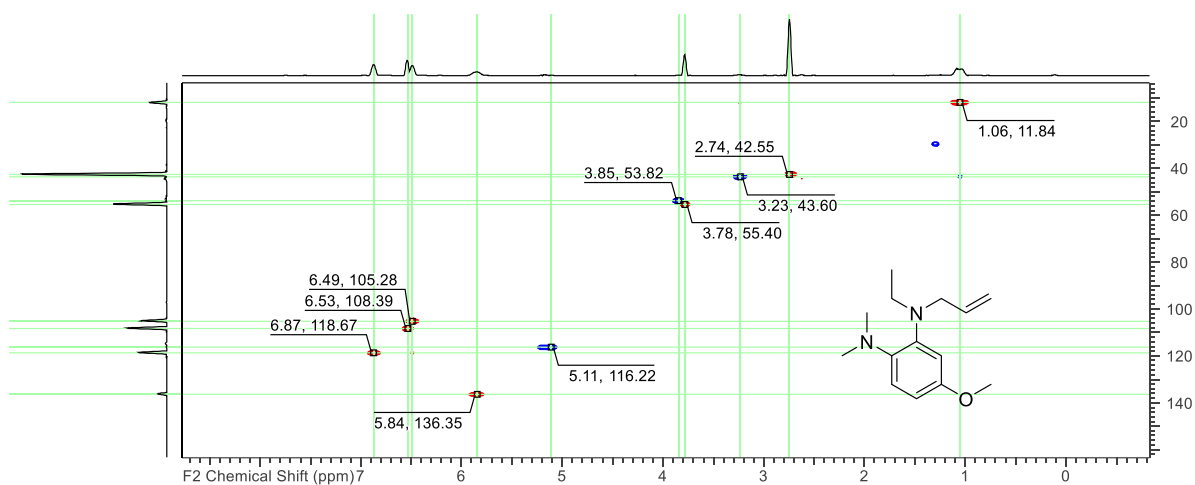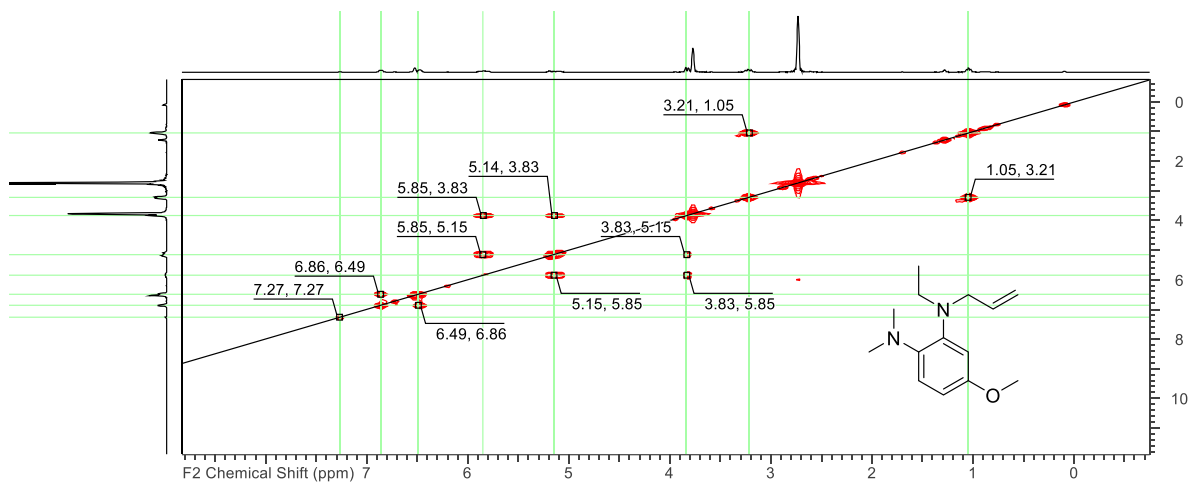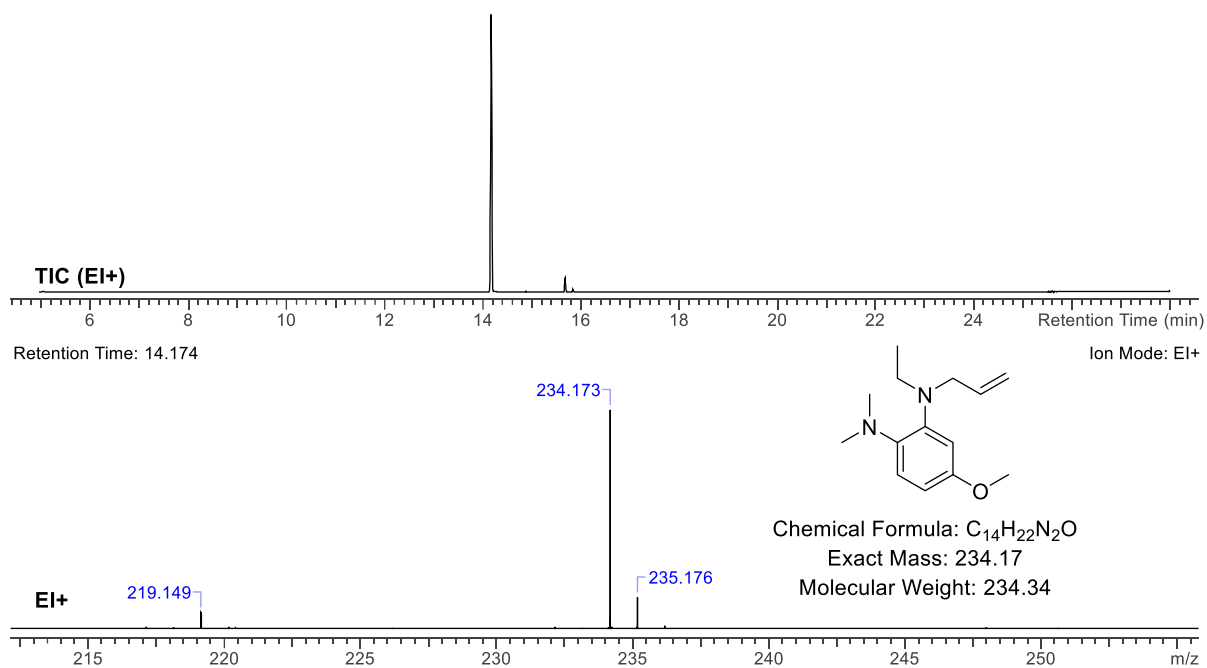
Figure 133 EI-HMRS spectrum of N^2-allyl-N^2-ethyl-4-methoxy-N^1,N^1-dimethylbenzene-1,2-diamine
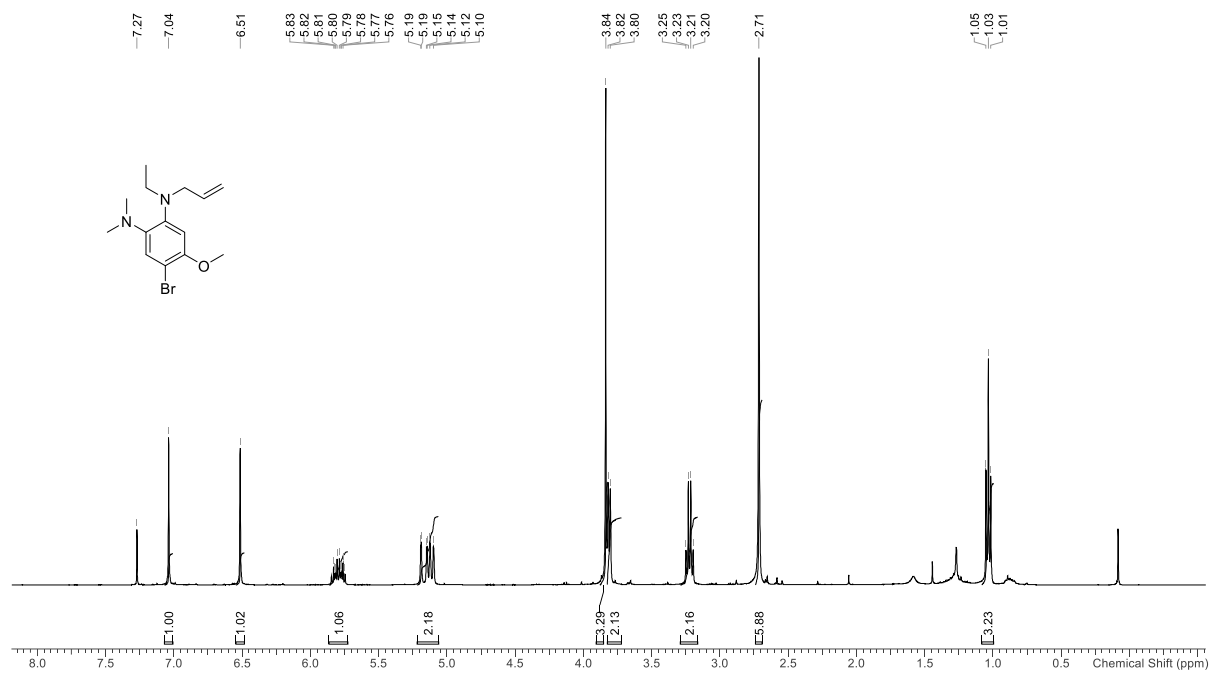
Figure 134 ¹H spectrum of N1-allyl-4-bromo-N1-ethyl-5-methoxy-N2,N2-dimethylbenzene-1,2-diamine (400 MHz Chloroform-d)
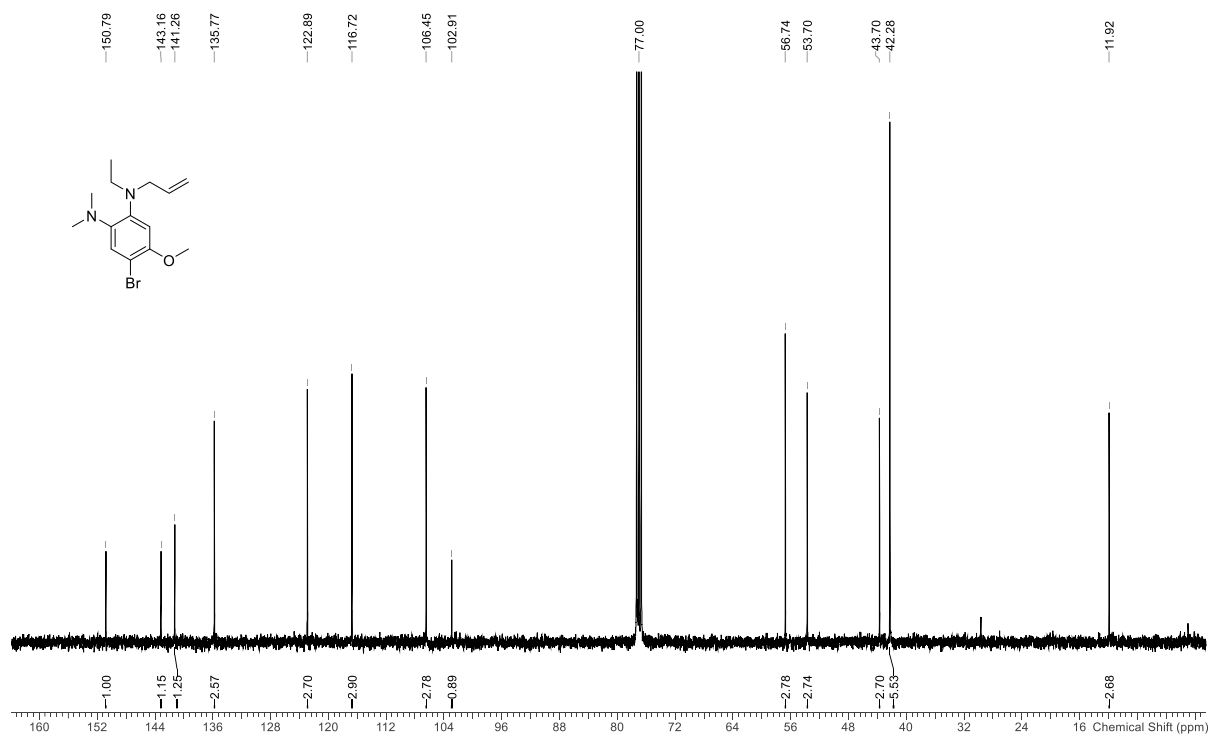
Figure 135 ¹³C spectrum of N1-allyl-4-bromo-N1-ethyl-5-methoxy-N2,N2-dimethylbenzene-1,2-diamine (101 MHz, Chloroform-d)
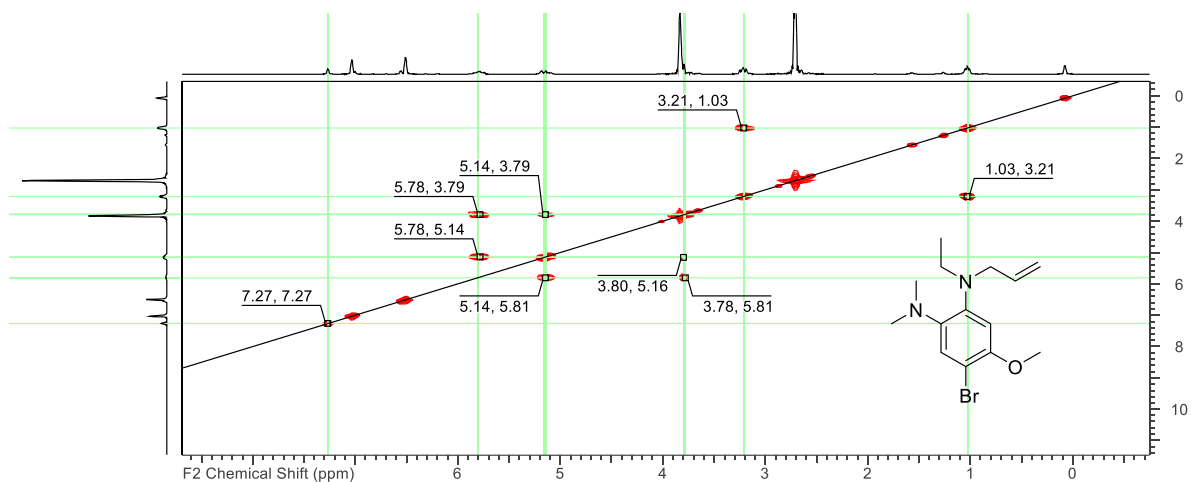
Figure 136 ^{1}H-^{1}H COSY spectrum of N1-allyl-4-bromo-N1-ethyl-5-methoxy-N2,N2-dimethylbenzene-1,2-diamine (Chloroform-d)
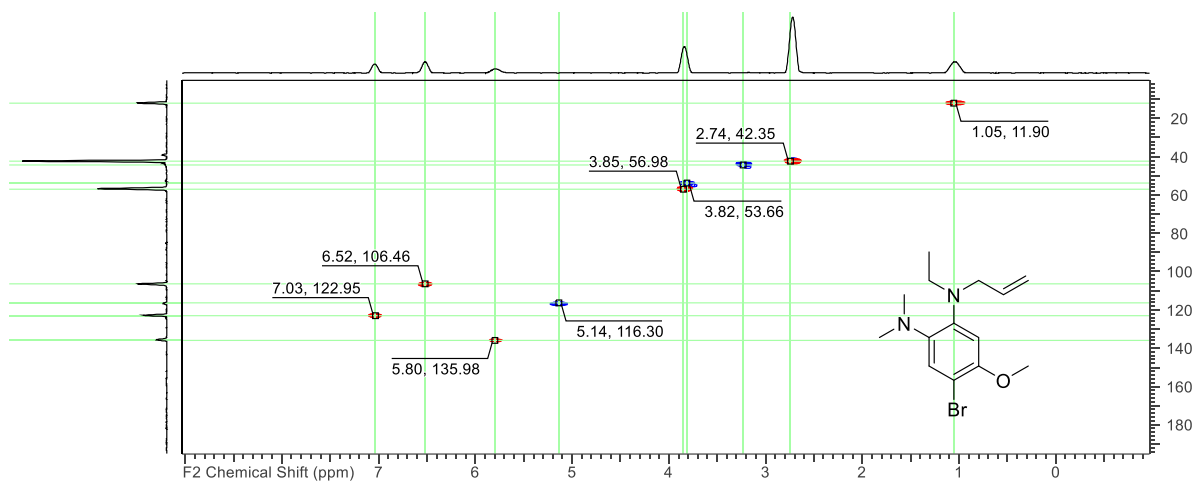
Figure 137 ^{1}H-^{13}C HSQC Spectrum of N1-allyl-4-bromo-N1-ethyl-5-methoxy-N2,N2-dimethylbenzene-1,2-diamine (Chloroform-d)
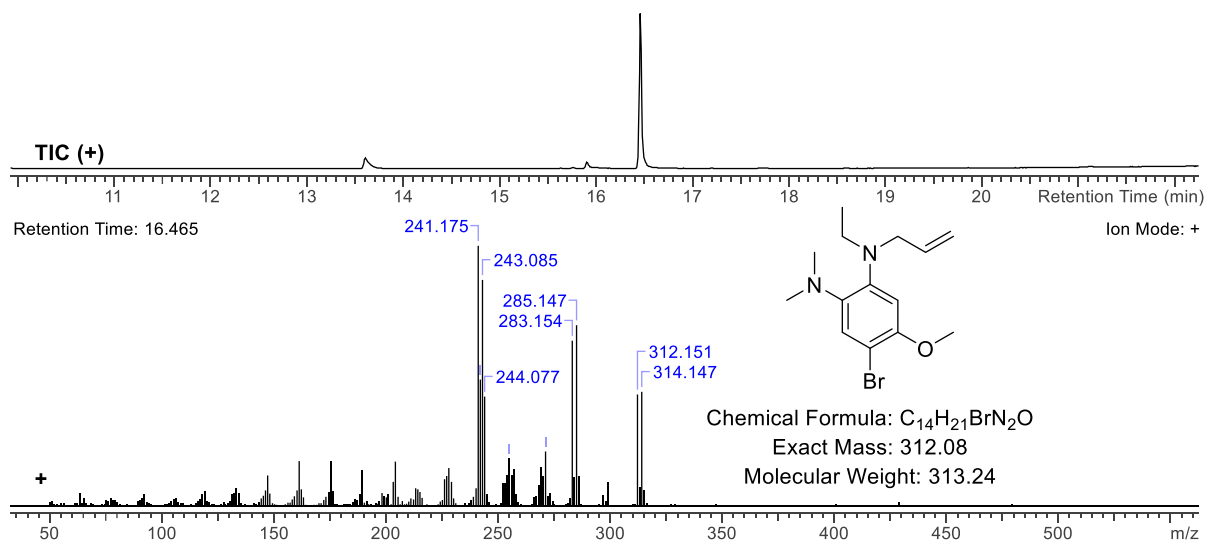
Figure 138 ESI-HRMS Spectrum of N^1-allyl-4-bromo-N^1-ethyl-5-methoxy-N^2,N^2-dimethylbenzene-1,2-diamine
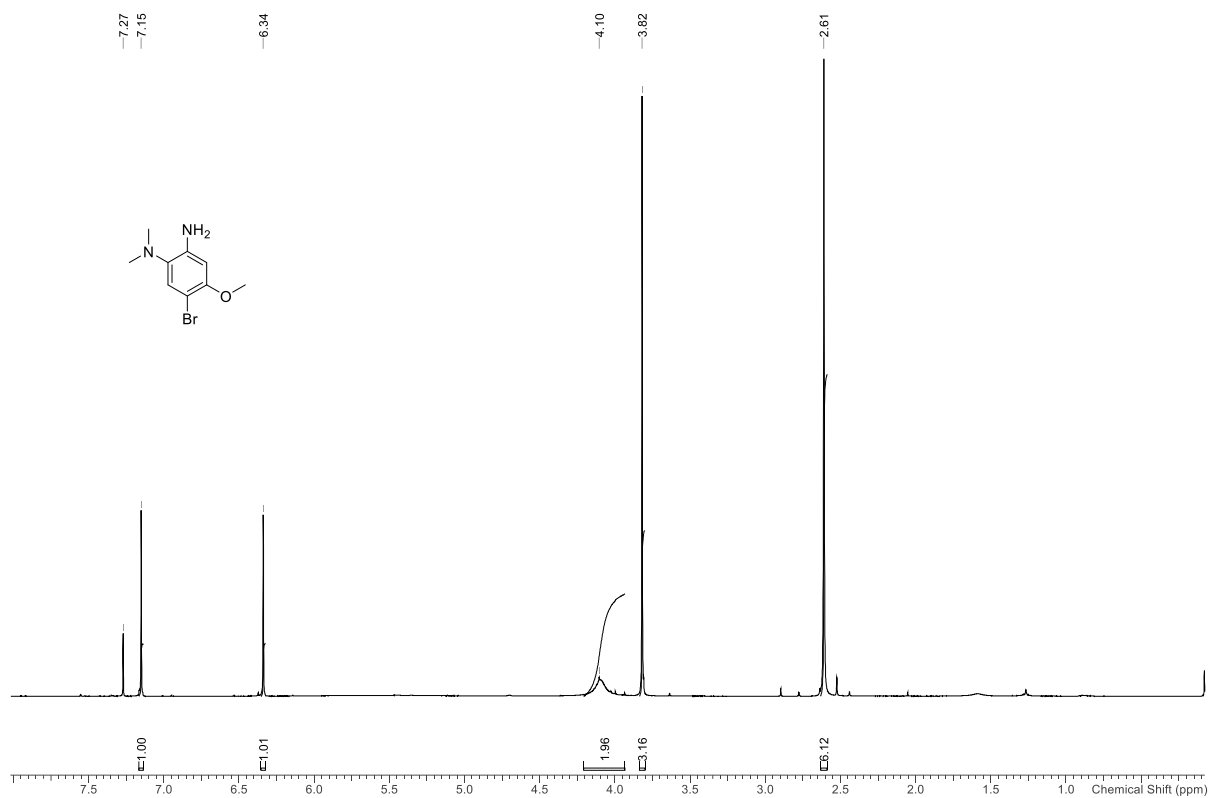
Figure 139 ^{1}H NMR Spectrum of 5-bromo-4-methoxy-N[1],N[1]-dimethylbenzene-1,2-diamine (400 MHz CHLOROFORM-d)
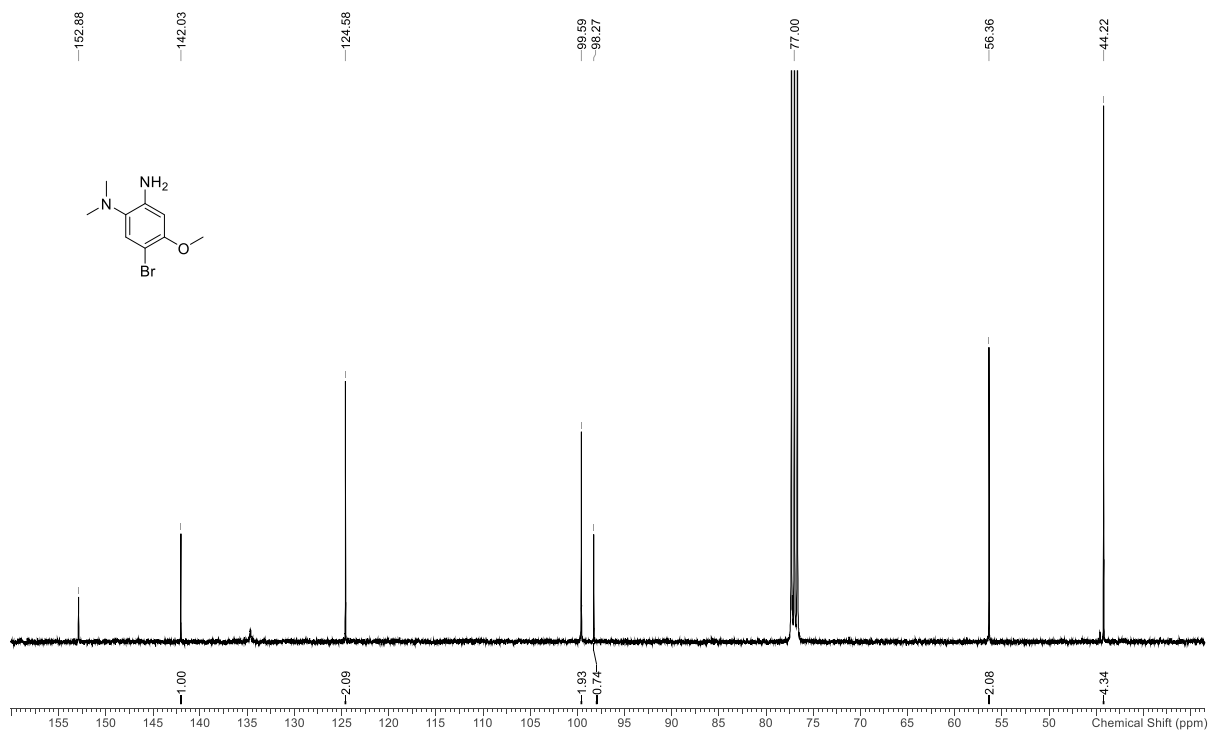
Figure 140 [13]C Spectrum of 5-bromo-4-methoxy-N[1],N[1]-dimethylbenzene-1,2-diamine (101 MHz, Chloroform-d)
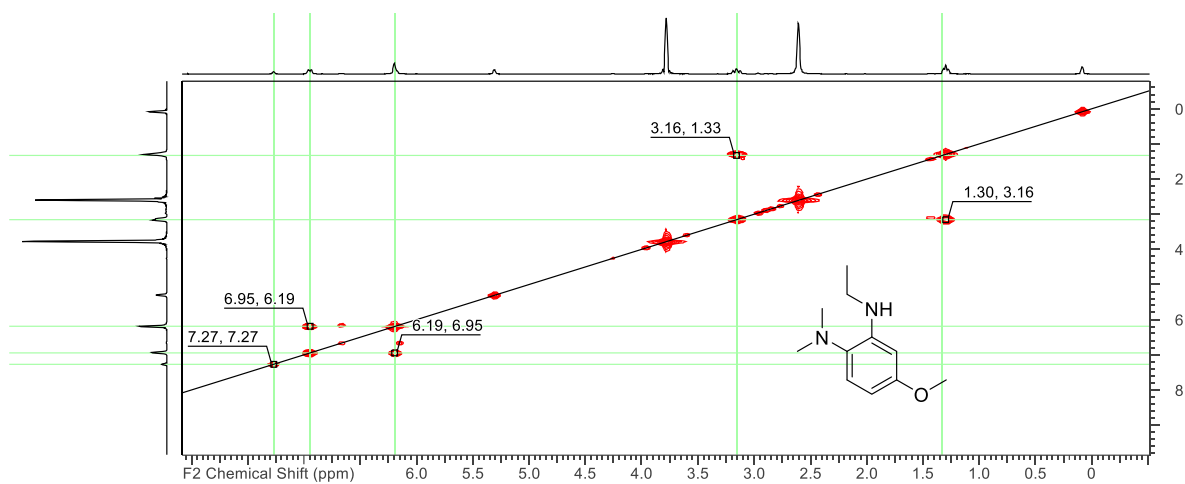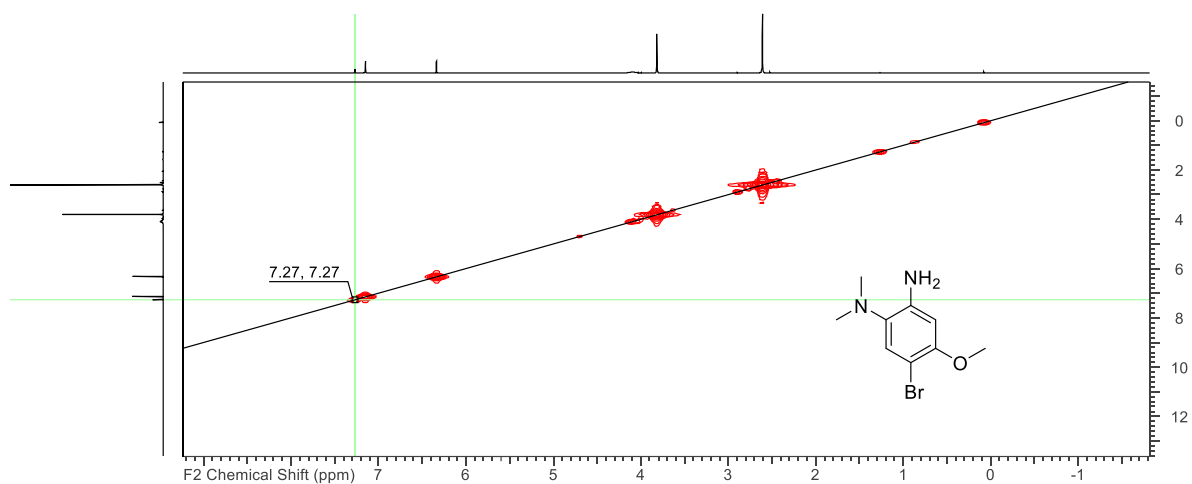
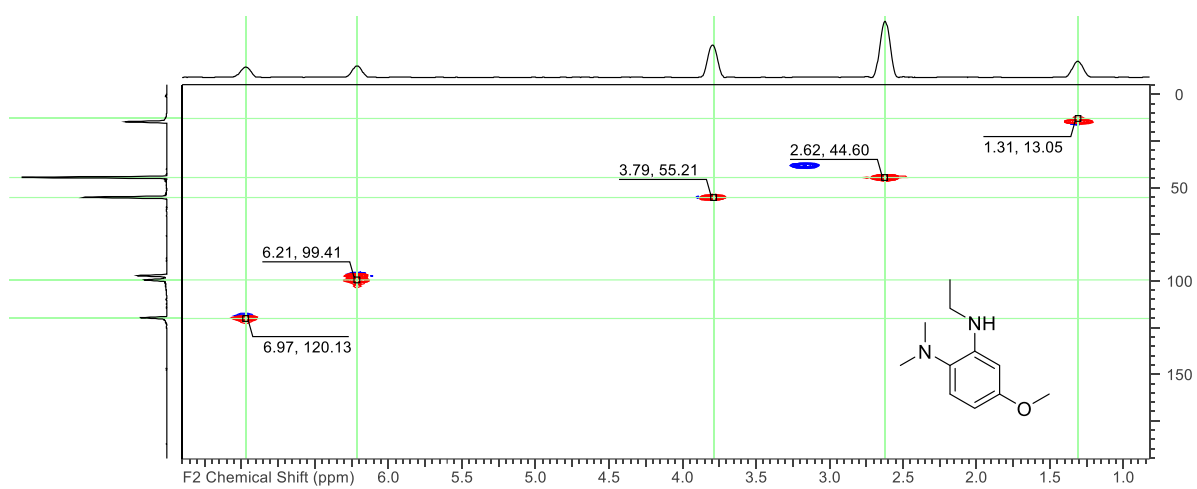Figure 141 ¹H-¹H COSY Spectrum of 5-bromo-4-methoxy-N1,N1-dimethylbenzene-1,2-diamine (Chloroform-d)
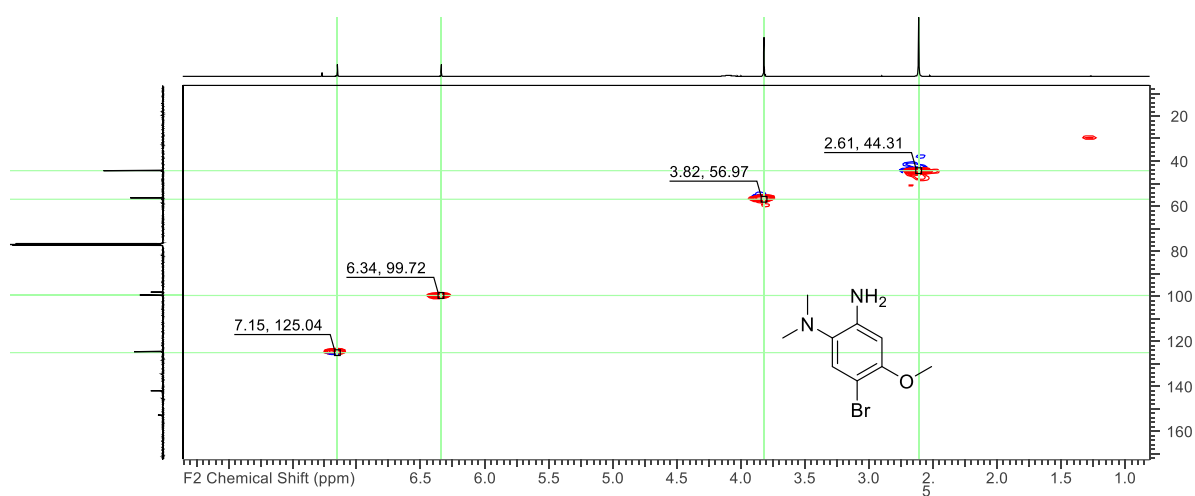
Figure 142 ¹H-¹³C HSQC Spectrum of 5-bromo-4-methoxy-N¹,N¹-dimethylbenzene-1,2-diamine (Chloroform-d)
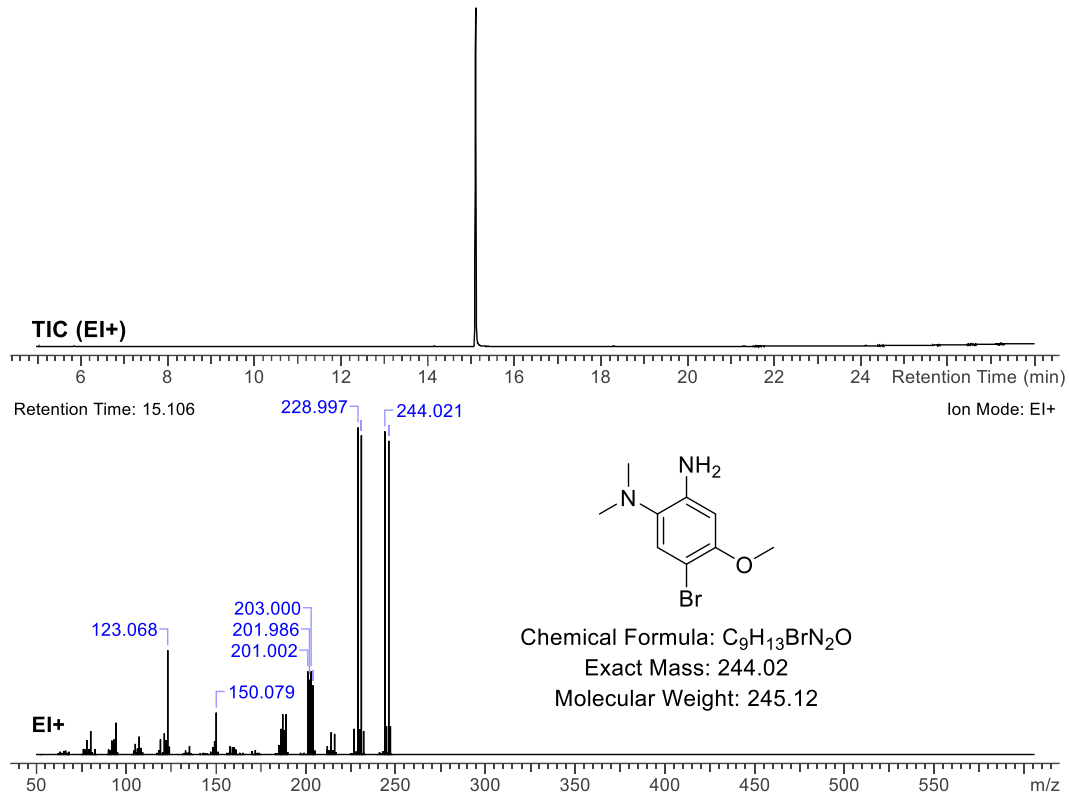
Figure 143 EI-HRMS 5-bromo-4-methoxy-N^1,N^1-dimethylbenzene-1,2-diamine
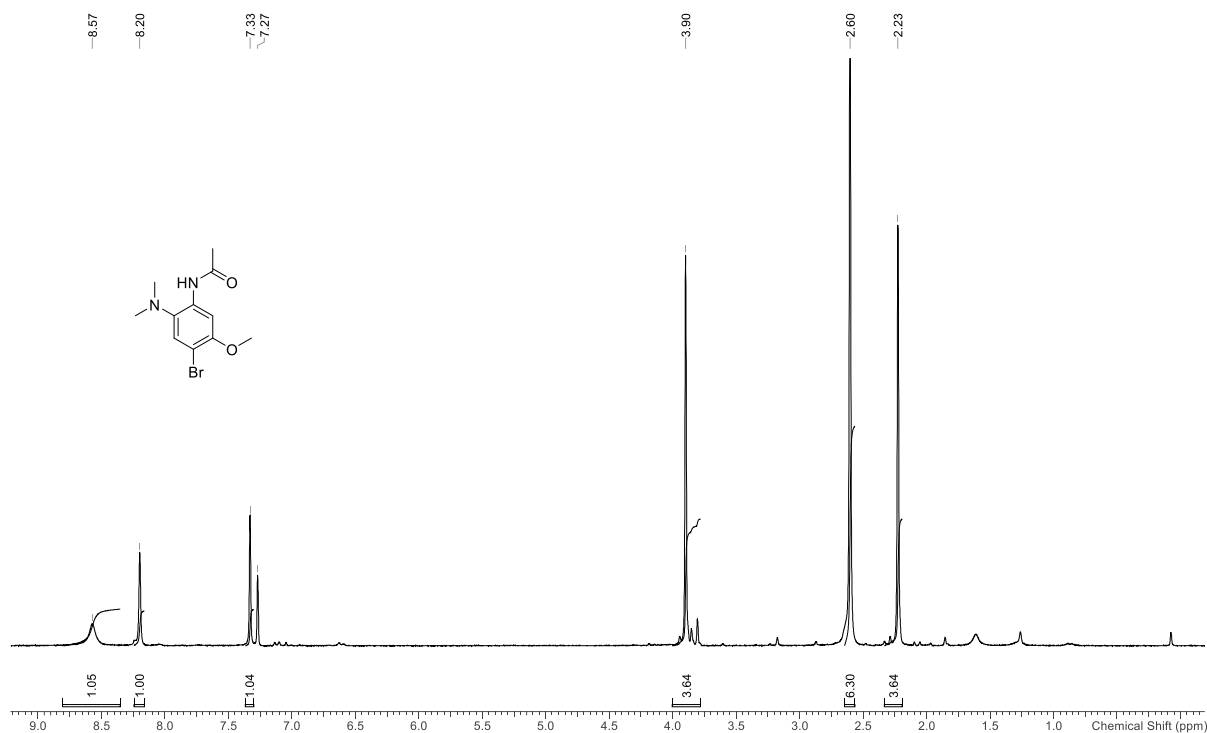
Figure 144 [1]H Spectrum of N-(4-bromo-2-(dimethylamino)-5-methoxyphenyl)acetamide (250 MHz, Chloroform-d)
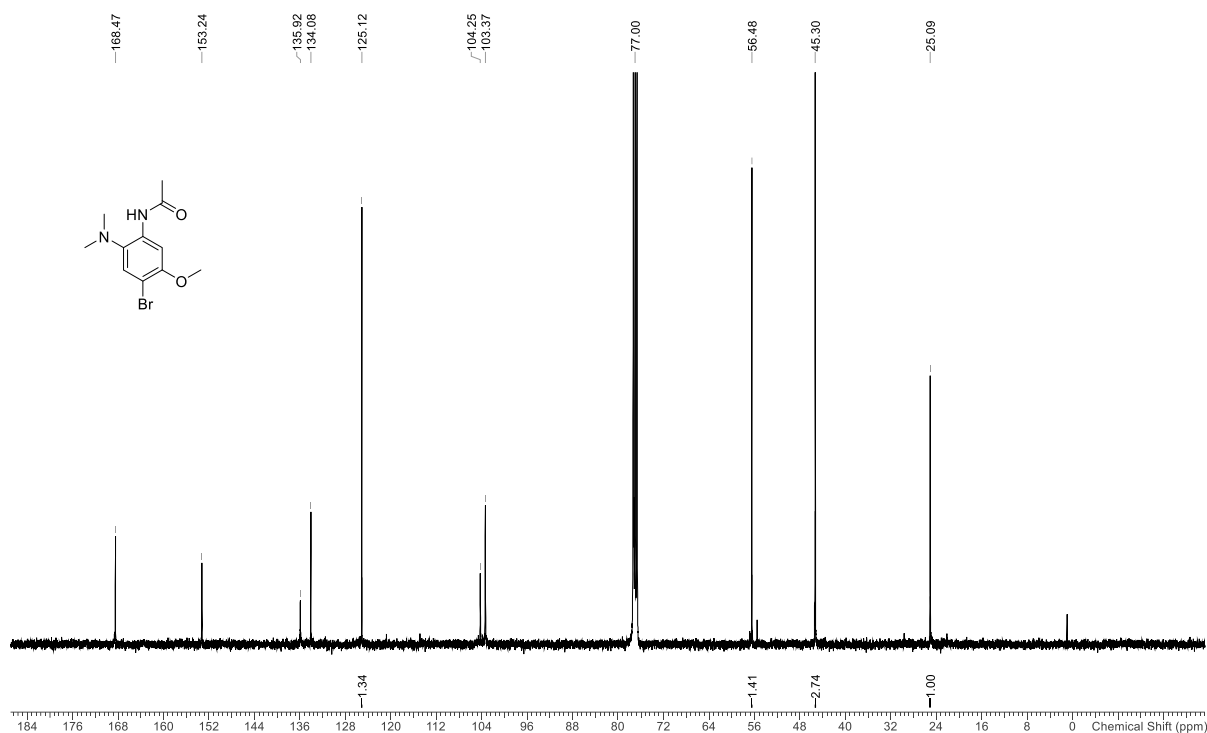
Figure 145 [13]C Spectrum of N-(4-bromo-2-(dimethylamino)-5-methoxyphenyl)acetamide (250 MHz Chloroform-d)
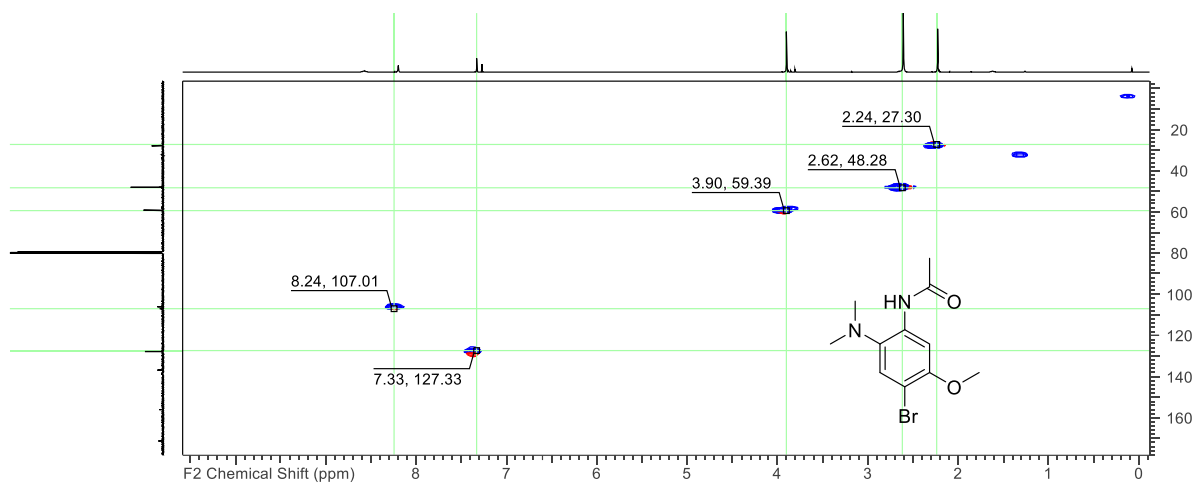
Figure 146 ^{1}H-^{13}C HSQC Spectrum of N-(4-bromo-2-(dimethylamino)-5-methoxyphenyl)acetamide (Chloroform-d)
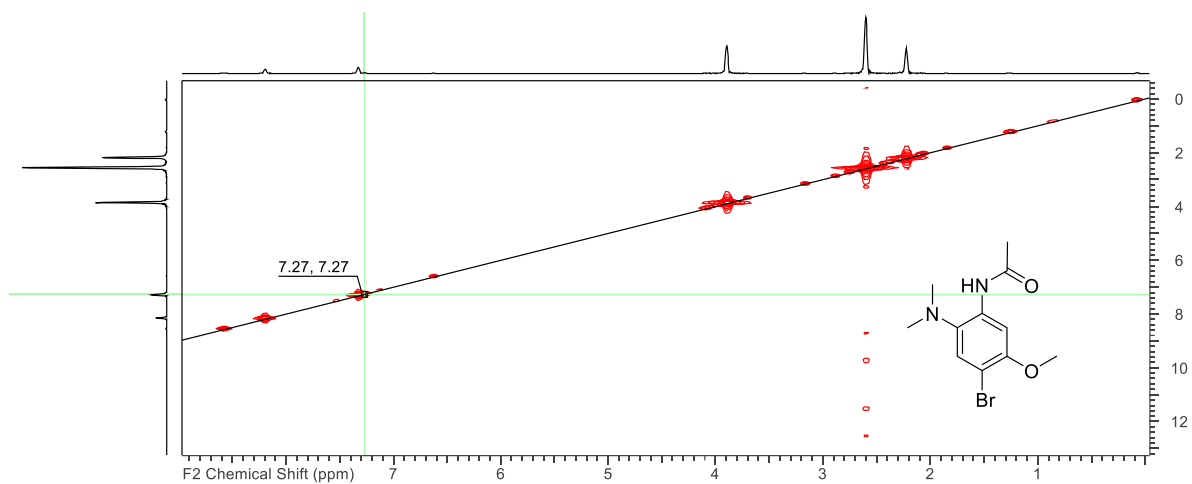
Figure 147 ^{1}H-^{1}H COSY Spectrum of N-(4-bromo-2-(dimethylamino)-5-methoxyphenyl)acetamide (Chloroform-d)
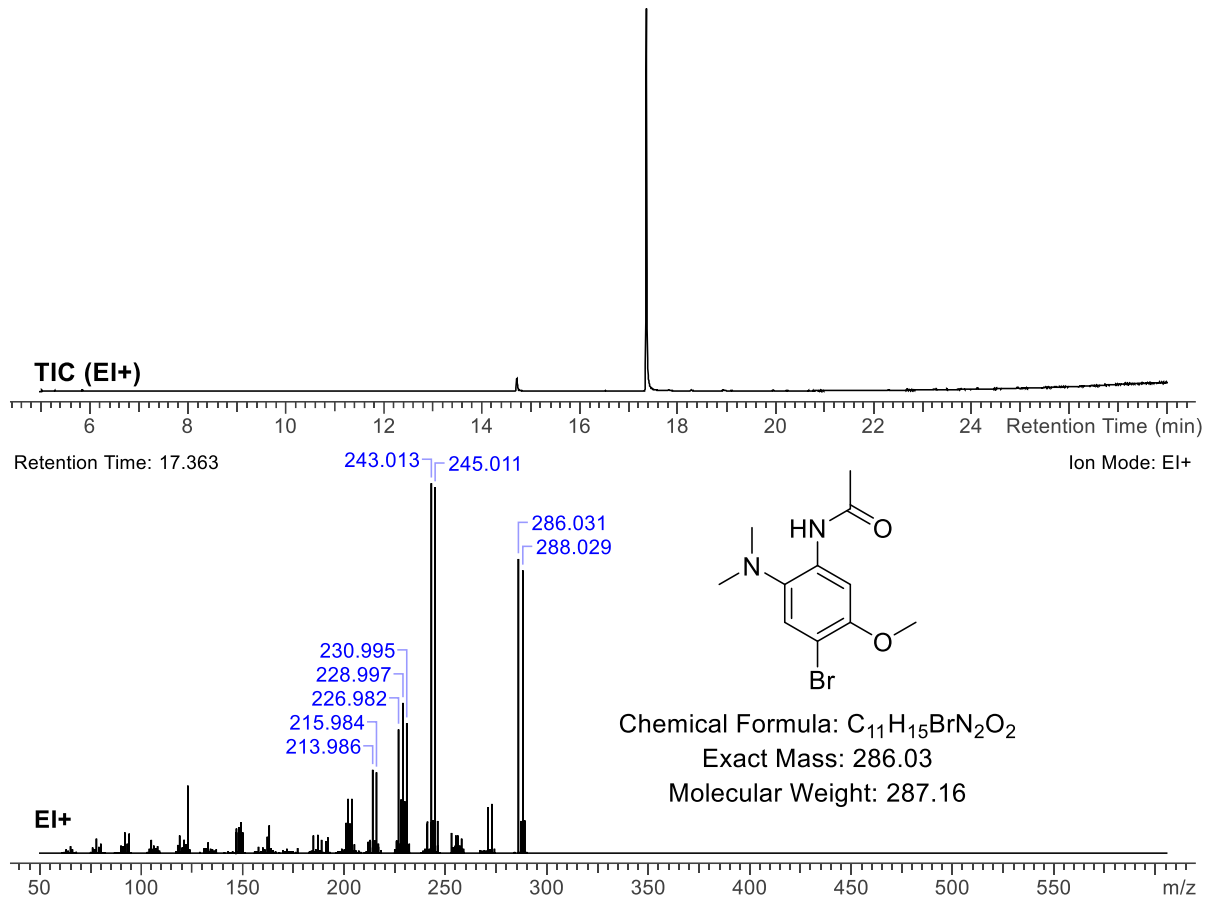
Figure 148 EI-HRMS Spectrum of N-(2-(dimethylamino)-5-methoxyphenyl)acetamide
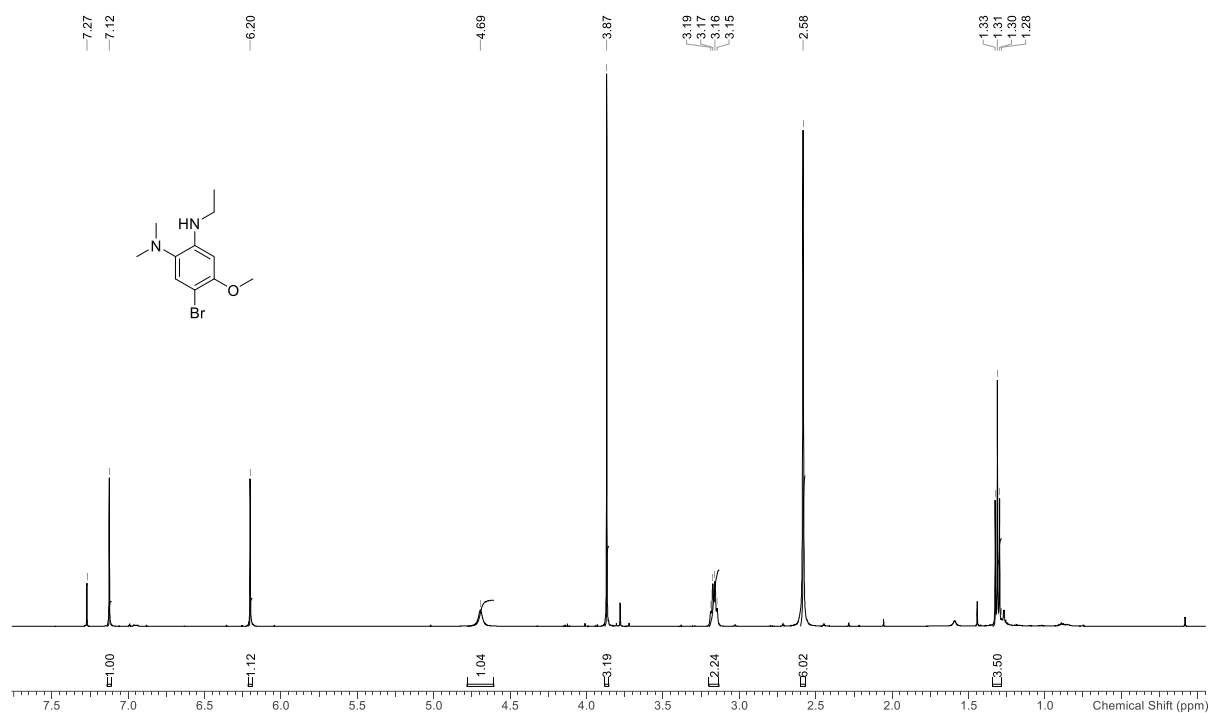
Figure 149 ^{1}H Spectrum of 4-bromo-N1-ethyl-5-methoxy-N2,N2-dimethylbenzene-1,2-diamine (500 MHz, Chloroform-d)
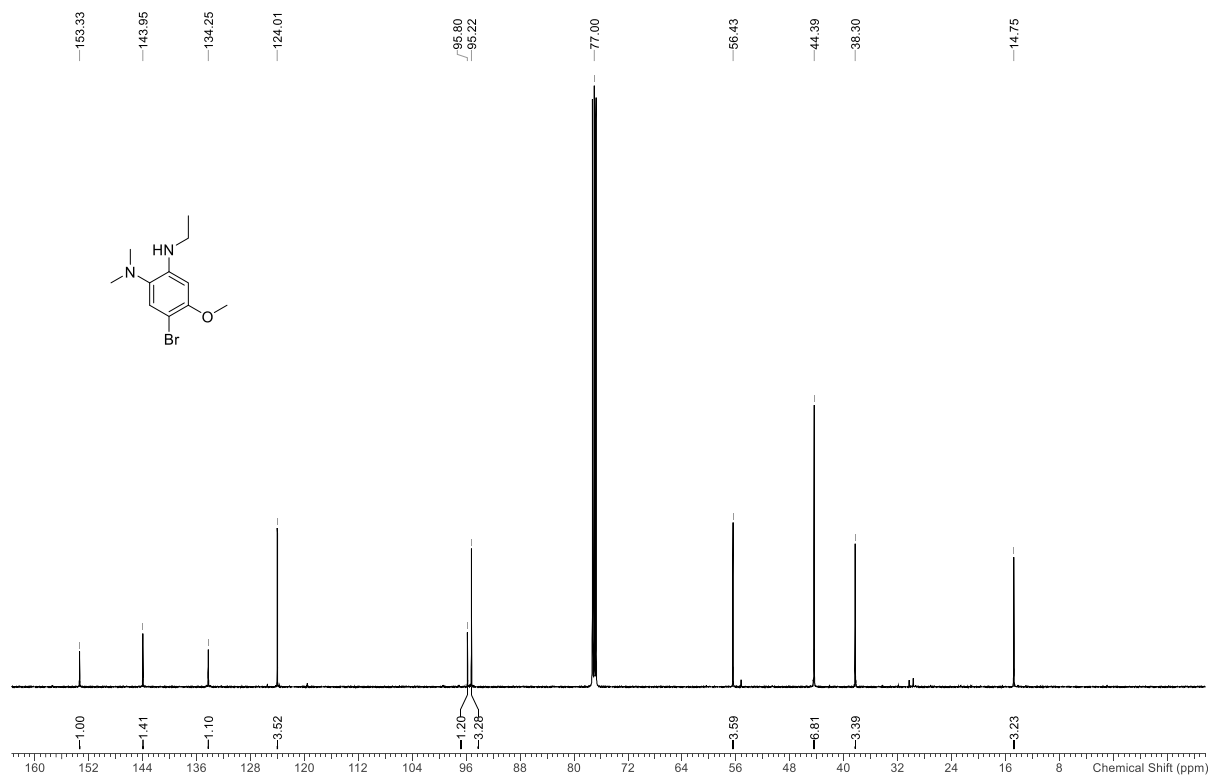
Figure 150 ^{13}C Spectrum of 4-bromo-N1-ethyl-5-methoxy-N2,N2-dimethylbenzene-1,2-diamine (126 MHz, Chloroform-d)
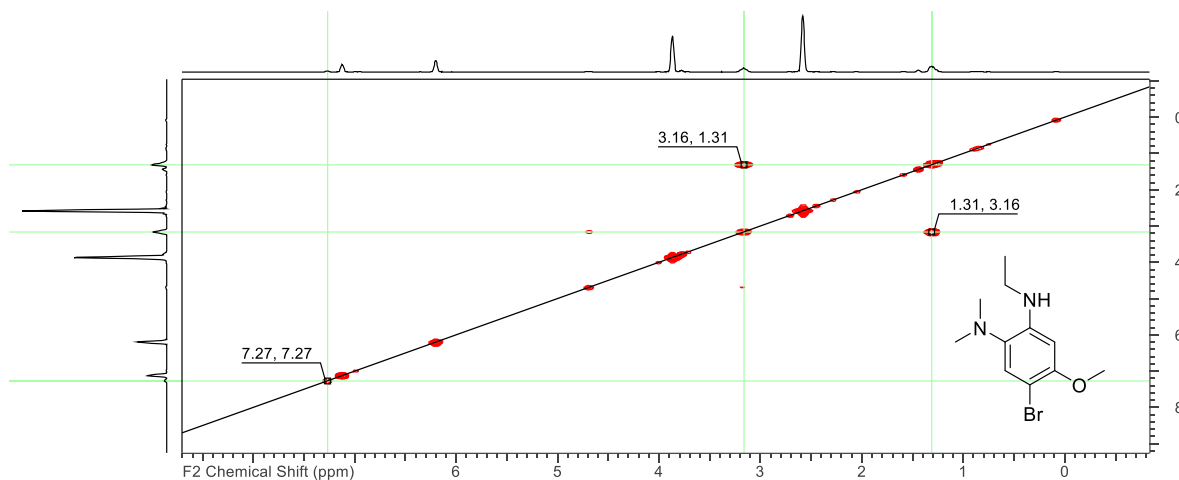
Figure 151 ¹H-¹H COSY Spectrum of 4-bromo-N1-ethyl-5-methoxy-N2,N2-dimethylbenzene-1,2-diamine (Chloroform-d)
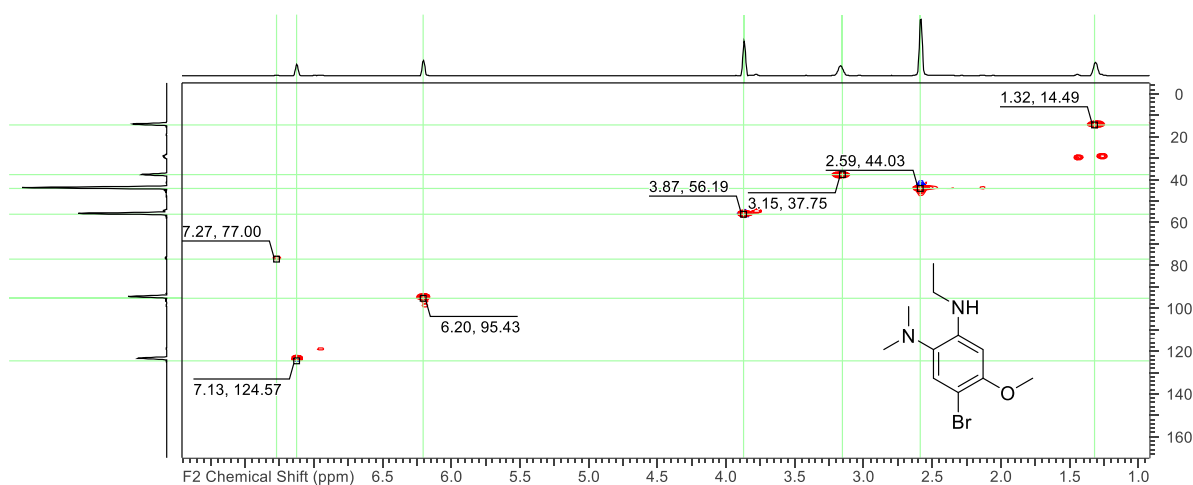
Figure 152 ¹H-¹³C HSQC Spectrum of 4-bromo-N1-ethyl-5-methoxy-N2,N2-dimethylbenzene-1,2-diamine (Chloroform-d)

2020-07-13_bt156b_1

TIC (EI+)

Retention Time: 16.545

Ion Mode: EI+

EI+

Chemical Formula: $C_{11}H_{17}BrN_2O$
Exact Mass: 272.05
Molecular Weight: 273.17
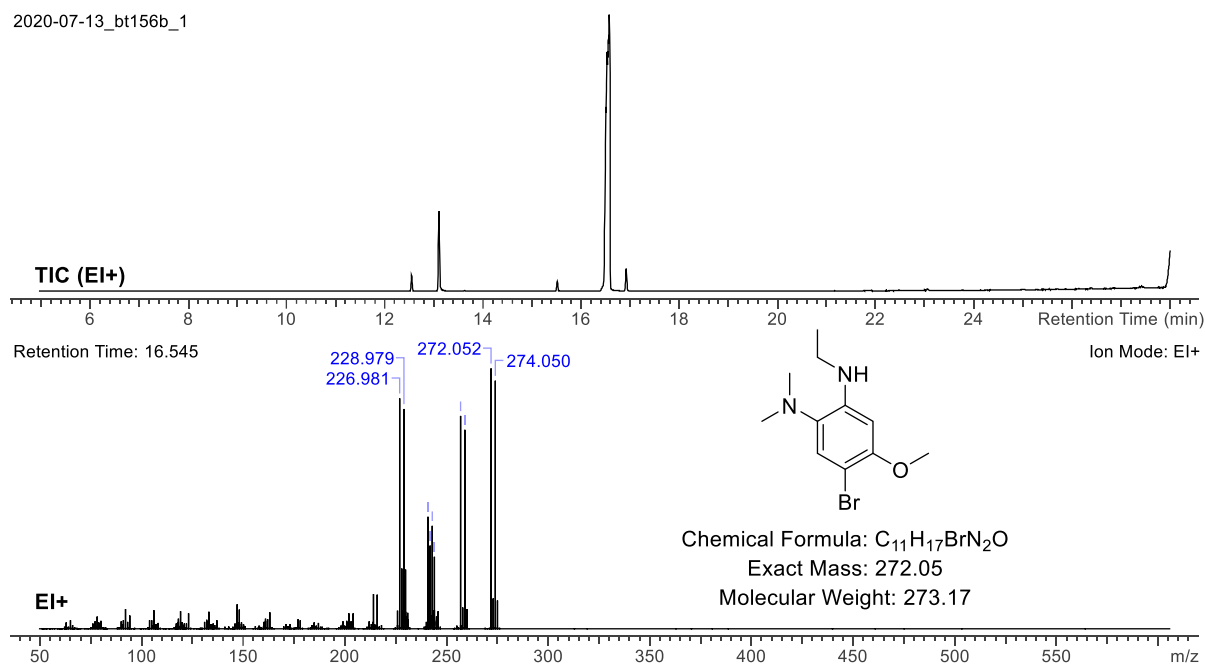
Figure 153 EI-HRMS of 4-bromo-N1-ethyl-5-methoxy-N2,N2-dimethylbenzene-1,2-diamine
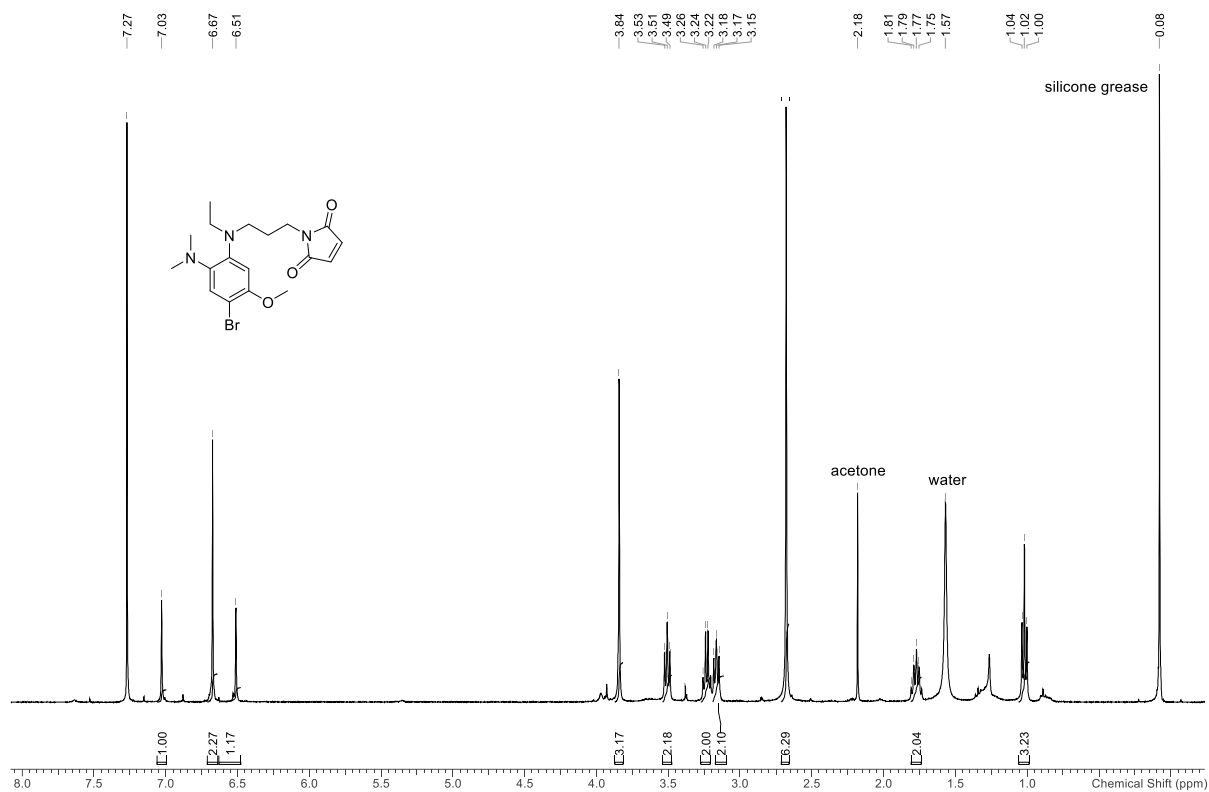
Figure 154 ¹H NMR Spectrum of 1-(3-((4-bromo-2-(dimethylamino)-5-methoxyphenyl)(ethyl)amino)propyl)-1H-pyrrole-2,5-dione (400 MHz, Chloroform-d)
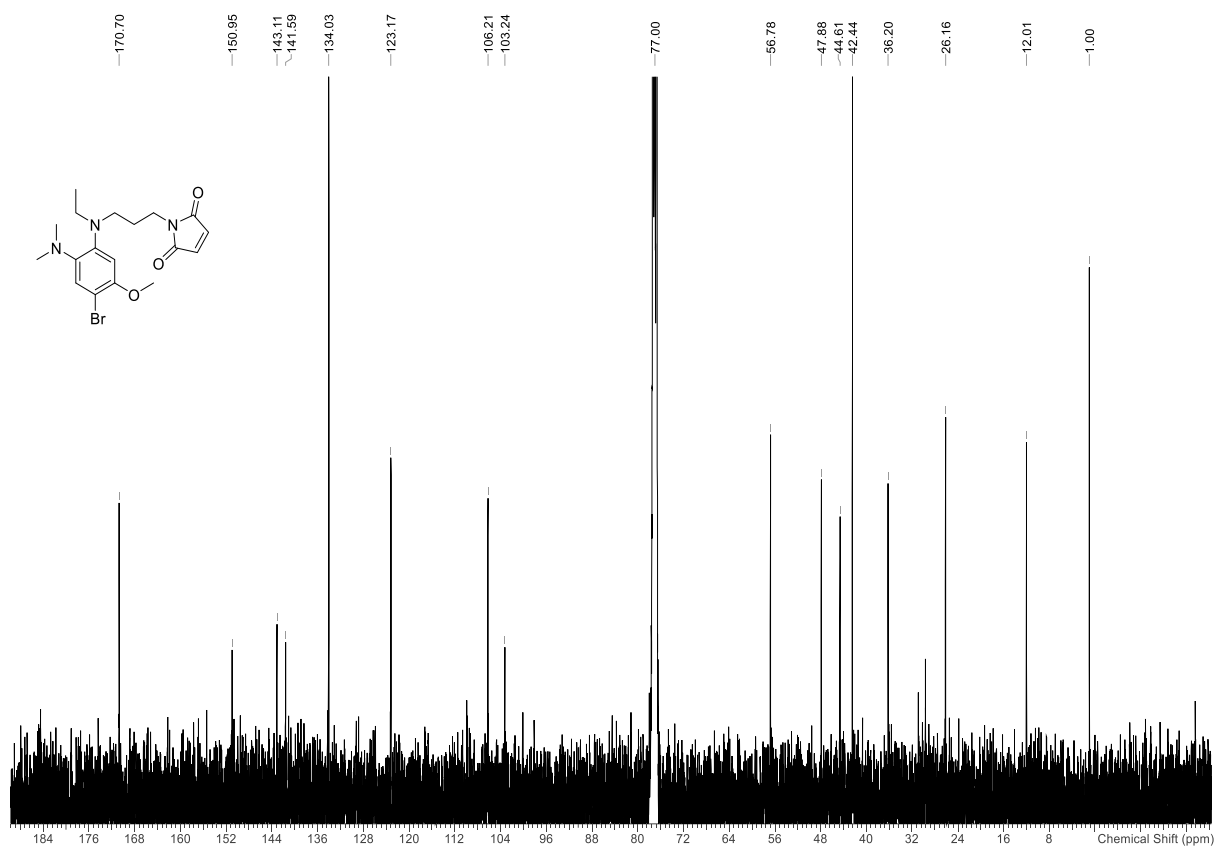
Figure 155 ¹³C Spectrum of 1-(3-((4-bromo-2-(dimethylamino)-5-methoxyphenyl)(ethyl)amino)propyl)-1H-pyrrole-2,5-dione (101 MHz, Chloroform-d)
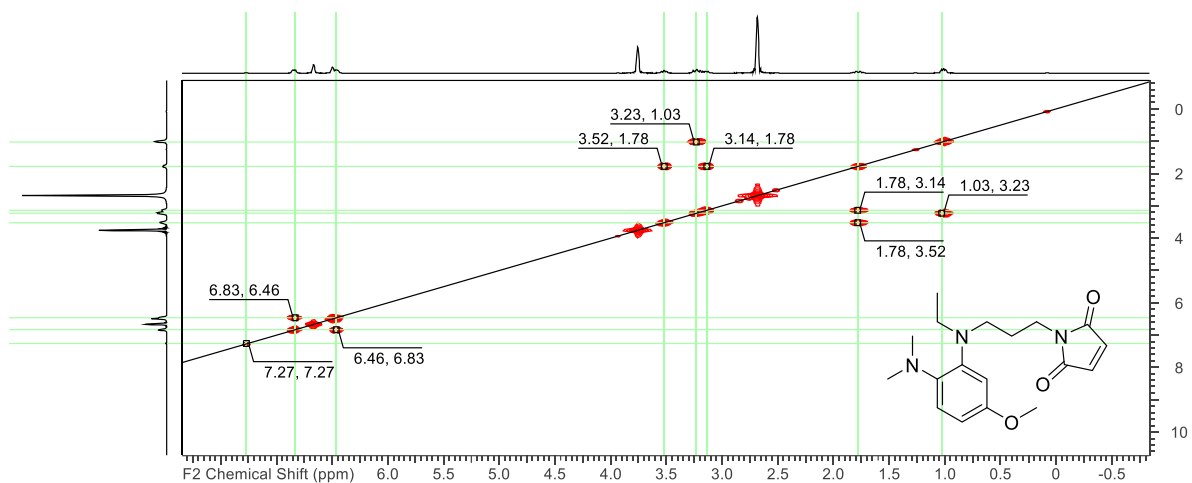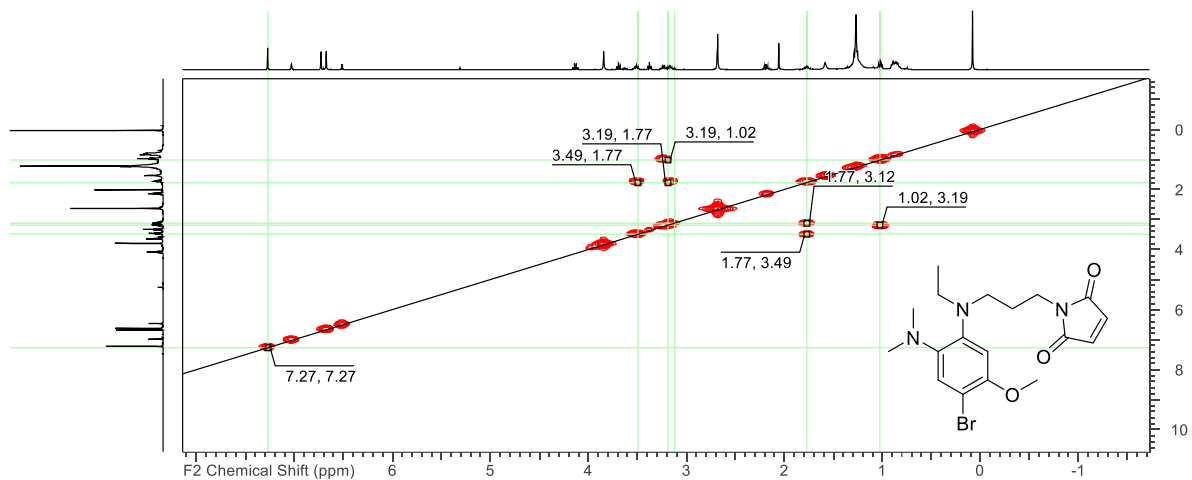
Figure 156 ¹H-¹H COSY Spectrum of 1-(3-((4-bromo-2-(dimethylamino)-5-methoxyphenyl)(ethyl)amino)propyl)-1H-pyrrole-2,5-dione (Chloroform-d)
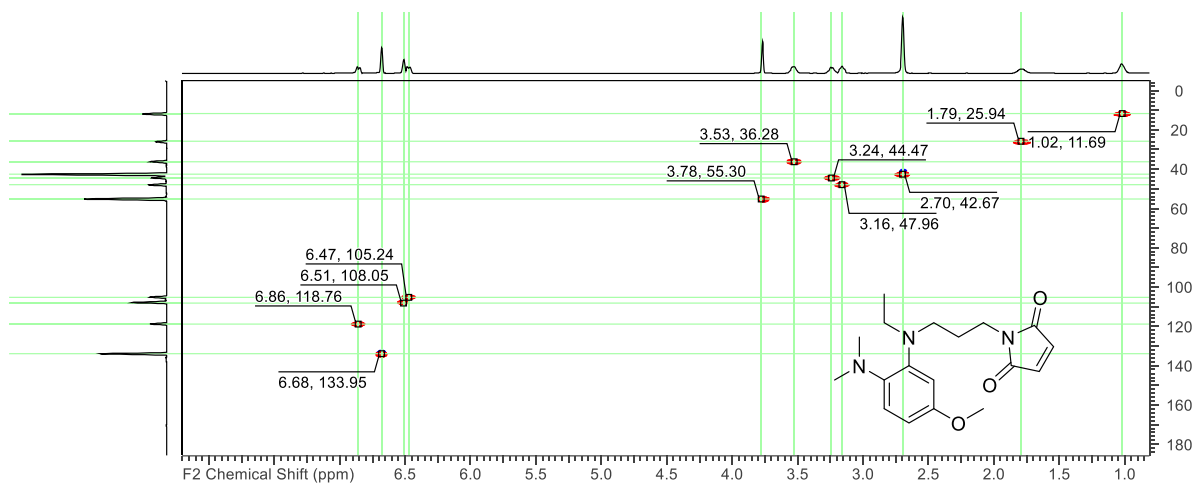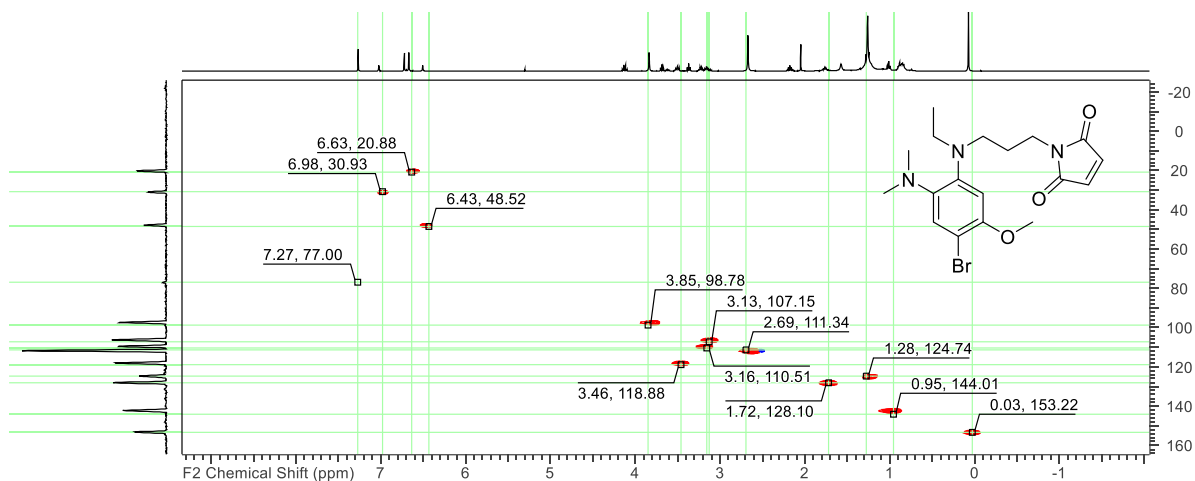

Figure 157 ¹H-¹³C Spectrum of 1-(3-((4-bromo-2-(dimethylamino)-5-methoxyphenyl)(ethyl)amino)propyl)-1H-pyrrole-2,5-dione (Chloroform-d)

Chemical Formula: $C_{18}H_{24}BrN_3O_3$
Exact Mass: 409.10
Molecular Weight: 410.31

TIC (Positive)

Retention Time (min)

Retention Time: 2.000

Ion Mode: Positive

Positive

m/z
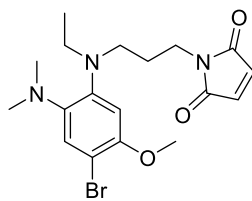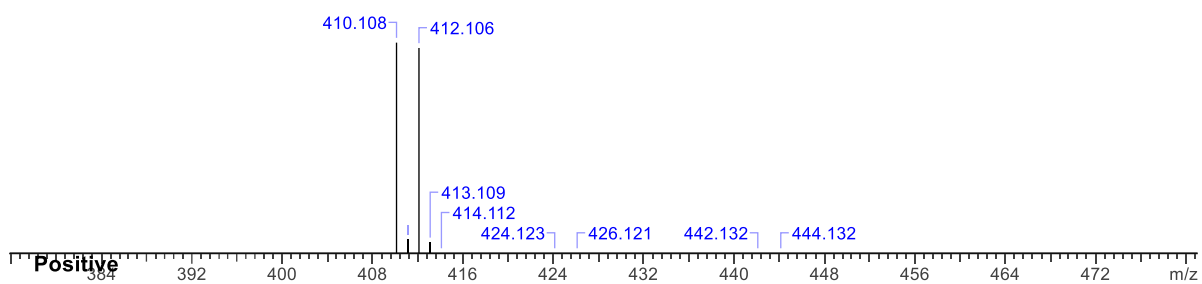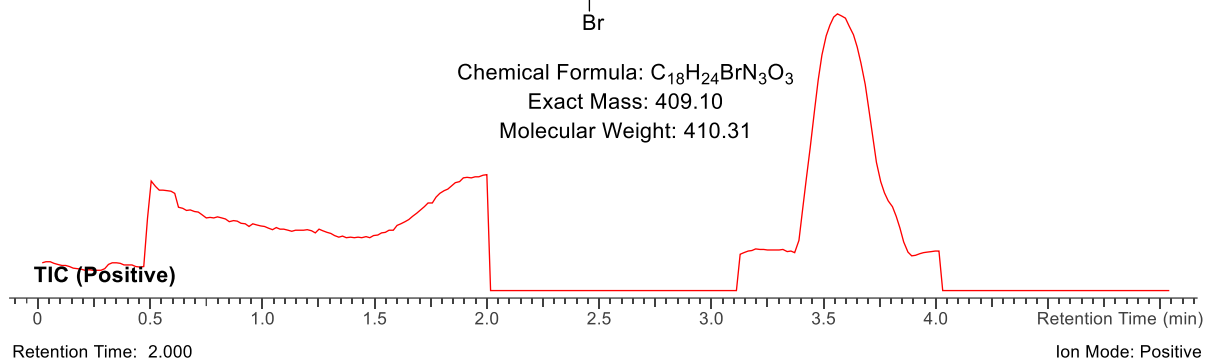
Figure 158 ESI-HRMS Spectrum of 1-(3-((4-bromo-2-(dimethylamino)-5-methoxyphenyl)(ethyl)amino)propyl)-1H-pyrrole-2,5-dione
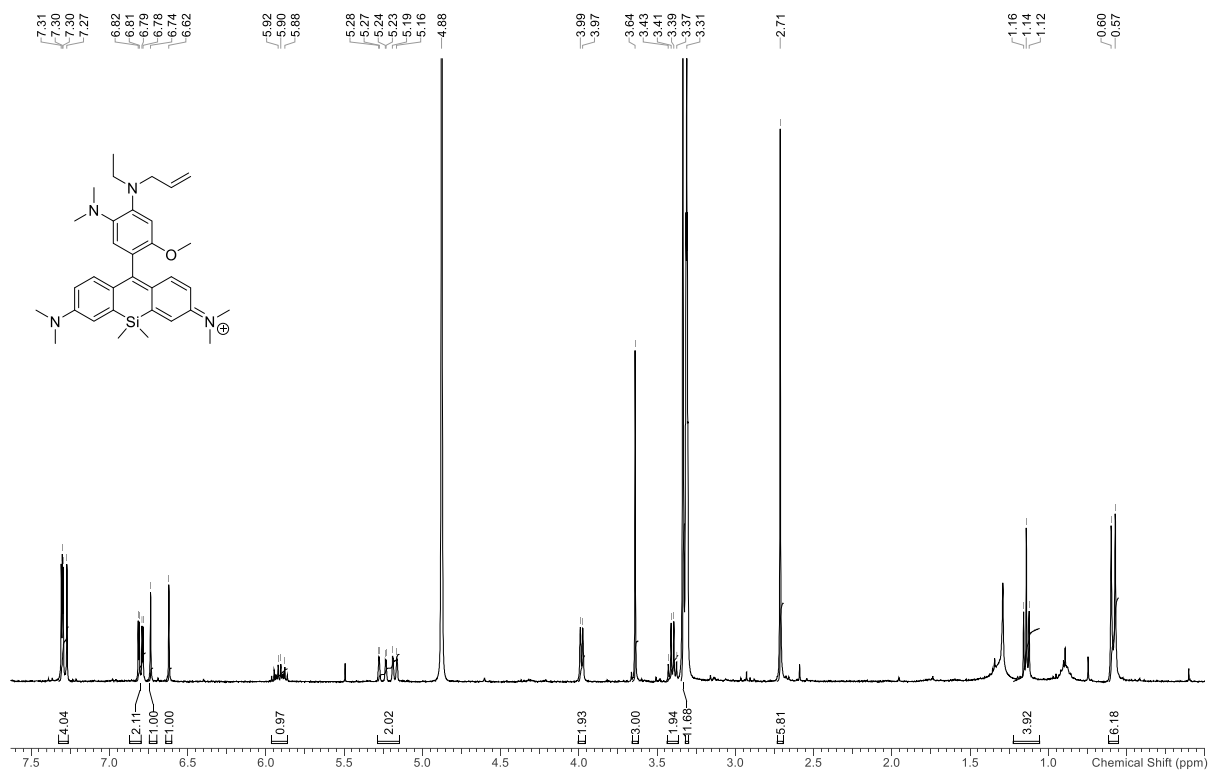
Figure 159 ¹H Spectrum of N-(10-(4-(allyl(ethyl)amino)-5-(dimethylamino)-2-methoxyphenyl)-7-(dimethylamino)-5,5-dimethyldibenzo[b,e]silin-3(5H)-ylidene)-N-methylmethanaminium (400 MHz Methanol-d)
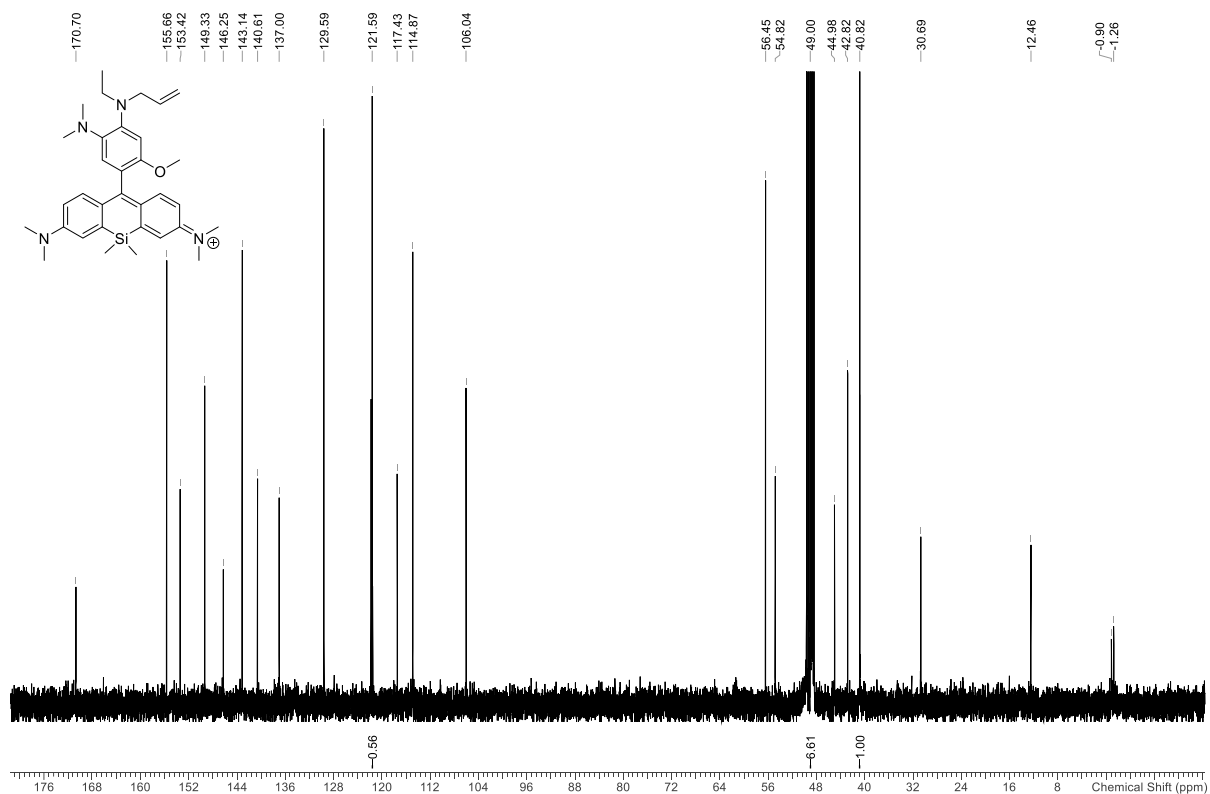
Figure 160 ¹³C Spectrum of N-(10-(4-(allyl(ethyl)amino)-5-(dimethylamino)-2-methoxyphenyl)-7-(dimethylamino)-5,5-dimethyldibenzo[b,e]silin-3(5H)-ylidene)-N-methylmethanaminium (101 MHz Methanol-d)
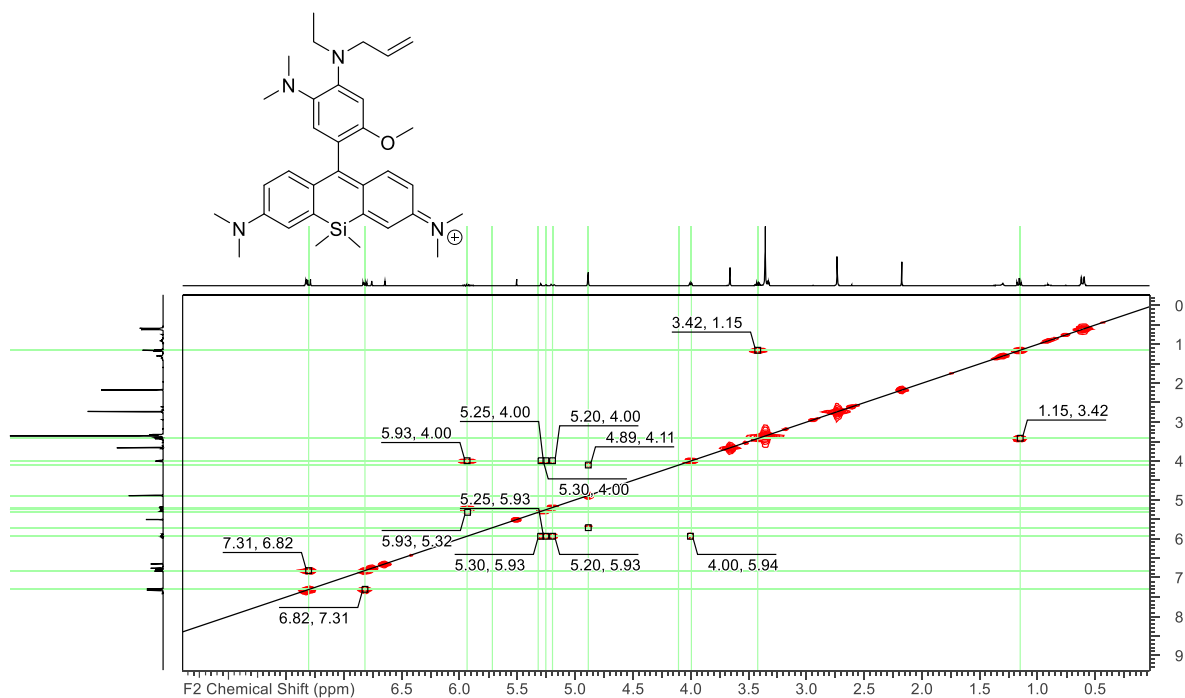
Figure 161 ¹H-¹H COSY spectrum of N-(10-(4-(allyl(ethyl)amino)-5-(dimethylamino)-2-methoxyphenyl)-7-(dimethylamino)-5,5-dimethyldibenzo[b,e]silin-3(5H)-ylidene)-N-methylmethanaminium (Methanol-d)
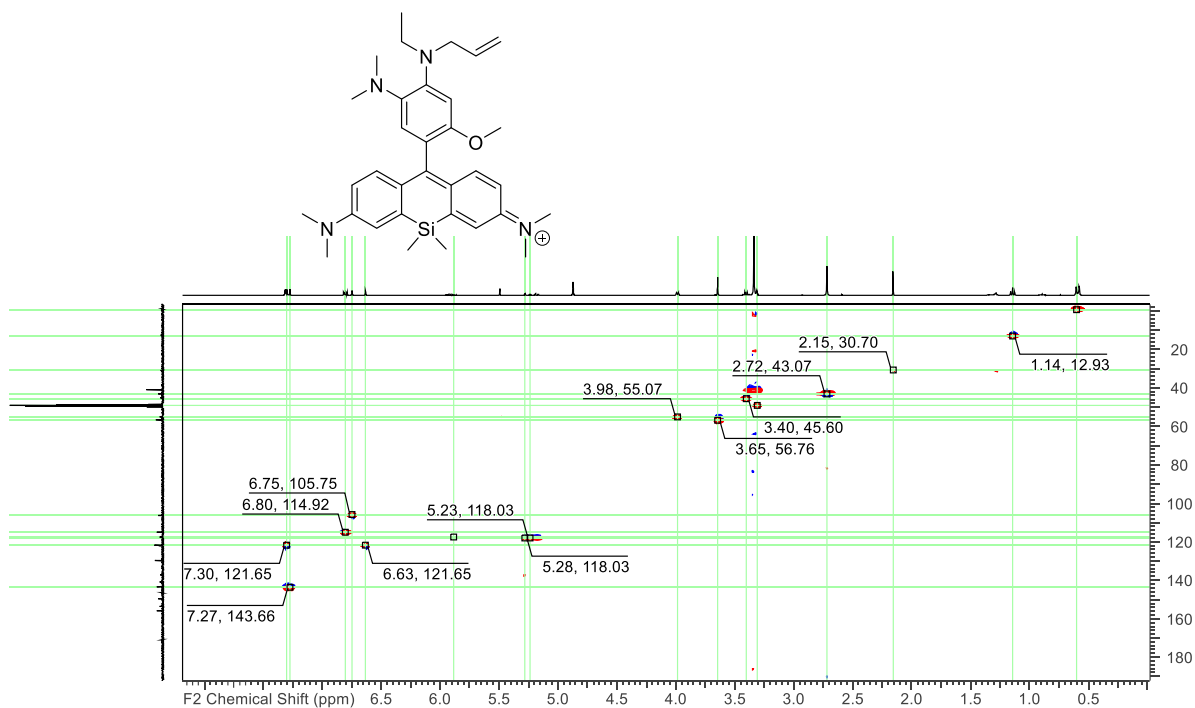
Figure 162 ¹H-¹³C HSQC spectrum of N-(10-(4-(allyl(ethyl)amino)-5-(dimethylamino)-2-methoxyphenyl)-7-(dimethylamino)-5,5-dimethyldibenzo[b,e]silin-3(5H)-ylidene)-N-methylmethanaminium (Methanol-d)

Chemical Formula: $C_{33}H_{45}N_4OSi^+$
Exact Mass: 541.34
Molecular Weight: 541.83
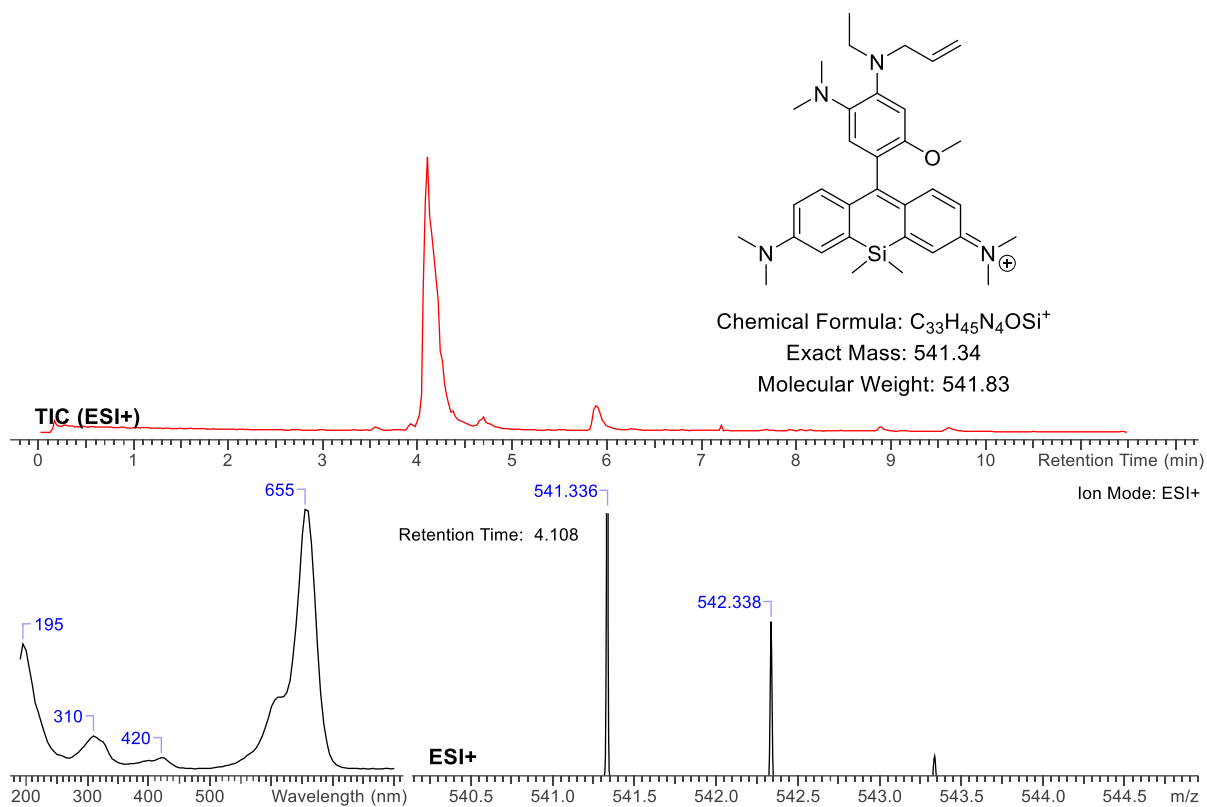
Figure 163 HPLC profile of N-(7-(dimethylamino)-10-(5-(dimethylamino)-4-(ethylamino)-2-methoxyphenyl)-5,5-dimethyldibenzo[b,e]silin-3(5H)-ylidene)-N-methylmethanaminium showing the retention time (TOP), the absorption profile (bottom left) and the ESI isotopic pattern (bottom right)
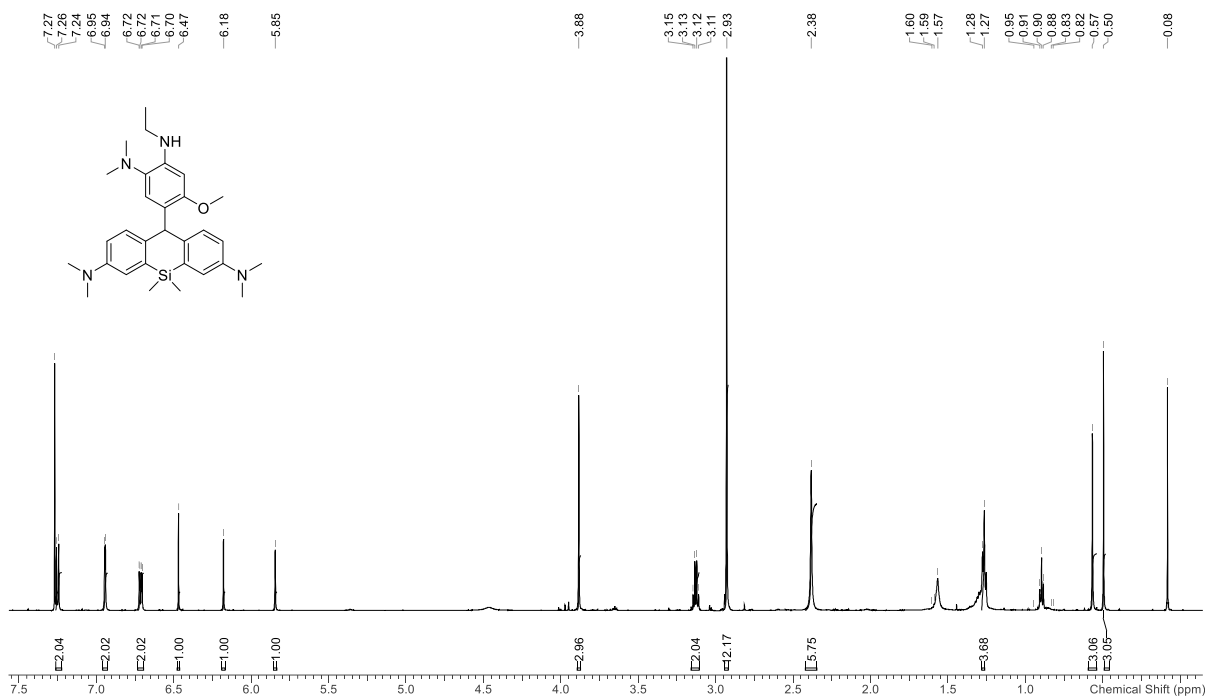
Figure 164 ¹H NMR Spectrum of N-(7-(dimethylamino)-10-(5-(dimethylamino)-4-(ethylamino)-2-methoxyphenyl)-5,5-dimethyldibenzo[b,e]silin-3(5H)-ylidene)-N-methylmethanaminium (400 MHz, Chloroform-d)
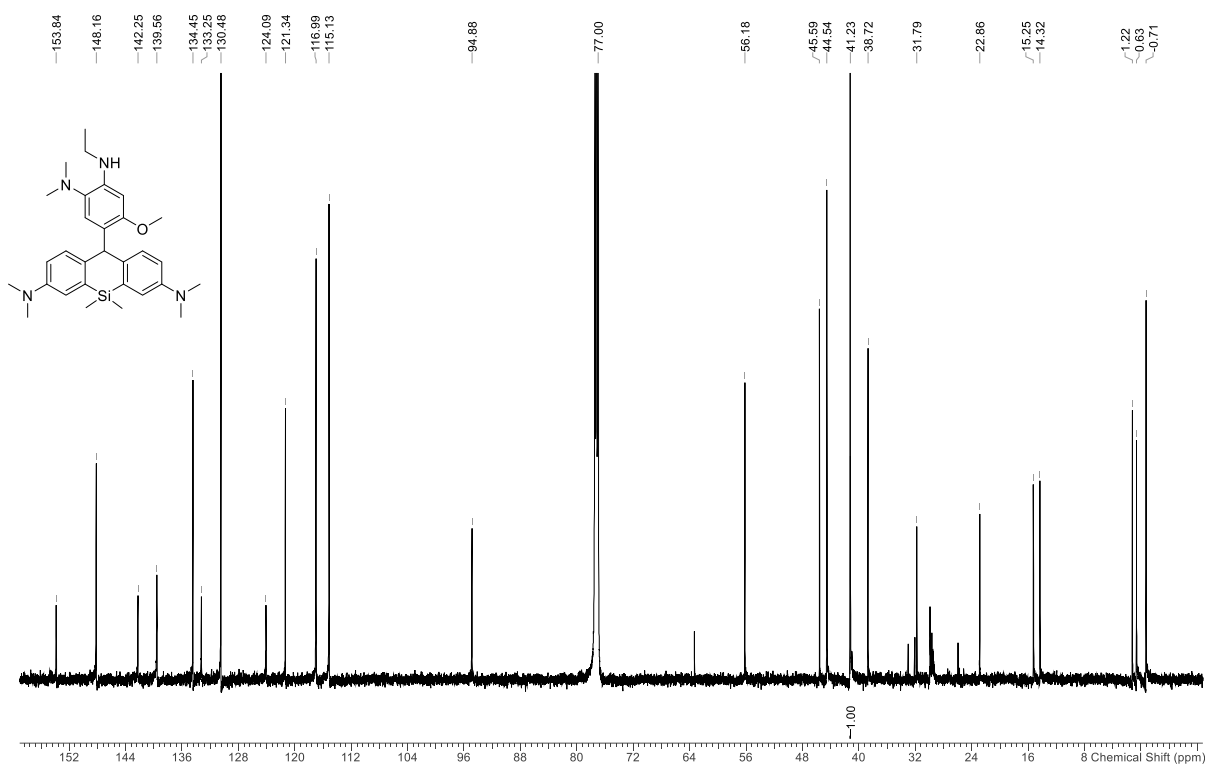
Figure 165 ¹³C NMR Spectrum N-(7-(dimethylamino)-10-(5-(dimethylamino)-4-(ethylamino)-2-methoxyphenyl)-5,5-dimethyldibenzo[b,e]silin-3(5H)-ylidene)-N-methylmethanaminium (126 MHz Chloroform-d)
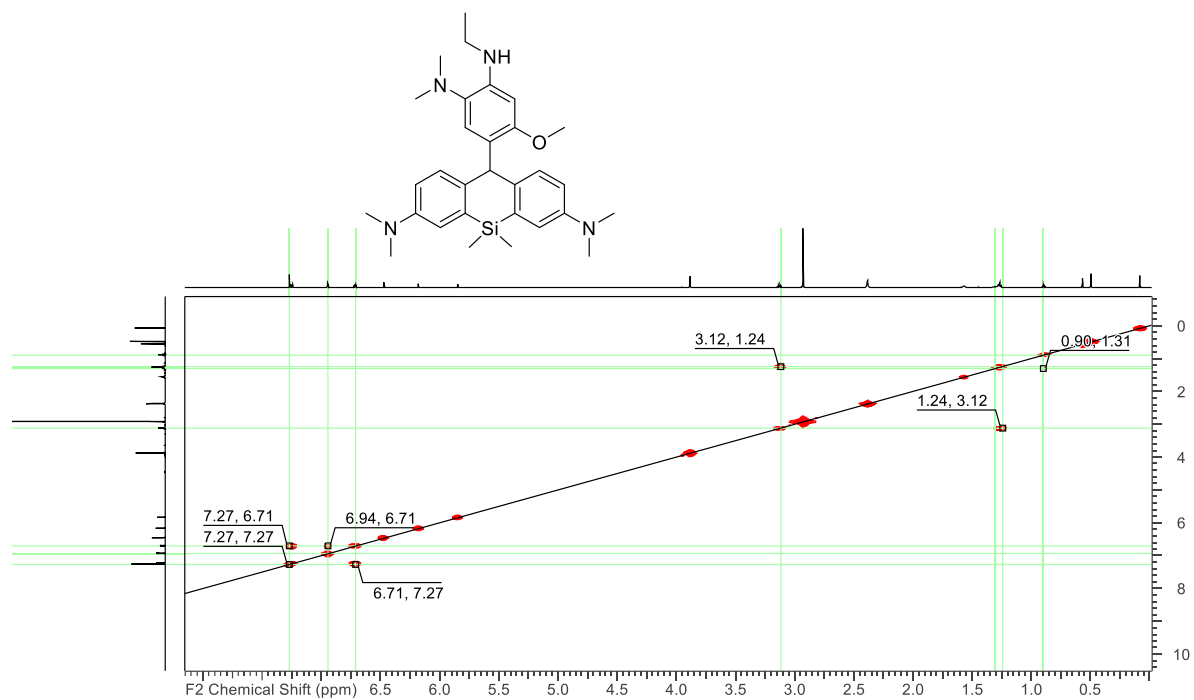
Figure 166 ¹H-¹H COSY Spectrum of N-(10-(4-(allyl(ethyl)amino)-5-(dimethylamino)-2-methoxyphenyl)-7-(dimethylamino)-5,5-dimethyldibenzo[b,e]silin-3(5H)-ylidene)-N-methylmethanaminium (Chloroform-d)
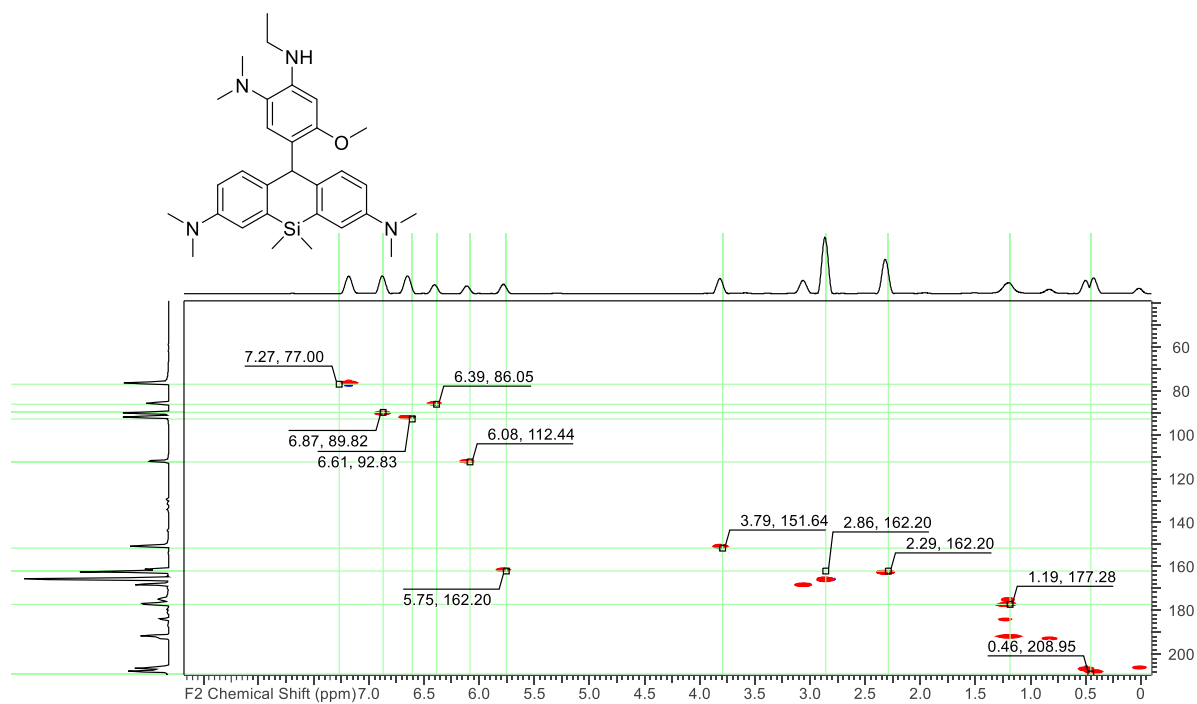
Figure 167 HSQC Spectrum of N-(10-(4-(allyl(ethyl)amino)-5-(dimethylamino)-2-methoxyphenyl)-7-(dimethylamino)-5,5-dimethyldibenzo[b,e]silin-3(5H)-ylidene)-N-methylmethanaminium (Chloroform-d)

Chemical Formula: $C_{30}H_{41}N_4OSi^+$
Exact Mass: 501.30
Molecular Weight: 501.77
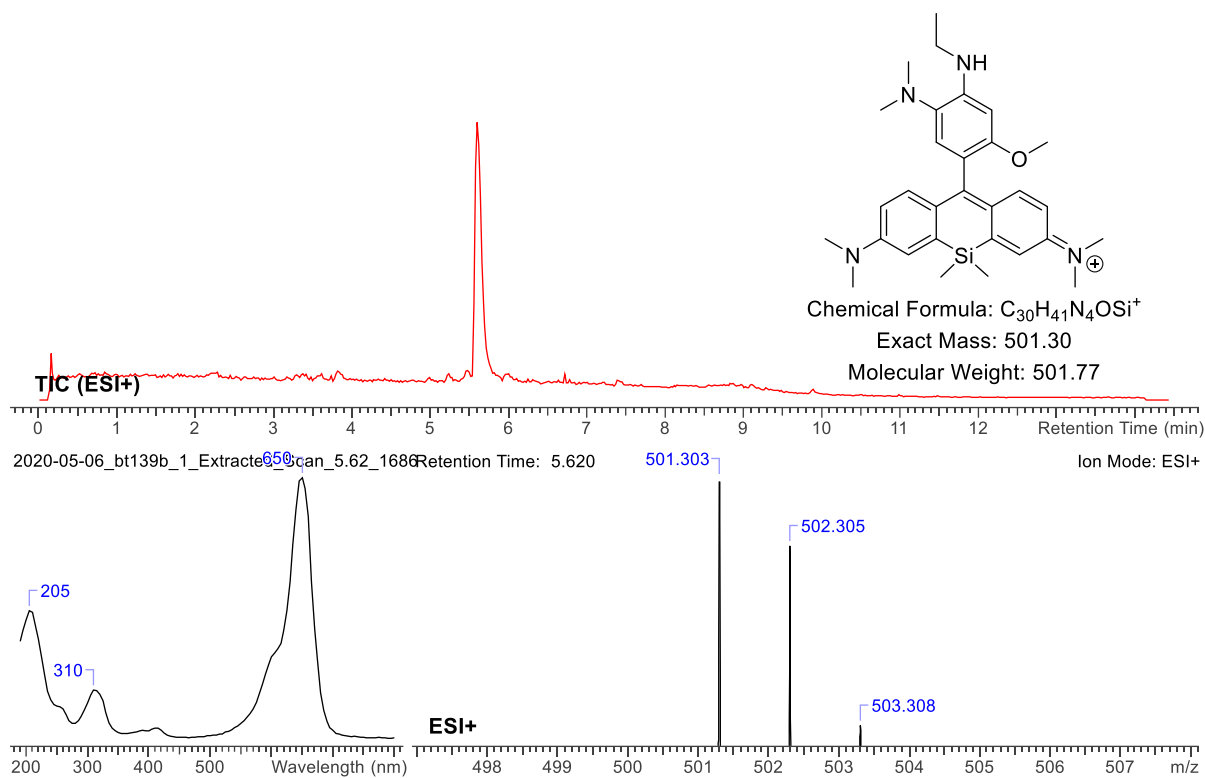
Figure 168 HPLC profile of N-(10-(4-(allyl(ethyl)amino)-5-(dimethylamino)-2-methoxyphenyl)-7-(dimethylamino)-5,5-dimethyldibenzo[b,e]silin-3(5H)-ylidene)-N-methylmethanaminium (oxidized form) showing retention time (top) absorption profile (bottom left) Isotopic pattern (bottom right)

Chemical Formula: $C_{30}H_{42}N_4OSi$
Exact Mass: 502.31
Molecular Weight: 502.78

TIC (ESI+)

Retention Time (min)

Retention Time: 4.346

Ion Mode: ESI+

ESI+

Wavelength (nm)

m/z
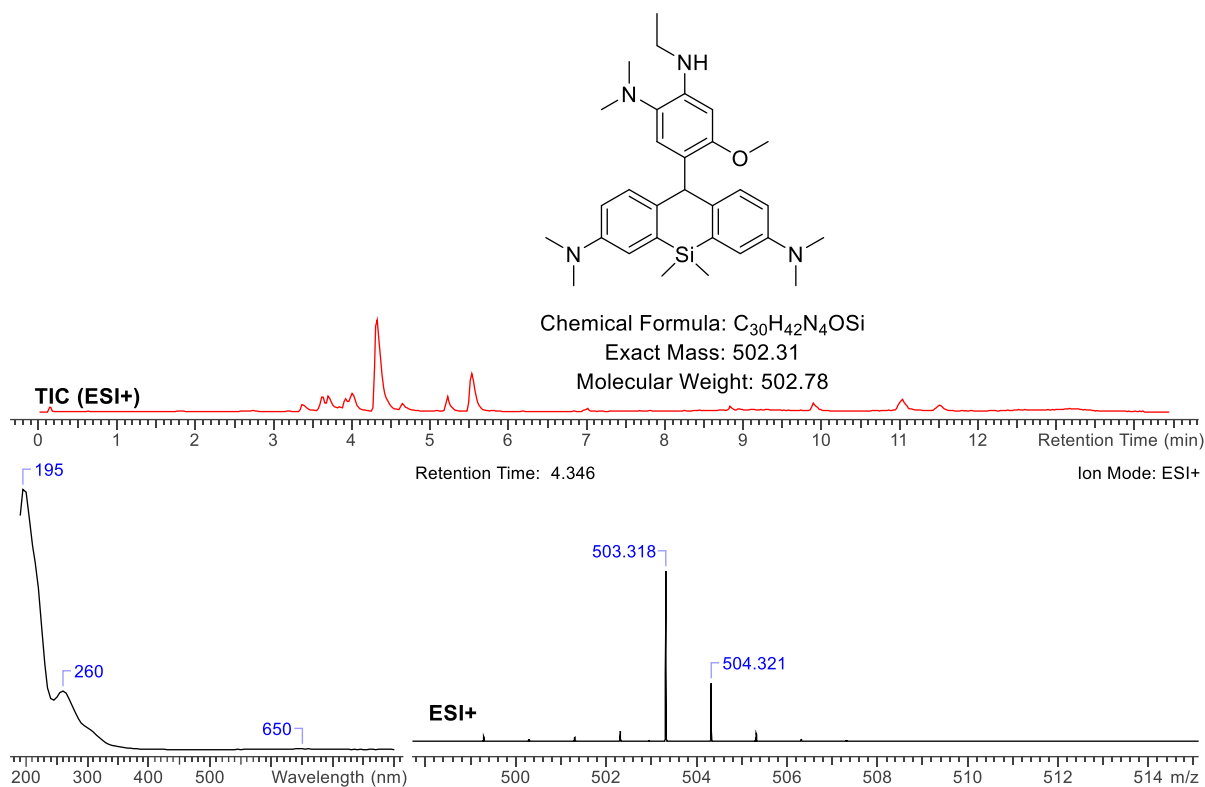
Figure 169 HPLC profile of N-(10-(4-(allyl(ethyl)amino)-5-(dimethylamino)-2-methoxyphenyl)-7-(dimethylamino)-5,5-dimethyldibenzo[b,e]silin-3(5H)-ylidene)-N-methylmethanaminium (reduced form) showing retention time (top) absorption profile (left) and ESI isotopic pattern (bottom right).

7. Bibliography

1.   Low, P. S.; Singhal, S.; Srinivasarao, M., Fluorescence-guided surgery of cancer: applications, tools and perspectives. *Curr Opin Chem Biol* **2018,** *45*, 64-72.

2.   Siegel, R. L. a. M., Kimberly D and Fuchs, Hannah E and Jemal, Ahmedin, Cancer statistics, 2021. *CA: a cancer journal for clinicians* **2021,** *71* (1), 7--33.

3.   Nagaya, T.; Nakamura, Y. A.; Choyke, P. L.; Kobayashi, H., Fluorescence-Guided Surgery. *Front Oncol* **2017,** *7*, 314.

4.   Li, H.; Yao, Q.; Sun, W.; Shao, K.; Lu, Y.; Chung, J.; Kim, D.; Fan, J.; Long, S.; Du, J.; Li, Y.; Wang, J.; Yoon, J.; Peng, X., Aminopeptidase N Activatable Fluorescent Probe for Tracking Metastatic Cancer and Image-Guided Surgery via in Situ Spraying. *J Am Chem Soc* **2020,** *142* (13), 6381-6389.

5.   Morawski, A. M.; Lanza, G. A.; Wickline, S. A., Targeted contrast agents for magnetic resonance imaging and ultrasound. *Curr Opin Biotechnol* **2005,** *16* (1), 89-92.

6.   AV, D. S.; Lin, H.; Henderson, E. R.; Samkoe, K. S.; Pogue, B. W., Review of fluorescence guided surgery systems: identification of key performance capabilities beyond indocyanine green imaging. *J Biomed Opt* **2016,** *21* (8), 80901.

7.   Gao, Z.; Hao, Y. C.; Zheng, M. L.; Chen, Y., A fluorescent dye with large Stokes shift and high stability: synthesis and application to live cell imaging. *Rsc Advances* **2017,** *7* (13), 7604-7609.

8.   Mishra, A.; Behera, R. K.; Behera, P. K.; Mishra, B. K.; Behera, G. B., Cyanines during the 1990s: A Review. *Chem Rev* **2000,** *100* (6), 1973-2012.

9.   Boni, L.; David, G.; Mangano, A.; Dionigi, G.; Rausei, S.; Spampatti, S.; Cassinotti, E.; Fingerhut, A., Clinical applications of indocyanine green (ICG) enhanced fluorescence in laparoscopic surgery. *Surg Endosc* **2015,** *29* (7), 2046-55.

10.   Alius, C.; Oprescu, S.; Balalau, C.; Nica, A. E., Indocyanine green enhanced surgery principle, clinical applications and future research directions. *J Clin Invest Surg* **2018,** *3* (1), 1-8.

11.   Schaafsma, B. E. a. M., J Sven D and Hutteman, Merlijn and Van der Vorst, Joost R and Kuppen, Peter JK and Löwik, Clemens WGM and Frangioni, John V and Van de Velde, Cornelis JH and Vahrmeijer, Alexander L, The clinical use of indocyanine green as a near-infrared fluorescent contrast agent for image-guided oncologic surgery. *Journal of surgical oncology* **2011,** *104* (3), 323-332.

12.   Mindt, S.; Karampinis, I.; John, M.; Neumaier, M.; Nowak, K., Stability and degradation of indocyanine green in plasma, aqueous solution and whole blood. *Photochem Photobiol Sci* **2018,** *17* (9), 1189-1196.

13.   Gao, B.; Li, H.; Liu, H.; Zhang, L.; Bai, Q.; Ba, X., Water-soluble and fluorescent dendritic perylene bisimides for live-cell imaging. *Chem Commun (Camb)* **2011,** *47* (13), 3894-6.

14.   Sahoo, D.; Sharma, V.; Roy, R.; Varghese, N.; Mohanta, K.; Koner, A. L., Synthesis of highly-soluble push-pull perylenemonoimide derivatives by regioselective peri-functionalization for switchable memory applications. *Chem Commun* **2019,** *55* (1), 103-106.

15.   Kaloyanova, S.; Zagranyarski, Y.; Ritz, S.; Hanulova, M.; Koynov, K.; Vonderheit, A.; Mullen, K.; Peneva, K., Water-Soluble NIR-Absorbing Rylene Chromophores for Selective Staining of Cellular Organelles. *J Am Chem Soc* **2016,** *138* (9), 2881-4.

16.   Chen, C.; Tian, R.; Zeng, Y.; Chu, C. C.; Liu, G., Activatable Fluorescence Probes for "Turn-On" and Ratiometric Biosensing and Bioimaging: From NIR-I to NIR-II. *Bioconjugate Chem* **2020,** *31* (2), 276-292.

17.   Voskuil, F. J.; Steinkamp, P. J.; Zhao, T.; van der Vegt, B.; Koller, M.; Doff, J. J.; Jayalakshmi, Y.; Hartung, J. P.; Gao, J.; Sumer, B. D.; Witjes, M. J. H.; van Dam, G. M.; Grp, S. S., Exploiting metabolic acidosis in solid cancers using a tumor-agnostic pH-activatable nanoprobe for fluorescence-guided surgery. *Nature Communications* **2020,** *11* (1).

18.   Widen, J. C.; Tholen, M.; Yin, J. J.; Antaris, A.; Casey, K. M.; Rogalla, S.; Klaassen, A.; Sorger, J.; Bogyo, M., AND-gate contrast agents for enhanced fluorescence-guided surgery. *Nat Biomed Eng* **2021,** *5* (3), 264-277.

19.   Wang, C.; Wang, Z.; Zhao, T.; Li, Y.; Huang, G.; Sumer, B. D.; Gao, J., Optical molecular imaging for tumor detection and image-guided surgery. *Biomaterials* **2018,** *157*, 62-75.

20.   Jacques, S. L., Optical properties of biological tissues: a review. *Phys Med Biol* **2013,** *58* (11), R37-61.

21.   Pellicciari, C.; Biggiogera, M., Histochemistry of Single Molecules: Methods and Protocols. *Springer* **2017**.

22.   Horvath, H., Gustav Mie and the scattering and absorption of light by particles: Historic developments and basics. *Journal of Quantitative Spectroscopy and Radiative Transfer* **2009,** *110*, 787-799.

23.   Bigio, I. J.; Bown, S. G., Spectrroscopic sensing of cancer and cancer therapy: Current status of translational research. *Cancer biology & therapy* **2004,** *3* (3), 259-267.

24.   Wang, T. D.; Van Dam, J., Optical biopsy: a new frontier in endoscopic detection and diagnosis. *Clin Gastroenterol Hepatol* **2004,** *2* (9), 744-53.

25.   DSouza, A. V.; Lin, H.; Henderson, E. R.; Samkoe, K. S.; Pogue, B. W., Review of fluorescence guided surgery systems: identification of key performance capabilities beyond indocyanine green imaging. *Journal of biomedical optics* **2016,** *21*, 080901.

26.   Ntziachristos, V.; Ripoll, J.; Wang, L. V.; Weissleder, R., Looking and listening to light: the evolution of whole-body photonic imaging. *Nat Biotechnol* **2005,** *23* (3), 313-20.

27.   Leblond, F.; Ovanesyan, Z.; Davis, S. C.; Valdes, P. A.; Kim, A.; Hartov, A.; Wilson, B. C.; Pogue, B. W.; Paulsen, K. D.; Roberts, D. W., Analytic expression of fluorescence ratio detection correlates with depth in multi-spectral sub-surface imaging. *Phys Med Biol* **2011,** *56* (21), 6823-37.

28.   Ntziachristos, V., Going deeper than microscopy: the optical imaging frontier in biology. *Nature methods* **2010,** *7*, 603-614.

29.   Barth, C. W.; Gibbs, S. L., Fluorescence Image-Guided Surgery - a Perspective on Contrast Agent Development. *Proc SPIE Int Soc Opt Eng* **2020,** *11222*.

30.   Nguyen, Q. T.; Tsien, R. Y., Fluorescence-guided surgery with live molecular navigation--a new cutting edge. *Nat Rev Cancer* **2013,** *13* (9), 653-62.

31.   Choi, H. S.; Gibbs, S. L.; Lee, J. H.; Kim, S. H.; Ashitate, Y.; Liu, F.; Hyun, H.; Park, G.; Xie, Y.; Bae, S.; Henary, M.; Frangioni, J. V., Targeted zwitterionic near-infrared fluorophores for improved optical imaging. *Nat Biotechnol* **2013,** *31* (2), 148-53.

32.   Sekijima, M.; Tojimbara, T.; Sato, S.; Nakamura, M.; Kawase, T.; Kai, K.; Urashima, Y.; Nakajima, I.; Fuchinoue, S.; Teraoka, S., An intraoperative fluorescent imaging system in organ transplantation. *Transplant Proc* **2004,** *36* (7), 2188-90.

33.   Watanabe, J.; M., O.; Suwa, Y.; Suzuki, S.; Suwa, H.; Momiyama, M.; Ishibe, A.; Watanabe, K.; Masui, H.; Nagahori, K., Evaluation of the intestinal blood flow near the rectosigmoid junction using the indocyanine green fluorescence method in a colorectal cancer surgery. *International journal of colorectal disease* **2015,** *30*, 329-335.

34.   Reuthebuch, O.; Haussler, A.; Genoni, M.; Tavakoli, R.; Odavic, D.; Kadner, A.; Turina, M., Novadaq SPY: intraoperative quality assessment in off-pump coronary artery bypass grafting. *Chest* **2004,** *125* (2), 418-24.

35.   Schirmer, R. H.; Adler, H.; Pickhardt, M.; Mandelkow, E., Lest we forget you—methylene blue…. *Neurobiology of aging* **2011,** *32* (12), 2325--e7.

36.   Matsui, A.; Tanaka, E.; Choi, H. S.; Kianzad, V.; Gioux, S.; Lomnes, S. J.; Frangioni, J. V., Real-time, near-infrared, fluorescence-guided identification of the ureters using methylene blue. *Surgery* **2010,** *148* (1), 78-86.

37.   Ohlow, M. J.; Moosmann, B., Phenothiazine: the seven lives of pharmacology's first lead structure. *Drug Discov Today* **2011,** *16* (3-4), 119-31.

38.   Matsui, A.; Tanaka, E.; Choi, H. S.; Kianzad, V.; Gioux, S.; Lomnes, S. J.; Frangioni, J. V., Real-time, near-infrared, fluorescence-guided identification of the ureters using methylene blue. *Surgery* **2010,** *148*, 78-86.

39.   Gauthier, T. W., Methylene blue-induced hyperbilirubinemia in neonatal glucose-6-phosphate dehydrogenase (G6PD) deficiency. *J Matern Fetal Med* **2000,** *9* (4), 252-4.

40.	Folaron, M.; Strawbridge, R.; Samkoe, K. S.; Filan, C.; Roberts, D. W.; Davis, S. C., Elucidating the kinetics of sodium fluorescein for fluorescence-guided surgery of glioma. *J Neurosurg* **2018,** *131* (3), 724-734.

41.	Pansare, V.; Hejazi, S.; Faenza, W.; Prud'homme, R. K., Review of Long-Wavelength Optical and NIR Imaging Materials: Contrast Agents, Fluorophores and Multifunctional Nano Carriers. *Chem Mater* **2012,** *24* (5), 812-827.

42.	Zhou, J. F.; Chin, M. P.; Schafer, S. A., Aggregation and degradation of indocyanine green. *Laser Surgery: Advanced Characterization, Therapeutics, and Systems IV* **1994,** *2128*, 495-505.

43.	Samanta, A.; Vendrell, M.; Das, R.; Chang, Y. T., Development of photostable near-infrared cyanine dyes. *Chem Commun (Camb)* **2010,** *46* (39), 7406-8.

44.	Hadjipanayis, C. G.; Stummer, W., 5-ALA and FDA approval for glioma surgery. *J Neurooncol* **2019,** *141* (3), 479-486.

45.	Chen, C.; Tian, R.; Zeng, Y.; Chu, C.; Liu, G., Activatable Fluorescence Probes for "Turn-On" and Ratiometric Biosensing and Bioimaging: From NIR-I to NIR-II. *Bioconjug Chem* **2020,** *31* (2), 276-292.

46.	Cilliers, C.; Nessler, I.; Christodolu, N.; Thurber, G. M., Tracking Antibody Distribution with Near-Infrared Fluorescent Dyes: Impact of Dye Structure and Degree of Labeling on Plasma Clearance. *Mol Pharm* **2017,** *14* (5), 1623-1633.

47.	Hyun, H.; Owens, E. A.; Narayana, L.; Wada, H.; Gravier, J.; Bao, K.; Frangioni, J. V.; Choi, H. S.; Henary, M., Central C-C Bonding Increases Optical and Chemical Stability of NIR Fluorophores. *RSC Adv* **2014,** *4* (102), 58762-58768.

48.	Kobayashi, H.; Griffiths, G. L.; Choyke, P. L., Near-Infrared Photoimmunotherapy: Photoactivatable Antibody-Drug Conjugates (ADCs). *Bioconjug Chem* **2020,** *31* (1), 28-36.

49.	Urano, Y.; Asanuma, D.; Hama, Y.; Koyama, Y.; Barrett, T.; Kamiya, M.; Nagano, T.; Watanabe, T.; Hasegawa, A.; Choyke, P. L.; Kobayashi, H., Selective molecular imaging of viable cancer cells with pH-activatable fluorescence probes. *Nat Med* **2009,** *15* (1), 104-9.

50.	Mochida, A.; Ogata, F.; Nagaya, T.; Choyke, P. L.; Kobayashi, H., Activatable fluorescent probes in fluorescence-guided surgery: Practical considerations. *Bioorg Med Chem* **2018,** *26* (4), 925-930.

51.	Ogawa, M.; Kosaka, N.; Choyke, P. L.; Kobayashi, H., H-type dimer formation of fluorophores: a mechanism for activatable, in vivo optical molecular imaging. *ACS Chem Biol* **2009,** *4* (7), 535-46.

52.	Lacivita, E.; Leopoldo, M.; Berardi, F.; Colabufo, N. A.; Perrone, R., Activatable fluorescent probes: a new concept in optical molecular imaging. *Curr Med Chem* **2012,** *19* (28), 4731-41.

53.	Han, J.; Burgess, K., Fluorescent indicators for intracellular pH. *Chem Rev* **2010,** *110* (5), 2709-28.

54.	Piechota, E. J.; Meyer, G. J., Introduction to Electron Transfer: Theoretical Foundations and Pedagogical Examples. *J Chem Ed* **2019,** *96* (11), 2450-2466.

55.	Murtagh, J.; Frimannsson, D. O.; O'Shea, D. F., Azide conjugatable and pH responsive near-infrared fluorescent imaging probes. *Org Lett* **2009,** *11* (23), 5386-9.

56.	Killoran, J.; Allen, L.; Gallagher, J.; Gallagher, W. M.; Donal, F., Synthesis of BF 2 chelates of tetraarylazadipyrromethenes and evidence for their photodynamic therapeutic behaviour. *Cheml comm* **2002,** (17), 1862-1863.

57.	Ogawa, M.; Kosaka, N.; Regino, C. A.; Mitsunaga, M.; Choyke, P. L.; Kobayashi, H., High sensitivity detection of cancer in vivo using a dual-controlled activation fluorescent imaging probe based on H-dimer formation and pH activation. *Mol Biosyst* **2010,** *6* (5), 888-93.

58.	Chen, J.; Tung, C. H.; Allport, J. R.; Chen, S.; Weissleder, R.; Huang, P. L., Near-infrared fluorescent imaging of matrix metalloproteinase activity after myocardial infarction. *Circulation* **2005,** *111* (14), 1800-5.

59.	Staudigl, C.; Concin, N.; Grimm, C.; Pfeiler, G.; Nehoda, R.; Singer, C. F.; Polterauer, S., Prognostic relevance of pretherapeutic gamma-glutamyltransferase in patients with primary metastatic breast cancer. *PLoS One* **2015,** *10* (4), e0125317.

60.   Iwatate, R. J.; Kamiya, M.; Urano, Y., Asymmetric Rhodamine-Based Fluorescent Probe for Multicolour In Vivo Imaging. *Chemistry* **2016,** *22* (5), 1696-703.

61.   Iwatate, R. J.; Kamiya, M.; Umezawa, K.; Kashima, H.; Nakadate, M.; Kojima, R.; Urano, Y., Silicon Rhodamine-Based Near-Infrared Fluorescent Probe for gamma-Glutamyltransferase. *Bioconjug Chem* **2018,** *29* (2), 241-244.

62.   Li, H.; Yao, Q.; Sun, W.; Shao, K.; Lu, Y.; Chung, J.; Kim, D.; Fan, J.; Long, S.; Du, J.; , Aminopeptidase N activatable fluorescent probe for tracking metastatic cancer and image-guided surgery via in situ spraying. *Journal of the American Chemical Society* **2020,** *142* (13), 6381-6389.

63.   Bures, F., Fundamental aspects of property tuning in push-pull molecules. *Rsc Advances* **2014,** *4* (102), 58826-58851.

64.   Misra, R.; Bhattacharyya, P., Intramolecular Charge Transfer: Theory and Applications. *John Wiley & Sons* **2018**.

65.   Raghavachari, R., Near-infrared applications in biotechnology. **2000**.

66.   Grabowski, Z. R.; Rotkiewicz, K.; Rettig, W., Structural changes accompanying intramolecular electron transfer: focus on twisted intramolecular charge-transfer states and structures. *Chem Rev* **2003,** *103* (10), 3899-4032.

67.   Galievsky, V.; Zachariasse, K., Intramolecular charge transfer with N, N-Dialkyl-4-(trifluoromethyl) anilines and 4-(dimethylamino) benzonitrile in polar solvents. Investigation of the excitation wavelength dependence of the reaction pathway. *Acta Physica Polonica A* **2007,** *112*, S-39.

68.   Catalan, J., On the dual emission of p-dimethylaminobenzonitrile and its photophysical implications. *Phys Chem Chem Phys* **2013,** *15* (22), 8811-20.

69.   Feiler, L.; Langhals, H.; Polborn, K., Synthesis of perylene-3, 4-dicarboximides—Novel highly photostable fluorescent dyes. *Liebigs Annalen* **1995,** *1995* (7), 1229-1244.

70.   Zagranyarski, Y.; Chen, L.; Jansch, D.; Gessner, T.; Li, C.; Mullen, K., Toward perylene dyes by the Hundsdiecker reaction. *Org Lett* **2014,** *16* (11), 2814-7.

71.   Tomizaki, K.-y.; Thamyongkit, P.; Loewe, R. S.; Lindsey, J. S., Practical synthesis of perylene-monoimide building blocks that possess features appropriate for use in porphyrin-based light-harvesting arrays. *Tetrahedron* **2003,** *59*, 1191-1207.

72.   Li, C.; Schoneboom, J.; Liu, Z.; Pschirer, N. G.; Erk, P.; Herrmann, A.; Mullen, K., Rainbow perylene monoimides: easy control of optical properties. *Chemistry* **2009,** *15* (4), 878-84.

73.   Zagranyarski, Y.; Chen, L.; Zhao, Y.; Wonneberger, H.; Li, C.; Mullen, K., Facile transformation of perylene tetracarboxylic acid dianhydride into strong donor-acceptor chromophores. *Org Lett* **2012,** *14* (21), 5444-7.

74.   Quante, H.; Geerts, Y.; Müllen, K., Synthesis of soluble perylenebisamidine derivatives. Novel long-wavelength absorbing and fluorescent dyes. *Chemistry of materials* **1997,** *9* (2), 495-500.

75.   Huang, C.; Barlow, S.; Marder, S. R., Perylene-3,4,9,10-tetracarboxylic acid diimides: synthesis, physical properties, and use in organic electronics. *J Org Chem* **2011,** *76* (8), 2386-407.

76.   Avlasevich, Y.; Li, C.; Müllen, K., Synthesis and applications of core-enlarged perylene dyes. *Royal Society of Chemistry* **2010,** *20*, 3814-3826.

77.   Fu, M.; Xiao, Y.; Qian, X.; Zhao, D.; Xu, Y., A design concept of long-wavelength fluorescent analogs of rhodamine dyes: replacement of oxygen with silicon atom. *Chem Commun (Camb)* **2008,** (15), 1780-2.

78.   Koide, Y.; Urano, Y.; Hanaoka, K.; Terai, T.; Nagano, T., Development of an Si-rhodamine-based far-red to near-infrared fluorescence probe selective for hypochlorous acid and its applications for biological imaging. *J Am Chem Soc* **2011,** *133* (15), 5680-2.

79.   Koide, Y.; Urano, Y.; Hanaoka, K.; Terai, T.; Nagano, T., Evolution of group 14 rhodamines as platforms for near-infrared fluorescence probes utilizing photoinduced electron transfer. *ACS Chem Biol* **2011,** *6* (6), 600-8.

80.   McCann, T. E.; Kosaka, N.; Koide, Y.; Mitsunaga, M.; Choyke, P. L.; Nagano, T.; Urano, Y.; Kobayashi, H., Activatable optical imaging with a silica-rhodamine based near infrared (SiR700) fluorophore: a comparison with cyanine based dyes. *Bioconjug Chem* **2011,** *22* (12), 2531-8.

81.   Koide, Y.; Urano, Y.; Hanaoka, K.; Piao, W.; Kusakabe, M.; Saito, N.; Terai, T.; Okabe, T.; Nagano, T., Development of NIR fluorescent dyes based on Si-rhodamine for in vivo imaging. *J Am Chem Soc* **2012,** *134* (11), 5029-31.

82.   Tamao, K.; Uchida, M.; Izumizawa, T.; Furukawa, K.; Yamaguchi, S., Silole derivatives as efficient electron transporting materials. *J Am Chem Soc* **1996,** *118* (47), 11974-11975.

83.   Yamaguchi, S.; Tamao, K., Silole-containing sigma- and pi-conjugated compounds. *J Chem Soc Dalton* **1998,** (22), 3693-3702.

84.   Takeda, N.; Shinohara, A.; Tokitoh, N., The first stable 9-silaanthracene. *Organometallics* **2002,** *21* (2), 256-258.

85.   Koide, Y.; Urano, Y.; Hanaoka, K.; Terai, T.; Nagano, T., Evolution of Group 14 Rhodamines as Platforms for Near-Infrared Fluorescence Probes Utilizing Photoinduced Electron Transfer. *Acs Chemical Biology* **2011,** *6* (6), 600-608.

86.   Pastierik, T.; Sebej, P.; Medalova, J.; Stacko, P.; Klan, P., Near-infrared fluorescent 9-phenylethynylpyronin analogues for bioimaging. *J Org Chem* **2014,** *79* (8), 3374-82.

87.   Pastierik, T.; Sebej, P.; Medalova, J.; Stacko, P.; Klan, P., Near-Infrared Fluorescent 9-Phenylethynylpyronin Analogues for Bioimaging. *Journal of Organic Chemistry* **2014,** *79* (8), 3374-3382.

88.   Grimm, J. B.; Brown, T. A.; Tkachuk, A. N.; Lavis, L. D., General Synthetic Method for Si-Fluoresceins and Si-Rhodamines. *Acs Central Sci* **2017,** *3* (9), 975-985.

89.   Butkevich, A. N.; Lukinavicius, G.; D'Este, E.; Hell, S. W., Cell-Permeant Large Stokes Shift Dyes for Transfection-Free Multicolor Nanoscopy. *J Am Chem Soc* **2017,** *139* (36), 12378-12381.

90.   Butkevich, A. N.; Lukinavicius, G.; D'Este, E.; Hell, S. W., Cell-Permeant Large Stokes Shift Dyes for Transfection-Free Multicolor Nanoscopy. *Journal of the American Chemical Society* **2017,** *139* (36), 12378-12381.

91.   Miksa, M.; Komura, H.; Wu, R.; Shah, K. G.; Wang, P., A novel method to determine the engulfment of apoptotic cells by macrophages using pHrodo succinimidyl ester. *J Immunol Methods* **2009,** *342* (1-2), 71-7.

92.   Huotari, J.; Helenius, A., Endosome maturation. *Embo J* **2011,** *30* (17), 3481-3500.

93.   Dombrowski, G. W.; Dinnocenzo, J. P.; Zielinski, P. A.; Farid, S.; Wosinska, Z. M.; Gould, I. R., Efficient unimolecular deprotonation of aniline radical cations. *Journal of Organic Chemistry* **2005,** *70* (10), 3791-3800.

94.   Ingold, C., Structure and mechanism in organic chemistry. *Cornell University Press* **1969**.

95.   Hall, H. K., Steric Effects on the Base Strengths of Cyclic Amines. *Journal of the American Chemical Society* **1957,** *79* (20), 5444-5447.

96.   Vlasenko, M. P.; Ozeryanskii, V. A., One-scale basicities of diaminobenzenes and diaminonaphthalenes: from aniline to proton sponge. *J Phys Org Chem* **2017,** *30* (2).

97.   van Beurden, F.; van Willigen, D. M.; Vojnovic, B.; van Oosterom, M. N.; Brouwer, O. R.; der Poel, H. G. V.; Kobayashi, H.; van Leeuwen, F. W. B.; Buckle, T., Multi-Wavelength Fluorescence in Image-Guided Surgery, Clinical Feasibility and Future Perspectives. *Mol Imaging* **2020,** *19*, 1536012120962333.

98.   Tanaka, E.; Chen, F. Y.; Flaumenhaft, R.; Graham, G. J.; Laurence, R. G.; Frangioni, J. V., Real-time assessment of cardiac perfusion, coronary angiography, and acute intravascular thrombi using dual-channel near-infrared fluorescence imaging. *J Thorac Cardiov Sur* **2009,** *138* (1), 133-140.

99.   Wada, H.; Hyun, H.; Vargas, C.; Gravier, J.; Park, G.; Gioux, S.; Frangioni, J. V.; Henary, M.; Choi, H. S., Pancreas-targeted NIR fluorophores for dual-channel image-guided abdominal surgery. *Theranostics* **2015,** *5* (1), 1-11.

100.   Jorzik, J. J.; Bindewald, A.; Dithmar, S.; Holz, F. G., Digital simultaneous fluorescein and indocyanine green angiography, autofluorescence, and red-free imaging with a solid-state laser-based confocal scanning laser ophthalmoscope. *Retina-J Ret Vit Dis* **2005,** *25* (4), 405-416.

101.   Sikka, P.; Bindra, V.; Kapoor, S.; Jain, V.; Saxena, K., Blue cures blue but be cautious. *Journal of pharmacy & bioallied sciences* **2011,** *3*, 543.

102.   Song, X. Z.;   Johnson, A.; Foley, J., 7-Azabicyclo[2.2.1]heptane as a Unique and Effective Dialkylamino Auxochrome Moiety: Demonstration in a Fluorescent Rhodamine Dye. *Journal of the American Chemical Society* **2008,** *130* (52), 17652-+.

103.   Toutchkine, A.; Nguyen, D. V.; Hahn, K. M., Merocyanine dyes with improved photostability. *Organic Letters* **2007,** *9* (15), 2775-2777.

104.   Fehniger, T. A.; Cooper, M. A., Harnessing NK Cell Memory for Cancer Immunotherapy. *Trends Immunol* **2016,** *37* (12), 877-888.

105.   Schumacher, T. N.; Schreiber, R. D., Neoantigens in cancer immunotherapy. *Science* **2015,** *348* (6230), 69-74.

106.   Rosenberg, S. A., IL-2: the first effective immunotherapy for human cancer. *J Immunol* **2014,** *192* (12), 5451-8.

107.   Kielland, N.; Vendrell, M.; Lavilla, R.; Chang, Y. T., Imaging histamine in live basophils and macrophages with a fluorescent mesoionic acid fluoride. *Chem Commun (Camb)* **2012,** *48* (59), 7401-3.

108.   Perrin, J.; Capitao, M.; Mougin-Degraef, M.; Guerard, F.; Faivre-Chauvet, A.; Rbah-Vidal, L.; Gaschet, J.; Guilloux, Y.; Kraeber-Bodere, F.;   Cherel, M.; Barbet, J., Cell Tracking in Cancer Immunotherapy. *Front Med (Lausanne)* **2020,** *7*, 34.

109.   Mellanby, R. J.; Scott, J. I.; Mair, I.; Fernandez, A.; Saul, L.; Arlt, J.; Moral, M.; Vendrell, M., Tricarbocyanine N-triazoles: the scaffold-of-choice for long-term near-infrared imaging of immune cells in vivo. *Chem Sci* **2018,** *9* (36), 7261-7270.

110.   Artico, M.; Spoletini, M.; Fumagalli, L.; Biagioni, F.; Ryskalin, L.; Fornai, F.; Salvati, M.; Frati, A.; Pastore, F. S.; Taurone, S., Egas Moniz: 90 Years (1927-2017) from Cerebral Angiography. *Front Neuroanat* **2017,** *11*, 81.

111.   Marmor, M. F.; Ravin, J. G., Fluorescein angiography: insight and serendipity a half century ago. *Arch Ophthalmol* **2011,** *129* (7), 943-8.

112.   Van Manen, L.; Handgraaf, H. J.; Diana, M.; Dijkstra, J.; Ishizawa, T.; Vahrmeijer, A. L.; Mieog, J. S. D., A practical guide for the use of indocyanine green and methylene blue in fluorescence-guided abdominal surgery. *Journal of surgical oncology* **2018,** *118*, 283-300.

113.   Raabe, A.; Beck, J.; Gerlach, R.; Zimmermann, M.; Seifert, V., Near-infrared indocyanine green video angiography: a new method for intraoperative assessment of vascular flow. *Neurosurgery* **2003,** *52* (1), 132-9; discussion 139.

114.   Seeliger, B.; Barberio, M.; D'Urso, A.; Agnus, V.; Longo, F.; Mascagni, P.; Marescaux, J.; Mutter, D.; Diana, M., Fluorescence in rectal cancer surgery. *Ann Laparosc Endosc Surg* **2018,** *3*, 47.

115.   Bates, D. D. B.; Paroder, V.; Lall, C.; Lalwani, N.; Widmar, M.; Garcia-Aguilar, J., Complete mesocolic excision and central vascular ligation for right colon cancer: an introduction for abdominal radiologists. *Abdom Radiol* **2019,** *44* (11), 3518-3526.

116.   Daskalaki, D.; Fernandes, E.; Wang, X. Y.; Bianco, F. M.; Elli, E. F.; Ayloo, S.; Masrur, M.; Milone, L.; Giulianotti, P. C., Indocyanine Green (ICG) Fluorescent Cholangiography During Robotic Cholecystectomy: Results of 184 Consecutive Cases in a Single Institution. *Surg Innov* **2014,** *21* (6), 615-621.

117.   Changalvaie, B.; Han, S.; Moaseri, E.; Scaletti, F.; Truong, L.; Caplan, R.; Cao, A.; Bouchard, R.; Truskett, T. M.; Sokolov, K. V.; Johnston, K. P., Indocyanine Green J Aggregates in Polymersomes for Near-Infrared Photoacoustic Imaging. *ACS Appl Mater Interfaces* **2019,** *11* (50), 46437-46450.

118.   Weber, J.; Beard, P. C.; Bohndiek, S. E., Contrast agents for molecular photoacoustic imaging. *Nat Methods* **2016,** *13* (8), 639-50.

119.   Yao, D.; Wang, Y.; Zou, R.; Bian, K.; Liu, P.; Shen, S.; Yang, W.; Zhang, B.; Wang, D., Molecular Engineered Squaraine Nanoprobe for NIR-II/Photoacoustic Imaging and Photothermal Therapy of Metastatic Breast Cancer. *ACS Appl Mater Interfaces* **2020,** *12* (4), 4276-4284.

120.   Xia, J.; Yao, J.; Wang, L. V., Photoacoustic tomography: principles and advances. *Electromagn Waves (Camb)* **2014,** *147*, 1-22.

121.   A., P. R.; Saugata, S., Performance of near-infrared dyes as effective contrast agents for breast cancer detection through simulation of photoacoustic imaging. *Journal of Modern Optics* **2020,** *67* (4), 307-328.

122.   Park, Y. D.; Park, J. E.; Kim, H. S.; Choi, S. H.; Park, J. E.; Jeon, J.; Park, S. H., Development of a Squaraine-Based Molecular Probe for Dual-Modal in Vivo Fluorescence and Photoacoustic Imaging. *Bioconjug Chem* **2020,** *31* (11), 2607-2617.

123.   Dessi, A.; Sinicropi, A.; Mohammadpourasl, S.; Basosi, R.; Taddei, M.; de Biani, F. F.; Calamante, M.; Zani, L.; Mordini, A.; Bracq, P.; Franchi, D.; Reginato, G., New Blue Donor-Acceptor Pechmann Dyes: Synthesis, Spectroscopic, Electrochemical, and Computational Studies. *Acs Omega* **2019,** *4* (4), 7614-7627.

124.   Bessho, T.; Zakeeruddin, S. M.; Yeh, C. Y.; Diau, E. W. G.; Gratzel, M., Highly Efficient Mesoscopic Dye-Sensitized Solar Cells Based on Donor-Acceptor-Substituted Porphyrins. *Angew Chem Int Edit* **2010,** *49* (37), 6646-6649.

125.   Chen, C.; Fang, C., Devising Efficient Red-Shifting Strategies for Bioimaging: A Generalizable Donor-Acceptor Fluorophore Prototype. *Chem-Asian J* **2020,** *15* (10), 1514-1523.

126.   Ren, T. B.; Xu, W.; Zhang, W.; Zhang, X. X.; Wang, Z. Y.; Xiang, Z.; Yuan, L.; Zhang, X. B., A General Method To Increase Stokes Shift by Introducing Alternating Vibronic Structures. *J Am Chem Soc* **2018,** *140* (24), 7716-7722.

127.   Mancini, L.; Terradot, G.; Tian, T.; Pu, Y.; Li, Y.; Lo, C.-J.; Bai, F.; Pilizota, T., A general workflow for characterization of Nernstian dyes and their effects on bacterial physiology. *Biophysical Journal* **2020,** *118*, 4-14.

128.   Slooter, M. D.; Mansvelders, M. S. E.; Bloemen, P. R.; Gisbertz, S. S.; Bemelman, W. A.; Tanis, P. J.; Hompes, R.; Henegouwen, M. I. V.; de Bruin, D. M., Defining indocyanine green fluorescence to assess anastomotic perfusion during gastrointestinal surgery: systematic review. *Bjs Open* **2021,** *5* (2).

129.   Gao, H. Q.; Duan, X. C.; Jiao, D.; Zeng, Y.; Zheng, X. Y.; Zhang, J. T.; Ou, H. L.; Qi, J.; Ding, D., Boosting Photoacoustic Effect via Intramolecular Motions Amplifying Thermal-to-Acoustic Conversion Efficiency for Adaptive Image-Guided Cancer Surgery. *Angew Chem Int Edit* **2021,** *60* (38), 21047-21055.

130.   Han, J. Y.; Burgess, K., Fluorescent Indicators for Intracellular pH. *Chemical Reviews* **2010,** *110* (5), 2709-2728.

131.   Huang, R.; Yan, S.; Zheng, X.; Luo, F.; Deng, M.; Fu, B.; Xiao, Y.; Zhao, X.; Zhou, X., Development of a pH-activatable fluorescent probe and its application for visualizing cellular pH change. *Analyst* **2012,** *137* (19), 4418-20.

132.   Shi, R.; Huang, L.; Duan, X.; Sun, G.; Yin, G.; Wang, R.; Zhu, J. J., Selective imaging of cancer cells with a pH-activatable lysosome-targeting fluorescent probe. *Anal Chim Acta* **2017,** *988*, 66-73.

133.   Wang, L.; Fan, Z.; Zhang, J.; Changyi, Y.; Huang, C.; Gu, Y.; Xu, Z.; Tang, Z.; Lu, W.; Wei, X.; Li, C., Evaluating tumor metastatic potential by imaging intratumoral acidosis via pH-activatable near-infrared fluorescent probe. *Int J Cancer* **2015,** *136* (4), E107-16.

134.   Hoogendoorn, S.; Blom, A. E.; Willems, L. I.; van der Marel, G. A.; Overkleeft, H. S., Synthesis of pH-activatable red fluorescent BODIPY dyes with distinct functionalities. *Org Lett* **2011,** *13* (20), 5656-9.

135.   Mu, H. Y.; Miki, K.; Harada, H.; Tanaka, K.; Nogita, K.; Ohe, K., pH-Activatable Cyanine Dyes for Selective Tumor Imaging Using Near-Infrared Fluorescence and Photoacoustic Modalities. *Acs Sensors* **2021,** *6* (1), 123-129.

136.   Pan, G. Y.; Jia, H. R.; Zhu, Y. X.; Wang, R. H.; Wu, F. G.; Chen, Z., Dual Channel Activatable Cyanine Dye for Mitochondrial Imaging and Mitochondria-Targeted Cancer Theranostics. *Acs Biomater Sci Eng* **2017,** *3* (12), 3596-3606.

137.   Koide, Y.; Kojima, R.; Hanaoka, K.; Numasawa, K.; Komatsu, T.; Nagano, T.; Kobayashi, H.; Urano, Y., Design strategy for germanium-rhodamine based pH-activatable near-infrared fluorescence probes suitable for biological applications. *Commun Chem* **2019,** *2*.

138.   Adie, E. J.; Francis, M. J.; Davies, J.; Smith, L.; Marenghi, A.; Hather, C.; Hadingham, K.; Michael, N. P.; Milligan, G.; Gamel, S., CypHer 5: A generic approach for measuring the activation and trafficking of G protein-coupled receptors in live cells. *Assay Drug Dev Techn* **2003,** *1* (2), 251-259.

139.   Asanuma, D.; Takaoka, Y.; Namiki, S.; Takikawa, K.; Kamiya, M.; Nagano, T.; Urano, Y.; Hirose, K., Acidic-pH-activatable fluorescence probes for visualizing exocytosis dynamics. *Angew Chem Int Ed Engl* **2014,** *53* (24), 6085-9.

140.   Akkapeddi, P.; Azizi, S. A.; Freedy, A. M.; Cal, P. M. S. D.; Gois, P. M. P.; Bernardes, G. J. L., Construction of homogeneous antibody-drug conjugates using site-selective protein chemistry. *Chemical Science* **2016,** *7* (5), 2954-2963.

141.   Ravasco, J.; Faustino, H.; Trindade, A.; Gois, P. M. P., Bioconjugation with Maleimides: A Useful Tool for Chemical Biology. *Chemistry* **2019,** *25* (1), 43-59.

142.   Richardson, M. B.; Gabriel, K. N.; Garcia, J. A.; Ashby, S. N.; Dyer, R. P.; Kim, J. K.; Lau, C. J.; Hong, J.; Le Tourneau, R. J.; Sen, S.; Narel, D. L.; Katz, B. B.; Ziller, J. W.; Majumdar, S.; Collins, P. G.; Weiss, G. A., Pyrocinchonimides Conjugate to Amine Groups on Proteins via Imide Transfer. *Bioconjug Chem* **2020,** *31* (5), 1449-1462.

143.   Walker, M. A., A High-Yielding Synthesis of N-Alkyl Maleimides Using a Novel Modification of the Mitsunobu Reaction. *Journal of Organic Chemistry* **1995,** *60* (16), 5352-5355.

144.   Baldwin, A. D.; Kiick, K. L., Tunable degradation of maleimide-thiol adducts in reducing environments. *Bioconjug Chem* **2011,** *22* (10), 1946-53.

145.   Hoyle, C. E.; Bowman, C. N., Thiol-ene click chemistry. *Angewandte Chemie International Edition* **2010,** *49* (9), 1540-1573.

146.   Dondoni, A., The emergence of thiol-ene coupling as a click process for materials and bioorganic chemistry. *Angew Chem Int Ed Engl* **2008,** *47* (47), 8995-7.

147.   Alonso, R.; Jimenez-Meneses, P.; Garcia-Ruperez, J.; Banuls, M. J.; Maquieira, A., Thiol-ene click chemistry towards easy microarraying of half-antibodies. *Chem Commun (Camb)* **2018,** *54* (48), 6144-6147.

148.   Northrop, B. H.; Coffey, R. N., Thiol-ene click chemistry: computational and kinetic analysis of the influence of alkene functionality. *Journal of the American Chemical Society* **2012,** *134* (33), 13804-13817.

149.   Das, R. C., Debashis, Silver triflate catalyzed acetylation of alcohols, thiols, phenols, and amines. *Synthesis* **2011,** *2011*, 1621-1625.

150.   Oscar Valdes Aguilera, D. C. N., Aggregation phenomena in xanthene dyes. *Acc. Chem. Res.* **1989,** *22*, 171-177.

151.   Ogawa, M.; Kosaka, N.; Choyke, P. L.; Kobayashi, H., In vivo molecular imaging of cancer with a quenching near-infrared fluorescent probe using conjugates of monoclonal antibodies and indocyanine green. *Cancer Res* **2009,** *69* (4), 1268-72.

152.   Heyne, B., Self-assembly of organic dyes in supramolecular aggregates. *Photoch Photobio Sci* **2016,** *15* (9), 1103-1114.

153.   Gatenby, R. A.; Gillies, R. J., Why do cancers have high aerobic glycolysis? *Nature reviews cancer* **2004,** *4* (11), 891-899.

154.   Feng, W.; Li, M.; Sun, Y.; Feng, G., Near-Infrared Fluorescent Turn-on Probe with a Remarkable Large Stokes Shift for Imaging Selenocysteine in Living Cells and Animals. *Anal Chem* **2017,** *89* (11), 6106-6112.

155.   Qi, Y.; Huang, Y.; Li, B.; Zeng, F.; Wu, S., Real-Time Monitoring of Endogenous Cysteine Levels In Vivo by near-Infrared Turn-on Fluorescent Probe with Large Stokes Shift. *Anal Chem* **2018,** *90* (1), 1014-1020.

156.   Sun, J.; Zhao, J.; Wang, L.; Li, H.; Yang, F.; Yang, X., Inner Filter Effect-Based Sensor for Horseradish Peroxidase and Its Application to Fluorescence Immunoassay. *ACS Sens* **2018,** *3* (1), 183-190.

157.   Ballou, B.; Ernst, L. A.; Waggoner, A. S., Fluorescence imaging of tumors in vivo. *Curr Med Chem* **2005,** *12* (7), 795-805.

158.   Egloff-Juras.; Bezdetnaya., C. a.; Gilles., L. a. D.; Lassalle, H.-P., NIR fluorescence-guided tumor surgery: new strategies for the use of indocyanine green. *International journal of nanomedicine* **2019,** *14*, 7823.
159.   Vargas, S. H.; Lin, C.; Cao, H. S. T.; Ikoma, N.; Amiri, S. A.; Ghosh, S. C.; Uselmann, A. J.; Azhdarinia, A., Receptor-Targeted Fluorescence-Guided Surgery With Low Molecular Weight Agents. *Frontiers in Oncology* **2021,** *11*.
160.   Attia, A. B. E.; Balasundaram, G.; Moothanchery, M.; Dinish, U. S.; Bi, R. Z.; Ntziachristos, V.; Olivo, M., A review of clinical photoacoustic imaging: Current and future trends. *Photoacoustics* **2019,** *16*.
161.   Mahalingam, S. M.; Kularatne, S. A.; Myers, C. H.; Gagare, P.; Norshi, M.; Liu, X.; Singhal, S.; Low, P. S., Evaluation of Novel Tumor-Targeted Near-Infrared Probe for Fluorescence-Guided Surgery of Cancer. *Journal of Medicinal Chemistry* **2018,** *61* (21), 9637-9646.
162.   Nguyen, Q. T.; Olson, E. S.; Aguilera, T. A.; Jiang, T.; Scadeng, M.; Ellies, L. G.; Tsien, R. Y., Surgery with molecular fluorescence imaging using activatable cell-penetrating peptides decreases residual cancer and improves survival. *P Natl Acad Sci USA* **2010,** *107* (9), 4317-4322.
163.   Tringale, K. R.; Pang, J.; Nguyen, Q. T., Image-guided surgery in cancer: A strategy to reduce incidence of positive surgical margins. *Wires Syst Biol Med* **2018,** *10* (3).
164.   Mochida, A.; Ogata, F.; Nagaya, T.; Choyke, P. L.; Kobayashi, H., Activatable fluorescent probes in fluorescence-guided surgery: Practical considerations. *Bioorgan Med Chem* **2018,** *26* (4), 925-930.
165.   Ogawa, M.; Kosaka, N.; Regino, C. A.; Mitsunaga, M.; Choyke, P. L.; Kobayashi, H., High sensitivity detection of cancer in vivo using a dual-controlled activation fluorescent imaging probe based on H-dimer formation and pH activation. *Molecular bioSystems* **2010,** *6*, 888-893.
166.   Dondoni, A.; Massi, A.; Nanni, P.; Roda, A., A new ligation strategy for peptide and protein glycosylation: photoinduced thiol-ene coupling. *Chemistry A European Journal* **2009,** *15* (43), 11444-11449.
167.   Piechota, E. J.; Meyer, G. J., Introduction to Electron Transfer: Theoretical Foundations and Pedagogical Examples. *Journal of Chemical Education* **2019,** *96* (11), 2450-2466.
168.   Jeffrey Dzubay, k. G., Vladimir Martin, Aleksey Rukavishnikov, Daniel Beacham WO2013180813 Fluorogenic pH sensitive dyes and their method of use. 2016.
169.   Perera, A. S.; Subbaiyan, N. K.; Kalita, M.; Wendel, S. O.; Samarakoon, T. N.; D'Souza, F.; Bossmann, S. H., A hybrid soft solar cell based on the mycobacterial porin MspA linked to a sensitizer-viologen Diad. *J Am Chem Soc* **2013,** *135* (18), 6842-5.
170.   Grimm, J. B.; Brown, T. A.; Tkachuk, A. N.; Lavis, L. D., General Synthetic Method for Si-Fluoresceins and Si-Rhodamines. *ACS Cent Sci* **2017,** *3* (9), 975-985.

8. ZUSAMMENFASSUNG

Die Zahl der krebsbedingten Todesfälle nimmt jedes Jahr zu und nach Angaben des National Cancer Institute starben 2017 1,7 Millionen Menschen an krebsbedingten Krankheiten. [1] Die Chirurgie ist gemeinsam mit adjuvanten Therapien wie Chemo- und Immuntherapien nach wie vor eine der nützlichsten Methoden zur Krebsbekämpfung.[2] Die Resektion von Krebs im Frühstadium ist der erste Ansatz zur Behandlung von nicht hämatogenem, lokalisiertem Krebs und die Erkennung und Visualisierung aller bösartigen Läsionen bleibt eine ständige Herausforderung für Chirurgen. Bis heute stützt sich die erste Operation, die zur Erkennung der Tumormasse erforderlich ist, auf die visuelle Lokalisierung, die Palpation und die pathologische Analyse im Schnellschnitt.[3] Die Schwierigkeit, Tumorränder zu erkennen, führt häufig zu einer unvollständigen Entfernung des Tumors. Während moderne, bildgebende Verfahren auf der Grundlage der Computertomographie (CT) und der Magnetresonanztomographie (MRT) Anomalien auf anatomischer Ebene wirksam aufspüren, können nur Verfahren, die auf dem Einsatz gezielter exogener molekularer Kontrastmittel beruhen, Aufschluss über die verbleibenden positiven Ränder auf zellulärer Ebene geben. Darunter fällt die fluoreszenzgesteuerte Chirurgie (FGS), die zunehmend Anklang in den Operationssälen findet.[1, 2] Als Alternative zur Radionuklid-Bildgebung reduziert die Verwendung von gewebetransparenten Photonen niedriger Energie im nahen Infrarotbereich (NIR) in Verbindung mit kompakten optischen Bildgebungssystemen den Platzbedarf der nuklearmedizinischen Ausrüstung und ermöglicht es Chirurgen, die Qualität chirurgischer Resektionen in Echtzeit zu verbessern, ohne gesunden Strukturen wie Nerven, Blutgefäße, Harnleiter und Gallengänge zu schädigen.[1] Bis heute wurde der Einsatz von fluoreszierenden Kontrastmitteln in verschiedenen medizinischen Anwendungen dokumentiert, die von der Sentinel-Lymphknotenkartierung bis hin zu laparoskopischen und robotergestützten Operationen reichen. Unter ihnen sind die vaskuläre Fluoreszenzangiographie in der rekonstruktiven Chirurgie und die Beurteilung der Leberfunktion die häufigsten Techniken.[4] Ein fluoreszierendes Kontrastmittel kann ein synthetisches organisches Chromophor in Form eines kleinen Moleküls oder eine makromolekulare Einheit (Molekulargewicht >1000 Da) sein. Es sollte einen hohen Extinktionskoeffizienten und eine hohe Quantenausbeute in Wasser, eine große Stokes-Verschiebung, Biokompatibilität und geringe Toxizität aufweisen. Im Jahr 1959 genehmigte die Food and Drug Administration (FDA) Indocyaningrün (ICG) als Kontrastmittel für die fluoreszenzgestützte Chirurgie, womit es das erste Fluorophor war, das in der Klinik eingesetzt wurde. Es gehört zur Familie der Cyaninfarbstoffe und lieferte beachtliche Ergebnisse in der Chirurgie zur Messung des Herzzeitvolumens, zur Untersuchung der Anatomie der Netzhautgefäße und zur Beurteilung der Leberfunktionsreserve vor der Leberresektion bei zirrhotischen Lebern. Bei Anregungslicht von 750-800 nm emittiert ICG bei 820 nm, weist eine geringe Toxizität auf, bindet an Plasmaproteine und hat eine kurze Halbwertszeit im Blutkreislauf (3-5 Minuten). Es wird schnell von der Leber extrahiert und unverändert in der Galle konzentriert. ICG bringt jedoch auch mehrere Nachteilen mit sich wie etwa schlechte Wasserlöslichkeit, kurze Stokes-Verschiebung und geringe Quantenausbeute in

---

[1] Low, P. S.; Singhal, S.; Srinivasarao, M., Fluorescence-guided surgery of cancer: applications, tools and perspectives. Curr Opin Chem Biol 2018, 45, 64-72.

[2] Nagaya, T.; Nakamura, Y. A.; Choyke, P. L.; Kobayashi, H., Fluorescence-Guided Surgery. Front Oncol 2017, 7, 314.

[3] Li, H.; Yao, Q.; Sun, W.; Shao, K.; Lu, Y.; Chung, J.; Kim, D.; Fan, J.; Long, S.; Du, J.; Li, Y.; Wang, J.; Yoon, J.; Peng, X., Aminopeptidase N Activatable Fluorescent Probe for Tracking Metastatic Cancer and Image-Guided Surgery via in Situ Spraying. J Am Chem Soc 2020, 142 (13), 6381-6389.

[4] AV, D. S.; Lin, H.; Henderson, E. R.; Samkoe, K. S.; Pogue, B. W., Review of fluorescence guided surgery systems: identification of key performance capabilities beyond indocyanine green imaging. J Biomed Opt 2016, 21 (8), 80901

Wasser von 1 bis 10 %. Dadurch ist das Fluoreszenzsignal von ICG nur schwer nachweisbar und es sind höhere Dosen und mehrere intravenöse Kontrastmittelinjektionen im selben OP-Setup erforderlich. Die Photostabilität des Farbstoffs ist ebenfalls ein wichtiger Parameter; ICG wird bereits nach kurzer Bestrahlungszeit mit sichtbarem Licht (20 Minuten) abgebaut. Aus diesen Gründen stellt die Synthese neuartiger bildgebender NIR-Farbstoffe, die die Verwendung von ICG-grün in der FGS ersetzen können, heute eine wichtige Herausforderung dar. Unternehmen verwenden heute NIR-Imaging-Mittel, die auf chemisch verbesserten Versionen von Cyanin-Farbstoffgerüsten basieren. Insbesondere LiCOR® biotechnology hat Erfahrung in der Forschung mit IRDye®-Sonden in klinischen Studien der Phasen I und II. NIR-Wirkstoffe sind nützlich für die Untersuchung von Medikamentenverabreichungssystemen, gezielten Therapeutika, chirurgischen Kontrastmitteln und die Überwachung der molekularen Grundlagen von Krankheiten. Dennoch geht die Forschung zu anderen Farbstoffklassen über, um die Einschränkungen der Cyaninfarbstoffe zu überwinden. Push-Pull-Perylenfarbstoffe stellen eine neue Klasse von NIR-absorbierenden Chromophoren mit ausgezeichneter Photostabilität und Wasserlöslichkeit dar. Sie werden von Perylenmonoimiden abgeleitet, indem an den Peri-Positionen elektronenspendende Gruppen wie primäre Arylamine oder wasserlösliche Gruppen wie Guanidinfunktionen angebracht werden. Push-Pull-Perylenfarbstoffe sind in der Literatur als Materialien bekannt, die resistent gegen Photobleichung sind und sich für die Langzeitbestrahlung bei der Bildgebung von lebenden Zellen eignen. Peneva und Mitarbeitern gelang erstmals die Synthese eines Push-Pull-Perylenfarbstoffs mit einer Emission im NIR-Bereich bis zu 720 nm unter Verwendung einer Guanidinfunktion als Donorgruppe an den Periposition.[5] Push-Pull-Perylenfarbstoffe und die meisten Cyaninfarbstoffe können als "immer eingeschaltete Sonden" eingestuft werden. Nach der Definition von Chen et al. bleibt das Emissionssignal von "always ON"-Sonden bei Bestrahlung mit der im Versuchsaufbau verwendeten Anregungswellenlänge konstant.[6] Aufgrund dieser Eigenschaft kann der Signalüberschuss, der von ungebundenen, immer eingeschalteten Sonden auf dem kranken Gewebe in vivo ausgeht, zu einem geringen Verhältnis zwischen Ziel und Hintergrund auf dem kranken Gewebe von Interesse führen. Um diese Nachteile zu überwinden, wurden aktivierbare Farbstoffe entwickelt. Diese Fluorophore emittieren im fernen Rotbereich (650-700 nm) und können so konzipiert werden, dass sie ihre Fluoreszenz von einem dunklen AUS-Zustand in einen EIN-Fluoreszenz-Zustand umschalten, um spezifische pathologische Bedingungen zu erkennen, die mit erkranktem Gewebe verbunden sind, z. B. die Änderung des pH-Wertes bei Tumorazidose.[7] Zu den aktivierbaren Farbstoffen, die heutzutage in vivo verwendet werden, zählen auch Silizium-Rhodamine. Sie können vielseitig eingesetzt werden, unter anderem um Antikörper und kleinen Peptide zu markieren. Ihre Syntheseroute kann so gestaltet werden, dass die Funktionalisierung von primären Thiolen in Cysteinresten in makromolekularen Einheiten ermöglicht wird, die als Vektormoleküle ausgewählt wurden. In den folgenden Kapiteln wird die potenzielle Verwendung von Push-Pull-Perylen-Farbstoffen und aktivierbaren Silizium-Rhodamin-Farbstoffen dargestellt, gefolgt von einer ausführlichen Beschreibung des Stands der Technik der bereits in der FGS verwendeten Substanzen.

[5] Kaloyanova, S.; Zagranyarski, Y.; Ritz, S.; Hanulova, M.; Koynov, K.; Vonderheit, A.; Mullen, K.; Peneva, K., Water-Soluble NIR-Absorbing Rylene Chromophores for Selective Staining of Cellular Organelles. J Am Chem Soc 2016, 138 (9), 2881-4.

[6] Chen, C.; Tian, R.; Zeng, Y.; Chu, C. C.; Liu, G., Activatable Fluorescence Probes for "Turn-On" and Ratiometric Biosensing and Bioimaging: From NIR-I to NIR-II. Bioconjugate Chem 2020, 31 (2), 276-292.

[7] Wang, C.; Wang, Z.; Zhao, T.; Li, Y.; Huang, G.; Sumer, B. D.; Gao, J., Optical molecular imaging for tumor detection and image-guided surgery. Biomaterials 2018, 157, 62-75.

8. SELBSTÄNDIGKEITSERKLÄRUNG

Ich erkläre, dass ich die vorliegende Arbeit selbständig und unter Verwendung der angegebenen Hilfsmittel, persönlichen Mitteilungen und Quellen angefertigt habe.

Ort, Datum   Unterschrift der Verfasserin/des Verfassers

Pavia 26.03.2022

9. CURRICULUM VITAE

Profile

I am currently working in contract development and manufacturing organization CBC Procos S.p.A as R&D researcher for the development, scale-up and production of active pharmaceutical ingredients (API) with potent immunosuppressant activity and advanced intermediates for the pharmaceutical industry. I worked at the Friedrich Schiller University of Jena supported by Carl Zeiss Stiftung under the supervision of Prof. Dr. K. Peneva on the preparation of targeted macromolecular probes for fluorescence image-guided surgery. During my experience, I earned knowledge and experience on near-infrared fluorescence angiography to improve the detection and surgery of solid tumors *in vivo*. I have a strong passion for scientific writing and experience as a teacher and tutor in scientific disciplines in schools and universities. In my free time, I help young people to pursue their dreams. I believe in the strength of empathy, creativity, and emotional intelligence in personal life and at the workplace.

Personal Data

Davide Botteri M.Sc.
Via Mazzucchelli Carlo 17, Cameri, Novara (NO), Italy
Via Montini 15, 27100 Pavia (PV), Italy
Tel: +39 3519579264
davide.botteri92@gmail.com
davide.botteri@uni-jena.de
Skype name: bott-92
Twitter: @Davide_Botteri
ORCID iD: https://orcid.org/0000-0001-8109-638X
Website:
https://www.penevagroup.uni-jena.de/group/former+members
13th June 1992
Pavia, Italy
Italian

Work experiences

20.09.2021 – Today	**CBC Procos SpA, Cameri, Novara.** R&D Organic process research and development chemist working on late-stage modifications of high potent drugs with immunosuppressant activity.	
12.05.2021 – 17.06.2021	**Eurofins BioPharma Product Testing, Vimodrone, Milano.** Internship in **Eurofins Biolab**, QC Chemical analyst trainee in Active Pharmaceutical Ingredients (API). Internship Analyst working in cGMP regime.	
09.11.2020 – 07.05.2021	**Istituto comprensivo statale di Landirano, Landriano, Pavia Scuola media statale "G.Marconi"** Technology Teacher. Lecturer in chemistry and earth sciences. Lecturer in emotional intelligence and time management at the workplace.	
01.09.2016 – 31.08.2020	**Institute of Organic and Macromolecular Chemistry, Friedrich Schiller University, Jena** PhD candidate, Carl Zeiss Stiftung Research Fellow, Research	

topic: Multistage imaging reagents for fluorescence guided surgery (The research group of Kalina Peneva).

I worked on the synthesis and late-stage modification of NIR emitting fluorophores based on perylene and silicon rhodamine scaffolds. The fluorescent probes I developed, possess a bioconjugation linker to label targeting moieties like small peptides or antibodies for the precise detection and visualization of solid tumors. I am currently involved in collaborations with Dr. Andrea Picchetto and Prof. Dr. Giancarlo D´Ambrosio, La Sapienza University of Rome (Italy), Dr. Michele Diana, "Institut de recherche contre les cancers de l´appareil digestif" IRCAD Strasbourg (France) Mark Vendrell, University of Edinburgh (United Kingdom), and Magdalena Steiner Fujifilm Visualsonics, Science Park, Amsterdam, (Netherlands).

29/11/2018 - 30/11/2018   **Department of Medicine and Surgery Paride Stefanini, Policlinico Umberto I, La Sapienza University of Rome**
Research project in collaboration with Dr.Andrea Picchetto, for the study of APMI dyes as NIR contrast agents in *in vivo* angiography in rats.

10/2014 - 07/2016   **Department of Organic Chemistry, University of Pavia**
Master thesis (110/110 L "Graduated with Distinction") (The group of Dr.Giuseppe Zanoni in collaboration with Dr. Lutz Ackermann, University of Göttingen)

Research project: "Palladium mediated C-H activation for the synthesis of biologically active compounds "

During my master thesis I exploited the thermodynamically favored intramolecular C-H activation for the synthesis of cyclic core structures of phosphodiesterase inhibitors PDE10. In particular, I have conducted several investigations on pyrazole and triazole reactivity toward intramolecular arylation for the synthesis of pentatomic and heptatomic cyclic molecules. I also have worked on the synthesis of palladium-based catalysts.

09/2011 - 07/2014   **Department of Organic Chemistry, University of Pavia**
Bachelor thesis (The group of Prof. Dr. Angelo Albini)

Research project: "Photochemical internalization in Drug Delivery "

I studied the role of porphyrins for the photochemical production of cytotoxic singlet oxygen in biological media as a new approach in Photodynamic Therapy. I investigated the reactions of singlet oxygen toward unsaturated lipids and glycolipids in cell membranes that leads the formation of lipid hydroperoxides.

08/2010 - 09/2010   **Department of Physical Chemistry, University of Pavia**
Internship (The group of Dr. Umberto Anselmi Tamburini in collaboration with Dr. Alberto Zeffiro)

Research Project: "Effect of nanosized crystallites on Zirconium and Cerium Oxides based materials"

Education and Awards

09.11.2020   **Urkunde über Förderung bei der Carl-Zeiss-Stiftung,**
Certificate of Promotion, Carl-Zeiss-Stiftung Fundation

14.07.2020   **Teaching license for middle and high schools,**   24
University credits, cultural anthropology, cognitive psychology, theory of teaching and learning, Mnemosine Telematic University, University Dante Alighieri.

11.06.2020	**Medicinal chemistry, the molecular basis of drug discovery**, certificate of achievement, course of study offered by DavidsonX, Davidson college and Novartis. Erland Stevens, Ph.D, professor and chair of chemistry, Davidson college.
18.06.2019	Winner of one-year prolongation, **Carl Zeiss Stiftung** Fellowship, Project: Development of multistage imaging agents for fluorescence guided surgery
23.03.2019	**Sapienza research call,** starting projects, winner of research funding for the project "novel APMI dyes for fluorescence guided surgery and detection of ureters in rats" in collaboration with Dr. Andrea Picchetto and Prof. Dr Giancarlo D´Ambrosio, Sapienza University of Rome (Italy)
11.08.2018	**Sapienza research call,** starting projects, winner of research funding for the project "pH responsive Si Rhodamines as activatable probes in fluorescence guided surgery" in collaboration with Dr. Andrea Picchetto and Prof. Dr. Giancarlo D´Ambrosio, Sapienza University of Rome (Italy)
06.11.2017	Winner of the 2017 award of the **FCA automobiles**, for outstanding students Torino (Italy)
01.09.2017	**Carl Zeiss Stiftung,** winner of Ph.D. fellowship at the Friedrich Schiller University Jena (Germany)
01.06.2017	Winner of the 2017 Fellowship **Fondazione Agnelli**, Torino (Italy)
2011-2016	**University of Pavia, Pavia, Italy** Bachelor in Chemistry (final grade: 106/110) Master thesis – Organic Chemistry (final grade: 110L/110 cum laude) (winner of the award for the early graduated young students)
2006-2011	**Liceo scientifico statale, T.Taramelli, Pavia, Italy** High school (final grade: 92/100) (internships: one moth spent at the Physical Chemistry department, University of Pavia)

Conferences

09.07.2021	**Circular Economy and Catalysis, Online Workshop** (Italy) Pharmaceutical green chemistry & catalysis.
09-11.03.2021	**UniTo-PoliTo Conference series in cancer. Nanoscience in cancer immunotherapy**. Poster session: Water soluble NIR absorbing chromophores based on perylene and silicon rhodamine scaffolds for fluorescence guided surgery. Link: https://youtu.be/M8TfZGKyWNs (Minute 12:05-12:52). Torino (Italy).
08.07.2020	**2nd ChemBioChem Virtual Symposium,** 8 July 2020, Davide Botteri Friedrich Schiller University, Jena (Germany) contribution: audience
27.05.2020	**1st ChemBioChem Virtual Symposium,** 27 May 2020, Davide Botteri Friedrich Schiller University, Jena (Germany) contribution: audience

13.08.2019	**T.O Sommerfest, Towards understanding polyplex mediated gene delivery,** Pharmaceutical technology and Biopharmacy, Institute of Organic Chemistry and Macromolecular Chemistry, Jena (Germany) Contribution: Speaker, Davide Botteri and Andrew Njau
15-17.07.2019	**Symposium on innovative polymers for the nanomedicine of the 21st century,** Jena (Germany) Contribution: Audience
10-12.09.2018	**26th Lecture Conference on Photochemistry,** Munich (Germany) contribution: Poster
25.07.2018	**T.O Sommerfest, NIR molecular probes for in vivo and in vitro imaging,** Pharmaceutical Technology and Biopharmacy, Institute of Organic Chemistry and Macromolecular Chemistry, Jena (Germany) Contribution: Speaker
07-09.03.2018	**Imaging of cancer dynamics,** Torino (Italy) contribution: Poster
08-10.10 2017	**Solchem symposium on Solar-Driven Chemistry** Ulm (Germany) contribution: Poster
07-09.06.2017	**Receptor light symposium,** Würzburg (Germany) Contribution: Audience
23.08.2017	**Catalight Workshop** Jena (Germany) Contribution: Speaker
26-28.09.2016	**Lecture Conference on Photochemistry** Jena (Germany) Contribution: Staff Member
19.04.2016	**The Chemistry of Rubber** Pavia (Italy) Contribution: Staff Member
15.06.2016	**The meaning of being a Chemist in Lombardia** Pavia (Italy) Contribution: Staff member

Qualifications and Skills

Synthetic skills
- Organic and organometallic Chemistry, design, and synthesis of small molecules by multistep synthesis with C-H activation as a key step. Strong background in Cross coupling chemistry
- Strong expertise in organolithium chemistry for the synthesis of Silicon Rhodamine dyes
- Expertise in Mitsunobu reaction for the synthesis of maleimide linkers for antibody - drug conjugates.
- Alkylation of enolates; reactions of carbon nucleophiles with carbonyl compounds; functional group interconversion; electrophilic additions to carbon-carbon multiple bonds; reduction and oxidation of carbon-carbon multiple bonds, carbonyl groups and other functional groups; aromatic substitution reactions; organometallic chemistry with strong background in cross coupling chemistry

- Design and synthesis of Palladium catalysts for C-H activation reactions
- General bioconjugation chemistry techniques with special focus on the preparation of maleimide linkers and terminal allyl linkers for UV-mediated Click thiol-ene coupling (TEC) reactions.

Analytical skills
- Strong background and expertise in silica gel column chromatography for the purification of organic compounds (extensive knowledge of physico-chemical and miscibility data of solvents, use of Snyder's classification of eluent strenght)
- Thin layer chromathography, determination of retention factor and translation to column chromathography.
- 1D, 2D NMR techniques 1H, 13C, 1H-1H COSY, 1H-13C HSQCY
- Mass spectrometry techniques EI-MS, chemical ionization, MALDI, ESI
- RP-HPLC-UV, RP-HPLC-MS, GC-MS. Experience with Jasco ® software and Empower® software Agilent and Waters instruments.
- UV-Vis spectroscopy Experience with Jasco ® V780
- Potentiometry experience with pH meter and potentiometric titrations.
- Gel electrophoresis techniques: EMSA, SDS-PAGE, Western Blot
- Fluorescence spectroscopy. Experience with Edinburgh Instruments ® FLS1000
- Experience in fluorescence titration techniques for the determination of pKa values in activatable dyes for fluorescence guided surgery
- Experience *In vivo* fluorescence guided surgery in rats with Quest Medical imaging ®
- Aptitude in working with vacuum pumps, rotary evaporators, ovens, small scale glassware

Oral presentation, scientific discussions, courses, scientific writing and teaching skills
- Active participation in scientific meetings and conferences with oral presentations
- Poster presentation of main scientific findings of research projects.
- Teaching skills and course design in scientific disciplines. Experience with Argo® and Google Classroom®.
- Scientific writing

Publications

Hassan Abul-Futouh, Artem Skabeev, Davide Botteri, Yulian Zagranyarski, Helmar Görls, Wolfgang Weigand, and Kalina Peneva Toward a Tunable Synthetic [FeFe]-Hydrogenase H-Cluster Mimic Mediated by Perylene Monoimide Model Complexes: Insight into Molecular Structures and Electrochemical Characteristics
Organometallics 2018. DOI**:** 10.1021/acs.organomet.8b00450

Botteri, Davide and Sittig, Maria and Dietzek, Benjamin and Peneva, Kalina
Water soluble NIR absorbing chromophores based on perylene and Si-Rhodamine scaffolds for fluorescence guided surgery
CANCERTO-NANOSCIENCE IN CANCER IMMUNOTHERAPY Frontiers event abstracts

Workshops, Events, MOOC, Courses, Competitions

15-19.03.21	**3rd Compound Challenge. Merck Open Innovation** Merck Open Innovation. Competition to identify the best submitted synthetic route for a given small molecule. Live session training with **SYNTHIA®** Proposal ranked Top 200.
11.06.2020	**Medicinal chemistry, the molecular basis of drug discovery** certificate of achievement, course of study offered by DavidsonX, Davidson college and Novartis. Erland Stevens, Ph.D, professor and chair of chemistry, Davidson college.

,

22.05.20	**The type setting system LaTeX** Two days training course. Dr. Jens Kubieziel, Graduate Academy, FSU Jena.
12.05.20	**Academic Writing Skills** One day training course. Dr. Sonja Pierce, Graduate Academy, FSU Jena.
12.2015	**"Mind maps and how they work"** Compact course by Sonia Cristofaro University of Pavia, Italy.
2008-2016	**"Corripavia" Half Marathon** Staff member for "Atletica 100 Torri Pavia" Castello Visconteo, Pavia, Italy.
11/2015 - 04/2016	**"Lievemente" School of Watercolors** Student of Elisabetta Mino, Milano, Italy.

Voluntary services

08/2014	Volunteer member of "**Casa del Giovane**" staff member of "Missione Scampia" project for helping orphans children Scampia, Naples, (Italy).
11/2013 - 04/2014	Volunteer member of the "**Frati Minori di Canepanova**" Waiter in the Mensa of the homeless Pavia, (Italy).
2010 - 2011	Creative writer for "Liceo T.Taramelli" newspaper "Il Busto".

Teaching experience

09.11.2020- 07.05.2021	Teacher of Technology, lecturer in chemistry and earth sciences scuola media statale "G.Marconi" **Istituto comprensivo statale di Landriano, Scuola Media G.Marconi.**
2016-2020	Teaching experiences as organic chemistry techniques tutor in the university of Jena for undergraduate chemistry students. **FSU Jena** (Germany)
2014-2021	Private tutor for middle, high school and university students in the subjects: inorganic and organic chemistry

2010-2015	Sport Teacher in middle distances running (800 mt- 1500 mt) for "**Atletica 100 torri**", Pavia.

Languages

Italian	mother tongue
English	fluent in speaking and writing
German	fluent in speaking and writing
French	good knowledge

IT qualifications

Writing and project planning:	Windows OS, Microsoft Office, EndNote, ChemBioDraw, Reaxys, SciFinder LaTeX
Graphical programs:	CorelDRAW, Photoshop, Image J.
Analytical programs:	MestReNova, GraphPad, Prism, Origin, ACD labs.

Hobbies & Interests

- Running (competitive runner in 1500 mt and 800 mt)
- Martial Arts (Karate, Kick boxing)
- Watercolor painting
- Creative writing

Place, Date   Signature

Pavia, 26.03.2022